



University
of Glasgow

Sheafi, Emadeddin A.Mansur (2015) *Effects of various test regimes on fatigue behaviour of PMMA bone cement: a comparative study*.
PhD thesis.

<http://theses.gla.ac.uk/6250/>

Copyright and moral rights for this thesis are retained by the author

A copy can be downloaded for personal non-commercial research or study, without prior permission or charge

This thesis cannot be reproduced or quoted extensively from without first obtaining permission in writing from the Author

The content must not be changed in any way or sold commercially in any format or medium without the formal permission of the Author

When referring to this work, full bibliographic details including the author, title, awarding institution and date of the thesis must be given



EFFECTS OF VARIOUS TEST REGIMES ON FATIGUE BEHAVIOUR OF PMMA BONE CEMENT: A COMPARATIVE STUDY

EMADEDIN A MANSUR SHEAFI

BSc & MSc

Submitted in fulfilment of the requirements for the
Degree of Doctor of Philosophy (PhD)

School of Engineering
College of Science and Engineering
University of Glasgow

December 2014

ABSTRACT

Numerous testing regimes have been used *in vitro* to assess the fatigue behaviour of acrylic bone cements. While some attempts have been made to introduce an optimal protocol that measures the fatigue life of bone cement under similar stress conditions to those exist *in vivo*, the effects of specific testing variables such as test specimen specification and stress parameters are still questionable. These factors can be important since inconsistency in results have been reported regarding the precise effects of other variables such as the mixing method of cement components and the resultant porosity.

For a given series of testing variables; namely, specimen cross sectional shape, surface production method and stress type and level (herein collectively termed testing regime), this study investigates the effect of each variable on both the fatigue life and the fatigue crack propagation properties (fatigue behaviour) of bone cement. Testing was constantly performed in 37°C saline under stress-controlled conditions at a frequency of 3Hz (2Hz for the CT specimens). All specimens were produced after vacuum mixing of the cement components and soaked in 37°C saline for 1- 6 weeks. Specimens were manufactured with two cross sectional shapes: rectangular (ISO 527-2) and circular (ASTM F2118), using two production methods: direct moulding or machining. Two different bone cements were used: SmartSet GHV and CMW1. For each specimen type, at least 10 specimens were fatigued to failure at a maximum stress of 20 MPa applying either fully reversed tension-compression ($R = -1$) or tension-tension ($R = 0.1$) loading, followed by Weibull analysis. For the fully reversed loading only, at least 5 specimens were tested for each group at other three levels: ± 12.5 , ± 15 and ± 30 MPa and the four stresses were compared using S-N curves. Behaviour of fatigue cracks were assessed based on the cyclic stress-strain responses. CT specimens were used to measure the crack growth rates in the two cements.

The findings of this study have emphasised the important role of the set of a testing regime variables included in testing and identified the influence of each testing variable on the fatigue behaviour of bone cement. Machining of test specimens and applying high stress levels, in particular, can lead to irrelevant findings when considering the *in vivo* conditions, depending also on the cement composition. While these “inappropriate” testing variables can be considered as possible reasons for the variations in fatigue results reported in previous work, it is suggested to consider the effects of these variables in future work.

TABLE OF CONTENTS

ABSTRACT	2
TABLE OF CONTENTS	3
LIST OF TABLES	9
LIST OF FIGURES	11
ACKNOWLEDGMENTS	16
AUTHOR’S DECLARATION	17
NOMENCLATURE	18
CHAPTER 1. INTRODUCTION	20
CHAPTER 2. FATIGUE TESTING OF BONE CEMENT: LITERATURE REVIEW	23
2.1 Fatigue testing of materials: an introduction	23
2.1.1 Types of fatigue loading	25
2.1.1.1 Fully reversed sinusoidal stress	26
2.1.1.2 Zero to tension stress	27
2.1.1.3 Sinusoidal fluctuating stress	27
2.1.1.4 Non-sinusoidal fluctuating stress	27
2.1.1.5 Strain controlled fatigue	28
2.1.2 Specimens for fatigue testing	29
2.1.2.1 Design of test specimens	29
2.1.2.2 Preparation of specimens	29
2.1.3 Fatigue testing and analysis approaches	30
2.1.3.1 Stress-life approach	31
2.1.3.2 Strain-life approach	33
2.1.3.3 Fatigue approach: stress-controlled or strain-controlled	34
2.1.3.4 Low-cycle versus high cycle fatigue.....	36
2.1.3.5 Stress-strain curve	37
2.1.3.6 Crack initiation and propagation	38
2.1.4 Weibull functions for fatigue data analysis	39

2.2 Bone cement as a biomaterial	44
2.2.1 Bone cement components	44
2.2.2 Preparation and curing of bone cement	46
2.2.3 The role of bone cement in medical applications	47
2.2.4 Concerns about bone cement	49
2.2.4.1 Heat of polymerisation: effects and suggested solutions	49
2.2.4.2 Bone resorption	51
2.2.4.3 Implant loosening in joint replacement.....	51
2.2.5 <i>In vivo</i> versus <i>in vitro</i> fatigue.....	53
2.3 Fatigue testing of bone cement	57
2.3.1 Fatigue fracture: influencing factors and controversy	57
2.3.1.1 Chemical composition of the cement	57
2.3.1.2 Mixing methods	59
2.3.1.3 Porosity	62
2.3.2 Previous consideration of the effects of testing conditions and data analysis approaches	65
CHAPTER 3. MATERIALS AND METHODS	75
3.1 Materials	75
3.1.1 SmartSet GHV bone cement.....	76
3.1.2 CMW1 bone cement	76
3.1.3 Bone cement in its solid form	76
3.1.4 Saline solution.....	77
3.2 Mechanical testing	77
3.2.1 Preparation of test specimen	77
3.2.1.1 Specimen shape reference standards.....	77
3.2.1.2 Mixing of bone cement components.....	79
3.2.1.3 Surface preparation of test specimen	80
3.2.1.4 Initial assessment of test specimens.....	81
3.2.1.5 Classification and numbering of specimens	81
3.2.1.6 Identification of specimen measurements and loading forces	82

3.2.1.7	Conditioning of specimens prior to testing	83
3.2.2	Configuration of fatigue testing	83
3.2.2.1	Specimen installation	83
3.2.2.2	Conditioning of specimens while testing	84
3.2.2.3	Fatigue data acquisition.....	85
3.2.2.4	Application of fatigue stress.....	86
3.2.2.5	Final assessment of test specimens	86
3.2.3	Fatigue testing of CT specimens.....	87
3.2.3.1	Specimens preparation	87
3.2.3.2	Installation of crack gauges on specimens	87
3.2.3.3	Fatigue of CT Specimens and data acquisition.....	89
3.3	Data analysis	90
3.3.1	Weibull analysis.....	91
3.3.1.1	significance of variations in fatigue results.....	92
3.3.1.2	two-parameter Weibull distribution	93
3.3.1.3	three-parameter Weibull distribution	94
3.3.1.4	fatigue performance index.....	97
3.3.1.5	skewness of Weibull distribution (density function)	97
3.3.2	Wöhler (S-N) curves	98
3.3.2.1	Comparison of S-N curves of various specimen types	99
3.3.2.2	Comparison of S-N curves of different cements.....	100
3.3.2.3	Consideration of the effect of individual stress levels	101
3.3.3	Cyclic stress-strain response (hysteresis curves)	101
3.3.3.1	Rationale for considering absorbed energy and secant modulus	102
3.3.3.2	Estimation of absorbed energy and secant modulus	102
3.3.3.3	Consideration of a strain correction factor.....	105
3.3.3.4	Fatigue cycles versus absorbed energy and modulus.....	105
3.3.4	Fatigue crack growth in CT specimens.....	106
3.4	Post-fatigue failure investigations	108
3.4.1	Microscopic investigations of fracture surfaces	108
3.4.2	Differential Scanning Calorimetry (DSC)	109

CHAPTER 4. TOTAL FATIGUE LIFE.....	110
4.1 Introduction.....	110
4.2 Methods.....	110
4.3 Results - Weibull analysis of fully reversed tension-compression fatigue ...	111
4.3.1 Fatigue results	111
4.3.2 Significance of variations in fatigue results: preliminary comparisons	112
4.3.3 Weibull functions: two-parameter analysis	113
4.3.3.1 Comparison of fatigue performance indices	114
4.3.3.2 Probability density functions of Weibull distributions	116
4.3.4 Weibull functions: Three-parameter analysis	117
4.3.4.1 Comparison of fatigue performance indices	117
4.3.4.2 Probability density functions of Weibull distributions	120
4.4 Results - Weibull analysis of tension-tension fatigue.....	121
4.4.1 Fatigue results	121
4.4.2 Significance of variations in fatigue results: preliminary comparisons	121
4.4.3 Weibull functions: two-parameter analysis	122
4.4.3.1 Comparison of fatigue performance indices	122
4.4.3.2 Probability density functions of Weibull distributions	125
4.4.4 Weibull functions: Three-parameter analysis	126
4.4.4.1 Comparison of fatigue performance indices	126
4.4.4.2 Probability density functions of Weibull distributions	126
4.5 Results – Wöhler (S-N) curves	129
4.5.1 General comparisons of S-N curves of various specimen types.....	129
4.5.2 Comparison of S-N curves of same specimen type of different cements ..	131
4.5.3 The effect of individual stress levels	133
4.6 Results – post-fatigue examinations	136
4.6.1 Microscopic observations of fracture and circumferential surfaces	136
4.6.2 Degree of polymerisation (DSC)	138
4.7 Discussion.....	139
4.7.1 Effects of specimen specifications	139
4.7.1.1 Specimen cross-sectional area and size.....	139

4.7.1.2 Surface preparation method (roughness)	142
4.7.2 Effects of cement powder inclusions	145
4.7.3 Effects of stress type	147
4.7.4 Description of fatigue behaviour: effects of analysis approaches	150
4.8 Conclusions	153
CHAPTER 5. BEHAVIOUR OF FATIGUE CRACK PROPAGATION	154
5.1 Introduction	154
5.2 Methods	154
5.3 Analysis of stress-strain curves	155
5.3.1 Stress-strain curves: fully reversed tension-compression fatigue	155
5.3.1.1 Changes in absorbed energy.....	156
5.3.1.2 Changes in secant modulus	157
5.3.2 Stress-strain curves: tension-tension fatigue.....	159
5.3.2.1 Changes in absorbed energy.....	159
5.3.2.2 Changes in secant modulus	160
5.4 Fatigue crack growth measurement	161
5.4.1 Fatigue crack length vs. fatigue cycles	161
5.4.2 Crack growth rate vs. stress intensity range.....	163
5.5 Discussion	164
5.5.1 Stress-strain cyclic curves as fatigue damage indicators	164
5.5.1.1 Specimen type and composition	165
5.5.1.2 Stress type and amplitude effect	165
5.5.1.3 Thermal stability of test specimens	167
5.5.1.4 Consideration of creep contribution	168
5.5.2 Crack growth in CT specimens.....	170
5.5.2.1 Compliance to Paris' power law	170
5.5.2.2 Effects of molecular and particle characteristics	171
5.6 Conclusions	173
CHAPTER 6. GENERAL DISCUSSION	175

CHAPTER 7. CONCLUSIONS AND FUTURE WORK.....	180
7.1 Conclusions.....	180
7.2 Future work	182
LIST OF REFERENCES	183
APPENDICES	197
PUBLICATIONS	211

LIST OF TABLES

CHAPTER 3

Table 3.1 The powder and liquid chemical contents of SmartSet GHV and CMW175

Table 3.2 Specimen shapes and variations in cross and surface areas and surface area to volume ratios78

CHAPTER 4

Table 4.1 Ranked fatigue results of all groups tested in fully reversed tension-compression of ± 20 MPa, classified according to specimen type and cement composition.....112

Table 4.2 Significance of variations in results among various specimen types and cement compositions for the tension-compression stresses at ± 20 MPa.....113

Table 4.3 Summary of the determined values of the shape and scale parameters (two-parameter Weibull for the tension-compression stresses) and the resultant fatigue performance indices116

Table 4.4 Summary of the determined values of the shape, minimum fatigue life and scale parameters (three-parameter Weibull at tension-compression) and the resultant fatigue performance indices120

Table 4.5 Fatigue results for tension-tension (2-20 MPa), classified according to specimen type and cement composition.....121

Table 4.6 Significance of variations in results among various specimen types and cement compositions for the tension-tension stress regimes122

Table 4.7 Summary of the determined values of the shape and scale parameters (two-parameter Weibull at tension-tension) and the resultant fatigue performance indices – based on the relevant functions in Figure 4.4125

Table 4.8 Summary of the determined values of the shape, minimum fatigue life and scale parameters (three-parameter Weibull at tension-tension) and the resultant fatigue performance indices128

Table 4.9 Comparison of the estimations of the degree of polymerisation for all specimen types138

Table 4.10 Comparison of the difference in fatigue performance index (I) for all specimen types at the fully reversed tension-compression (± 20 MPa) and tension-tension (2 to 20 MPa) stress conditions (based on the three-parameter Weibull analysis).....148

CHAPTER 5

Table 5.1 Comparison of secant moduli of various specimen types tested in tension-compression measuring the modulus at an early fatigue cycle (the 10th cycle) and a late fatigue cycle (the 5th cycle before failure) with the total reduction in modulus in percentage between these two cycles158

Table 5.2 Comparison of secant moduli of various specimen types tested in tension-tension measuring the modulus at an early fatigue cycle (the 10th cycle) and a late fatigue cycle (the 5th cycle before failure) with the total reduction in modulus in percentage between these two cycles161

Table 5.3 Comparison of fatigue crack lengths at the failure point for the two cements..162

LIST OF FIGURES

CHAPTER 2

Figure 2.1 Various cyclic loading types shown as stress-time relations. a) Fully reversed tension-compression loading, b) zero to tension loading, c) tension-tension loading and d) non-sinusoidal fluctuating loading	26
Figure 2.2 Cycle-dependant material responses under (a) strain control and (b) stress control	28
Figure 2.3 Typical stress-life (S-N) curves for ferrous alloys (with an endurance limit) and non-ferrous alloys (with no endurance limit)	32
Figure 2.4 Schematic representation of the typical variation of stress amplitude with the number of cycles to failure for polymers	33
Figure 2.5 A total strain-life curve showing the elastic and plastic components.....	34
Figure 2.6 Fatigue testing of the same material under (a) stress-controlled and (b) strain-controlled conditions	35
Figure 2.7 Fatigue testing of two types of bone cements prepared by two mixing methods under (a) Stress-controlled and (b) strain-controlled fatigue conditions	35
Figure 2.8 Low-cycle versus high- cycle fatigue for steel	37
Figure 2.9 Schematic of stress-strain curve for a tension-compression cycle.	38
Figure 2.10 Different phases of fatigue life and related fracture factors	39
Figure 2.11 One pack of 40g SmartSet GHV bone cement (DePuy CMW manufacturing)	44
Figure 2.12 a) Methyl methacrylate (MMA) and b) Polymethylmethacrylate (PMMA) ..	45
Figure 2.13 Schematic of a cemented total hip replacement.....	48
Figure 2.14 Sketch diagram shows a possible polymerisation temperature curve	51
Figure 2.15 Images of a fractured stainless steel prosthesis due to failure of the bone cement mantle followed by implant loosening: (a) fracture position and (b) fracture surfaces.....	53
Figure 2.16 Fatigue life versus strain level for centrifuged and uncentrifuged Simplex P cement at 3 different probabilities of survival levels	61

Figure 2.17 Fatigue Summary of the mean fatigue test results and standard deviations, when prepared using different mixing systems and tested at 0.3-22 MPa in 22°C	62
--	----

CHAPTER 3

Figure 3.1 Test specimen shapes: (a) rectangular according to ISO 527-2 and (b) circular according to ASTM F2118	78
---	----

Figure 3.2 Close up of a specimen fully covered by saline spray during testing.....	85
--	----

Figure 3.3 Geometry and nominal dimensions of CT specimens used in testing of crack growth rate	88
--	----

Figure 3.4 An electrical circuit showing the prescriptive method of connecting the crack gauge and the readout instrument	89
--	----

Figure 3.5 A CT specimen with a crack measurement gauge during testing.....	90
--	----

Figure 3.6 An example of a diagram illustrates the determination of b and N_a for the two-parameter Weibull functions	94
--	----

Figure 3.7 An example of a diagram illustrates the determination of N_0 for the three-parameter Weibull functions	96
--	----

Figure 3.8 An example of a diagram illustrates the determination of N_a and b for the three-parameter Weibull functions.....	96
---	----

Figure 3.9 The density function of the Weibull distribution showing the effect of skewness of the shape parameter b	98
--	----

Figure 3.10 A hysteresis loop showing the distribution of data points where the absorbed energy was estimated as the area of the loop	104
--	-----

Figure 3.11 Illustration of changes in absorbed energy (increase in loop area), secant modulus reduction (decrease in secant slope) and creep (point where secant line crosses the horizontal axis) as the cyclic fatigue progresses	105
---	-----

CHAPTER 4

Figure 4.1 Illustration of porosity assessment of fracture surfaces after fatigue failure: (a & b) accepted specimens with no pores or pores diameter of $\leq 1\text{mm}$ and (c) a rejected specimen with a pore diameter of $>1\text{mm}$	111
---	-----

Figure 4.2 Plots of the two-parameter Weibull relationships showing the variations in fatigue behaviour of four different specimen types tested in fully reversed tension-compression ($\pm 20\text{ MPa}$) for (a) SmartSet GHV and (b) CMW1	115
--	-----

Figure 4.3 Plots of the three-parameter Weibull relationships showing the variations in fatigue behaviour of four different specimen types tested in fully reversed tension-compression (± 20 MPa) for (a) SmartSet GHV and (b) CMW1	119
Figure 4.4 Plots of the two-parameter Weibull relationships showing the variations in fatigue behaviour of four different specimen types tested in tension-tension cyclic loading between 2 and 20 MPa for (a) SmartSet GHV and (b) CMW1	124
Figure 4.5 Plots of the three-parameter Weibull relationships showing the variations in fatigue behaviour of four different specimen types tested in tension-tension cyclic loading between 2 and 20 MPa for (a) SmartSet GHV and (b) CMW1	127
Figure 4.6 General comparison of S-N curves generated from testing at four fully reversed tension-compression stress levels, comparing fatigue behaviour of four specimen types for (a) SmartSet GHV and (b) CMW1 bone cements	130
Figure 4.7 Comparison of S-N curves of SmartSet GHV cement (blue) and CMW1 cement (red) using specimen types of a) RDM, b) RMM, c) CDM and d) CMM.	132
Figure 4.8 Comparisons of the median fatigue lives of different specimen types at different stress levels for (a) SmartSet GHV and (b) CMW1	134
Figure 4.9 SEM of fracture surfaces of the median specimens of different specimen types of (a, c, e & g) SmartSet GHV and (b, d, f & h) CMW1, showing (a & b) RDM specimens, (c & d) RMM specimens, (e & f) CDM specimens and (g & h) CMM specimens	137
Figure 4.10 Examples of fracture surfaces that showed early failure of rectangular specimens due to localisation of pores or defects in the corners (circled) showing (a) for tension-tension and (b) for tension-compression of SmartSet GHV and (c) tension-tension and (d) tension-compression for CMW1. $R = 0.1$ and $R = -1$ respectively with a stress level of 20MPa.....	141
Figure 4.11 Examples of the defects observed on the outer surface of some moulded specimens	143
Figure 4.12 Micrographs of fracture surfaces compare the likely spread and accumulation of the two different opacifier particles in (a, c, e) SmartSet GHV and (b, d, f) CMW1, at three magnification levels	147
 CHAPTER 5	
Figure 5.1 Variations in the increase in absorbed energy per fatigue cycle for the different specimen types tested in tension-compression, showing (a) SmartSet GHV and (b) CMW1	157

Figure 5.2 Variations in the reduction in modulus per fatigue cycle for the different specimen types tested in tension-compression, showing (a) SmartSet GHV and (b) CMW1	158
Figure 5.3 Variations in the increase in absorbed energy per fatigue cycle for the different specimen types tested in tension-tension, for (a) SmartSet GHV and (b) CMW1	160
Figure 5.4 Variations in the reduction in modulus per fatigue cycle for the different specimen types tested in tension-tension, comparing (a) SmartSet GHV and (b) CMW1	160
Figure 5.5 Comparison between the fatigue crack propagation in (a) SmartSet GHV and (b) CMW1	162
Figure 5.6 Comparison of the regression lines fitting the fatigue crack growth rate (da/dN) against the stress intensity range (ΔK) for SmartSet GHV and CMW1	164
Figure 5.7 Comparable illustration of the strain creep behaviour for different specimen types of (a) SmartSet GHV and (b) CMW1 at 20 MPa tension-tension stress level ($R=0.1$)	169
Figure 5.8 Micrographs of a SmartSet GHV fracture surface illustrating (a) the disconnection of the PMMA beads without being fractured and (b) interaction between a PMMA bead and accumulated ZrO_2 particles	172

To:

*My parents; my wife, Amal; my sons, Anas and Amjad and
my daughter, Aala*

ACKNOWLEDGEMENTS

All praise is due to Allah (God). Peace and blessings of Allah be upon the one after whom there is no prophet.

Much effort has been made to complete this thesis. I am grateful to all those who, by one way or another, provided me with guidance and support during the years of my research.

I would like to express my gratitude to my research supervisor, Professor K. E. Tanner, who constantly provided me with valuable advice, useful feedback and explanations and, above all, encouragement and motivation throughout the course of this research.

I would, at the same time, thank and appreciate the Ministry of Higher Education and Scientific Research of Libya for the financial support provided to do this research. In the same regard, thanks are due to the Cultural Attaché of the Libyan Embassy in London for their help and support.

I would also like to acknowledge DePuy CMW for the supply of the bone cement materials and mixing systems. Special thanks to Bill McGregor in DePuy CMW1 for arranging to deliver the materials and for the useful information and comments he gave.

Thanks for the help and assistance I received from many individuals here at University of Glasgow. Special thanks to Mr John Davidson, Mr Alan Yuill, Mr Denis Kearns, Mr Wilson MacDougall and Mr Tom Dickson for their help. Thanks to Ross Colquhoun, Alex Vasiev, Zaleha Mustafa, Isaiah Adekanmbi and all others for being helpful and supportive.

Above all and foremost, I am truly grateful to my parents and my wife who have always provided me with the support and encouragement needed. I would just say I owe you all much more than I can possibly express. I would like also to thank my brothers, sisters, relatives, and friends for their concern and help.

AUTHOR'S DECLARATION

I hereby declare that, unless otherwise specified within the context, this thesis entirely represents my own work and it has not been previously submitted for any other degree or qualification.

Emadeddin Sheafi

Nomenclature

A	Amplitude ratio
a	Fatigue crack length [mm]
a_0	CT specimen pre-crack length [mm]
$\frac{da}{dN}$	Fatigue crack growth rate [mm/cycle]
A_{loop}	Area of a hysteresis loop = absorbed energy per cycle [kJ/m ³]
B	CT specimen thickness [mm]
b	Weibull modulus (or shape parameter)
b	Fatigue strength exponent (Basquin's exponent)
C	Material constant for Paris' power law
c	Fatigue ductility exponent
I	Fatigue performance index [cycles]
i	The rank of a testing specimen in the group
K	Stress intensity factor [MPa (m) ^{1/2}]
K_{max}	Maximum stress intensity factor [MPa (m) ^{1/2}]
K_{min}	Minimum stress intensity factor [MPa (m) ^{1/2}]
K_t	Stress concentration factor
m	Material constant for Paris' power law
n	Number of specimens per testing group
N	fatigue life [cycles]
N_a	Fatigue characteristic (or scale) parameter [cycles]
N_0	Weibull guaranteed (or minimum fatigue life) parameter [cycles]
N_f	Number of cycles to failure (fatigue life) [cycles]
P_{max}	Failure force for CT specimens in tension [N]
$P(N_f)$	Probability of failure (also P)

R	Stress ratio
R^2	Coefficient of determination
S	Stress [MPa]
W	CT specimen width [mm]
Y	dimensionless function that depends on the crack geometry (a/W)
Γ	Gamma function
Δa	Crack growth increment [mm]
ΔK	Stress intensity factor range [MPa (m) ^{1/2}]
ΔK_{TH}	Threshold stress intensity factor range [MPa (m) ^{1/2}]
ΔP	Difference between max and min fatigue forces (CT specimens) [N]
ε_a	Strain amplitude
ε_e	Elastic deformation
ε'_f	Fatigue ductility coefficient
ε_p	Plastic deformation
λ	Hazard function (failure rate) for Weibull distributions
σ	Axial stress [MPa]
σ_a	Stress amplitude [MPa]
σ_e	Fatigue endurance limit [MPa]
σ_f	Axial stress limit [MPa]
σ'_f	Fatigue strength coefficient
σ_m	Mean stress [MPa]
σ_{max}	Maximum stress [MPa]
σ_{min}	Minimum stress [MPa]
σ_r	Stress range [MPa]
τ	Torsional stress [MPa]
τ_f	Torsional stress limit [MPa]

CHAPTER 1. INTRODUCTION

Fatigue testing and characterisation are essential in improving the mechanical integrity of any material, including if this material is used in orthopaedic applications and subjected to cyclic loads. Bone cement is used in implant fixations as a grout material subjecting it to the various loads generated from body weight and movements. An artificial hip joint, for example, depending on the patient's age and activity, encounters an average of between 0.5 to 2 millions of stress cycles every year (Wallbridge and Dowson, 1982) which are transmitted by the cement mantle in a cemented hip or knee replacement. In some cases, early failure of the cement mantle has been reported, leading to serious clinical consequences. These consequences stem from not only losing the key roles of the cement mantle in securing the implant into the bone and stability transferring the loads between them but also other issues subsequent to this failure including mainly implant loosening associated with pain experienced by the patient. Therefore, enhancing the fatigue fracture resistance of bone cement is essential. Much research has been conducted to examine the variables that can play a role in controlling fatigue performance of bone cement materials. *In vitro*, the effects of variables such as chemical composition, mixing method and resultant porosity have been examined extensively. However, there is inconsistency in findings regarding the effect of particular variables amongst different studies. Lewis (2003a) in his review, which included examining the "intrinsic" and "extrinsic" factors that can affect the fatigue performance of bone cement as reported in previous work, concluded that there are "only a few areas of agreement" and "many areas of disagreement". It has been stated that using different fatigue testing methods makes it inappropriate to compare the findings from different studies (Johnson et al., 1989; Harper and Bonfield, 2000). In addition to using a range of testing conditions, Lewis and Nyman (2000) argued that many of these studies "have employed inappropriate statistical methods" and "have not addressed the issue of possible interactions between the parameters being investigated". These considerations have made it important to closely examine the effect of each testing regime variable on the fatigue characterisation of bone cement while maintaining all the other testing conditions and variables constant. For the same material and under the same environmental conditions and test frequency, these variables include specimen cross sectional shape, specimen production method and cyclic loading type and level.

Limited studies have simultaneously examined the effects of these variables comparing only two testing regimes under the same other "controlled" testing conditions. Carter et al.

(1982) and Gates et al. (1983) studied the fatigue properties of one bone cement brand using the same testing conditions except applying different cyclic loading type (fully reversed tension-compression and zero-tension, respectively) and using only one specimen type (circular in cross section and machined). Also, they used strain-controlled fatigue, which has now been agreed to be less representative than stress-controlled loading. Paravic et al. (1999) investigated the effect of specimen preparation on porosity and fatigue longevity comparing two specimen production methods (moulding and machining). They used circular cross sectional specimens only, prepared from one cement formulation, and performed the fatigue tests in tension-tension loading only, reporting longer fatigue lives for the moulded specimens. Using moulded specimens and considering the effect of specimen shape only, Lewis and Janna (2003) compared the fatigue life of rectangular and circular cross sectional specimens of three different cements. All specimens were subjected to one fully reversed tension-compression stress level of 15 MPa, and longer fatigue lives were found for the circular specimens. More recently, Tanner et al. (2010) compared two fatigue testing methods, using four bone cements, where the first method used rectangular moulded specimens at one tension-tension stress level, followed by Weibull analysis, and the second method used circular machined specimens in fully reversed tension-compression at a range of stress levels, followed by Wöhler analysis. While this study compared closely two different testing methods and reported substantial variations in results, there are interactions between the different variables amongst the two methods making it difficult to decide which variable (specimen shape, production method, stress conditions or the data analysis approach) is specifically important. Moreover, none of the published studies has attempted to examine and compare the behaviour of fatigue crack progress of different bone cement specimen types and under various stress parameters (i.e. when using different testing regimes). Apparently, all the studies that compared particular testing methods aimed to examine their effect on the total fatigue life with no sufficient consideration of the fatigue crack behaviour within the same testing method comparative studies under “controlled” conditions. Simulation studies of the fatigue damage accumulation *in vivo* have shown that failure progress is affected by the stress amplitude, where using one peak stress alone would be a “misleading measure of durability” (Lennon and Prendergast, 2001), the “load-profile”, with the muscle loading “to provide increased confidence” compared to the non-muscle loading (Britton et al., 2003), the periods of rest during testing, and hence *in vivo* (Roques et al., 2004), the stiffness and creep damage response at the cement-bone interface that is influenced by loading magnitude, number of loading cycles and the cement-bone contact area (Mann et al., 2009).

This thesis provides a comprehensive study that has been performed to investigate and compare the effects of different testing regime variables on fatigue behaviour of bone cements, using different data analysis approaches. Two different composition bone cements were used in the study: SmartSet GHV and CMW1. For each cement, two testing standards were used to have two different cross sectional shape specimens: ISO 527-2 (rectangular shape – half-sized specimen) and ASTM F2118 (circular shape), which both have been adopted in many studies of fatigue testing bone cement, with the first standard being for the determination of tensile properties of plastics in general and the second being for fatigue testing of bone cements in particular. Since both standards refer to the possibility of producing specimens by either direct moulding or machining and since both production methods have been used for bone cement, both moulded and machined specimens were produced for each testing group of both specimen shapes. Using an adequate number of specimens per group, all specimens were fatigued to failure in either fully-reversed tension-compression ($R=-1$) or tension-tension ($R=0.1$) cyclic loading at the same maximum stress level (20 MPa), followed by Weibull analysis of fatigue life results for each stress type. The fully reversed fatigue was also performed on all specimen types at other maximum stress levels (12.5, 15 and 30 MPa) to allow the generation of S-N curves to compare the fatigue results. All fatigue life testing was conducted at 3 Hz in flowing saline at 37°C. To obtain an estimation of the fatigue crack behaviour in each specimen type, the cyclic stress-strain curves were examined at different intervals and the changes in hysteresis and secant modulus per cycle were used to indicate the fatigue damage. Additionally, direct measurements of the fatigue crack growth in the two cements were performed on a number of CT specimens subjected to tension-tension loading at 2 Hz.

Overall, this thesis is divided into seven chapters, including this introduction as the first chapter. Chapter 2 is a literature review that starts with a brief introduction to fatigue testing of materials in general followed by introducing bone cement as a biomaterial and its fatigue testing in previous work. Chapter 3 outlines the materials used, the experimental procedures followed and the data analysis approaches adopted. The results are presented and discussed in two chapters: Chapter 4 compares the total fatigue life, that is the number of cycles to failure, for all testing regimes included in the research and Chapter 5, first, estimates and compares the crack propagation trend under these testing regimes and, second, measures and compares the fatigue crack propagation in the two cements using the ASTM E647 standard. General discussion of the findings is provided in Chapter 6, followed by the main conclusions and future work in Chapter 7.

CHAPTER 2. FATIGUE TESTING OF BONE CEMENT: LITERATURE REVIEW

2.1 FATIGUE TESTING OF MATERIALS: AN INTRODUCTION

The term *fatigue* is widely used in materials science and engineering and refers to the progressive damage in a material's structure as a result of being exposed to repeated stresses or strains. Fatigue damage has been reported to occur over various successive stages that depend mainly on the structure of the material and the existence of defects. These stages have been reported as a general description of the progressive growth of fatigue cracks in materials. Suresh (1998), for instance, described these crack initiation and propagation stages saying:

“... the progression of fatigue damage can be broadly classified into the following stages:

- 1) Substructural and microstructural changes which cause nucleation of permanent damage
- 2) The creation of microscopic cracks
- 3) The growth and coalescence of microscopic flaws to form ‘dominant’ cracks, which may eventually lead to catastrophic failure
- 4) Stable propagation of a dominant macrocrack
- 5) Structural instability or complete fracture”

Fatigue fracture is the most important phenomenon by which the failure of mechanical components occurs. It “is the most unexpected service failure” (McClintock and Argon, 1966). The fatigue life that a component can provide in service depends on many factors including mainly the material properties, stress amplitude and temperature. Two general reasons are considered if a component failed exceptionally early: the material resistance to fatigue is particularly low or the applied stress is excessively high; “however, the list of questions is larger” (Schijve, 2009). One of the trailblazing studies on the subject of fatigue and its crack mechanisms was provided by William John Macquorn Rankine when he was

examining the fatigue fractures of train axles at the University of Glasgow in the middle decades of the 19th century. As mentioned in Cotterell (2010), Rankine (1843) examined the fatigue fracture of five axles that had fractured within four years and observed that the cracks started with regular forms of smooth minute fissures that extended around the journal neck. Due to initially being uncertain that the iron of the axles changed its structure, Rankine performed his study to find more logical reasons that led to the failure of the components. It was reported that the axles failed when the central part of the axle iron became insufficient to take its role in supporting the continued loads (Cotterell, 2010).

Over the last few decades, and due to the availability of advanced optical and electron microscopic systems, detailed observations on the underlying microstructural factors have become possible. This evaluation process is, of course, performed along with the consideration of the effect of mechanical factors (e.g. load spectrum) and environmental factors (e.g. temperature). The main benefit gained from fatigue assessment is, therefore, providing a chance to investigate the factors that control the fatigue life in order to help improve the strength and, accordingly, the life of stressed components. This enhancement process (*design against fatigue*) can be important whenever the properties of a material need to be enhanced to provide greater fatigue performance. Techniques that are typically used to improve fatigue fracture resistance include, for instance, surface treatment, heat treatment and modifying chemical compositions (Manson, 1971; Pokluda et al., 2005).

As fatigue of components is the most commonly described failure mechanism, various fatigue testing standards have been developed to assess the fatigue characteristics of different materials. Over the time, fatigue test methods have varied in terms of procedures and applications depending essentially on the properties and use of the material in question. This variation includes, but is not limited to, using different test specimen shapes prepared using different surface production methods along with applying different stress modes and parameters, providing a range of methods that each of which can be valid for testing fatigue and fracture of a particular component depending on its 'real life' usage. However, for fatigue testing of a particular material such as bone cement, various testing methods have been adopted with limited consideration to the effect of these variations on describing fatigue behaviour of the material.

2.1.1 Types of fatigue loading

Materials are subjected to various stress conditions depending on their positions under operation. A component might encounter a single direction stress (uniaxial) or interference of two (biaxial) or more (multiaxial) stresses. Fatigue stresses are classified depending upon the position and direction of the applied cyclic load on a particular component. To assess the fatigue properties of a material, fatigue testing specimens are cyclically loaded by applying axial tension and/or compression, bending or torsion loads as required. For each of these loading cases, specimens are fatigue tested by applying a particular stress type. Combinations of different stress modes such as axial tension and torsion may be applied. These combined stresses lead to more complex situations as they might differ in phase or frequency or both depending on the sources of cyclic loading (Dowling, 2007). An early study by Gough and Pollard (1935), for instance, proposed an elliptical quadrant criterion (Equation 2.1) to consider the combined effect of and the relation between the bending stress (σ) and the torsion stress (τ) in metals considering their fatigue limits in single load cases (σ_f & τ_f respectively).

$$\frac{\sigma^2}{\sigma_f^2} + \frac{\tau^2}{\tau_f^2} = 1 \quad (2.1)$$

Stress types are classified according to the ratio between the minimum and the maximum applied cyclic stresses. The main stress types of fatigue testing are listed below and illustrated in Figure 2.1. The main relations between the main stress components (σ_m , mean stress; σ_a , stress amplitude; σ_r , stress range; A , amplitude ratio and R stress ratio) are given in equations 2.2 - 2.5.

$$\sigma_m = \frac{\sigma_{max} + \sigma_{min}}{2} \quad (2.2)$$

$$\sigma_a = \frac{\sigma_{max} - \sigma_{min}}{2} \quad (2.3)$$

$$R = \frac{\sigma_{min}}{\sigma_{max}} \quad (2.4)$$

$$A = \frac{\sigma_a}{\sigma_m} \quad (2.5)$$

where, σ_{max} is maximum stress and σ_{min} is minimum stress, noting that tension is considered to be positive and compression is negative.

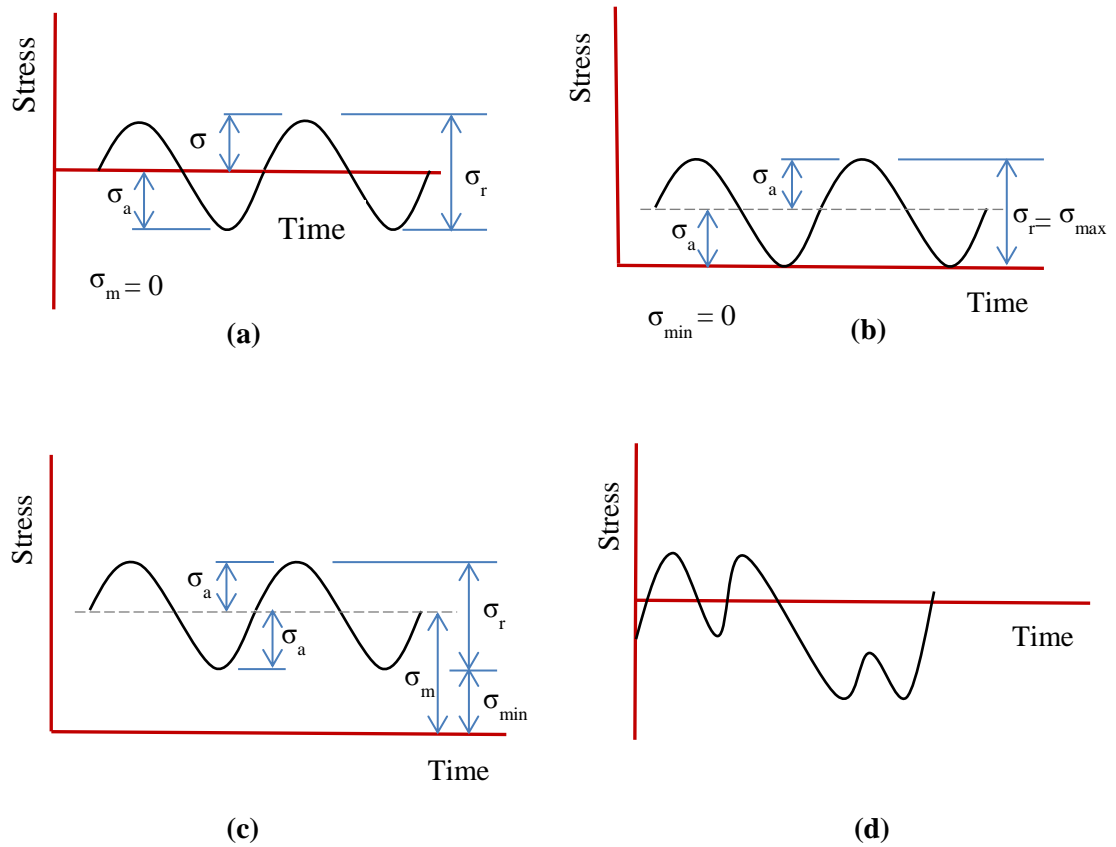


Figure 2.1 Various cyclic loading types shown as stress-time relations. **a)** Fully reversed tension-compression loading, **b)** zero to tension loading, **c)** tension-tension loading and **d)** non-sinusoidal fluctuating loading [redrawn from Shigley and Mischke (1989)]

2.1.1.1 Fully reversed sinusoidal stress

This type of stress (also known as fully reversed tension-compression) exists when a material is subjected to a fluctuating stress where it is loaded in tension and compression to the same load levels providing a sinusoidal shape of the cycle curve. As illustrated in Figure 2.1a, identical level fluctuating stresses occur alternately providing a zero mean stress value. This is only obtained when the absolute values of the maximum (tension) and minimum (compression) applied loads are equal, providing the fully reversed fatigue conditions, leading the stress components for this case to be defined as follows:

$$\sigma_m = 0 \quad (2.6)$$

$$\sigma_a = |\sigma_{max}| = |\sigma_{min}| \quad (2.7)$$

$$R = -1 \quad (2.8)$$

$$A = \infty \quad (2.9)$$

2.1.1.2 Zero to tension stress

This cyclic stress is when a material is loaded from zero force to a positive force repeatedly as can be seen from Figure 2.1b. The components of stress in this case have the following characteristics:

$$\sigma_m = \sigma_a = \frac{\sigma_{max}}{2} \quad (2.10)$$

$$\sigma_{min} = 0 \quad (2.11)$$

$$R = 0 \quad (2.12)$$

$$A = 1 \quad (2.13)$$

2.1.1.3 Sinusoidal fluctuating stress

This is another type of uniform fatigue; however, it fluctuates between two positive (tension-tension) or between two negative (compression-compression) stresses never reaching zero. The tension fluctuation for this case is illustrated in Figure 2.1c. The component is stressed continuously throughout its time of operation between a lower and a higher stress values. This leads to the mean stress and stress amplitude to be determined according to Equations 2.2 and 2.3 while the stress ratio and stress amplitude are identified as in Equations 2.13 and 2.14, respectively.

$$R > 0 \quad (2.13)$$

$$1 > A > 0 \quad (2.14)$$

2.1.1.4 Non-sinusoidal fluctuating stress

There are two types of non-sinusoidal fatigue testing. The first is when the signal fluctuates between the stress levels providing a non-sinusoidal signal shape such as a saw tooth or square wave. The second stress type includes the occurrence of various uneven fluctuating stresses throughout the working time of a component. Thus, the relations between the stress components are not constant over the cyclic loading period. An example to the shape of the stress-time relation with uneven cyclic fluctuation is shown in Figure 2.1d.

2.1.1.5 Strain controlled fatigue

The cyclic loading types listed above may apply to strain controlled fatigue where the load limits are based on the strain rather than stress fatigue such that a specimen or a component is loaded between two upper and lower displacement limits (instead of the force limits). For fatigue testing, the selection between these two testing approaches is controlled by various factors as explained in section 2.1.3.3.

In terms of the comparable cycling waves during testing, and as illustrated by Hertzberg (1996), when the process is controlled by strain conditions, the inconstant limits of the dependent stress waves would be produced by the material being subjected to hardening or softening deformation (Figure 2.2a). Similarly, when the specimen is tested under stress controlled fatigue, the strain response would be driven by the applied stress, showing either hardening or softening behaviour with the latter deformation providing a higher strain range that leads to earlier fracture (Figure 2.2b).

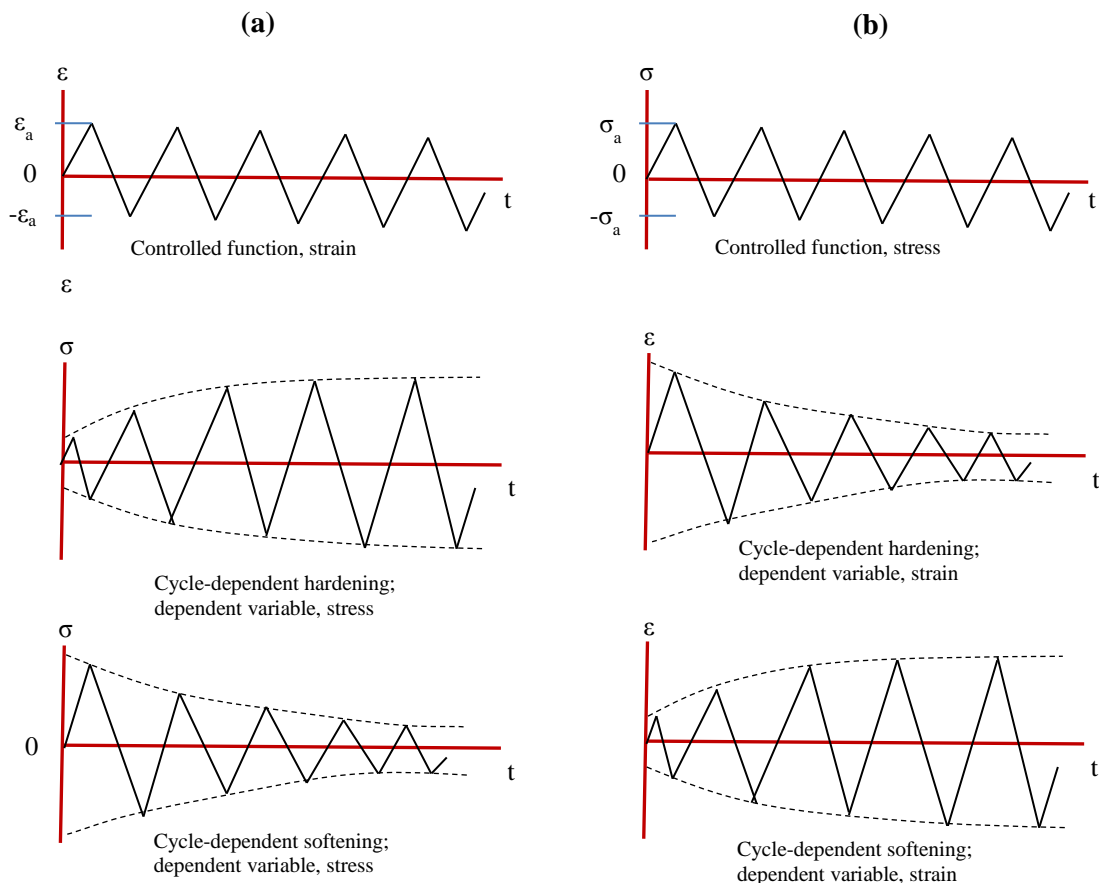


Figure 2.2 Cycle-dependant material responses under (a) strain control and (b) stress control [adapted from Hertzberg (1996)]

2.1.2 Specimens for fatigue testing

Fatigue testing specimens are usually designed in such a way that “the required test conditions are simulated as closely as possible” (Swanson, 1974). Fatigue specimens can be either unnotched (smooth) without a stress raiser in the gauge section of the specimen or notched to produce a stress concentration in the failure section where the latter is characterised by the elastic stress concentration factor (Dowling, 2007). Specimens are designed with a particular shape gauge section providing circular or rectangular cross sectional areas and the outer surface of the specimen is prepared by a specified production method.

2.1.2.1 Design of test specimens

Fatigue specimens usually have rectangular or circular cross sections. Review of the literature shows that a typical fatigue life testing specimen generally is divided into three to five regions: the gauge section in the centre of the specimen that has a significantly reduced cross sectional area compared to the other parts of the specimen, two grip ends to be used for fixing the specimen in the testing machine, and two transitional sections between the gauge and the grips through which the cross area is gradually reduced from the grips to the gauge section. The specimens, particularly the circular cross sectional ones, can be either solid or hollow as appropriate to represent the real-life conditions. Although the cross sectional shape options are limited, the dimensions of the gauge sections and the geometry of the non-gauge sections vary substantially depending upon the properties of the material being tested. Generally, two main criteria should be considered when designing fatigue specimens: (1) ensuring the occurrence of the failure in the gauge section and (2) avoiding the presence of stress raisers unless deliberately required (Swanson, 1974). The stress concentrations mentioned in the latter criterion such as notches are included in specimens of special testing requirements as the Compact Tension specimens used in measuring the fatigue crack growth rate within a material.

2.1.2.2 Preparation of specimens

Various manufacturing techniques have been reported to prepare testing specimens. These techniques can be classified, as in Bhandari (2010), into three categories: casting processes (e.g. mould casting), deformation processes (e.g. extrusion) and material removal or machining processes (e.g. milling). Although casting can be “one of the easiest methods to convert the raw material into finished component” (Bhandari, 2010), the most common method in preparing fatigue specimens is to machine them from non-waisted oversized

rods, presuming that the specimen is not overheated or excessively stressed by the machining process (Swanson, 1974). The material removing approach is particularly applicable for specimens with circular sections that are cyclically loaded under various deformation modes including rotating bending (Suresh, 1998).

Numerous standards have been published to provide guidelines for specimen preparation and testing, such as the ISO and ASTM standards. ISO, for example, has specified standards that describe the procedures to be followed when preparing testing specimens by injection and moulding (e.g. ISO 293) or machining from compression- or injection-moulded rods (e.g. ISO 2818). ISO 527-2 specifically recommends the use of rectangular shape for determining the tensile properties of plastics; however, the specimens can be prepared by either moulding or machining in accordance with other relevant standards as appropriate (BSI, 2012a). With either production method, specimens may need to be polished to remove scratches or sharp edges. It is generally recommended that the surface roughness measurements should be between 0.05 μm and 0.8 μm (Swanson, 1974). The preparation of specimen process may be specified to be followed by other treatments or aging environments before testing depending upon the material being investigated. ISO 291, for instance, provides general atmospheres to be used for conditioning of plastic specimens unless other conditions have been agreed. This environmental factor can have different effect on materials depending on their structure. With polymers, for example, it is possible to obtain higher or lower fatigue resistance levels due to the effect of specific surface environments, as fatigue fractures are more likely to develop from sources on these surfaces (Sauer and Richardson, 1980).

2.1.3 Fatigue testing and analysis approaches

Once the specimens have been prepared and conditioned as appropriate, they are installed in the test machines to be subjected to the required loading test. For the typical dumbbell specimens, this includes placing the specimen in the test machine aligning its longitudinal axis with the axis of the machine (BSI, 2012a). Other non-uniform specimens are installed as specified in the relevant testing standards. The typical Compact Tension specimens that are used for measuring the fatigue crack growth have to be fatigue loaded in tension-tension only where a specific gripping assembly “is used at both the top and bottom of the specimen to allow in-plane rotation as the specimen is loaded” (ASTM, 2013). For fatigue testing, it is required to select an appropriate total-life approach to be stress-controlled (the

stress-life or S-N curve approach) or strain-controlled (the strain-life approach) which should respectively be decided according to whether components would mainly undergo elastic or plastic deformation in their real life usage (Suresh, 1998). While testing, in general, the case is considered to be high cycle fatigue when there is no plastic deformation whereas low cycle fatigue is associated with plastic deformation. There are general concepts that occur in all specimen types when exposed to fatigue loading including specimen deformation, crack initiation and propagation and changes in the strain energy. This leads to gradual reduction in the mechanical properties of the material resulting in fatigue failure when the specimen fractures due to the growth of fatigue cracks.

2.1.3.1 Stress-life approach

Stress-life (or S-N curve) approach is the most classical technique to characterise fatigue behaviour of elements, predicting the total fatigue life according to the variability in cyclic stress. It, therefore, provides a graphical analysis showing the stress parameters as a function of the cycles to failure. An S-N curve can be generally described as:

“...a plot of stress against the number of cycles to failure. The stress can be maximum stress, σ_{max} ; minimum stress, σ_{min} ; stress range, σ_r ; or alternating stress, σ_a . The curve indicates the S-N relationship for a specific value of σ_a , A or R and a specific probability of survival. For N , a log scale is commonly used. For S , either a logarithmic or a linear scale is used” (Bauman, 2008).

It also illuminates the endurance limit (σ_e) which is the stress amplitude below which fatigue failures never occur. Figure 2.3 shows an example of two types of S-N curves where the upper curve represents ferrous alloys and titanium providing an endurance limit and the lower curve is a representative of non-ferrous alloys (e.g. aluminium) without an endurance limit. While the shape of an S-N curve is mathematically controlled by the stress amplitudes and the resultant cycles to failure data, more underlying factors have been reported to govern the process. The fatigue data is primarily associated with two periods of fatigue life: the crack initiation period involving the micro-crack growth and the crack propagation period (Schijve, 2009).

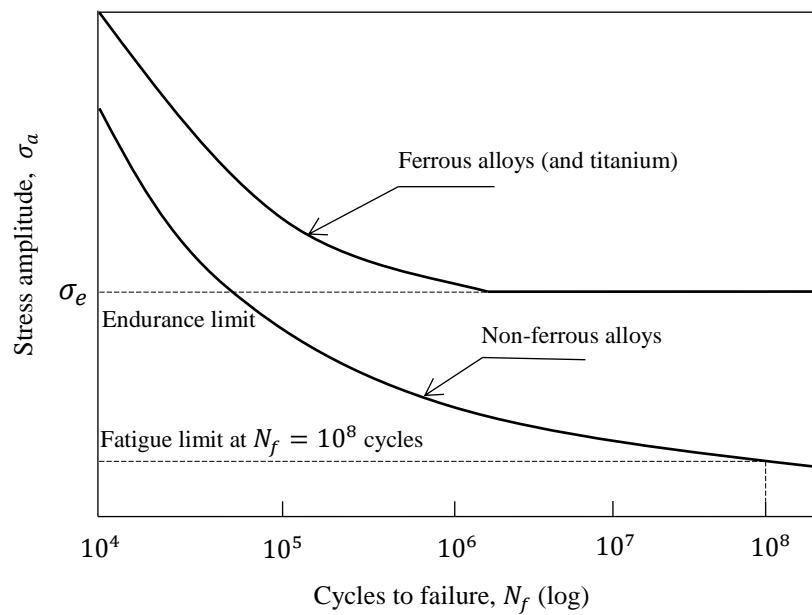


Figure 2.3 Typical stress-life ($S-N$) curves for ferrous alloys (with an endurance limit) and non-ferrous alloys (with no endurance limit) [redrawn from Milella (2013)]

Although a typical $S-N$ curve is developed in the same way for all materials, its shape can be obviously different. Polymeric materials, for instance, provide $S-N$ curves that can generally be divided into three distinct regions (I, II and III) as shown schematically in Figure 2.4 (Suresh, 1998). In the cases of recording insufficient maximum tensile stress in the early loading cycles, which is required to form the crazes that lead to the nucleation of micro-cracks over this stage, the curve in region I would follow the same trend as that in region II which can be characterised by “a slope of 14 MPa per decade of N_f ” for many polymers (Suresh, 1998). In terms of determining and representing the fatigue endurance limits using the conventional $S-N$ method, it has been mentioned to be difficult to achieve this in polymers due to the effect of the localized thermal fatigue on the mechanisms of failure resulting in inaccuracy in fatigue durability obtained (Teoh, 2000).

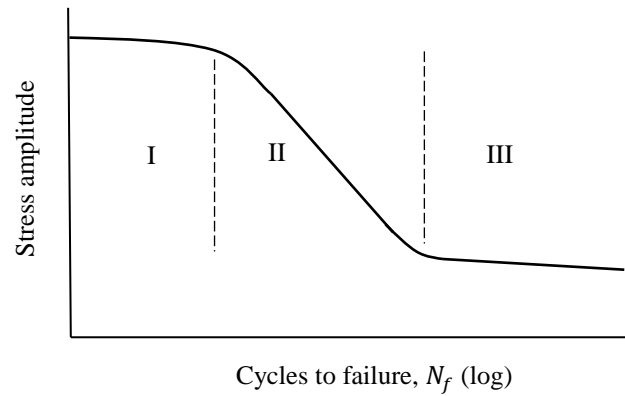


Figure 2.4 Schematic representation of the typical variation of stress amplitude with the number of cycles to failure for polymers [adapted from Suresh (1998)]

2.1.3.2 Strain-life approach

The strain-life approach (or ε - N curve) is performed to show the strain amplitude as a function of the cycles to failure. The basic strain-life relationship is represented in equation 2.15 (Mitchell, 1996). The right side of the equation consists fundamentally of two parts representing the elastic (ε_e) and the plastic (ε_p) deformations as represented in equation 2.16. Figure 2.5 illustrates this relationship in materials such as metals showing how a total ε - N curve can be developed. The crossing point between the elastic and plastic curves meets the reversals to failure ($2N_t$) before which the plastic deformation controls the process and after which the elastic strain dominates.

$$\frac{\Delta\varepsilon}{2} = \frac{\sigma'_f}{E} (2N_f)^b + \varepsilon'_f (2N_f)^c \quad (2.15)$$

$$\frac{\Delta\varepsilon}{2} = \varepsilon_e + \varepsilon_p \quad (2.16)$$

where $\frac{\Delta\varepsilon}{2}$ is the strain amplitude = ε_a , σ'_f is fatigue strength coefficient, ε'_f is fatigue ductility coefficient, b is the fatigue strength exponent (Basquin's exponent) and c is the fatigue ductility exponent

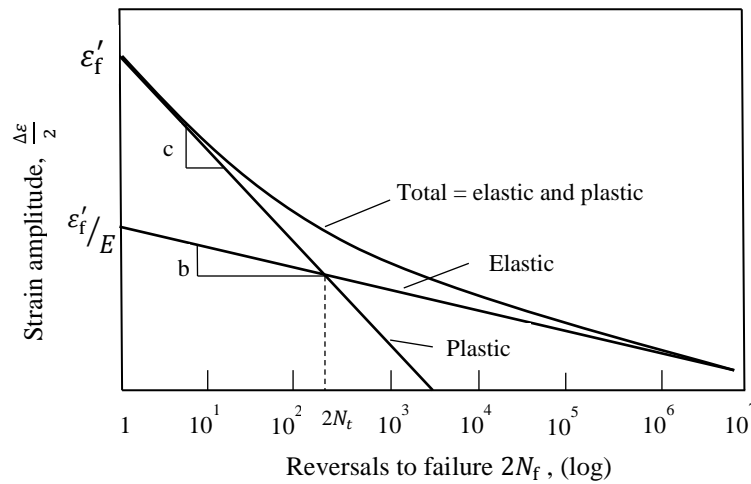


Figure 2.5 A total strain-life curve showing the elastic and plastic components [redrawn from Mitchell (1996)]

2.1.3.3 Fatigue approach: stress-controlled or strain-controlled

The degree of plastic deformation is largely controlled by the material property in terms of being ductile or brittle. Ductile materials show obvious deformation before failure whereas the brittle materials show low or no deformation. If a material was fatigued and started to deform, strain hardening would start to progress. According to Suresh (1998), in materials such as single crystals, this hardening occurs rapidly under fully reversed loading from even the early cycles until reaching a state known as quasi-steady deformation or saturation. Other materials can show either brittle and rigid or tough and ductile behaviour as was pointed out by Ehrenstein (2001) for plastics:

“Brittle behaviour is characterised by a small deformation at failure and the absence of a well-defined yield point on the stress-strain curve. In contrast, a plastic is tough if a distinct yield stress can be defined before failure and/or the deformation is both large and irreversible.”

Due to these suppositions, it is important to consider the effect of the selection of a particular total-life approach on the fatigue results. Figure 2.6 shows a schematic for a possible difference between a stress-controlled S-N curve and a strain-controlled S-N curve that can be obtained when testing the same material (Milella, 2013). This difference can be observed for the materials that undergo a cyclic strain hardening under stress-controlled fatigue where this hardening is not observed with strain-controlled fatigue that shows a greater apparent fatigue resistance (Milella, 2013).

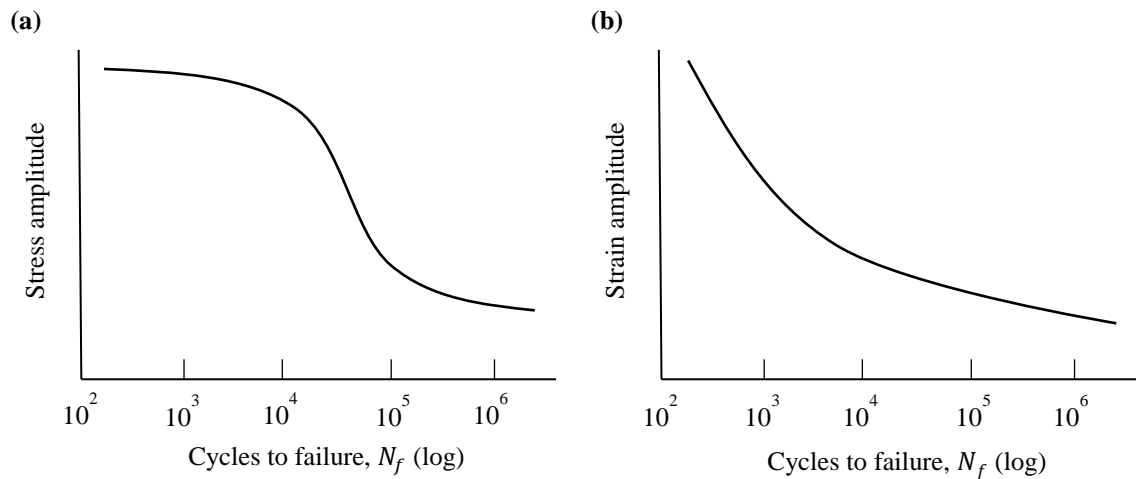


Figure 2.6 Fatigue testing of the same material under (a) stress-controlled and (b) strain-controlled conditions [adapted from Milella (2013)]

One more detailed explanation to the variation in fatigue results, due to the adoption of the stress-controlled or the strain-controlled approach, is the comparable findings of Kindt-Larsen et al. (1995) regarding the fatigue performance of two bone cements: Boneloc[®] prepared by vacuum mixing and Simplex P[®] prepared by vacuum and non-vacuum mixing. As shown in Figure 2.7, they found superior fatigue properties for the Boneloc[®] compared to the Simplex P[®] under strain-controlled conditions and totally opposite results when the stress-life approach was used. The low glass-transition temperature of 52°C for the Boneloc[®] was considered as a reason to lead to these dissimilar results as the stress-controlled cycling generates more heat, providing a disadvantageous factor for this cement. Moreover, Boneloc[®] is known to undergo high creep, which contributes to providing fast stress reduction when strain control is used.

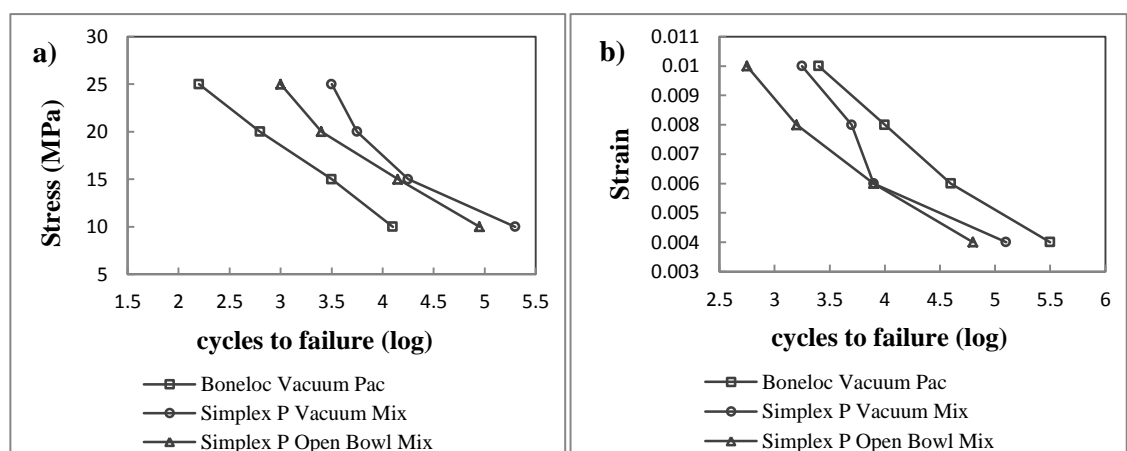


Figure 2.7 Fatigue testing of two types of bone cements prepared by two mixing methods under (a) Stress-controlled and (b) strain-controlled fatigue conditions [redrawn from Kindt-Larsen et al. (1995)]

In general, fatigue fracture that results when exceeding the elastic limit is associated with the existence of cyclic plastic strain (Shigley and Mischke, 1989). For the cases in which the nominal elastic stresses and strains exist, the stress-based fatigue life technique is preferable (Lee et al., 2005). The strain analysis fatigue approach, which was developed in the late 1950s, has been reported to be a more valuable option in analysing fatigue testing data in the cases where local cyclic plastic deformation arises on components due to the availability of notches, welds or other stress concentration factors (Lee et al., 2005; Dowling, 2007). The stress- and strain-controlled systems are more recent options of describing fatigue behaviour compared to testing under low-cycle and high-cycle loads (Collins, 1993).

2.1.3.4 Low-cycle versus high-cycle fatigue

In practice, components are considered to show low-cycle fatigue when the number of cycles to failure is reasonably low whereas elements that survive longer provide high-cycle fatigue, that is affected by the existence of plastic deformation as discussed earlier. The transitional point from the low to the high cycle fatigue is not fixedly specified but mostly ranges between 10^3 and 10^5 cycles (Collins, 1993; Bhandari, 2010). As can be seen from the S-N diagram in Figure 2.8, this aspect is mainly driven by the applied stress levels where the lower the cycling stress level the longer the fatigue life. This trend remains valid, particularly within the high-cycle fatigue domain, until reaching the fatigue endurance limit (S_e). The resultant deformation type (elastic or plastic) and the degree of deformation would depend on the material properties (brittle or ductile) along with the applied stress amplitude. For metals, the fundamental difference between the elastic and plastic deformation is that elastic deformation preserves the locally arranged atoms, whereas the plastic deformation, that involves shape change, leads to the breakage of the atomic bonds of these arrangements and the formation of new bonds (Mittemeijer, 2010).

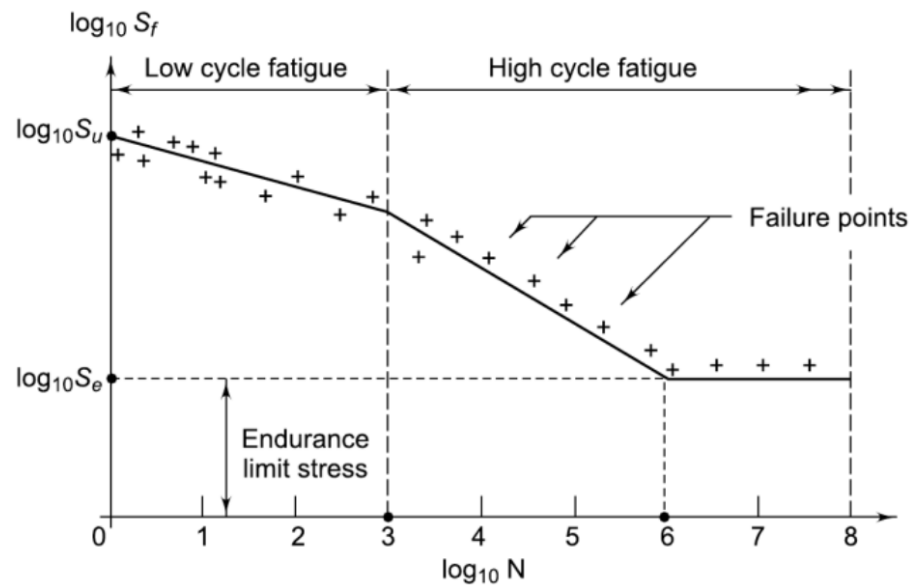


Figure 2.8 Low-cycle versus high-cycle fatigue for steel [taken from Bhandari (2010)]

2.1.3.5 Stress-strain curve

The relation between the stress and the strain is described by the stress-strain curve. A fatigue cycle can be represented by a hysteresis loop that its area and shape can change over the loading time depending on the properties of the material under plastic deformation. Also, the loop characteristics are affected by the type and level of stress loading applied. Figure 2.9 shows a schematic of a stress-strain loop for a tension-compression loading cycle. A cyclic stress-strain curve (loop) exists for both: stress-controlled and strain-controlled fatigue. Its behaviour would therefore be controlled by the fatigued component being subjected to stress or strain limits. The examination of the stress-strain behaviour can be of importance since “the hysteresis loop contains all the basic information on the cyclic stress-strain response” (Polák, 2003).

This information can particularly provide indications of the fatigue damage progressing in a stressed component. For polymers, many investigations have characterised fatigue damage by evaluating the stress-strain relationships reflected in the hysteresis loop area which remains almost constant at the early loading fatigue cycles and then increases noticeably (Moet and Aglan, 2003).

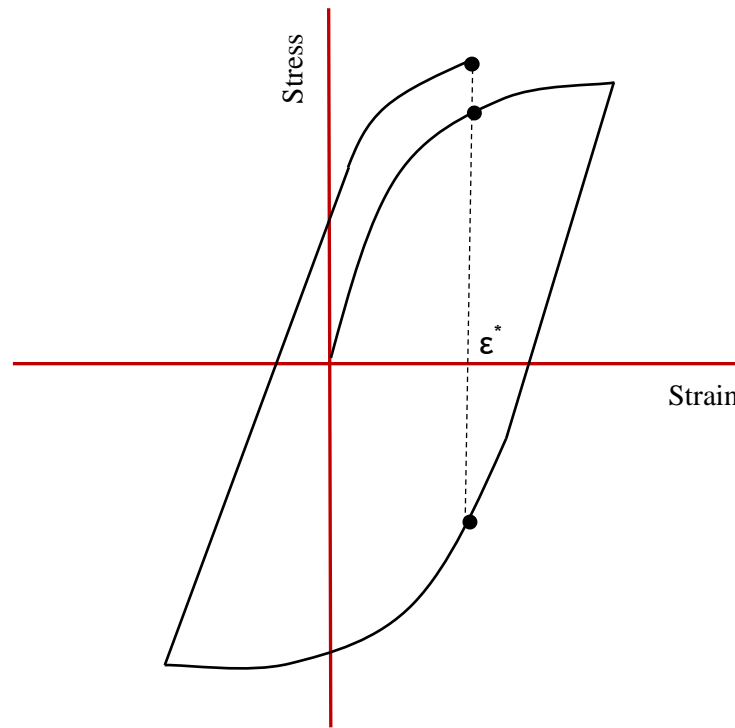


Figure 2.9 Schematic of stress-strain curve for a tension-compression cycle. “The stress at a given strain ϵ^* , depends on prior loading history” [redrawn from Anderson (2005)]

2.1.3.6 Crack initiation and propagation

The fatigue life of materials is often defined through three subsequent main stages: initiation of micro-cracks, propagate into macro-cracks and the occurrence of failure (Figure 2.10). “When design defects or metallurgical flaws are pre-existent, the initiation stage is shortened drastically or completely eliminated, resulting in a reduction in potential cyclic life” (Hertzberg, 1996). This can be seen as the reason to correlate this stage with the stress concentration factor (K_t) to control the fracture process. The crack propagation stage is entirely controlled by the stress intensity factor (K) which is usually described by Paris’ law (Equation 2.17).

$$\frac{da}{dN} = C(\Delta K)^m \quad (2.17)$$

where $\frac{da}{dN}$ is the fatigue crack growth rate, ΔK is the stress intensity factor range = $K_{max} - K_{min}$ and C and m are material constants.

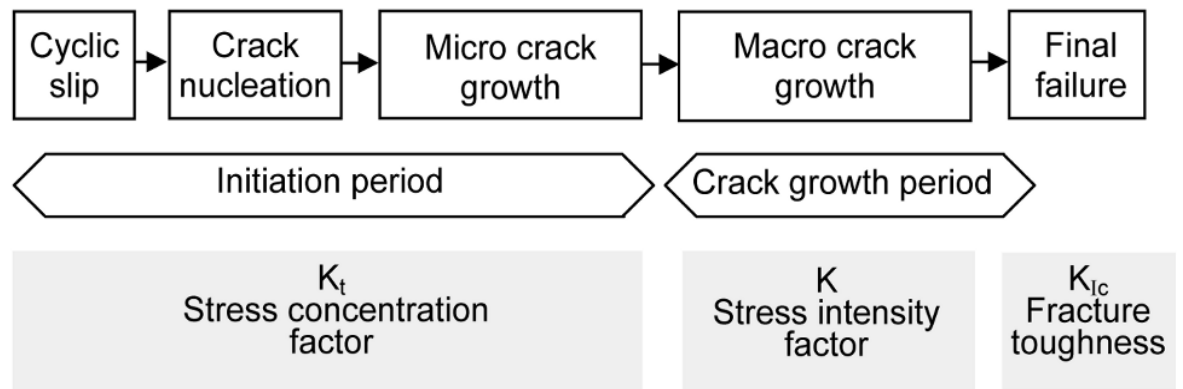


Figure 2.10 Different phases of fatigue life and related fracture factors [taken from Schijve (2009)]

It is obvious that, as can be deduced from Equation 2.18, the stress intensity factor range ($\Delta K = K_{max} - K_{min}$) is controlled by the values of the maximum and minimum applied cyclic stress loads. The crack growth rate is therefore driven by the variability in the stress intensity factor (K) that is affected by the applied stress level.

$$K = \sigma Y (\pi a)^{\frac{1}{2}} \quad (2.18)$$

where, σ is the applied stress and Y is a dimensionless function that depends on the crack length a and specimen width W [$Y = f(a/W)$].

2.1.4 Weibull functions for fatigue data analysis

Weibull analysis has been widely used in fracture and fatigue analysis. In general, Weibull distribution is flexible and includes within it excellent representations of both normal and exponential distributions (Shigley and Mischke, 1989). The method of analysing fatigue results depends on the graphical and analytical methods developed and reported originally by the Swedish scientist Waloddi Weibull during the middle decades of the last century. Over this period, as reported in Weibull (1961), Weibull methods for fatigue testing were developed to provide the most accurate analysis of results.

Weibull (1961) started his graphical and analytical representation of strength and life distribution by returning to the basic relation between the probability P and a random variable X as written in Equation 2.19 which is called the cumulative distribution function, where $X \leq x$.

$$P = P(X \leq x) = F(x) \quad (2.19)$$

If i was the order number of a result in a set of n results, and if this result was assumed here to be recorded at N_f cycles to failure, then the probability $P(N_f)$ can be calculated using one of the equations given below. These expressions have continuously been corrected to reduce statistical bias errors. Weibull (1961), for example, used Equation 2.20, and because he thought this might introduce bias in the estimate of the slope parameter (variance) in particular and the other parameters in general, Weibull also advised that Equation 2.21 could be used. This expression had gained significant acceptance because it could be interpreted theoretically (Cunnane, 1978). When using his probability graph papers for analysis, however, Weibull pointed out that the former expression can be used as plotting position even if a bias error would result (Weibull, 1961).

$$P(N_f) = \frac{i}{n+1} \quad (2.20)$$

$$P(N_f) = \frac{i-3/8}{n+1/4} \quad (2.21)$$

The cumulative failure has also been estimated using other equivalent formulas. Equation 2.22 shows another approximation (Weibull, 1961; Soh Fotsing et al., 2010). This has been reported in many literature resources such as Faucher and Tyson (1988), Lewis and Sadhasivini (2004) and ASTM (2007). It is widely agreed though the correction given in Equation 2.23 below (also known as Bernard's median rank correction) is a good estimator of the $P(N_f)$ value which has been reported in several studies including Faucher and Tyson (1988), Dunne et al. (2003), Janna et al. (2005) and Harris (2006). It should be noted that, for all the given cumulative failure probability expressions, to calculate the probability of failure for the i th observation, the results must be arranged in ascending order of magnitude (Weibull, 1961; Dunne et al., 2003).

$$P(N_f) = \frac{i-0.5}{n} \quad (2.22)$$

$$P(N_f) = \frac{i-0.3}{n+0.4} \quad (2.23)$$

These equations are important since they are required for the determination of the probability of failure. This probability is substituted in the Weibull functions to determine Weibull parameters as discussed below. Overall, Weibull functions are classified to two types: two-parameter or three-parameter probability functions. The literature shows that

fatigue results have been analysed using the two- or three-parameter functions of the Weibull probability distribution using either exponential or linearized expressions. The exponential distribution function of the two-parameter according to Weibull (1951, 1961), and as in Shigley and Mischke (1989), Danzer et al. (2007), ASTM (2007) and Soh Fotsing et al. (2010), is:

$$P(N_f) = 1 - \exp[-(N_f/N_a)^b] \quad (2.24)$$

And the linearised transformation of this formula is given in Equation 2.25 (Hertzberg, 1996, Askeland et al., 2011), which is derived by applying the natural logarithm twice on Equation 2.24.

$$\ln \ln \left[\frac{1}{1-P(N_f)} \right] = b \ln(N_f) - b \ln(N_a) \quad (2.25)$$

Where, $P(N_f)$ is the probability of failure at N_f stress cycles, N_a is the characteristic fatigue life (also known as scale parameter) and b is Weibull modulus (also known as shape parameter).

Although a reasonable number of papers have used the two-parameter Weibull distribution, many researchers have used the three-parameter functions. The use of the latter distribution involves, in addition to the shape parameter (b) and scale parameter (N_a), a third parameter (N_0) that represents the Weibull guaranteed or minimum fatigue cycles to failure (Dunne et al., 2003, Lewis and Janna, 2003). The exponential form of the three-parameter distribution function is given in Equation 2.26 (Shigley and Mischke, 1989, Lewis and Li, 2010). Equation 2.27 shows the widely used linearised transformation of this exponential equation (Lewis, 1999a; Murphy and Prendergast, 2000; Dunne et al., 2003; Janna et al., 2005).

$$P(N_f) = 1 - \exp[-\{(N_f - N_0)/(N_a - N_0)\}^b] \quad (2.26)$$

$$\ln \ln \left[\frac{1}{1-P(N_f)} \right] = b \ln(N_f - N_0) - b \ln(N_a - N_0) \quad (2.27)$$

Having briefly summarised the main Weibull probability functions as have been reported in the relevant literature, it is important to understand the significance of these equations and the function of each parameter and how can these parameters help in data analysis. It should be said that, as it is clear from the published studies including Weibull's work, there

has been no one specific manner to apply Weibull distribution functions either graphically or analytically. The symbols of the Weibull parameters in the equations have been differently named according to the authors' philosophy to simplify the functions. Also, the use of both base 10 and natural logarithms within the functions has been reported.

One method given by Weibull (1961) to present data graphically is to plot the double logarithm of $1/[1 - P(N_f)]$ against the logarithm of the variable x in Equation 2.19 (i.e. N_f), originally with the use of Weibull graph papers. Similar methods of presenting data on graphs according to Weibull analysis are reported by Faucher and Tyson (1988) with the only exception the abscissa represents the natural logarithm of strength results rather than of fatigue results. Weibull (1961) considering the determination of fatigue-life distributions and to overcome possible relevant analysis issues, developed graphical and analytical based methods to be used in the analysis of fatigue results. He states that "since the distribution of fatigue life in the region of the mean is frequently approximately log-normal, it is better to plot $\log N$ rather than N ".

The analysis of results is, as mentioned earlier, associated with the analysis of Weibull functions and parameters. Once fatigue results of a test group were obtained, a graphical Weibull function can be presented. "A typical ordinate scale assumes values from +2 to -6. This approximately corresponds to a range in probability of failure from 0.25 to 99.9%" (ASTM, 2007). For this case, Weibull modulus (the shape parameter, b) can be determined as the slope of the fitted line (Askeland et al., 2011). It can also be determined from Equation 2.26 (Faucher and Tyson, 1988) for the two-parameter and Equation 2.28 for the three-parameter Weibull functions. The scale parameter, N_a , is estimated at 63.2% of the N_f results (ASTM, 2007; Askeland et al., 2011). More discussion on the determination of Weibull parameters is provided in the Methods section.

Having obtained the Weibull parameters, the data of fatigue results is usually explained using various statistical methods, depending mainly on these parameters. One approach that has been reported, particularly with regard to bone cement, is to use the Fatigue Performance Index, I , to compare different fatigue results. Two methods have largely been used to calculate the fatigue performance index for bone cement fatigue results. The first is to use Equation 2.28 to calculate the fatigue performance index, introduced originally by Britton et al. (1990) when they were investigating the strengths of dental constructs. This approach has been used by many workers to comment on fatigue results of bone cement such as Lewis (1999b), Dunne et al. (2003) and Janna et al. (2005).

$$I = N_a \sqrt{b} \quad (2.28)$$

The fatigue index has also been estimated through the determination of the mean. In this case, Equation 2.29 for determining the mean (Shigley and Mischke, 1989) is used. This has been reported in a number of papers, particularly those considering fatigue testing of bone cements, such as Lewis (2003a) and Lewis et al. (2005a).

$$I = N_0 + (N_a - N_0) \Gamma(1 + 1/b) \quad (2.29)$$

Where, Γ is the gamma function and can be obtained from relevant tables (Shigley and Mischke, 1989).

2.2 BONE CEMENT AS A BIOMATERIAL

2.2.1 Bone cement components

Polymethylmethacrylate based bone cement is commercially available in the form of two main components: liquid monomer (methyl methacrylate, MMA) and powder polymer (polymethylmethacrylate, PMMA). These two components are typically provided by the manufacturers as ready to use proportions of polymer in a pouch and liquid in an ampoule (Figure 2.11). Kurtz et al. (2005) states that more than 60 brands of bone cements are available all over the world, mainly to treat joint diseases and bone fractures.



Figure 2.11 One pack of 40g SmartSet GHV bone cement (DePuy CMW manufacturing)

In implant fixations, the polymer and monomer are blended with the aim of producing homogeneous cement dough that is used as a grout between the bone and the implant. The combination of the two components leads to chemical reactions, polymerisation and changes in the material's properties. Understanding these processes requires in the first instance knowledge of the chemical formula of the polymer and the monomer as well as the different additives that are included in each component and the role of each additive. Figure 2.12 shows the chemical structure of the monomer and the polymer. The double bond in the monomer is broken during mixing the components allowing the start of the free radical polymerisation process. This process is mainly driven by the range of chemical substances added to both the powder and the liquid (Hasenwinkel et al., 2002).

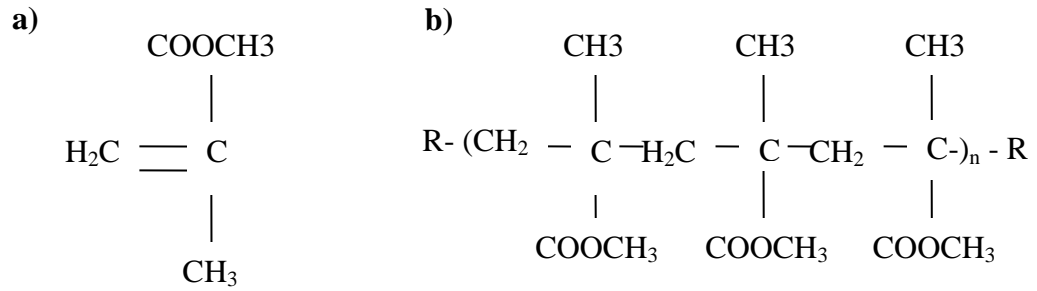


Figure 2.12 a) *Methyl methacrylate (MMA)* and b) *Polymethylmethacrylate (PMMA)* [adapted from Kühn (2005)]

The two components are therefore substantially different and contain different added substances. The powder is based on pre-polymerised beads of PMMA with the following additions:

- (i) An initiator (benzoyl peroxide, BPO) that starts the free polymerisation reaction.
- (ii) Radiopacifiers (zirconium dioxide, ZrO_2 , or barium sulphate, BaSO_4) that provides X-ray opacity and thus the ability to identify failures.
- (iii) Antibiotics in medicated cements (usually gentamicin sulphate)

The liquid monomer includes the following chemical additives:

- (i) An activator, usually N,N-dimethyl-p-toluidine (DMPT), that accelerates the polymerisation process.
- (ii) An inhibitor that helps in preventing the monomer from spontaneous pre-polymerisation.

Once the monomer and liquid components are mixed at room temperature, a reaction between the initiator BPO and the activator DMPT is generated leading to the formation of benzoyl free radicals which in turn starts the polymerisation process by breaking the reactive MMA double bond (Kühn, 2005). Due to the increase in these free radicals, gradual growth of the polymer occurs. This growth continues until reaching the termination stage which is the last stage of the polymerisation process where the polymer growth stops as the free radicals are depleted (Hasenwinkel et al., 2002).

2.2.2 Preparation and curing of bone cement

Bone cement is prepared by mixing the powder polymer and the liquid monomer in typical room conditions using an appropriate mixing technique. The usual mixing temperature in the operating theatre is 21-24 °C and humidity above 50% (Stillwell, 1987). The mixing techniques that have been used and reported in the literature are "hand mixing (HM), centrifugation mixing (CM), vacuum mixing (VM), vibratory and shaking mixing (VISM), sonication (SM), and rotary drum mixing (RDM)" (Lewis, 2003a). Among these, HM, VM and CM are the methods that the majority of studies have reported. The aim of these techniques is to obtain homogeneous cement mixture either exposed to air such as in the HM or evacuated such as in the VM. Moreover, methods such as VM and CM (known as the third-generation mixing techniques) were introduced in order to reduce porosity within the produced cement after years of depending on HM (first-generation).

Once the cement components are mixed, various phases with various characteristics will be sequentially observed in the produced material until it becomes solid in about 10-20 minutes (different cements have different forming times). Four main stages take place in conjunction with the polymerisation process: mixing, waiting, working and hardening stages. During these phases, the cement viscosity shows a rapid change from runny dough at the first stage to a solid material by the end of the last stage. The temperature starts to increase slowly during the first stage and then rapidly to reach its highest value when the monomer is depleted (Madigan et al., 2006).

The cure of bone cement, therefore, starts with the mixing stage which includes adding the powder to the liquid using a mixing ratio that is specified by the manufacturer. The ratio is usually two parts of powder to one part of liquid (Kühn, 2000). During the next stage (waiting), the cement changes gradually to become a more uniform mixture. Over this stage, however, the cement viscosity starts to decrease steadily but it remains too low when it comes to applying the cement in a joint fixation during this period (Hasenwinkel et al., 2002). The third phase (working), is the time during which the cement is inserted between the bone and the implant because the viscosity becomes moderate at this stage (Kühn, 2000). Finally, the cement starts to harden gradually until it becomes completely solid (hardening stage). During this stage also the polymerisation of MMA monomer in the mixture is dramatically enhanced which generally lasts for about six to twelve minutes (Hasenwinkel et al., 2002). Although cement hardening is the final stage of setting process, experimental experience has proved that the factual end of the polymerisation process

might take up to 24 hours, which *in vivo* does not put a barrier on patients from safe and careful moving once the hardening stage has finished (Tanner et al., 2010).

2.2.3 The role of bone cement in medical applications

The essential application of bone cement is to connect the implant to the bone in joint replacement surgery. It has been utilized in this purpose for more than five decades. In 1958, Sir John Charnley managed to anchor femoral prostheses using acrylic bone cement (Kühn, 2005). This was the first attempt of employing bone cement in total hip replacements benefiting from its earlier use in dental treatment. The application of PMMA bone cement in joint arthroplasty however did not remain confined to hip surgery as other joint replacements such as knees, shoulders and elbows have been cemented. “It has also been used for joint reconstruction, cranioplasties, investment of aneurysms, fixation of pathological fractures, artificial eyeballs and bone replacements” (Deb and Koller, 2008). This clinical use was enhanced by the promising findings of initial use of PMMA reported in 1961 by Sir John Charnley which became more reliable when Charnley and other surgeons validated these findings (Mehlhoff and Sledge, 1990). The first addition of antibiotics to bone cement was in 1969 by Professor Buchholz as a start to antibiotic containing bone cements (Kühn et al., 2005).

Revising the history of using bone cement in different joint replacements shows that the dependency on applying this material as a grout between bones and implants (Fig. 2.13) has become more important. This is apparently due to the significance of having such a substance that can work as a buffer to distribute the loads resulting from a patient weight and movement. Moreover, the formed cement mantle in the interface area between a bone and a prosthetic component helps in securing the artificial component to the bone.

Regarding total hip replacements (THRs), according to the Swedish Hip arthroplasty Register (Garellick et al., 2012; 2013), a total of 15,978 replacement operations were performed in Sweden only during the year 2012 and 16,299 replacements during 2013. In the UK, according to the 10th Annual Report of the National Joint Registry for England, Wales and Northern Ireland (NJR, 2013), a total of 86,488 hip replacements were performed in 2012 by an increase of 7.5% from the previous year. Internationally, Malchau et al. (2002) mentioned that 800,000 THR surgeries are performed yearly all over the world. Slightly higher number of replacements (1 million) was reported by Schierholz and Beuth (2001). This figure has increased rapidly over the last decades and is expected to

double by the year 2025, considering the usage history as well as the growing population (Monge Jodra et al., 2006).

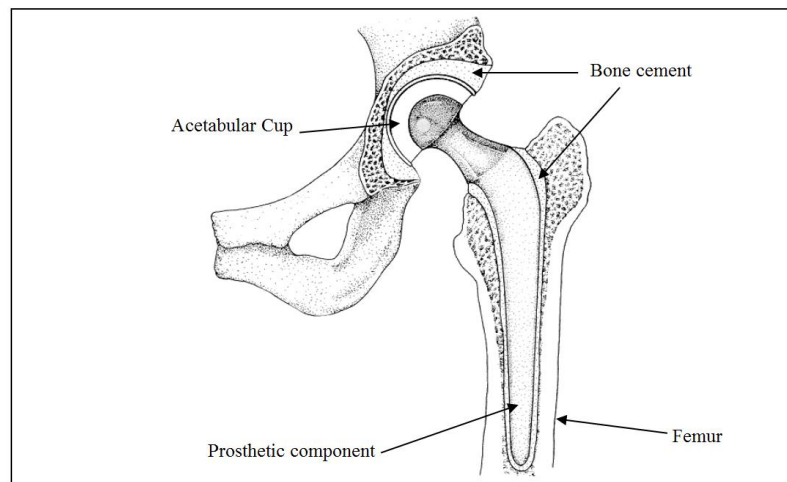


Figure 2.13 Schematic of a cemented total hip replacement [adapted from Hardinge (1983)]

As for total knee replacements (TKRs), the figures are no less important where hundreds of thousands of surgeries are performed every year worldwide in patients who have fracture or infection knee issues. The replacements of knee joints have increased rapidly over the last two decades and expected to record higher rate in the future which is estimated, according to Moran and Horton (2000), to increase by 40% over the years 2000 to 2030. In the US only, for example, the number of primary knee replacements that were performed in 2004 was just over 430,000 which is almost double that number recorded for the year 2000 in the same country (Kim, 2008). In the UK, more recent figures indicated that the total number of knee replacement operations was 90,842 during 2012, an increase of 7.3% compared to 2011 (NJR, 2013).

Apart from the typical use of bone cement in joint replacement, it has more recently been employed in spine reconstructive surgeries in order to help in treating vertebral compression fractures (Kurtz et al., 2005). This object has been safely and effectively achieved in particular patients who have pain associated with osteoporotic vertebral compression fractures with no chance of addressing the problems of vertebral height loss and kyphotic spinal deformity (Theodorou et al., 2002). The application of bone cement in spine surgery, however, usually involves increasing the radiopacifier content of the cement to visualise the flow during the insertion of the dough to ensure the cement does not spread beyond the confines of the vertebral body (Kurtz et al., 2005). Although there is a

concern over the higher level of barium sulphate content, Kurtz et al. (2005) analysed the collected static and fatigue testing data of different BaSO₄ content percentages and concluded that “bone cement can be designed with barium sulphate levels sufficiently high to permit fluoroscopic visualization while retaining the overall mechanical profile of a conventional bone cement under typical *in vivo* loading conditions”.

In terms of the necessity of applying bone cements in joint replacements, surgeons need to decide whether they will use cemented or uncemented fixation to treat the joint disease, as both approaches are used. Nevertheless, correct use of the cemented fixation method might be preferred because of the expected role of the cement in securing the prostheses especially in patients older than 60 years (Harper, 1998). Havelin et al. (2000) stated that using PMMA bone cements in THR fixation has been considered by many specialists as the gold standard. In general, a considerable proportion of all total joint replacements (TJR) including hip, knee, shoulders and elbows are cemented (Lewis, 2009). This confirms the statement mentioned earlier in Hasenwinkel et al. (2002) that well above 50% of all joint replacement operations performed worldwide make use of bone cement in implant fixation for one or more components. Dunne et al. (2014) stated that “at present with longer life expectancy and younger patient populations requiring TJR, an increase in cemented revisions seems inevitable”. What seems to have been more important consideration when it comes to the decision making on whether to use bone cement in implant fixations or not, however, is the drawbacks and concerns that have been reported as a result of using bone cement in implant fixation.

2.2.4 Concerns about bone cement

Despite of the initial positive results, long-term follow-ups of patients with cemented joints have revealed a number of controversial discussions about the detrimental side effects of bone cement. One concern, for instance, is the effect of heat generated during polymerisation process of bone cement on bone tissues. Another vitally important issue is the possible contribution of the cement failure to implant loosening. Below is a brief review of the main concerns discussed in the literature.

2.2.4.1 Heat of Polymerisation: effects and suggested solutions

The bone cement mixture is injected between the implant and the bone during the working stage. The polymerisation and viscosity increase rapidly generating exothermic heat of about 57 kJ per mole MMA (Kühn et al., 2005; Kühn, 2005). According to many studies,

the temperature of the produced cement over the polymerisation period can be high, as reported by Hansen and Jensen (1990), can rise to a maximum of between 66°C and 91.5°C, depending essentially on the variation in cement compositions.

This high temperature is considered to be a major issue due to its possible contribution to bone necrosis (Starke et al., 1998). During cement application, bone necrosis can arise because of the presence of heat in conjunction with the existence of residual methacrylate monomer, which is noxious to bone tissue. This concern has led to developing many research studies to find what factors can help in reducing the polymerisation heat and, accordingly, alleviating its effect on the bone tissue.

One consideration, for example, is to implement the minimum thickness possible of the cement mantle in order to reduce the released heat. This heat has been found to be cement layer thickness dependant. Although heat generated during polymerisation process might detrimentally affect the biological tissue adjacent to the cement, minimising the cement mantle thickness can diminish the temperature and accordingly reduce the tissue deterioration (Ramaniraka, 2002). The thickness value has been recommended in many research studies to be maintained at the maximum thickness of 5mm which, according to Liptáková et al. (2009), “cannot cause thermal necrosis of bone cells and the surrounding tissues”. In addition to the significance of having the thinnest possible cement mantle, Toksvig-Larsen et al. (1991) in their interpretation of this issue state that blood flow adjacent to the cemented area cools the polymerising cement.

Another aspect that can affect the temperature is the chemical formulation of bone cement. This simply means using specific brands of acrylic bone cement in joint arthroplasty can lead to lower peak of polymerisation temperature. Wykman and Sanderjöo (1995) examined the thermal characteristics of one brand of bone cement (Boneloc®) *in vivo* by means of measuring the temperature of polymerised cement during total hip replacement of 11 patients. They found that the maximum cement temperature in 10 out of the 11 samples was below 43°C, however, this cement is based on polybutylmethacrylate with a lower polymerisation exotherm than polymethylmethacrylate. The polymerisation temperature behaviour in this study was presented as shown in Figure 2.14 which can be a general indicator of the trend of polymerisation temperature, considering the variations in the peak temperature amongst various cement compositions. Although the maximum polymerisation temperature in the study was substantially lower than those obtained from

earlier studies, Boneloc® has been demonstrated to show high creep leading the cement to be insecure in implant fixation.

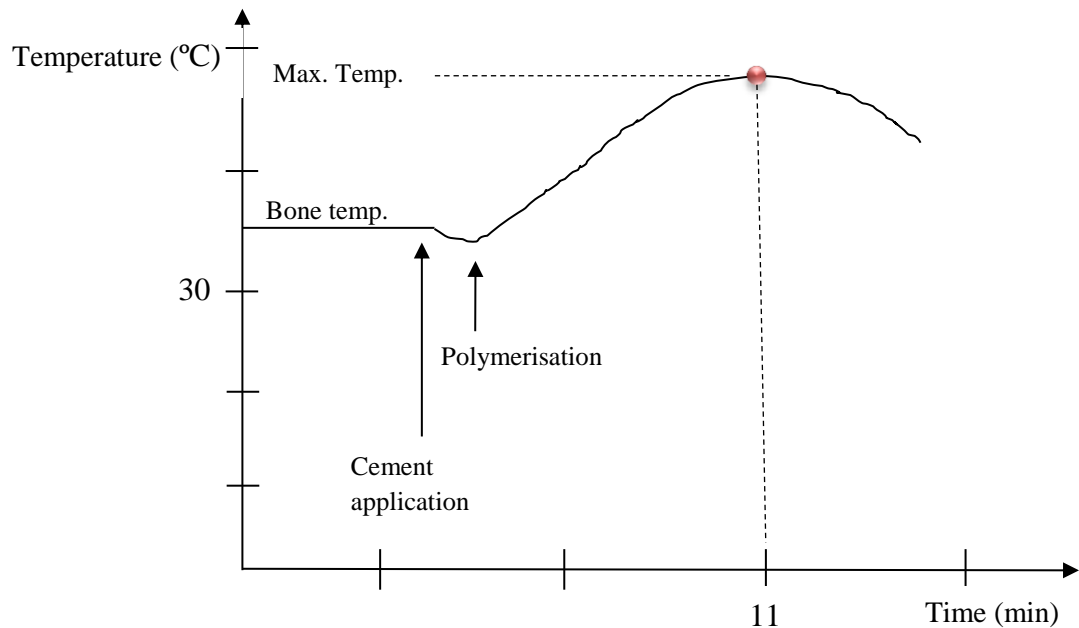


Figure 2.14 Sketch diagram shows a possible polymerisation temperature curve (Boneloc® bone cement) [adapted from Wykman and Sanderjöö (1995)]

2.2.4.2 Bone resorption

Another biological effect that might be encountered is the bone resorption produced by cement particles subsequent to the fracture of the cement mantle, mainly due to fatigue failure. The cement fracture leads to the detrimental production and spread of PMMA and opacifier particles that are believed to be absorbed by the adjacent bone (Quinn et al., 1992; Sabokbar et al., 1996) leading to various biological responses depending on particle shape and size (Gelb et al., 1994; Mitchell et al., 2003) as well as the type of opacifying agent included (Lezarus et al., 1994; Mitchell et al., 2003; Wang et al., 2005). It is not bone cement only, however, that can be responsible for releasing third-body wear damage particles, as the implanting metals can also produce debris mainly due to metal-on-metal (MOM) contact. The tendency of the transfer of the bone cement particles into the implants can be low compared to the transfer into the bone, whereas the metallic particles might work reversely. This is according to a recent study by Halim et al. (2014) that investigated the damage produced in the surfaces of CoCr implants by bone cement, CoCr, and Ti6Al4V debris found that “compared to third-body abrasion with metal debris, polymethylmethacrylate debris had minimal effect on the CoCr surfaces”.

2.2.4.3 Implant loosening in joint replacement

Despite the fact that medical results of total joint replacements are often excellent, a number of implants will face aseptic loosening and need to be revised (Bauer and Schils, 1999). Aseptic loosening refers to the failure of the bond between the prosthesis and the bone in a total joint replacement (Tong et al., 2006). Although more than 90% of implants last for more than 10 years, approximately three quarters of the failures come as a result of prosthesis loosening (Malchau et al., 2002). While implant loosening can be attributed to both biological and mechanical effects, the underlying reasons are still under discussion (Yang et al., 2010).

Fatigue failure of the *in vivo* bone cement mantle, however, is widely considered to be a major cause of implant loosening (Malchau et al., 2002). Many studies and radiographic images of reconstructed prosthesis after loosening have shown that bone cement failure is fundamentally responsible for implants loosening. Figure 2.15 shows a stainless steel implant broken *in vivo* after loosening due to the failure of the proximal bone cement mantle with the section below the fracture still held firm.

Harrigan et al. (1992) suggested that the failure of fixations starts at the prosthesis-cement interface because of cracks initiated in the cement due to the existence of pores and voids. The voids can arise because of many reasons, one of which is the substances that are added to the cement such as the opacifier additives. According to Topoleski et al. (1990), barium sulphate (BaSO_4) particles lead to the formation of voids around them resulting in lower fracture toughness and fatigue life which can be the cause of bone cement failure.

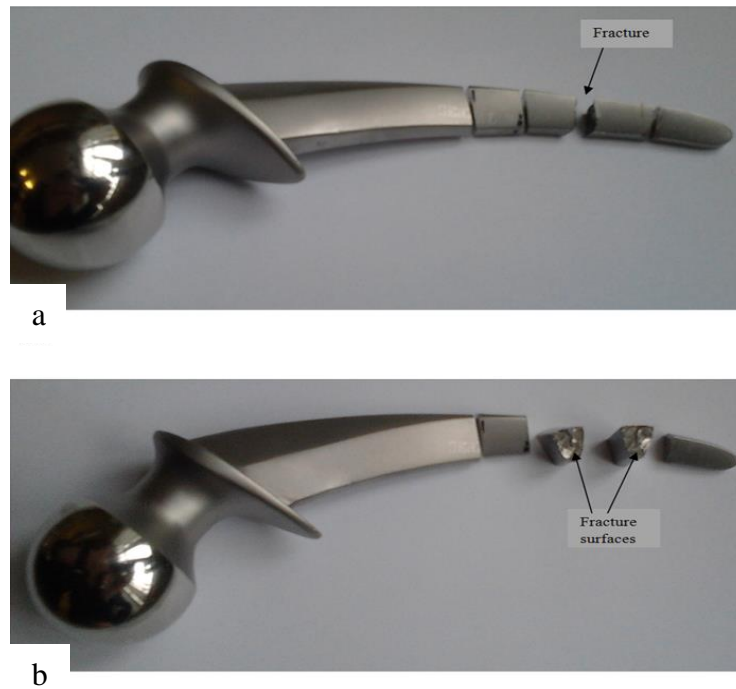


Figure 2.15 Images of a fractured stainless steel prosthesis due to failure of the bone cement mantle followed by implant loosening: (a) the position at which the implant fractured in vivo and (b) the fracture surfaces of this implant.

Murphy and Prendergast (1999) suggested a similar reason for the likely contribution of bone cement into implant loosening confirming that the initiation and propagation of many microcracks within the cement mantle can be a cause for joint reconstruction. This is basically because, as they interpreted, the growth in these resultant microcracks leads to a steadily reduction in the mechanical integrity of the bone cement mantle which, in turn, leads to the failure of the mantle and subsequently implant loosening. Murphy and Prendergast demonstrated that the main reason behind the cracks is the pores formed within the cement that can work as crack initiation sites and therefore the number of initiated cracks can be porosity dependent.

Minari et al. (2001) mentioned that the weakest link in aseptic loosening of a total hip implant is the cement mantle around the femoral stem. A study performed by Jasty et al. (1991) to follow up 16 patients who had cemented total hip replacements in order to verify the initial mechanisms involved in implant loosening showed that separation at the cement-implant interface and fracture in the cement mantle are more likely to happen. Longer and more precise observations to the samples in this study revealed that circumferential and radial fractures initiated and extended from the cement-prosthesis interface particularly near to sharp corners of the implant, in the thinner sections of the cement mantle, and starting from existing pores.

The phenomenon of implant loosening therefore is a significantly vital issue. For cemented fixation, it seems to be extremely crucial to focus on the fatigue of bone cement and what are the most important factors that can accelerate the failure of the cement. Although many fatigue studies have been performed, more research is required to improve the mechanical integrity of bone cement including fatigue fracture resistance in order to achieve greater fatigue performance. It is apparent that fatigue studies on bone cements have been mainly performed based on *in vitro* test conditions to simulate the *in vivo* conditions. While the *in vitro* tests are generally believed to reflect the *in vivo* conditions, there seems to be no consensus or even controversial regarding the use of particular testing variables.

2.2.5 *In vivo* versus *in vitro* fatigue

Considering the failure of the cement mantle as a main reason of implant loosening in cemented joint replacement has led to developing many studies that focus on fatigue behaviour of bone cement and the factors that can have effects on this feature. Fatigue of bone cement *in vivo* occurs, in general, as a result of continued patient activity, which is simultaneously affected by the patient's weight and age. The cement mantle in its position, around a hip joint for example, can be affected by a load of up to 2.5 times body weight during walking increasing to about 8 times of the body weight during recovery from a stumble (Bergmann et al., 2001; Schoellner et al., 2003). These loads, in conjunction with the continuous movement, work as repeated cyclic loading that, with the passage of time, leads to the initiation and propagation of fatigue cracks and subsequently to the failure of the cement mantle.

Many fatigue studies have shown that there is obvious similarity between the *in vivo* and *in vitro* fatigue behaviour. Culleton et al. (1993) examined fracture surfaces of 6 pieces of a fractured cement mantle during the revision operation of a total hip replacement to assess the mechanisms of fatigue failure in the mantle. The results of the microscopic investigation of crack surfaces were found to be identical to those examined during laboratory experiments for the same cement. These results were consistent with those reported earlier by Topoleski et al. (1990) who similarly studied fracture surfaces of cement samples taken from revised joints which were simultaneously compared with fracture surfaces of experimentally fatigued specimens. The findings of the latter study showed that the examined crack surfaces are similar from both *ex vivo* and *in vitro* loading. Topoleski et al. (1990) confirmed that fatigue of bone cement is a key factor when it comes to the collapse of the cement mantle because of many reasons that they identified:

“... the primary *in vivo* failure mechanism of bone cement is fatigue, and the fatigue cracks grow by developing a microcraze shower damage zone. Agglomerates of BaSO₄ particles can be implicated in some bone cement failures, large flaws or voids *in vivo* can lead to a rapid, unstable fracture, pores in the PMMA mass have a clear influence on a propagating crack, and wear of the fracture surfaces occurs, and may produce PMMA debris, exacerbating bone destruction.”

The correlation and similarity reported in several studies between the mechanisms of fatigue failure in both *ex vivo* and *in vitro* bone cement samples have emphasised that *in vitro* fatigue findings can largely be representative to the *in vivo* fatigue characteristics. This, in turn, has inspired researchers to conduct further research to more fully understand the fatigue failure factors of bone cement and attempt to improve its fatigue life. The fatigue life enhancement includes, for example, optimising the cement compositions, working conditions and mixing techniques, therefore, control or alleviate of the underlying failure causes such as porosity. In brief, it has been broadly believed to be of importance to follow the achieved *in vitro* fatigue studies and work to develop further fatigue research in order to constantly improve the *in vivo* fatigue lives of bone cements.

The mechanical properties of acrylic bone cements are significantly important in terms of providing long-term *in vivo* performance of the material and consequently longer stability of artificial joints. Many studies have been experimentally established in order to investigate, compare, and hence improve the mechanical characteristics of bone cements. Various cements with various compositions have been tested *in vitro* providing different fatigue performance results. Harper and Bonfield (2000), for example, studied the mechanical properties of 10 cements commercially available at that time: 6 older formulations (Palacos[®] R, Simplex[®] P, CMW[®] 1 & 3, Sulfix[®]-60, Zimmer[®] Dough) and 4 newer formulations (Endurance[®], Duracem 3, Osteobond[™] and Boneloc[®]). Important variations in tensile and more clearly in fatigue characteristics of these cements were seen. This study concluded that the cements that have greater clinical performance showed longer experimental fatigue lives, which confirms the importance of subjecting newly developed bone cements to static and fatigue testing regimes prior to the medical usage in order to have initial evaluations to their clinical performance.

While it is mostly agreed that experimental testing of bone cements can, to a large extent, be a good representative of the performance in medical applications, this has not been

always the case. Bargar et al. (1986), for instance, found significant differences in the physical and mechanical properties between PMMA samples polymerised *in vivo* and others from the same batch prepared *in vitro*. Moreover, the *in vitro* results obtained from different studies in the literature have shown similarity in many research papers and dissimilarity in others. Lewis (2003a) reviewed the literature that focussed on studying the variables that can affect the fatigue life of bone cement in order to compare the results of relevant published studies. His research confirmed that there are areas of agreement and others of disagreement on the effect of particular factors on the fatigue of acrylic bone cements. He mentioned, for example, there is consensus that increases in the molecular weight of the powder components enhance the fatigue life of the cement, whereas this review states that vacuum mixing has been controversially reported in the literature as to whether this technique can improve the totally cured cement's fatigue life compared to the hand mixing approach.

Another example for these various findings is the influence of the opacifier content on the fatigue life where different results were reported with different chemical formulation of cements. Interestingly, other studies such as that performed by Tanner et al. (2010) found variations in fatigue lives of different bone cements under different testing regimes. This study that compared two methods of fatigue testing concluded that "increases in the opacifier content leads to earlier failure in tension-only testing than in fully reversed testing". Hence, the effect of the opacifier content is an independent variable that has impact on fatigue life of bone cement not only because of differences in chemical compositions, but also as a result of other factors including even testing regimes. Indeed, there are underlying factors that have led to reporting these variations in results some of which have largely been examined by researchers such as the difference in chemical composition and porosity and other possible influences need to be comprehensively investigated such as the effect of specimen surface preparation as well as the effect of applying different testing regimes.

2.3 FATIGUE TESTING OF BONE CEMENT

2.3.1 Fatigue fracture: influencing factors and controversy

Many variables that have been thought to influence fatigue behaviour of bone cement have been investigated in various studies. The effects of particular variables, whether or not it exists, have been reported with no or limited debate. For example, a wide range of test frequency (mainly between 1 Hz and 50 Hz) has been used with little attention paid to the effect of this factor particularly in early studies. Johnson et al. (1989) included examining the effect of frequency on fatigue behaviour of bone cement (comparing a range of frequencies including a minimum of 1 Hz and a maximum of 20 Hz in room temperature under stress-controlled tension-tension conditions) and recommended to consider the effect of test frequency. Lewis et al. (2003), however, examined this factor within two frequencies (1 Hz and 10 Hz), but in stress-controlled tension-compression conditions, and concluded that “test frequency (over the range used) does not exert a statistically significant effect on the fatigue life of the cements tested”. It is also widely agreed that performing fatigue testing in 37°C flowing saline solution or a similar environment to simulate the *in vivo* conditions is preferable; however, this consideration has not been adopted in all studies, presumably because testing in dry conditions is easier, with no acute criticism noted in the literature. The effect of initiation chemistry has widely been discussed with similar trend of deductions that this factor does largely or slightly control fatigue life of bone cement. More controversial topics regarding the effect of other factors, in contrast, have been reported including the effect of mixing methods and porosity as discussed below.

2.3.1.1 Chemical composition of the cement

The basic components of bone cements, as detailed in Section 2.2.1.1, are the components of both the powder and the liquid. The powder includes the pre-polymerised beads of PMMA along with the initiator and the radiopacifier. The liquid mainly includes the methyl methacrylate MMA and the accelerator. When comparing various bone cement brands, however, the formulations may vary including the polymerised beads type. These can be pure PMMA beads with an opacifier that can be either BaSO₄ (e.g. CMW1) or ZrO₂ (e.g. SmartSet GHV). The polymer beads can also be a combination of PMMA and methyl methacrylate-styrene-copolymer P(MMA, S), such as that in Simplex P (Stryker, 2006). If the cement is medicated to contain antibiotics, a specific fraction of gentamicin is added to

the powder. Addition of particular substances to reinforce the material's strength may also need to be considered.

The effect of the change in cement composition on fatigue fracture has been broadly studied by many researchers and manufacturing companies, using various sets of test conditions. One of the most pertinent of these studies is perhaps that reported by Hasenwinkel et al. (2002) that simultaneously examined the effect of the concentration of the initiator (BPO), the concentration of the activator (DMPT) and the BPO:DMPT molar ratio of a two-solution acrylic bone cement on fatigue and fracture of bone cements. They concluded that “the fracture toughness and fatigue life of the solution compositions were not strongly influenced by the BPO concentration or the BPO:DMPT molar ratio, whereas the highest amine concentration produced significantly lower K_{IC} values and fatigue strength”.

Lewis (2003a) in his state of the art review, however, reported that, although the findings of many studies that focused on the effect of cement formulation, including Hasenwinkel et al. (2002), had shown variations in fatigue results, “the cements compared have differences in more than one basic constituent; thus, no clear conclusions may be drawn regarding the role of basic composition”. Subsequently, however, a study by Deb et al. (2003) focused on determining the influence of changing the activator type only (one compositional variable) on the fatigue behaviour and fracture toughness of bone cement, under the same testing conditions. Three sets of cements were used where each cement included a different activator. One cement included the conventional activator, 4-*N,N* dimethyl p-toluidine (DMPT) and the other two were modified with long-chain amine activators 4-*N,N* dimethylaminobenzyl oleate (DMAO) and 4-*N,N* dimethylaminobenzyl laurate (DMAL). They concluded that “for a given acrylic bone cement formulation, replacing DMPT with either DMAO or DMAL leads to a cement with increased fatigue life and fracture toughness”. While this finding provided generally confirmed the previous statement that chemical composition influences fatigue life, it emphasised that the effect of this variable exists even if one basic constituent was uniquely compared.

When it comes to altering the basic cement composition by adding newly introduced or developed particles in order to reinforce the cement, several studies have investigated the effect of this alteration reporting either increase or decrease in the fatigue longevity. Kane et al. (2010), for instance, examined the influence of adding zirconia fibres to enhance the fatigue properties of acrylic bone cement. They found that “the mean fatigue life of

cements reinforced with 15 and 20 vol% straight zirconia fibres was significantly increased by 40-fold, on average, compared to a commercial benchmark (Osteobond™) and cements reinforced with 0.10 vol% straight zirconia fibres”. A recent study by Slane et al. (2014) included studying the effect of modifying the polymer of the same bone cement (Palacos R+G) with three ratios (0.5%, 2% and 5% wt/wt) of mesoporous silica nanoparticles on the fatigue and fracture of the material. Their study, unlike Kane et al. (2010), found that reinforcing bone cement with silica nanoparticles leads to severe degradation in the cement’s fatigue and fracture toughness characteristics. It was accordingly suggested by the authors that “mesoporous silica, as used in this study, is not an effective reinforcement material for use in acrylic bone cement”. Again, the effect of altering the chemical formulation of acrylic bone cement appeared to have influences on the fracture and fatigue properties considering, however, the variations in testing regimes and conditions among the different reported studies.

2.3.1.2 Mixing methods

The various mixing methods, that are used to blend the powder and the liquid components to prepare the doughy bone cement, have been developed to increase cement strength. They are classified to three main categories: first, second, and third generations. The first generation was initially used where the bone cement is mixed by hand using a spatula and a bowl which later developed to the second generation technique by reducing mixing pressure (-30 kPa) as an attempt to decrease porosity and also to significantly alleviate the levels of the noxious monomer fumes (Dunne and Orr, 2001). Early clinical results reported regarding the use of second generation technique showed improved cement performance (Murphy, 2001). Despite this improvement, a third generation technique was introduced to also provide cement with less porosity (-70 kPa mixing pressure) and less human exposure to the monomer emissions (Dunne and Orr, 2001). In general, further improvements were achieved with the third generation techniques including, in particular, centrifugation and vacuum mixing methods (Jasty et al., 1990).

A study performed by Lewis (1999a), that included investigating the effect of mixing method (vacuum mixing vs. hand mixing) on the fatigue and porosity of bone cement considering simultaneously the effect of storage temperature of cement components, concluded that vacuum mixing can clearly increase the uniaxial tension-compression fatigue life, irrespective of the cement constituents temperature prior to mixing, referring to the influence of the reduction in porosity associated with the vacuum mixing on enhancing fatigue performance. The uniaxial fully reversed tension-compression fatigue test in this

study was conducted using cylindrical dumbbell specimens of Palacos[®] cement that were machined from moulded rods to have final specimens as specified by ASTM F2118.

These results seem to contradict an earlier report by Fritsch et al. (1996) who tested the fatigue properties of the same brand of bone cement (Palacos[®]). They stated that vacuum mixing or applying additional pressure during the setting of the cement cannot increase fatigue resistance of the cement regardless of the achieved decreases in porosity. These differences in findings lead to consider the variations in testing conditions that each study adopted. These include specimen configuration and fabrication method as well as the stress type and magnitude. Unlike Lewis (1999a), the specimens in Fritsch et al. (1996) were made as flat dumbbell specimens (rectangular cross section), according to the German Industrial Standard (DIN) 53442 for the fatigue testing of plastics, with total length of 90 mm, gauge length of 40 mm and gauge width of 20 mm. More importantly, the fatigue properties were evaluated according to the DIN standard depending on the bending characteristics of the cement rather than tensile properties where bending moments were applied till failure or 20 million cycles. Therefore, it might be unreliable to compare the variations in conclusions in these two and other similar studies without considering the extent to which these investigations were similar in terms of all testing conditions unless a particular condition has been demonstrated to have no significant effects on the final results.

Thus, it might be more reliable to consider variations in findings that are obtained under the same testing conditions excluding those variables that are identified to be examined. Davies et al. (1987), for example, compared fatigue behaviour of circular machined specimens made from only one cement formulation (Simplex P) prepared under the same conditions except either centrifuged or non-centrifuged mixing techniques. The specimens were all subjected to fully reversed tension-compression strain-controlled fatigue at 2 Hz. The results for this test are illustrated in Figure 2.16 where the fatigue lives, at different strain levels and probabilities of survival, were found to be significantly higher for the centrifuged bone cement when compared to the non-centrifuged cement. The longer fatigue life associated with the lower strain values in both techniques is considered by these authors to be highly important as these smaller strains are more likely to exist *in vivo* and therefore the longer fatigue lives are better representations. However, these suggestions were not similarly considered in many similar fatigue studies, particularly those that adopted stress control conditions, making it impractical to compare the results of this study with the other studies. The question that needs to be answered here is, for a

particular mixing method, would the findings remain the same if the applied stress conditions and specimen specification were changed?

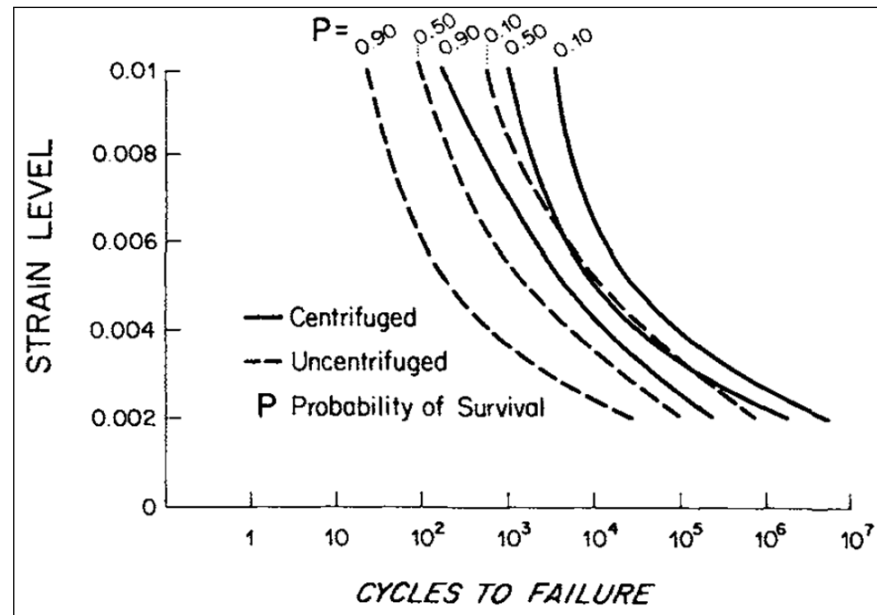


Figure 2.16 Fatigue life versus strain level for centrifuged and uncentrifuged Simplex P cement at 3 different probabilities of survival levels [adapted from Davies et al. (1987)]

The development and variation in mixing methods used to prepare the bone cement have continuously attracted researchers to examine the effect of this factor on the material fatigue strength. The aim of this has been to reach a commonly agreed conclusion on defining which techniques can have positive effect in terms of producing the solid cement with increased fatigue strength. A study by Dunne et al. (2003) involved comparing the influence of 6 mixing systems, one of which is hand mixing (first generation) and the others are reduced pressure techniques (third generation). For each mixing system, 18 half sized ISO 527-2 specimens of Palacos R[®] bone cement (with gentamicin) were prepared by moulding. All the specimens were subjected to tension-tension cyclic loading (0.3 - 22 MPa) at room temperature (22°C). The results, as reported by Dunne et al. (Figure 2.17), showed, in general, double the number of cycles to failure when the reduced pressure systems were used compared to the hand mixing. They have also reported, however, variation in fatigue lives among these reduced pressure cements can also be great. Generally, the researchers concluded that, in comparison to hand mixing (atmospheric conditions), using reduced pressure systems leads to greater fatigue strength, but the mixing mechanism can have more important effect when preparing the cement using different reduced pressure devices.

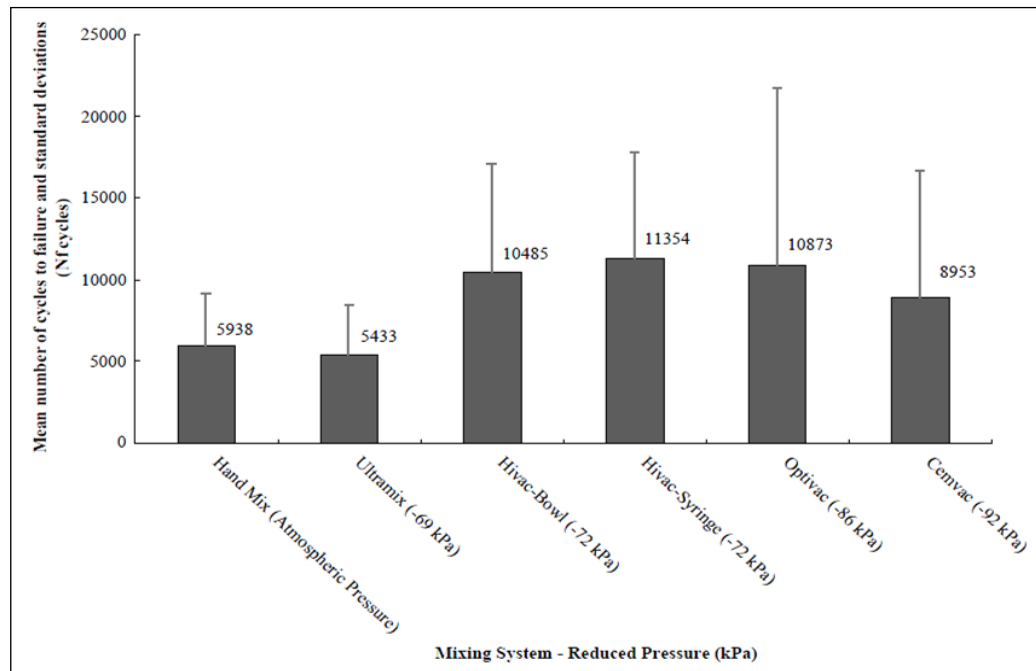


Figure 2.17 Fatigue Summary of the mean fatigue test results and standard deviations, when prepared using different mixing systems and tested at 0.3-22 MPa in 22°C [adapted from Dunne et al. (2003)]

The effect of mixing approach might also be influenced by other factors including the difference in chemical composition and viscosity of bone cements. Lewis (1999b) found variation in fatigue behaviour of two low and high viscosity cements when tested using hand or vacuum mixing methods. The two cements showed no major differences in number of cycles to failure when vacuum mixing was used, whereas the high viscosity specimens lasted significantly longer when hand mixed.

2.3.1.3 Porosity

It is vitally important to focus on the underlying factors that have been discussed in the literature to affect the fatigue life of bone cement including porosity as the main factor. As discussed earlier, porosity can, to a large extent, be controlled by the mixing method adopted. Porosity has been considered by many researchers to play a key role when it comes to the failure of bone cement, particularly *in vitro*. Pore size and distribution can be, in some measure, affected by the mixing approach adopted and thus influencing the fatigue results. The effect of porosity and its characteristics on fatigue behaviour of bone cement, however, seems to be an area of controversy in the literature.

Fracture of bone cement is certainly controlled by the strength of the cement structure which is in turn affected by various factors including pore density and size. The porosity in

the cement exists essentially from air bubbles that arise during mixing the powder and the liquid as well as the possibility of having these bubbles as a consequence of monomer evaporation that occurs because of the heat generated from the polymerisation process (Bishop et al., 1996). It has been argued that porosity weakens acrylic bone cement since the resultant pores promote the initiation of micro-cracks that extend to form major fatigue cracks (Dunne et al., 2003). Although many studies have experimentally demonstrated that cement porosity has a major role in shortening the fatigue life of the material, there have fairly been different interpretations of the mechanisms how pore size and distribution contribute to cement failure. Moreover, Janssen et al. (2005b) argued that the effect of porosity on *in vitro* and *in vivo* fatigue longevity of bone cement differs due to the cement being exposed to homogeneous stress for the *in vitro* testing that certainly leads to reduction in fatigue life whereas this homogeneous state of stress distribution does not exist *in vivo* since, as considered by the authors, the “fatigue failure of the cement mantle is governed by local stress singularities” and “the process of fatigue failure was not affected by the level of porosity”.

Considering the pore size, Murphy and Prendergast (2000) showed experimentally that the effect of porosity on fatigue life can be a function of the mixing method used to prepare specimens. They suggested that, according to their findings, a large pore within a specimen made by vacuum mixing can obviously reduce the fatigue strength of the specimen more than the reduction that can be recorded from a similar specimen made by hand mixing. While the variability in fatigue life according to the study can be higher in vacuum mixing, the authors confirm the belief that, in general, the average fatigue life is greater for vacuum mixed specimens than for similar hand mixed ones. In brief, this study pointed out that the effect of porosity on fatigue properties exists; however, this effect can vary among different specimens because of other factors even if the same mixing methods were used.

Differently and without focusing on the effect of mixing systems, Evans (2006a) concluded that the void size itself has no significant influence on the initiation of cracks unless the void would obviously occupy an important proportion of the cross sectional area of the specimen. It has been pointed out though such laboratory specimens should be disregarded as porosity exists with importantly large pore size which undoubtedly will decrease the fatigue lives of those specimens substantially (Murphy and Prendergast, 2000; Dunne et al., 2003). For acceptable specimens, however, the findings of Evans (2006a) emerged that the presence of other stress concentration raisers, such as radiopacifier particles or rougher surfaces inside a void, would largely enhance the crack propagation

around this void and from here, as he deduces, appears the role of voids, particularly the large ones, in affecting the growth but not the initiation of cracks. The study also emphasised that the stress concentration around a void is a function of Poisson's ratio and not clearly affected by the void diameter. This study accordingly suggested for future work to focus on alleviating the other existing stress concentration risers in order to improve fatigue life rather than paying attention solely to porosity.

Similar trend with different interpretation was provided by James et al. (1992) to show the correlation between porosity and fatigue life. Using scanning electron microscopy, this research illustrated how pore distribution and pore size can simultaneously play an important role in initiating fatigue cracks. The researchers supposed that the presence of small pores in close proximity to larger ones lead to greater stress concentrations than those that can result from individual large pores. They depended in their analysis on the concept of stress concentration theory where they assumed that two small pores adjacent to a large pore can be considered as an elliptical hole that according to the theory causes a larger stress concentration than that caused by a rounded void, thus providing better conditions for a crack to develop.

Other studies, however, have assumed that pores can still have a considerable effect on reducing the fatigue strength of bone cement whether they are singular or combined in a cluster of pores. Hoey and Taylor (2009b) performed a quantitative analysis to assess the effect of porosity on the fatigue strength of bone cement. Using the so called "theory of critical distances (TCD)" to predict the effect of porosity on the fatigue of bone cement, they concluded saying single pores can increase stress concentration that leads to crack generation and failure of the material. Contradicting Evans (2006a) and other similar findings, and enhancing the opposite conclusions, Hoey and Taylor (2009b) also mentioned that the pore size has an important effect on reducing fatigue performance. However, the TCD prediction method used in this study confirmed the analysis of James et al. (1992), stated above, regarding the increase in stress concentration because of close localisation of several pores. They supposed that this distribution of pores and accordingly stress concentrations can result in cracks between the pores forming new and more complex shaped pores. The TCD prediction and the following analysis they used indicated that this clustering of pores can be detrimental to the fatigue strength of bone cement. It might be worth mentioning here, however, the authors in this study supported that having a low degree of porosity throughout the cement mantle can be importantly beneficial, as discussed in greater detail below. In order to properly benefit from this feature and prevent

the damaging effects, they recommended trying to allow and optimise the availability of few small pores evenly distributed within the mantle.

The hypothesis of the positivity of having a controlled number of pores inside the cement mantle has been supported by other studies, assuming that these pores would not significantly contribute to reducing the overall fatigue life. One of the main reasons behind this supposition is to provide a chance to help in releasing the antibiotics that are added to many PMMA brands to prevent any possible infection (Hoey and Taylor, 2009b). A reasonable number of studies have considered the factors that affect this phenomenon focusing basically on the role of bulk porosity. van de Belt et al. (2000) concluded that the amount of antibiotics that is initially released from the polymer matrix is somewhat surface dependent while the overall elution rate is mainly controlled by pore density. Other supposed beneficial results that porosity can contribute to are referred to in fewer instances in the literature which are summarised in Hoey and Taylor (2009b) including, in addition to the antibiotic release, two further advantages. The pores and their size might provide a chance for a bone ingrowth leading to securer fixation of implants. The authors also referred to the benefit suggested by Topoleski et al. (1993) that porosity at a crack tip can disperse the energy leading to a reduction in crack growth rate. Janssen et al. (2005a) also supported the hypothesis that controlled porosity can play a positive role suggesting that the location of pores in the crack path would determine its beneficial or detrimental role. It is worth remembering though the porosity is mostly discussed in the literature as a defective factor when it comes to influencing fatigue life of bone cement.

2.3.2 Previous consideration of the effects of testing conditions and data analysis approaches

Despite the extensity in investigating the effect of precise variables such as those discussed above, and even though the findings of these investigations have shown inconsistency in results, there have been insufficient findings regarding the effect of a particular set of a testing method on fatigue behaviour. Bone cement fatigue testing methods have varied considerably with no accord among researchers as to the optimal testing protocols. Lewis and Nyman (2000) referred to these drawbacks in testing procedures when they examined the literature pointing out that “a plethora of test conditions have been used” adding that “many literature parametric studies employed inappropriate statistical methods” and “these studies have not addressed the issue of possible interactions between the parameters being investigated”.

Obviously, specimens that have been used in fatigue testing of bone cement have varied in terms of shape, size and surface characteristics. Many international, national and researchers own standards have been reported for the measurement of fatigue and strength of bone cement. Although the majority of the relevant studies adopted either solid rectangular or circular cross sectional gauge section profile, the size of these gauge sections have varied. Moreover, particular studies used totally different own designs of specimens for the fatigue testing of bone cement. The surface preparation techniques have also varied depending mostly on direct moulding or machining of previously cast blanks. It may therefore be valuable to make mention (by way of example, not exhaustive enumeration) of a number of these studies in a *historical sequence*, focusing in particular on the specifications of test specimens and stress conditions that were used for fatigue testing in each study and refereeing to some of the main data analysis approaches used.

Pilliar et al. (1976) compared the fatigue properties of a carbon fibre-reinforced bone cement against a conventional bone cement using a rectangular specimen shape with a total length of 90 mm, grip width of 25 mm, a gauge width of 12.5 mm and a thickness of 6 mm (gauge length not reported). The specimens were all prepared by direct moulding using silicone rubber moulds. Fatigue testing was performed in tension-tension sinusoidal loading at 1 Hz, using stress control conditions (testing environment not specified). In terms of data analysis, S-N curves were used to compare the fatigue lives of the two cements that (in a non-linear shape) showed greater fatigue resistance of the carbon fibre-reinforced cement. It is to be noted though, the results are for too small sample size (1 to 3 specimens) were plotted at a range of stress levels (between 10 and 35 MPa), which is insufficient according to today's standards.

Dissimilarly, Freitag and Cannon (1977) examined the fatigue fracture characteristics of two types of bone cement using circular cross sectional specimens that were moulded at pressures of 5, 25 and 50 psi (34.5, 172.4 and 334.7 kPa) and subsequently 'machined and polished with jeweller's rouge to produce a standard cylindrical fatigue test specimen' (jeweller's rouge being fine powder compound of ferric oxide, Fe_2O_3 , used originally for polishing and buffing precious metals). Although the general shape and production method of the specimens used were referred to in this study, the exact dimensions of the test specimen were not reported. Considering the effects of specimen moulding pressure and conditioning environment of cements with zero and 10 wt% BaSO_4 on fatigue life, rotating bending fatigue cycling mode was applied into the specimens until failure and the fatigue lives were recorded for four different stress levels between 7 and 28 MPa, in air at 22°C

and in bovine serum at 37°C. S-N curves were generated only for the testing performed in air, with the use of Student's *t*-test to describe the obtained differences between curves at the different fabrication pressures. Due to obtaining insufficient data for the serum conditions, the main comparison was conducted numerically, using the mean of fatigue life and standard deviation, which showed variations for the effect of all of these variables.

Investigating the strain-controlled fatigue of bone cement, Carter et al. (1982) used similar circular sectional specimen shape, produced at one fabrication pressure. The researchers primarily produced moulded bone cement blanks that were afterwards machined down to produce dumbbell cylindrical specimens with total length of 61.8 mm, a gauge section length of 10 mm and a gauge diameter of 5mm. Uniaxial fully reversed tension-compression fatigue was performed on the specimens in 37°C and 100% humidity environment, after 6-22 days soaking in water at 37°C. Carter et al. used the strain controlled conditions stating that “all previous fatigue tests of bone cement have been conducted under load or stress control”. The authors used mainly the Weibull distributions of survival probability as a function of strain, such that the probability of failure was plotted against the cycles to failure for four different strain amplitudes. By using this technique, they concluded that this form of Weibull plots “not only describe the median specimen behaviour but also quantify the distribution of specimen survival probability under specific test conditions”. With the exception of using zero-tension cyclic loading instead of the tension-compression loading, the same procedures were repeated later by Gates et al. (1983) to study the tensile fatigue failure of acrylic bone cement; and in order to compare the findings with the older study. The comparison of the findings of the two studies indicated that fatigue lives were mostly governed by the tension portion of the fatigue cycles. Almost, the same specimen specifications, dimensions and fatigue loading and controlling conditions mentioned for the former study were adopted later by Davies et al. (1987) as mentioned in section 2.2.2.1 above.

Later, Krause et al. (1988) introduced what they described as a standard test method to determine the fatigue behaviour of bone cement. Krause et al. believed that the type of specimen used by Carter et al. (1982), Gates et al. (1983) and Davies et al. (1987) is inappropriate due to particular objections as they reported:

“The first objection was that the cross sectional area of the specimen was too small. The gage diameter is 5 mm, thus giving an area of 19.63 mm². Considering the inherent tendency of bone cement to contain voids, such a

small cross-sectional area may cause a void to occupy a large percentage of the area and may cause premature failure. In addition, their samples were machined which entailed an additional manufacturing operation and the possibility of introducing cracks on the surface”.

Krause et al. (1988), accordingly, proposed a different specimen type with different shape, size and surface finish. After consulting the ASTM specifications for tensile testing of plastics, the Type IV specimen of ASTM D638 was adopted by these researchers. This type is a rectangular cross sectional dumbbell specimen with a total length of ~152mm, gauge length of 44.5mm, and a gauge width of 6.35mm. The researchers supposed the thickness of ~5mm can be representative to that of the cement mantle around a hip prosthesis, providing a 50% larger cross area than that in the previous work. Moulding rather than machining of specimens was specifically recommended in this study. It is to be noticed however the authors proposed using sinusoidal zero-tension loading type at a frequency of 10 Hz, assuming that this frequency will be adequately low to obviate any internal heating of the specimen and also reach run outs of 10^7 cycles within a reasonable period of time (11.5 days). With these propositions, a specific statistical approach was introduced in this study based on the concept that a combination of two typical analysis approaches (namely; *S-N* relationship and *P-N* relationship) are joined together to provide a *P-S-N* (probability of failure-stress-cycles to failure) relationship.

Regardless of the introduction of this fatigue testing and analysis protocol, different specimen specifications, stress conditions and data analysis were used in subsequent research. Johnson et al. (1989), in their study considering the effect of frequency and environment on fatigue of bone cement, used circular cross sectional specimens that were produced by Silicone rubber moulds which included cavities made using stainless steel blanks that, as the authors reported, were machined according to the ASTM E466 Standard. Although the shape of this specimen type is similar to that reported earlier by Carter et al. (1982) and Davies et al. (1987), the gauge section length was 2.5 times longer, its diameter was 6.1mm and directly moulded to have the moulded surface characteristics. Johnson et al. stated that “although a comparison of results would appear valid within any one methodology, the validity of comparisons amongst studies is questionable”. Based on this supposition, they conducted their testing in dry (room temperature) and saline (both room temperature and 37°C) conditions using sinusoidal tensile loading only at a range of 0.3-20.0 MPa and frequencies of 1, 2, 5, 10 and 20 Hz for testing in dry conditions and a frequency of 10 Hz for testing in saline at 24°C and 37°C. Although this study concluded

that the effects of both testing frequency and environment on fatigue results exist and should be considered, using one stress level was mentioned as a limitation due to having insufficient data to establish an S-N curve, ending to only suggest that these effects are expected to be the same at other stress levels.

With time, and due to the increasing usage of bone cement in arthroplasty, more concern has been shown about fatigue failure of the material and, meanwhile, more variations in fatigue testing specimen specifications have appeared. Neither of these introduced specimen types had been agreed to be uniquely optimal for the usage with adequate stress conditions. Topoleski et al. (1995) used two specific types of machined specimens with circular cross sections to examine the influences of centrifugation and titanium fibre reinforcement on fatigue behaviour. Atypically, testing was performed on the specimens using fully reversed bending fatigue at three stress levels: 15, 20 and 30 MPa. One specimen was non-notched with a total waisted length of 38 mm, a minimum diameter in the waisted section of 6.4 mm and grips diameter of 13 mm. The other specimen had no waisted section, keeping a diameter of 13 mm throughout the total length of 108 mm, but, instead, included a circumferential notch at the mid length providing a smaller diameter of 6.4 mm at the notch tip. This study, that examined the effects of centrifugation and titanium fibre reinforcement on fatigue failure mechanisms of bone cement using three different modified cements, showed variations in fatigue lives depending on the cement reinforcement, centrifugation, stress level and, more importantly here, effect of notching the test specimens.

Murphy and Prendergast (2000), considering the magnitude and variability of fatigue results of vacuum and hand mixed bone cement specimens, used a rectangular shape of moulded specimens, but with a relatively short gauge length of 8 mm, whereas the total length of the specimen was 100mm. After a minimum of two weeks soakage in a 37°C water bath, the specimens were fatigue tested in water at 37°C applying uniaxial zero to tension cycling at 10 Hz under stress control. Four stress levels were used for both vacuum and hand mixed cement: 13 MPa, 17 MPa, 21 MPa and 25 MPa to allow establishing an S-N diagram to compare the fatigue results. One of the main findings of this study was that “the mean fatigue strength of vacuum-mixed cement can be greater than that of hand-mixed cement. However, the variability in fatigue strength of vacuum mixed cement can be greater”. It is still not clear though what the case would be if different stress regimes (different specimen and stress types) were used to measure the magnitude and variability of fatigue results of hand and vacuum mixed cements.

At the same time, Harper and Bonfield (2000) examined the fatigue properties of ten commercial bone cements in one study and using one testing method in order, as they believed, to provide more reliable comparisons between the fatigue characteristics of these cements. In this context, they stated that “following the introduction of bone cement by Sir John Charnley in the 1950s, there have been numerous investigations into its fatigue properties” and that “these reviews demonstrate the large variety of fatigue protocols that have been followed and the limited number of cements studied using any given testing technique”. The authors commented accordingly that “this background makes it almost impossible to compare results from different investigations”. To achieve their comparable investigations, they used a specimen shape according to ISO 527-2 (half-sized) and produced the specimens by direct moulding of hand mixed cement mixture, providing a dumbbell rectangular specimen shape with 75 mm total length, 5 mm gauge width and ~ 3.5 mm thickness and with a gauge length of 25 mm. To perform the fatigue testing, the specimens of all cements were stored in dry conditions at 37°C for at least a week prior to being subjected to sinusoidal tension-tension cyclic stress that was controlled between a minimum of 0.3 MPa and a maximum of 22 MPa at a frequency of 2 Hz, in air at room temperature. The comparison of fatigue results by means of Weibull analysis showed significant variations in fatigue behaviour, but, more importantly, it was concluded that “the cements that perform best clinically gave the highest results in this study”. The authors ended by mentioning certain limitations to the study including using hand mixing, testing in dry conditions and using one stress level only which they reported to be considered more fully in a subsequent study. Exactly the same testing method was used by Dunne et al. (2003) to study the relationship between porosity and fatigue characteristics of bone cement (discussed above), except they stored the specimens in air at 22°C. Jeffers et al. (2005), in their study considering the fatigue damage and creep behaviour of vacuum mixed bone cement, however, used the same test specimen shape and production method, but with different size (total length of 150 mm and a 12mm x 12mm gauge with a thickness of 3.5 mm). While the stress conditions in this study were generally similar to those in Harper and Bonfield (2000), four maximum stress levels were used (7, 11, 15 and 20 MPa) with $R = 0.1$ and at a frequency of 5 Hz in 37°C distilled water. Also, the results were assessed by means of S-N analysis where it was deduced that porosity was the main factor to control the fatigue life which was considered as a reason to cause “a large amount of data scatter”. In all of these studies, though, there was no mention of changing the test regime in terms of specimen and stress types and investigating their effects on the fatigue behaviour.

Within the same decade of performing and reporting these studies, other researchers were investigating the same or other variables in terms of controlling the fatigue life of bone cement, however, using totally different specimen types and stress conditions. Lewis (2000), for instance, examined the relative roles of cement molecular weight and mixing method on fatigue of two acrylic bone cements using a dumbbell specimen (circular section) with a total length of 61.8mm, a gauge length of 10 mm and a gauge diameter of 5mm [To clarify, this specimen geometry was later adopted in the ASTM standards (ASTM F2118), which is similar to that reported by Carter et al. (1982) who tested their specimens in strain controlled conditions as discussed above]. The specimens were produced by machining of previously moulded bone cement rods that were left to cure in room temperature for at least 24 hours before machining. After being investigated for porosity and discarding the specimens that had voids greater than 1 mm in diameter, the specimens were soaked in Ringer's solution for a week that was followed by testing in uniaxial fully reversed tension-compression stress conditions of ± 20 , ± 17.5 , ± 15 , ± 12.5 , ± 10 or ± 5 MPa, at 2 Hz and using a small sample size of 3 to 5 specimen per testing group. The fatigue results in this study were analysed using the probability-of-fracture method, the three-parameter Weibull, fit to the Olgive-type equation, and a fatigue performance index, I , approach. Under these testing and data analysis circumstances, it was generally concluded that "these results point to the greater influence of cement molecular weight over the mixing method on cement's fatigue performance".

In brief, there have been no agreed guidelines to be consensually followed by all researchers and, accordingly, more fatigue testing methods have been reported. In terms of specimen shape, Cristofolini et al. (2000), for instance, used a 4mm thickness flat dumbbell shape "in order to approximate the *in vivo* cement mantle thickness closely"; returning back to the suggestions and specimen shape provided by Krause et al. (1988), but using different specimen size (whole size ISO 527-2). In contrast, many studies have continued to test a circular shape according to specific standards such as ASTM F2118. Lewis and Janna (2003), nonetheless, stated that using either shape can be acceptable as the aim is to characterise the material *in vitro*. It is noted though the specimens with rectangular cross section have been mostly tested under either zero-tension or tension-tension fatigue, whereas those with circular cross section have been particularly used with the tension-compression fatigue for both stress- and strain- controlled conditions. Limited discussion, however, has considered the influence of surface preparation on fatigue behaviour of bone cement specimens. Although it has been suggested that the moulded specimens would be preferable to the machined (Krause et al., 1988; Paravic et al., 1999;

Lewis and Nyman, 2000), both specimen production methods continued to be used. As for the effect of deformation mode fatigue control conditions on fatigue behaviour of bone cement, there are few studies considered this factor, but again not comprehensively investigated. Most studies, applied only one mode preferring to use uniaxial tension or compression cyclic deformation modes. Tension-tension or tension-compression stress types, in particular, have been reported in the cement mantle *in vivo* (Lewis and Nyman, 2000). Tension-compression loading above all can be particularly preferred because this loading, according to Dowling (2007), provides a good indicator of fatigue performance of materials. Due to these considerations, only very few studies have applied other stress deformation modes such as rotating bending or flexural fatigue of bone cement specimens.

Regardless of the debate reported concerning the effects of using various stress regimes on describing the fatigue behaviour of bone cement, there has been limited number of studies that have tried to comparably investigate the effect of this factor while all the other testing variables are constant. Nevertheless, each of these studies has, under particular conditions, compared only two stress regime variables. That is to say, a study might compare, for example, the effect of specimen shape only using one mode and type of stress. Another study, using different cements and not ensuring the same conditions as the previous, might consider the effect of specimen production method at different stress levels of a particular stress type, and so on. The comparison of two studies performed by Carter et al. (1982) and Gates et al. (1983) discussed above (section 2.3.2.1) is an example of these limited investigations. The two studies considered only the effect of changing the loading type (zero-tension vs. tension-compression) on fatigue life of bone cement using, however, strain-controlled conditions and testing one specimen type.

In terms of considering specimen production method only, Paravic et al. (1999) examined the effect of this factor on porosity and fatigue behaviour of bone cement. Using circular cross sectional shape only and one cement, they compared the fatigue lives of a number of moulded specimens to approximately the same number of machined specimens. Half of each specimen type was prepared following centrifugation mixing method and the other half was produced by hand-mixing. The fatigue tests were conducted in tension-tension cyclic loading ($R=0.1$) to maximum stress levels of 15, 20, 25, 30 and 35 MPa at a frequency of 5Hz in 37°C circulating saline. The results of this study was analysed using Weibull analysis and showed that moulded specimens, when hand mixed, provide significant increase in fatigue life compared to the equivalent machined specimens. This difference in fatigue lives was not observed between the two specimen types when

centrifugation was used. It was also reported that centrifuged specimens had greater fatigue lives compared to the hand mixed. The difference of porosity distribution was provided as a reason to have these variations in results which is controlled originally by the difference in mixing technique and finally affected by the surface finish method as machining of specimens, particularly when hand mixed, causes the internal voids to appear on the outer surface which facilitates fatigue failure.

Another study by Lewis and Janna (2003) also involved two different methods of mixing the cement components (hand and vacuum mixing) for each of three cement formulations in order to investigate the effect of specimen cross sectional area shape on the fatigue life, using one specimen production method (moulding). Two specimen shapes were used: circular cross sectional according to ASTM F2118-01a and rectangular cross sectional according to ASTM D638-01 (Type IV specimen). The total length of the circular shape was 62mm with a gauge of 10mm in length and 5mm in diameter. The total length of the rectangular specimen was 155 mm with a gauge length of 25mm, width of 6mm and thickness of 3.2mm. The specimens were assessed for porosity and those that had pores of greater than 0.25mm in diameter were rejected and the accepted specimens were stored in ambient room temperature for a minimum of 48 hours prior to testing. The specimens were subjected to a uniaxial fully reversed tension-compression loading at stress levels of ± 15 MPa and a frequency of 5 Hz, until fatigue fracture. The fatigue data was analysed using the three-parameter Weibull relation, with the use of the Weibull mean as the fatigue performance index. Lewis and Janna (2003) found that, with either mixing method, the fatigue lives were greater for the circular specimens compared to the rectangular. Difference factors of between 2 and 36 times were found between the fatigue lives of both specimen types. The authors considered the difference in the residual monomer (about 10% lower for the circular specimen) as the main reason to lead to the difference in fatigue lives between the two specimen shapes.

Tanner et al. (2010) provided a wider comparison of two fatigue testing methods after performing two fatigue studies in two different laboratories, using four bone cement formulations. Although mixing conditions and procedures that were followed in both laboratories were similar, the moulding considerations were not totally similar with moulded rectangular specimens (half-size ISO 527-2) tested in one laboratory and moulded cylindrical rods, which were subsequently machined to provide waisted circular specimens (ASTM F2118), in the other laboratory. In both studies, only the specimens that had micro pores (<1.0 mm) were included in testing performed under stress-controlled conditions.

The study that tested the moulded rectangular specimens included performing single sinusoidal cyclic loading in tension-tension manner between 0.3 and 22 MPa at 2Hz in continuously flowing 37°C saline solution. A minimum of 11 specimens from each cement were tested after 1 to 6 weeks soakage in 37°C saline. The cycles to failure data in this study was analysed using Weibull functions where the probability of failure was determined using Bernard's correction (Equation 2.23). The other study tested the circular machined specimens at five stress levels of fully reversed tension-compression loading examining eight specimens at each stress level (± 10 , ± 12.5 , ± 15 , ± 20 or ± 30 MPa). All the other testing conditions were similar to that used for the rectangular specimens except of using 5 Hz frequency in this study, providing another dissimilar factor among the two studies that its effect on fatigue results cannot be ensured to not exist. The fatigue results of this study were analysed using the S-N analysis, plotting the base 10 logarithm of the cycles to failure against the maximum stress levels.

The comparison of the findings of the two testing methods reported by Tanner et al. (2010) showed that the difference between fatigue lives among the tested cements varied depending on the testing method. They found that "the fatigue lives between the cements were up to a factor of 15 different for the single stress level tension only tests, while they were only a factor of 2 different in the fully reversed tension-compression testing". This indicated that using different fatigue testing methods of the same cements can lead to dissimilar fatigue behaviour.

Although, as just discussed, there have been a limited number of studies that each of which considered the effect of changing particular variables of stress regimes on fatigue behaviour, no comprehensive study has been established to compare the effects of all stress regime variables. The question remains, therefore, what would the findings be if the same cement formulations were tested using various specimen types (more than one shape and production method) and different stress types and levels, while ensuring the constancy of all the other testing conditions (such as frequency and environment), with the fatigue results being analysed and compared using different data analysis approaches?

CHAPTER 3. MATERIALS AND METHODS

3.1 MATERIALS

SmartSet GHV and CMW1 bone cements were used to produce test specimens for the fatigue testing. These two cements were produced and supplied by DePuy CMW (Blackpool, UK) in packets, each of which includes two portions: 40g bone cement powder in a pouch and 18.88g bone cement liquid in an ampule. The powder composes mainly of a polymethyl methacrylate based polymer whereas the liquid component is based on the monomer methyl methacrylate. The composition and characteristics of the two bone cement materials are provided in Table 3.1. These two bone cements were used in this study since SmartSet GHV has zirconium dioxide as opacifier filler along with gentamicin sulphate and CMW1 contains barium sulphate filler with no antibiotic additives. Both of these cements have been classified as having high viscosity, thus excluding the influence of the difference of this factor on the results. To obtain the applicable solid bone cement, the powder and the liquid portions were mixed and moulded as appropriate. Phosphate buffered saline (PBS) was used to produce specimen soaking solutions that were kept at 37°C environment prior to and during fatigue testing of the prepared specimens.

Table 3.1 *The powder and liquid chemical contents* of SmartSet GHV and CMW1*

	SmartSet GHV		CMW1	
	% w/w	gram	% w/w	gram
Composition of bone cement powder:				
Polymethyl Methacrylate	0	0	88.85	35.54
Methyl Methacrylate/Methyl Acrylate Copolymer	80.45	32.18	0	0
Benzoyl Peroxide	0.96	0.384	2.05	0.82
Gentamicin Sulphate	4.22	1.688	0	0
Barium Sulphate	0	0	9.1	3.64
Zirconium Dioxide	14.37	5.748	0	0
Composition of bone cement liquid:				
Methyl Methacrylate	97.5	18.408	98.5	18.5968
N,N-Dimethyl-p-toluidine	≤2.5	≤0.47	≤1.5	≤0.282
Hydroquinone	75ppm	75ppm	75ppm	76ppm

*The contents represent a 40g unit (40g powder & 18.88g liquid)

3.1.1 SmartSet GHV bone cement

SmartSet GHV cement is a self-curing radiopaque formulation that has been developed, according to the manufacturer, to satisfy a range of clinical requirements and surgical approaches. Its powder component contains 14.37wt% zirconium dioxide (ZrO_2) as an opacifier which leads to having 9.76wt% of ZrO_2 in the final mixture. The powder also contains 4.22wt% of gentamicin sulphate, providing 2.867wt% in the mixture. The aim of impregnating the cement with this antibiotic filler is, according to the manufacturer, to provide ancillary local antibacterial therapy after the interference and cohesion between the bone cement and the adjacent bone surfaces. The cement powder, according to the manufacturer's description, is sterilised using ethyleneoxide and sealed in an inner paper / polyethylene peelable pouch, that is protected in a third non-sterile foil pouch. Due to being classified a high viscosity cement, SmartSet GHV, according to the supplier, is basically developed for either manual or syringe applications.

3.1.2 CMW1 bone cement

This cement is similar to the SmartSet GHV in specific aspects including curing properties, viscosity range and primary applications. Although it is also available in the form of antibiotic impregnated cement, the formulation used in this study was unmedicated to provide further consideration to the effect of variations in chemical composition on the fatigue results. Different from the SmartSet GHV cement, the powder portion of this cement contains 9.1wt% barium sulphate ($BaSO_4$) as an opacifier which leads to having 6.18wt% of $BaSO_4$ in the mixture of the polymer and the monomer. Also, when produced, the powder of this cement is sterilised with gamma radiation and sealed in an inner polyethylene bag followed by a non-sterile peelable pouch which is finally protected by an outer foil pouch.

3.1.3 Bone cement in its solid form

Mixing of the powder and liquid of each of the two cements (as explained in Section 3.2.1.2) provides the doughy applicable bone cement that hardens in a short period of time providing the solid structure (cement matrix). This structure is represented by the test specimens that were produced to provide four different types of specimens which

were later soaked in 37°C phosphate buffered saline to provide the desirable properties required for testing of such a material.

3.1.4 Saline solution

Distillate water was used to produce specimen soaking solutions. In order to obtain a moderate solution in terms of pH value and concentration, one phosphate buffered saline (PBS) powder packet (pH of 7.4) that yields 0.01M PBS solution when dissolved in 1 litre of distilled water, was used for the preparation of each litre of the solution. To maintain the test specimens in this solution at the specified temperature of 37°C prior to testing, the solution containing the specimens was stored in an incubator that was previously adjusted to the required temperature. The 37°C saline was also sprayed on to the test specimens during the testing period.

3.2 MECHANICAL TESTING

3.2.1 Preparation of test specimens

The basic requirements were to obtain both rectangular and circular cross sectional specimens prepared by two different surface finishing techniques. These preparation methods, which were performed in parallel throughout the experimental time of this research, were direct moulding of the cement mixture into the final dumbbell specimens or machining of oversized moulded non-waisted blanks into the final dumbbell shapes.

3.2.1.1 Specimen shape reference standards

Two standards were used to obtain specimens with two different cross sectional shapes by either direct moulding or machining of cast blanks. The first shape was rectangular according to ISO 527-2 (type 1BA, i.e. half-size) as shown in Figure 3.1a (BSI, 2012b) whereas the second shape was circular according to ASTM F2118 as shown in Figure 3.1b (ASTM, 2003). Both shapes have a nominal gauge cross sectional area of approximately 20 mm². The difference in the two shapes was considered because of their differences in gauge surface areas, gauge volumes and surface area to volume

ratios (Table 3.2) and due to the possible effect of these geometry variations on the fatigue behaviour.

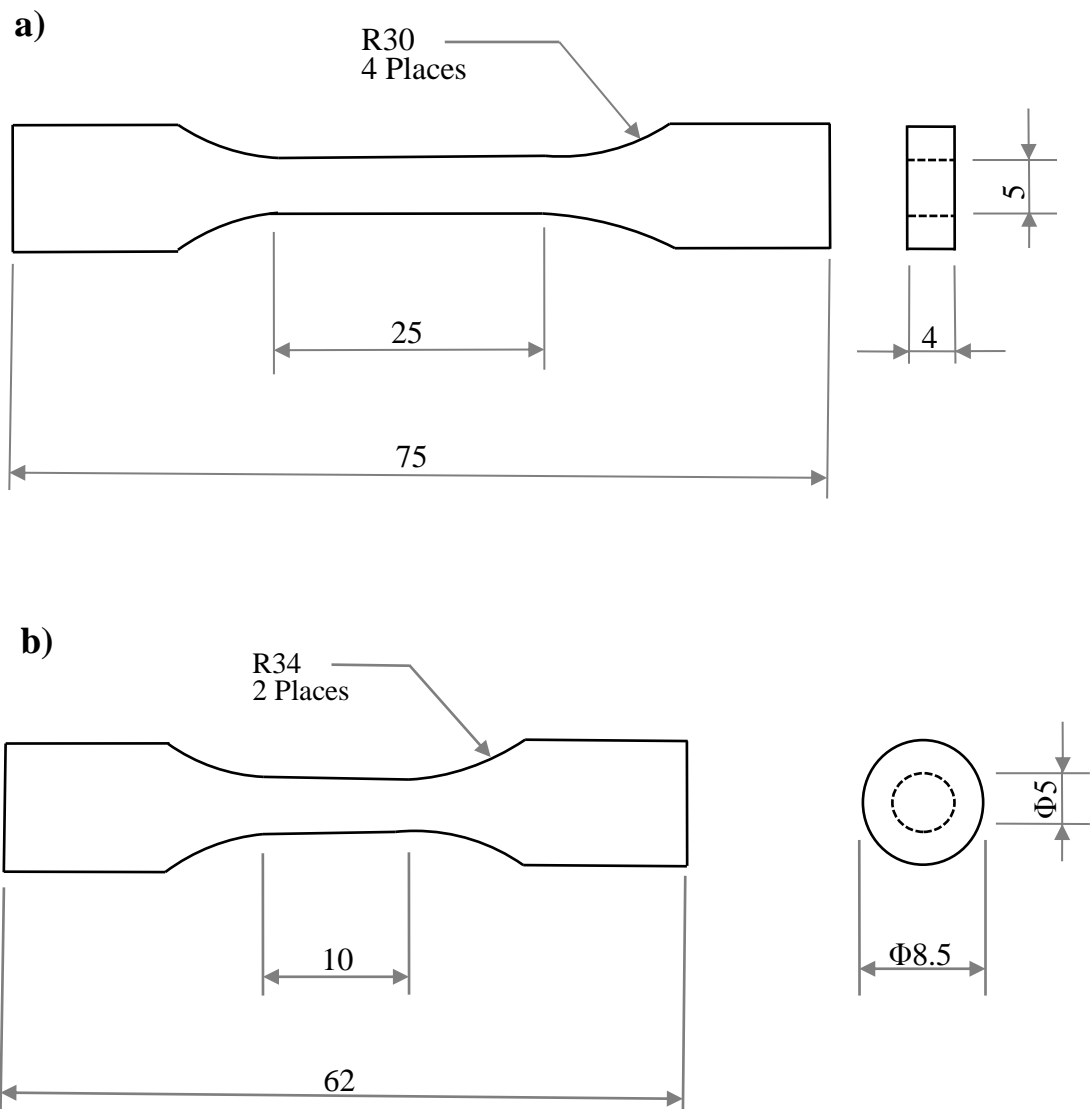


Figure 3.1 Test specimen shapes: (a) rectangular according to ISO 527-2 and (b) circular according to ASTM F2118 (units in mm – dimensions not to scale)

Table 3.2 Specimen shapes and variations in cross and surface areas and surface area to volume ratios

	Gauge cross sectional area (mm ²)	Surface area of gauge section (mm ²)	Volume of gauge section (mm ³)	Surface area to volume ratio
Rectangular	20	450	500	0.9
Circular	19.64	157.14	196.43	0.8

To have the specimens produced according to the two shape standards by both direct moulding or machining, four different polytetrafluoroethylene (PTFE) moulds were designed and made to include the exact shape cavities for the direct moulded specimens or oversized hollows to produce blanks that were later machined to the final dimensions. This consideration was to obtain the following four specimen types:

1. Rectangular directly moulded dumbbell specimens (RDM)
2. Rectangular moulded and then machined dumbbell specimens (RMM)
3. Circular directly moulded dumbbell specimens (CDM)
4. Circular moulded and then machined dumbbell specimens (CMM)

Due to the cylindrical geometry of the ASTM based specimens, each mould used to produce these specimens was made of two halves. Each half included 5 cavities each of which with a longitudinal hollow shape of half a circular cross sectional specimen (half longitudinal waisted circular specimen) or half an oversized cylindrical rod (half longitudinal cylindrical oversized rod) where each of these cavities was facing a same shape and size cavity on the other half of the mould so that, when filling these cavities with the cement mixture and pressing the two halves together, 5 whole circular moulded specimens (directly moulded or oversized rods) were produced at a time. The oversized rods were machined later to the final ASTM F2118 dimensions.

In the case of producing the rectangular specimens, single PTFE moulds were used to have 5-6 cavities of either final half-sized ISO 527-2 specimen shape or rectangular blanks that were afterwards machined to the final half-sized shape. Unlike moulding of the circular cross sectional specimens, two metal sheets, of a thickness of about 1mm and area larger than that of the main mould, were used to surround the mould from its two main sides so that, when injecting the bone cement mixture into the cavities of the mould, one metal sheet works as a base bottom and the other is used to cover the mould after the injection process.

3.2.1.2 Mixing of bone cement components

The moulding procedures started with mixing of the powder and the liquid of one pack (40g powder and 18.88g liquid) under vacuum-mixing conditions at room temperature

($21 \pm 2^\circ\text{C}$) using a CEMVAC mixing system (DePuy CMW, Blackpool, UK). From each individual mixture, 5-6 specimens were obtained. The mixing process was implemented following the manufacturer's instructions focusing, in particular, on mixing time, waiting time and working time for each cement type. During the mixing period, evacuation pressure (~ -70 kPa) was applied to the CEMVAC system with mixing speed of about 1 beat/s for a total mixing time of 30-45 seconds. Once the components were mixed, the mixture was left in the mixing system syringe for certain time (waiting time) that was specified by the manufacturer at 23°C and 19°C to be respectively 50 and 65 seconds for SmartSet GHV and 70 and 90 seconds for CMW1. If this time was reached and the cement mixture was felt to be gluey, which is judged by the cement dough easily sticking to the gloved fingers, a few more seconds were waited before the injection of the cement into the mould. Once injected into the mould at the beginning of the working time, the doughy specimens inside the mould were pressurised to about 50 bar using a hydraulic pressure machine and kept under pressure for 20-30 minutes. This pressure is to eject the excess cement and to ensure the formation of the required specimens with low porosity. The pressure was then released and the specimens were left in the mould for at least an hour before they were carefully removed. The specimens were then left for at least 24 hours before being prepared for testing, to allow sufficient time to ensure maximum polymerisation processes.

3.2.1.3 Surface preparation of test specimens

Both ISO 527-2 and ASTM F2118 standards refer to the possibility of producing test specimens, with the specified shapes and geometries, using either direct moulding or machining of previously moulded plates. To obtain directly moulded specimens, the specimens in their final dumbbell shape, either rectangular or circular, were removed from the mould, at least an hour after the injection process, and no further actions were performed except of slightly polishing any sharp marks that were created on the specimens due to the ejection of excess cement dough. This was performed using 600-grit or higher abrasive papers with occasional sprays of water on the specimen while grinding these undesirable sharp fragments in the longitudinal direction as specified by ASTM F2118. Machined specimens were obtained by moulding oversized rods which were subsequently machined to the final shape and size at least 24 hours after the completion of the polymerisation process. The difference of the machining processes

between the two shapes, due to the differences in shape, was that the machining tool movement, and thus the removal of the material, was in the longitudinal direction for the rectangular shape and perpendicular to the gauge length for the circular shape.

3.2.1.4 Initial assessment of test specimens

All obtained specimens were assessed for the presence of any undesirable defects including large pores, scratches or lack of material in the gauge and/or transition sections. As described by both ISO-527 and ASTM F2118, specimens that were found to have remarkable scratches and pores in these sections were rejected and excluded from any further testing except they were added to the discarded specimens in order to calculate and report the rejection rate. The porosity assessment was conducted visually in a clear vision area or under focusing light. As recommended by the ASTM F2118 and other relevant fatigue of bone cement papers [e.g. (Cristofolini et al., 2000) and (Lewis, 1999a)], the exclusion was applied to the specimens that had one defect or more where, at least, one of these defects had a length of 1 mm or greater in its major diameter (the 1 mm discard criterion). If a specimen was assessed to have no significant defects, it proceeded to the next stage of preparation for testing.

3.2.1.5 Classification and numbering of specimens

The specimens that were adequate for testing were classified according to their bone cement structure and their shape and production method. SmartSet GHV and CMW1 were fixedly denoted to as A and B, respectively. The numbers 1, 2, 3 and 4 were used to denote to a particular shape and production method (specimen type) as follows:

1 = Rectangular directly moulded (RDM)

2 = Rectangular machined (RMM)

3 = Circular directly moulded (CDM)

4 = Circular machined (CMM)

To make test specimens distinguishable, each test specimen number started with 1, 2, 3, or 4 followed by A (for SmartSet GHV) or B (for CMW1). This is followed by two digits that refer to the specimen in its group as well as the stress type and level as follows:

From 01 to 15 = tension-compression stress at ± 20 MPa

From 16 to 30 = tension-compression stress at ± 15 MPa

From 31 to 40 = tension-compression stress at ± 30 MPa

From 41 to 50 = tension-compression stress at ± 12.5 MPa

From 61 to 75 = tension-tension stress between 2 and 20 MPa

A specimen group here refers to the group of specimens that were made from the same cement, characterised by the same shape and surface production method and tested for fatigue under the same stress type and level, thus representing a unique stress regime. For example, the specimen 2-B-18 belongs to the testing group that its specimens had a rectangular machined shape, were made from CMW1 cement and were tested under fully reversed tension-compression of 15 MPa.

3.2.1.6 Identification of specimen measurements and loading forces

The measurements of the thickness and width of the gauge sections of the rectangular specimens were performed according to ISO 527-2. Three measurements were taken for the thickness of each specimen along the gauge section at different distances and the average of the three readings was used. In a similar manner, three widths were measured and the average width was determined. The average thickness and width were used to calculate the average cross sectional area of the specimen. For the circular specimens, the diameters of the gauge sections were measured at three different points along the gauge as described by ASTM F2118. The average diameter was used to calculate the cross sectional area of the gauge section.

Once the cross area was obtained, the required loading range for the specimen was determined depending on the stress level required for testing of that particular specimen using the basic relation between the stress, force and cross area. Excel spreadsheets were used to perform the calculation functions starting from computing the average thickness and width or the diameter from which the cross areas were obtained. Accordingly, the maximum loading force (in Newton) that was required to stress a particular specimen at particular stress levels was determined by multiplying of the assigned axial stress (in MPa) by the cross area (in mm^2).

3.2.1.7 Conditioning of specimens prior to testing

Once the specimens were prepared, numbered, measured and the appropriate loading forces were identified, they were soaked in the PBS solution and stored in an incubator (Sanyo, MIR-262) for a period of time that has been recommended to be between a minimum of 1 week and a maximum of 8 weeks, but, “as reasonably possible, all of the test specimens should have the same soaking time before testing” (ASTM 2118). To alleviate any possible effect of the variations of this period, therefor, specimens were mainly tested during the second and third weeks of aging time or, at the longest, during the fourth week. This was achieved by approximating the times required for testing at a particular stress level where a balance was always judged between the number of specimens entered into the solution and those that were tested. Particular attention was paid to control the soaking time when testing at lower stress levels as the specimens lasted for multiple days under testing.

3.2.2 Configuration of fatigue testing

The main considerations when performing the fatigue tests were to install the specimens in a uniaxial fatigue frame ensuring that the specimen was sufficiently covered by saline during testing, any loads generated from installing the specimen were removed and the required stress levels were correctly applied. An MTS machine (MTS – 858 Mini Bionix[®] II, MTS, Minneapolis, MN, USA) was used to perform this testing after it was properly prepared to fulfil the requirements of this study.

3.2.2.1 Specimen installation

Two stainless steel grips, attached to the hydraulically driven upper shaft and the lower fixed axial shaft within the MTS load frame, were used to firmly fix the test specimen at its ends. These ends were fully gripped ensuring that both of the shoulder sections are excluded from the gripping process. The steel grips were vertically aligned so that, when a specimen is installed between the two grips, the longitudinal centreline of the specimen coincides with the centre of the loading axis. Each fixing grip consists of two adjustable parts where each part has two roughened fixing faces, to prevent the slippage of the specimen. These roughened faces are flat from one side to allow the fixation of rectangular specimens and has a V shaped cavity on the other side along the centre of

the fixing face parallel to the loading axis to help in the fixation of the circular specimens.

In each case, a rod or a bar of the same cross section as the circular or rectangular specimen respectively, but each with upper and lower circular cross-sectional aligning extensions of 2mm in diameter, was first fitted into the central alignment hole on the lower grip followed by moving the upper grip down gradually so that the upper extension of the rod or the bar fits into the upper central aligning hole. The upper and lower grips were then tightened from one side ensuring it is totally aligned and in contact with the rod or the bar. The aligning rod or bar was then removed to start the installation process of a test specimen. For each specimen shape, the installation started with tightening the lower end of the specimen between the two parts of the lower grip by tightening the moving part of the grip into the other. The upper gripping assembly that was attached to the controlled fluctuating shaft of the MTS machine was gradually moved into the specimen using the MTS computerised controller until adequate positioning of the specimen's upper end was observed. The specimen was then tightened from the upper gripping side in a similar manner to that for the lower side.

3.2.2.2 Conditioning of specimens while testing

To provide physiological testing environment following the steps of many articles reported in the literature, a test specimen was taken from the soaking solution, installed in the testing machine and immediately remained in continuously flowing PBS solution. This can particularly be important if the specimen lasted in testing for many hours or days. To ensure the continuation of the flowing solution during testing, a fluid circulating system of adjustable temperature (Grant, GD120) was used to spray the solution on the specimen maintaining it wet at 37°C. In order to recollect the spray and condensate the evaporated portion, the specimen and the multi-holes flexible spray pipe around it were both surrounded by an environmental chamber. The view of a specimen during testing is shown in Figure 3.2, with the circulating saline solution covering the specimen.



Figure 3.2 *Close up of a specimen type fully covered by saline spray during testing*

3.2.2.3 Fatigue data acquisition

The MTS software program includes variety of processes and procedures that can be selected and modified according to the mechanical fatigue test requirements. Fatigue testing was selected from the program as the main process of testing. This selection provides the chance of choosing the required testing mode (axial only for the purpose of this study), entering the load parameters to provide the required stress and specifying the test start time and failure detection limits. Testing parameters such as test frequency and failure limits, that were to be constant throughout testing, were selected and saved in the specified testing procedure. Other inputs, such as the cyclic loading levels, were often modified as appropriate when changing the test specimen and/or test requirements. To remove any loads that could be generated from placing the specimens in the grips and allow stress relaxation before starting the fatigue test, a ramp to zero load process was selected from the MTS program while a subsequent holding process keeps the specimen under no load for 30 minutes. The aim was to relieve any stresses generated during the fixation of specimens.

To specify the type and range of data required for this study, the selected MTS procedure was programmed to record the number of cycles to failure and, for particular loading cycles, 10 data points were recorded throughout the testing period such that

each point reads the instantaneous force and displacement. The procedure was programmed to logarithmically record the first 10 cycles from each 100, the first 10 cycles from each 1,000, the first 10 cycles from each 10,000 and so on. The program was also set to include recording the data for all the last 1,000 cycles before failure.

3.2.2.4 Application of fatigue stress

Once a test specimen was adequately installed and covered by the saline and an appropriate MTS test procedure was configured by setting the required test parameters, the specimen was subjected to the required fatigue stress type (fully reversed tension-compression or tension-tension) between the maximum and minimum load limits as identified for the specimen. To adopt a moderate test frequency to allow obtaining enough fatigue results over the research time and, in the meantime, to not test at high testing speed that might generate undesirable effects such as specimen heating; a test frequency of 3Hz was used for all fatigue life testing methods. Testing was allowed to continue until the failure of test specimen, identifying that if a specimen reached 5 million cycles without failure, the result was considered as “runout” at this fatigue limit.

For the fully reversed tension-compression regimes ($R = -1$), the maximum force that was calculated for each specimen to provide the relevant maximum stress was entered as the maximum load in the MTS procedure providing the tension stress limit for that particular specimen. The negative value of this force was used as the minimum load in the MTS program representing the compression limit. In the case of applying the tension-tension regimes, a stress ratio of $R = 0.1$ was assigned to perform this stress type. The minimum load was, therefore, entered as 10% of the allocated maximum load that corresponded to a maximum stress of 20 MPa.

3.2.2.5 Final assessment of test specimens

For many cases, it was difficult to ensure that the test specimen had no inner macropores. Therefore, the specimen was tested for fatigue and the fracture surface was investigated for porosity. As explained in Section 3.2.1.4, if the specimen had one or more pores with a diameter of 1mm or longer, the obtained results were discarded and a replacement specimen was tested.

3.2.3 Fatigue testing of CT specimens

To provide further investigation and comparison to the fatigue crack propagation for the two test cements apart from the effect of specimen type, Compact Tension (CT) specimens were used for this purpose according to ASTM-E647 (ASTM, 2013). The geometry and dimensions of the test specimens are given in Figure 3.3a. The thickness of the specimen, B , was selected to be 3mm (within the recommended thickness range: $\frac{W}{20} \leq B \leq \frac{W}{4}$) and the width $W= 32\text{mm}$ (suggested minimum width $W= 25\text{mm}$). The pre-crack length, a_0 , was identified to equal $0.5W$ (suggested minimum length $a_0= 0.2W$).

3.2.3.1 Specimens preparation

The process of preparing the CT specimens started with making a 3mm thickness PTFE mould that was used to provide moulded 38.4mm x 40mm x 3 mm initial blank samples, following the same steps of mixing bone cement components used to make the dumbbell fatigue specimens (Section 3.2.1.2). After total hardening of the injected mixture, the blanks were removed from the mould and cured in an incubator at 37°C for 24 hours. As described by the ASTM standard, a pre-crack of the details shown in Figure 3.3b was then made by machining in addition to making two circular holes of 8mm diameter to be used to load the specimen while testing. Prior to testing, the specimens were aged in saline at 37°C between 1 and 6 weeks.

3.2.3.2 Installation of crack gauges on specimens

While setting the test conditions and before subjecting a CT specimen to fatigue cycling, a crack propagation gauge (Model TK-09-CPA01-005/DP, from Vishay Precision Group) was adhered to the specimen covering the area where the fatigue crack is expected to grow from the notch tip. This type of crack measurement gauges has 20 grid lines (strands) with a distance of 0.25mm between each two adjacent strands, providing a total grid width of 5mm.

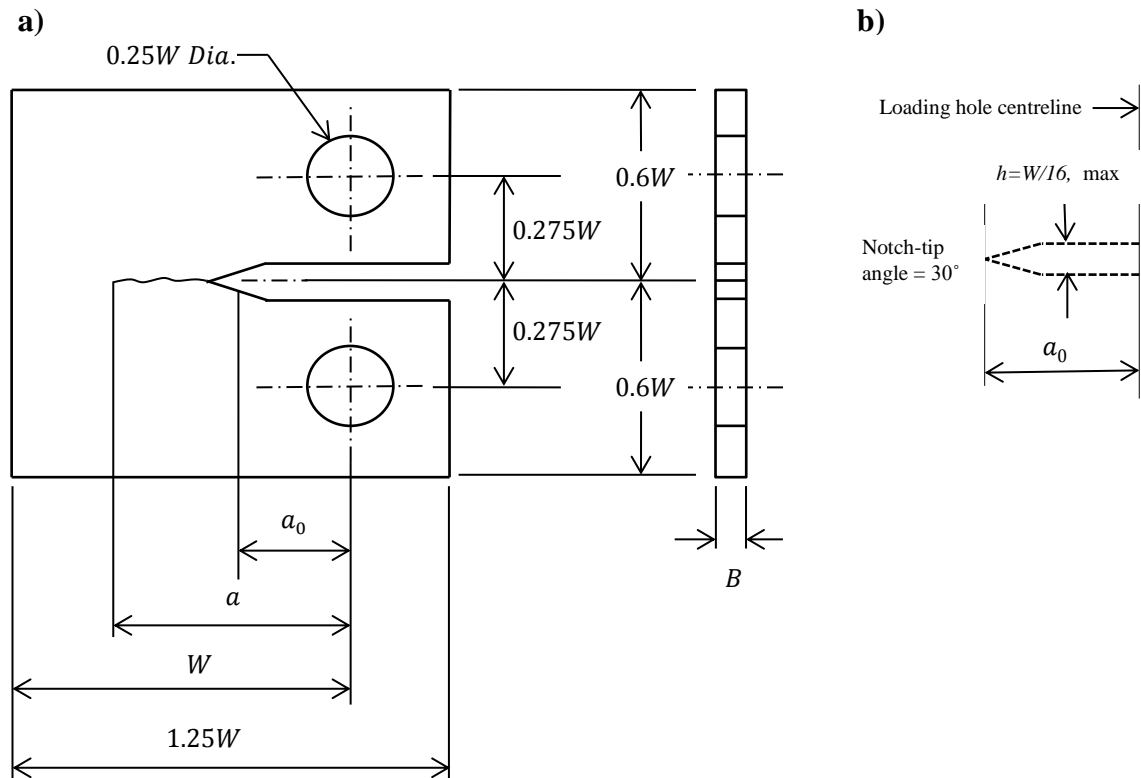


Figure 3.3 Geometry and nominal dimensions of CT specimens used in testing of crack growth rate: (a) specimen and (b) notch details [according to ASTM-E647 (ASTM, 2013)]

Following the manufacturer's instructions in terms of cleaning and preparing the area of the specimen onto which the gauge will be adhered, the gauge was installed on the specimen using specified glue (Micro-Measurement, M-Bond 200 Adhesive) ensuring that its grid lines were perpendicular to the length of the pre-crack. This is to relate the crack growth rate within the bone cement matrix on which the gauge is installed to an identical tear of the gauge grid and provide more accurate crack growth measurements. Two ends of isolated wires were welded into the gauge sides to be connected later to an adequate electrical circuit connected in the manner shown in Figure 3.4. To prevent any possible electrical shorting in the gauge due to the flow of the saline solution on the specimen, the gauge was covered by a thin layer of transparent nail varnish that worked as a waterproof coating for the gauge.

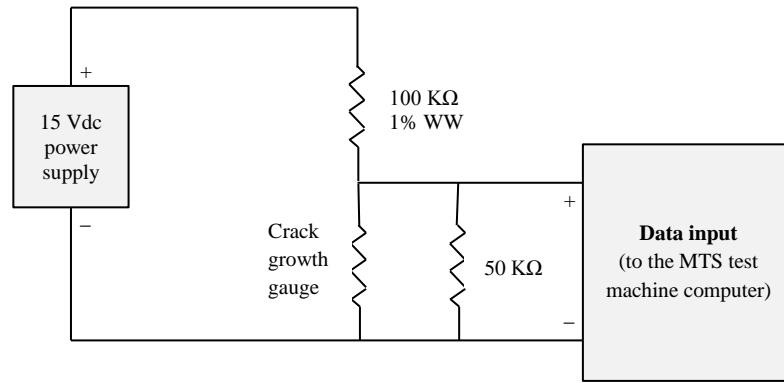


Figure 3.4 An electrical circuit showing the prescriptive method of connecting the crack gauge and the readout instrument [redrawn from Vishay (2014)]

3.2.3.3 Fatigue of CT specimens and data acquisition

For each test, a CT specimen, with a crack gauge adhered to it, was installed in the MTS machine by two metal grips through the machined holes where the pre-crack was aligned horizontally to ensure a perpendicular cyclic loading on the crack growth direction. Once the specimen was properly installed and the gauge connected to the electrical circuit that was connected to the MTS system, using specified input points. The selected MTS fatigue procedure included choosing a data acquisition feature that allows measuring the gradual change in voltage in the circuit due to the gradual breakage of the gauge strands. The specimen was covered by continuously flowing 37°C saline inside the closed environmental chamber and subjected to uniaxial tension-tension cyclic loading at a frequency of 2 Hz until failure, repeating this for all the CT specimens. Figure 3.5 illustrates the fixation of a CT specimen, the crack measurement gauge position and connections and the flowing saline.

For the purpose of having adequate time to monitor the crack growth over testing, the range of the stress was performed between $0.1P_{max}$ and $0.5P_{max}$ where P_{max} is the force required to break a CT specimen under tensile loading. In order to obtain a reference value of this failure force, two CT specimens from each of the two bone cements were selected randomly and subjected to tensile loading of speed of 1 mm/min until failure, recording the failure force as P_{max} . If a specimen was found to have macro-porosity or other defects that might provide misleading results, a replacement CT specimen was tested to obtain the required tension failure force. It is to be noted that the maximum level of test stress was below that reported *in vivo* due to the effect of the pre-

cracked notch in accelerating the crack initiation and propagation as the aim is only to monitor the fatigue crack propagation and measure its rate.

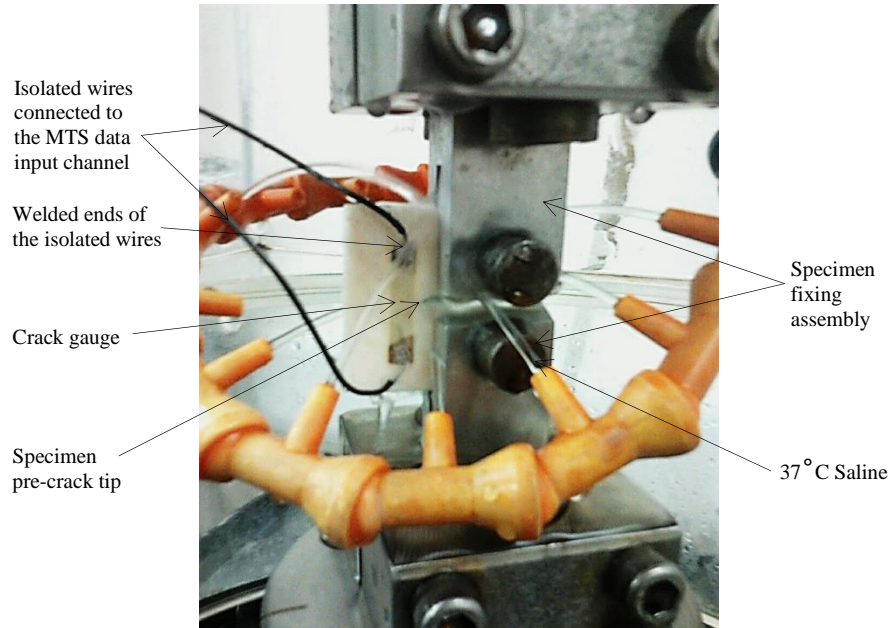


Figure 3.5 A CT specimen with a crack measurement gauge during testing

Once the fatigue test had started, data was collected in the manner specified within the selected MTS procedure. This included recording the force, displacement and cycles to failure data against time points in conjunction with the sudden changes in voltage. Since the gauge has a number of parallel strands that are gradually fractured as the crack propagates in the specimen, the break of each strand shows as a step increase in voltage which reflects crack growth of a length equalling to the width of the fractured strand that corresponds to a certain number of cycles to failure.

3.3 DATA ANALYSIS

Fatigue testing data, which was collected as described above, was compared and analysed using various theoretical and statistical methods. Two main fatigue data analysis techniques were used to compare results: Weibull analysis and Wöhler (or S-N curve) analysis. These were selected due to being widely used in analysing fatigue results of bone cement. One of the considerations of this study was to examine the effect of adopting particular analysis techniques, if existed, on the interpretation of fatigue

results. With either technique, further statistical analysis approaches, such as ANOVA (analysis of variance) and Student's *t*-test, were used, as appropriate, to measure the significance of variance. If further investigation or analysis was required, that could not be performed on every specimen in each group; the median cycles to failure specimen was usually used as an indicator of the performance of all specimens of a particular group. For particular analyses, the specimens with the highest and lowest fatigue lives in each group were included whenever it was appropriate and possible. This was specifically used for the analysis and comparison of fracture growth behaviour of various stress regimes using the changes in the absorbed energy and apparent modulus as the specimen encounters gradual increase in the fatigue damage over the cyclic loading period.

3.3.1 Weibull analysis

Graphical and analytical descriptions of Weibull functions were used to evaluate and compare the fatigue results of the testing regimes. Due to the longer testing time and more material required to provide sufficient data to perform Weibull analysis, only fully reversed tension-compression cyclic loading at 20 MPa ($R = -1$) and tension-tension loading of maximum stress of 20 MPa with $R = 0.1$ were included in the Weibull analysis. Fatigue testing of the fully reversed manner was performed at ± 20 MPa due to particular considerations. First, although it has been reported the *in vivo* stress levels range between 3-11 MPa (Krause and Mathis, 1988), most of the *in vitro* studies have been performed at higher stress ranges due to the fact that testing at the *in vivo* levels will require extremely long periods of time, particularly when testing a large number of specimens. Second, the stress of ± 20 MPa lies in the mid-range when it comes to the various *in vitro* fully reversed tension-compression stress levels reported in the literature, which are mainly in the range of between 10 MPa and 30 MPa (Lewis and Nyman, 2000). Third, the maximum stress level of 20 MPa corresponds to approximately 50% of the tensile strength of that reported for the leading cement brands (Webb and Spencer, 2007).

As both the two- and three-parameter Weibull distributions have been used in analysing fatigue results of bone cement and since it has been reported that the three-parameter Weibull may perhaps provide more accurate estimation to the Weibull modulus (Curtis

and Juszczyk, 1998), both distributions were used in the analysis of results and the effect of adopting one distribution rather than the other was examined. For both distributions, the number of cycles to failure of a group of specimens was plotted against the Weibull variate (Y) that was calculated according to Equation 3.1. The testing groups were then compared within the same Weibull graph or using various graphs as appropriate. The only difference between the two- and three-parameter Weibull distributions is that the cycles to failure for the latter were plotted after considering the subtraction of the third parameter value from each cycle to failure result, providing corrected values to the other two parameters.

3.3.1.1 Significance of variations in fatigue results

Since it is advised that “Weibull distributions should be derived using a significant number of data points” (Ramulu, 1999) which was estimated for fatigue testing of bone cement to be a minimum of either 7 or 11 specimens for the two- and three-parameter Weibull distribution functions respectively (Lewis and Sadhasivini, 2004) or a minimum number of 10 specimens as used in other studies that included either three-parameter Weibull analysis such as Deb et al. (2003) or two-parameter analysis such as Harper and Bonfield (2000) and Tanner et al. (2010), at least 10 specimens were tested and accepted per test group. The results of these groups were compared, considering the effect of a single or combination of particular variables at a time, to measure the significance of variance at a 5% confidence level, using ANOVA analysis followed by Student’s t -test as appropriate. This variation analysis was adopted to provide more reliable conclusions in terms of comparing Weibull functions as these functions afford excellent indicators of the trend of fatigue results, but they do not include a precise statistical hypothesis test that leads to confident conclusions whether or not the variations in results, or even in Weibull parameters, are significant.

To begin with, for a given bone cement composition, the effect of the combination of specific specimen shape and production method was assessed by statistically measuring the significance of variations in results of the four specimen type groups. The p -values that were obtained for these groups of each cement composition were compared against each other (RDM vs RMM vs CDM vs CMM). Likewise, for a given shape and production method, the effect of the chemical composition variable was examined by comparing each specimen type group of one cement to its counterpart of the other

cement. Subsequently, the same cement specimens were compared according to the difference in specimen shape or production method only. This statistical approach was conducted prior to the Weibull analyses to assess the significance of variations in results for both the fully reversed tension-compression stress regimes and the tension-tension stress regimes.

3.3.1.2 Two-parameter Weibull distribution

To perform the two-parameter Weibull, the number of cycles to failure of the specimens in each testing group of a particular type of stress were ranked in ascending order to plot the logarithm of life data [$X = \ln(N_f)$] against Weibull variate [Y]. This variate was determined using Equation 3.1 which requires calculating the cumulative probability of failure $P(N_f)$ using Bernard's approximation (Equation 2.23). Fatigue results for all specimen groups, of each stress type, were subsequently presented according to their cement formulation on two comparable graphs to obtain four two-parameter Weibull relationships (regression curves) for each cement.

$$Y = \ln \ln \left[\frac{1}{1 - P(N_f)} \right] \quad (3.1)$$

The two-parameter Weibull distribution relationship used for the analysis (the linearised form) is given in Equation 2.25. The importance of Equation 2.25 is that the left hand side of the equation represents the Weibull variate where the higher this number, the greater the fatigue performance. The right hand side of the equation is dependent on the variables b and N_a . The Weibull modulus for a testing group was obtained as the slope of the regression curve that best fits the set of data points of this group. The scale parameter N_a is obtained as the N_f value that meets with a Weibull variate of $Y = 0$ in Equation 3.1 which represent the value that below which lie 63.2% of the N_f results. The determination of b and N_a parameters is illustrated in Figure 3.6.

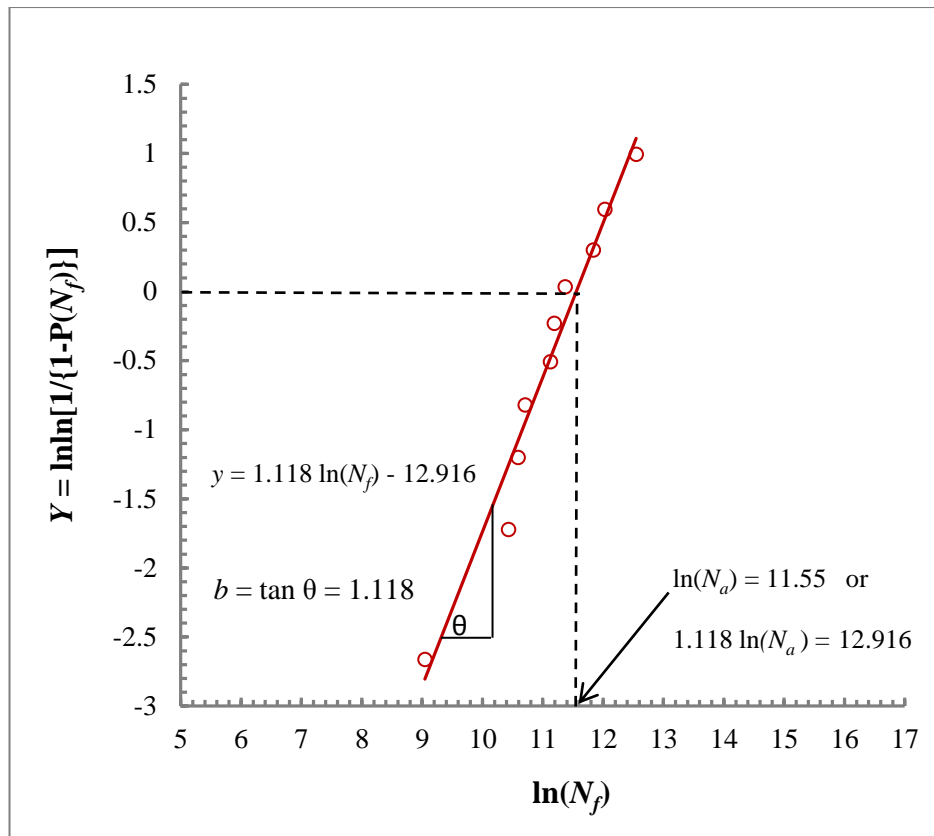


Figure 3.6 An example of a diagram illustrates the determination of b and N_a for the two-parameter Weibull functions (actual results of one of the testing groups)

3.3.1.3 Three-parameter Weibull distribution

The three-parameter Weibull distribution is generally similar to the two-parameter distribution. This three-parameter approach, however, is performed by considering a third parameter (N_0) that is known as the guaranteed or the minimum fatigue life (the number of cycles below which the probability of failure is zero) which is assumed to be zero cycles for the two-parameter distribution. To establish the three-parameter Weibull, the specimens were fundamentally arranged and ranked in the same manner used for the two-parameter analysis. The Weibull variate (Y) and the probability of failure were also determined in the same way using Equations 3.1 and 2.23, respectively. The three-parameter Weibull distribution relationship used for the analysis (the linearised form) is given in Equation 2.27.

Unlike the two-parameter function, the determination of the Weibull parameters started with estimating the guaranteed parameter N_0 , as in Shigley and Mischke (1989), where, for each testing group, the fatigue data was initially plotted providing $N_0 = 0$ and the

best fit of a “French curve” was drawn as illustrated in Figure 3.7. Three points were then located on the curve so that the reflection of these points on the Y axis leads to equal distances between the middle point and each of the upper and lower points. The reflection of these points on the $\ln(N_f)$ axis identifies three values of $\ln(N_f)$ that were used according to Equation 3.2 to estimate N_0 (Shigley and Mischke, 1989). Similar way of estimating the third parameter was suggested by Janna et al. (2005) for their method of analysing results using the Weibull distribution functions.

$$N_0 = N_{f2} - \frac{(N_{f3} - N_{f2})(N_{f2} - N_{f1})}{(N_{f3} - N_{f2}) - (N_{f2} - N_{f1})} \quad (3.2)$$

Once the fatigue life parameter was estimated, its value was subtracted from the cycles to failure results to obtain $(N_f - N_0)$ values. To generate a Weibull function, the natural logarithm of each of these values [i.e. $\ln(N_f - N_0)$] was plotted against the corresponding Y value from Equation 3.1. As can be seen from Figure 3.8, $\ln(N_a - N_0)$ corresponds to $Y = 0$, providing the point on the curve at which, according to Equation 3.1, 63.2% of specimens would have fractured. The determination of N_a and b was then performed as illustrated in Figure 3.8.

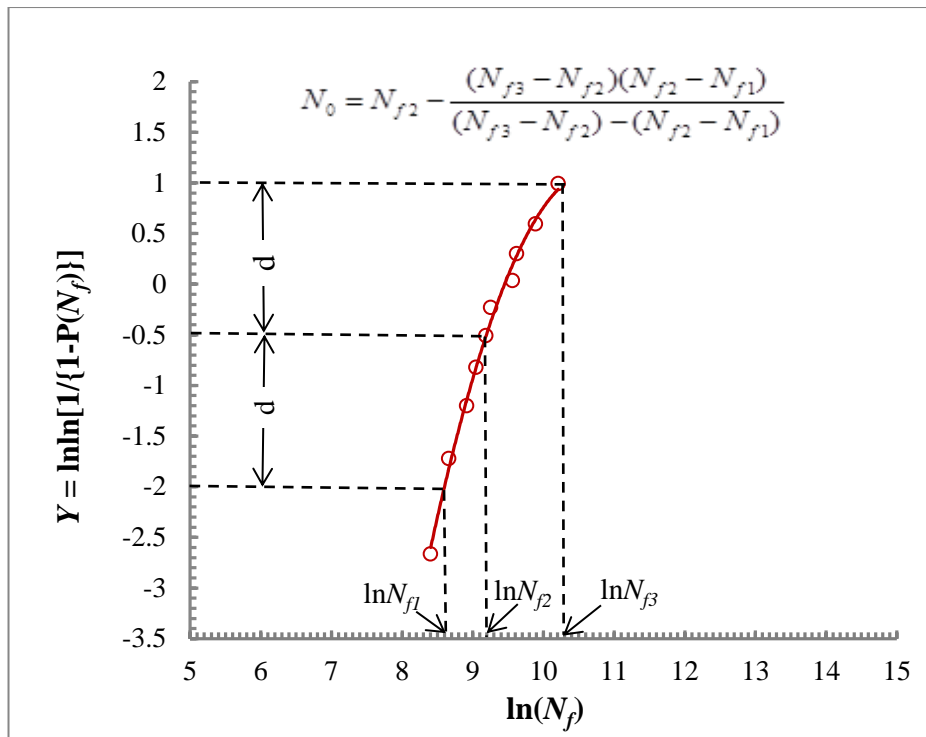


Figure 3.7 An example of a diagram illustrates the determination of N_0 for the three-parameter Weibull functions (Actual results of one of the testing groups)

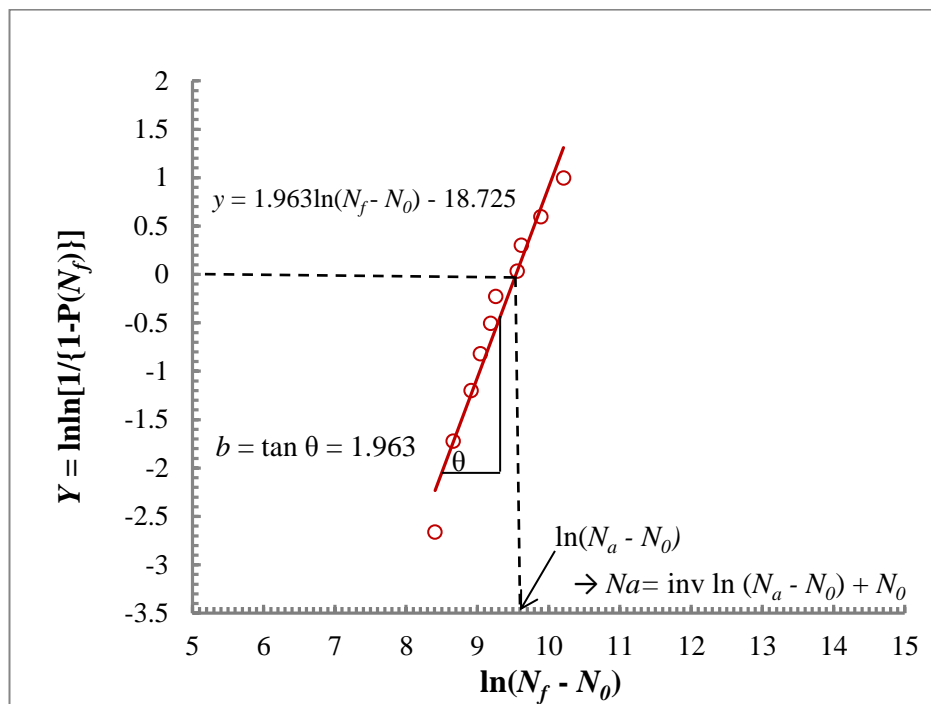


Figure 3.8 An example of a diagram illustrates the determination of N_a and b for the three-parameter Weibull functions (same data set as Figure 3.7)

3.3.1.4 Fatigue performance index

Providing further analysis to the comparable Weibull distribution functions can be of importance since the description of fatigue results, according to these functions, is achieved mainly graphically along with comparing the Weibull parameters that each of which is an indicator of a particular property, as discussed above. To provide an overall indicator that provides easier and more consistent comparison to the Weibull functions, including the combined indication of the Weibull parameters, a fatigue performance index, I , was determined for each testing group (Weibull function) using Equation 2.28. For the two-parameter Weibull, this index is a function of the estimated N_a and b only. For the three-parameter analysis, however, the index is a function of N_0 as well, as it is determined using the corrected N_a and b . The fatigue performance index has been reported in several studies of fatigue testing of bone cement including (Lewis, 1999a), Lewis (1999b), Dunne et al. (2003) and Janna et al. (2005).

3.3.1.5 Skewness of Weibull distribution (density function)

Weibull modulus (b) is a measure of skewness of data away from a certain optimal range (approximately $3 < b < 4$) during which “approximate symmetry is obtained along with a good approximation to the normal distribution” (Shigley and Mischke, 1989) and that, as illustrated by Figure 3.9, “large b ’s skew the distribution to the left and small b ’s skew the distribution to the right ” (Shigley and Mischke, 1989). If all b values are below this range, the dispersion of the N_f data is relatively measured so that the higher b value the lower the skewness to the right. According to these hypotheses, the skewness of fatigue results of a particular testing method (density function of the Weibull distribution) was assessed by means of the value of the Weibull modulus. This was applied to all the testing methods and the Weibull moduli were compared and the differences in the effect of these moduli on the Weibull distributions were identified.

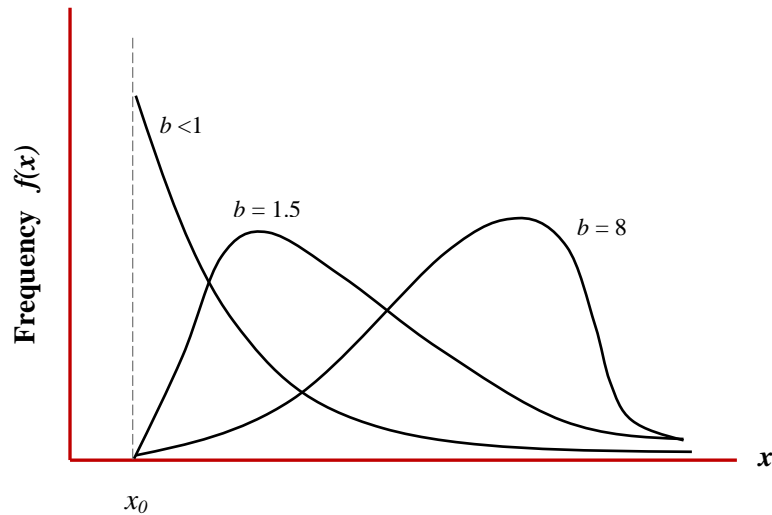


Figure 3.9 The density function of the Weibull distribution showing the effect of skewness of the shape parameter b [adapted from Shigley and Mischke (1989)]

The probability density functions were determined for the two- and three-parameter Weibull using Equations 3.3 and 3.4 respectively, which are derived by the integration of Equations 2.24 and 2.26 respectively.

$$f(N_f) = \frac{b}{N_a} \left(\frac{N_f}{N_a} \right)^{b-1} \exp \left[- \left(\frac{N_f}{N_a} \right)^b \right] \quad (3.3)$$

$$f(N_f) = \frac{b}{N_a - N_0} \left(\frac{N_f - N_0}{N_a - N_0} \right)^{b-1} \exp \left[- \left(\frac{N_f - N_0}{N_a - N_0} \right)^b \right] \quad (3.4)$$

3.3.2 Wöhler (S-N) curves

Considering the reality that bone cement has been tested *in vitro* at various stress levels, it can be important to examine the effect of changing the stress amplitude on the fatigue life of a particular specimen type made from a particular bone cement composition. In order to provide findings that compare the trends of various fatigue test regimes considering a range of stress levels that include most of the *in vitro* testing stresses as they have been reported in the literature, S-N curves (Wöhler curves) were used to achieve this comparison using four fully reversed tension-compression stress levels; namely, ± 12.5 MPa, ± 15 MPa, ± 20 MPa and ± 30 MPa. For each specimen type at each

of these stress levels, a minimum of five specimens were tested as recommended in ISO 527-1 “for each of the required directions of testing” (BSI, 2012a). This sample size is close to that postulated by ASTM E739 (ASTM, 2004) which is a minimum of 6 specimens when performing S-N curves for preliminary and exploratory research. For S-N analysis of bone cement fatigue results, a sample size of 5 specimens was used by Jeffers et al. (2005) while a sample size of 8 was used by Tanner et al. (2010).

All the S-N curves were performed in the form of stress-life diagrams that plot the maximum applied fatigue stress (independent controlled variable) against the logarithm to base 10 of the cycles to failure (dependent random variable), following the same manner of particular studies such as Davies et al. (1987), Murphy and Prendergast (2000) and Tanner et al. (2010). As all tests were performed in fully reversed tension-compression conditions, the maximum applied stress is equal to the stress amplitude (σ_a). At least five data points for each specimen type were obtained for each of the four stress levels.

An S-N curve was generated for each specimen type, representing the trend of the fatigue life of each type over the examined range of stress levels. The S-N curves were presented as regression lines that were fitted to the complete data set of each specimen type. This can, as reported by Murphy and Prendergast (2000), help in predicting fatigue lives at lower stress amplitudes based on the assumption that the relationship between the stresses and number of cycles to failure is approximately linear. The fatigue results were compared according to these curves that represent the fatigue behaviour of particular specimen shapes and production methods and, meanwhile, considering the effect of variations in cement composition. The equations of the S-N lines involve identifying the regression coefficients (slopes) where the analysis of variance between these slopes can be valuable in predicting and comparing the fatigue life of various sets at the lower stress levels.

3.3.2.1 Comparison of S-N curves of various specimen types

To provide an overall comparison of the fatigue results of different specimen shapes and production methods for both cements at various stress levels, two comparable S-N diagrams were plotted. Each diagram included four S-N curves that each of which describes the fatigue behaviour of a particular specimen type as the maximum stress of

the constant stress ratio ($R = -1$) changes between the four given values (± 12.5 MPa, ± 15 MPa, ± 20 MPa and ± 30 MPa).

One main advantage of performing this comparison is providing general diagrammatic illustration that includes within it numeric estimations of the fatigue life for all stress regimes. The assumption is that, if the fatigue life of various specimen types would differ, the S-N curves representing these types of specimen would appear dissimilar in terms of their regression coefficients and the position of the curves. When comparing the curves to each other, the curves with the greater slope refer to increased fatigue life as the stress amplitude declines. The curves where their position on the diagram is largely or totally to the right indicate greater fatigue performance compared to their counterparts.

3.3.2.2 Comparison of S-N curves of different cements

Separate S-N diagrams were performed to compare the fatigue behaviour of the similar shape and production method specimens according to their chemical composition. Each diagram, therefore, compared two S-N curves to see whether (or not) the chemical composition has a significant influence on the stress regime being controlling the fatigue life. Considering the variations in regression coefficients, the results shown on each diagram were, in the first instance, compared separately to consider the effect of cement composition when the same specimen type was used and, subsequently, the results of a total of four diagrams were compared together to obtain comparable conclusions on the effect of specimen type in each case.

Previously, for the fully reversed tension-compression, Tanner et al. (2010) found a maximum difference factor of only 2 between the median fatigue lives of four cements. They tested only one specimen type at these conditions (that is circular machined) comparing their findings as S-N curves, where three curves showed similar trend and the only one curve of the cement that provided an increased fatigue life (up to double) was matchlessly located to the right of all the other three curves over the entire stress range involved in testing. Based on this, the findings of the current study were compared in the same manner for the two cement compositions; however, this process was performed for the four specimen types considered in the study, providing wider range of comparisons in terms of stress regimes.

3.3.2.3 Consideration of the effect of individual stress levels

Since the S-N curves were established on the base of fatigue data points that were collected from testing of specimens at specific fully reversed stress amplitudes, the fatigue results at each of these stress levels were compared individually for all specimen types to closely assess the effect of stress amplitude on fatigue results, thus providing more interpretation to the trends of the S-N curves. Typically, it is expected that, when comparing the S-N curves of similar structure materials that were tested in the same manner and under the same conditions, the curves would be identical or nearly identical. If this was not the case, logical reasons need to be provided in order to justify the variations between the curves. Accordingly, for the considerations of this study, any significant differences between the S-N curves were related to the effect of the specimen shape and production method when one cement composition was considered or the effect of the cement composition when the same specimen types of two cements were compared.

In order to provide further explanations to the variations of the S-N curves, the statistical median of each specimen type group at each stress level was used to represent the fatigue performance of each group. At each stress level, factors of difference between the median fatigue lives were determined between the specimen types of each bone cement composition and also between the same shape and production method of both cements. Subsequently, additional comparisons were performed between the findings of fatigue lives at each of the stress amplitudes particularly when the S-N curves provided apparent dissimilar trends. This statistical comparison was considered since it can provide two advantages: first, comparable fatigue lives at various stress amplitudes individually and, second, therefore, understanding the effect of changing the stress amplitude on fatigue lives of specimen types in contrast with each other, comparing these findings for the two cement compositions.

3.3.3 Cyclic stress-strain response (hysteresis curves)

Weibull functions and Wöhler curves consider the fatigue life only (i.e. the last recorded load cycling data point before failure), but provide no clear indications of how fatigue cracks initiate and propagate. To investigate and compare the behaviour of fatigue

cracks, hysteresis loops were used to estimate the changes in absorbed energy and apparent modulus per loading cycle, using these as fatigue damage indicators.

3.3.3.1 Rationale for considering absorbed energy and secant modulus

The idea of using the absorbed energy concept is built on what has widely been reported regarding the proportional relation between the fatigue crack growth and the hysteresis energy. This energy based criterion is generally divided into two categories depending on the hypothesis being considered: the amount of absorbed energy is constant and independent of the number of cycles to failure or the amount of absorbed energy changes as the cycles to failure progress (Ellyin, 1997). To simplify the process, it is supposed that “a fatigue crack growth can be thought of as resulting from energy dissipation (or energy absorption) in the plastic zone” (McCartney, 1996). The change in energy absorption, however, is theoretically attributed to the creation of new free surfaces within the crack zone (Milella, 1999), reflecting the process of crack initiation and propagation. For most materials, the energy required for a crack to propagate increases as the crack extends (Spurgeon, 2009).

Likewise, it is well known that the apparent elastic modulus decreases as the fatigue crack propagates since it is a measure of the stiffness of materials. Therefore, the general relation between the change in absorbed energy and apparent modulus is that the increase in energy follows the same trend as the decrease in moduli (Hoppel and Pangborn, 1994). From here, the secant modulus is widely used to evaluate the fatigue damage, which is controlled by the shape of the hysteresis loop. It is defined as the “ratio of stress to the corresponding strain at any specific point on the stress-strain curve” (Rosato et al., 2001). Therefore, the modulus can be represented by the secant modulus, knowing that it is not necessarily equal to the Young’s or tangent moduli (Rosato et al., 2001). Accordingly, the reduction in the secant modulus throughout cyclic loading can be used to describe the degradation of the material integrity, indicating the gradual growth of the fatigue cracks.

3.3.3.2 Estimations of absorbed energy and secant modulus

To compare the progress of fatigue damage in various specimens according to the concept of absorbed energy and secant modulus variations, the data of a “typical

specimen” from each testing group, that is the median or the one close to the median cycles to failure, was selected to compare a total of 8 median specimens. The force and displacement data of these specimens was converted into stress-strain after selecting data points of certain loading cycles throughout testing. Depending on the fatigue life, the 10 data points of particular cycles, such as the 10th, 100th, 1000th, 5000th, 10000th, 20000th, 50,000th, 100,000th, 200,000th, 500,000th and so on, were used in the analysis, ensuring the inclusion of the data of at least one cycle within each base 10 logarithmic unit on the logarithmic scale of the cycles to failure count. To ensure recording data points for the last cycles before failure to estimate the crack growth behaviour when close to failure, the 5th, 100th and 1000th cycles before the failure cycle were also considered.

Each point of the 10 data points of each of the considered cycles included calculating the instantaneous stress and strain (correction factor was applied to the strain results as explained in the next section). Each cycle has a stress-strain loop that was identified by these 10 data points. On the stress-strain diagram, the area inside the loop is representative to the energy absorbed during that particular loading cycle. The area of this enclosure loop was estimated using Trapezoid rule for the determination of the area of an enclosed (polygonal) shape which, for stress strain variables, can be written as Equation 3.5. To validate the calculations of this Equation, Green’s theorem (Equation 3.6), which here affords the same service as the trapezoid rule, was used simultaneously. As illustrated by Figure 3.10, the area of the loop is approximately equal to the area of the polygonal that is formed from connecting the data points of the cycle, moving (clockwise) in order from a first point, $(\varepsilon_1, \sigma_1)$, and finishing by a last point, $(\varepsilon_{10}, \sigma_{10})$, that is connected to the original point to close the loop.

$$A_{loop} = \frac{1}{2} \sum_{i=1}^n (\sigma_i + \sigma_{i+1})(\varepsilon_{i+1} - \varepsilon_i) \quad (3.5)$$

$$A_{loop} = -\frac{1}{2} \sum_{i=1}^n (\varepsilon_i \sigma_{i+1} - \varepsilon_{i+1} \sigma_i) \quad (3.6)$$

where A_{loop} is the area of the loop, i is the data point rank number ($i = 1, 2, 3 \dots 10$), n is the number of data points ($n = 10$), σ_i is the instantaneous stress and ε_i is the instantaneous strain at the point i .

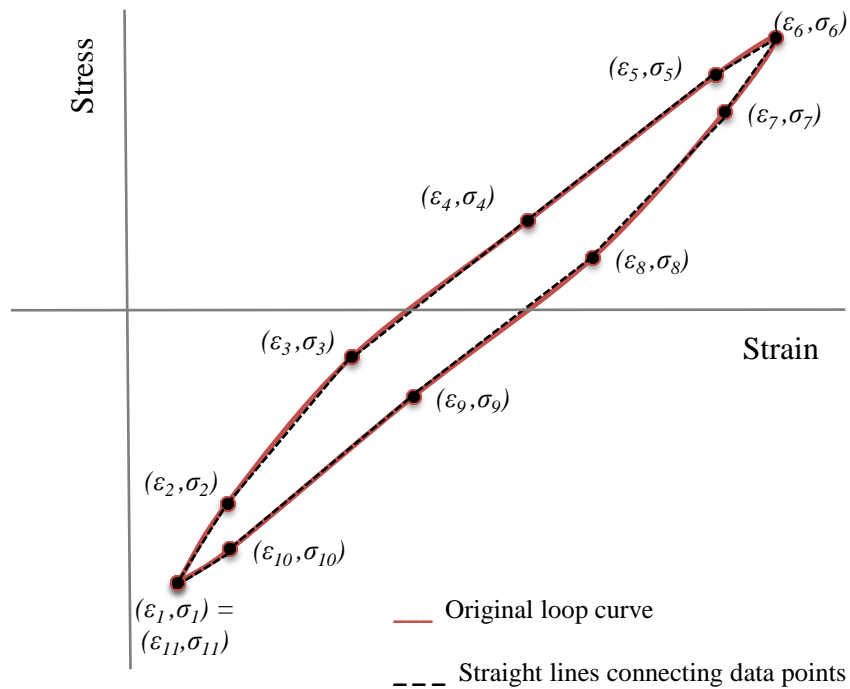


Figure 3.10 A hysteresis loop showing the distribution of data points of a fatigue cycle where the absorbed energy was estimated as the area of the loop (cycle data was taken from the last fatigue stages of actual results of a SmartSet CMM specimen fatigued at ± 20 MPa)

On the stress-strain diagram also, the secant modulus, for the fatigue cycles, was determined as the slope of the line that connects the two extreme points of the hysteresis loop. Figure 3.11 shows three hysteresis loops where each loop was drawn from 10 stress-strain data points of the same fatigue cycle (the three cycles were selected from the actual results of one specimen at various testing stages). This Figure illustrates that, as the cyclic fatigue progresses, the area inside the loop increases and the slope of the secant line decreases. In view of that, the fatigue fracture behaviour was compared for different specimen types and the variations in results were reported and analysed. The creep occurred in specimens can also be assessed from the points the secant line crosses the horizontal (strain) axis.

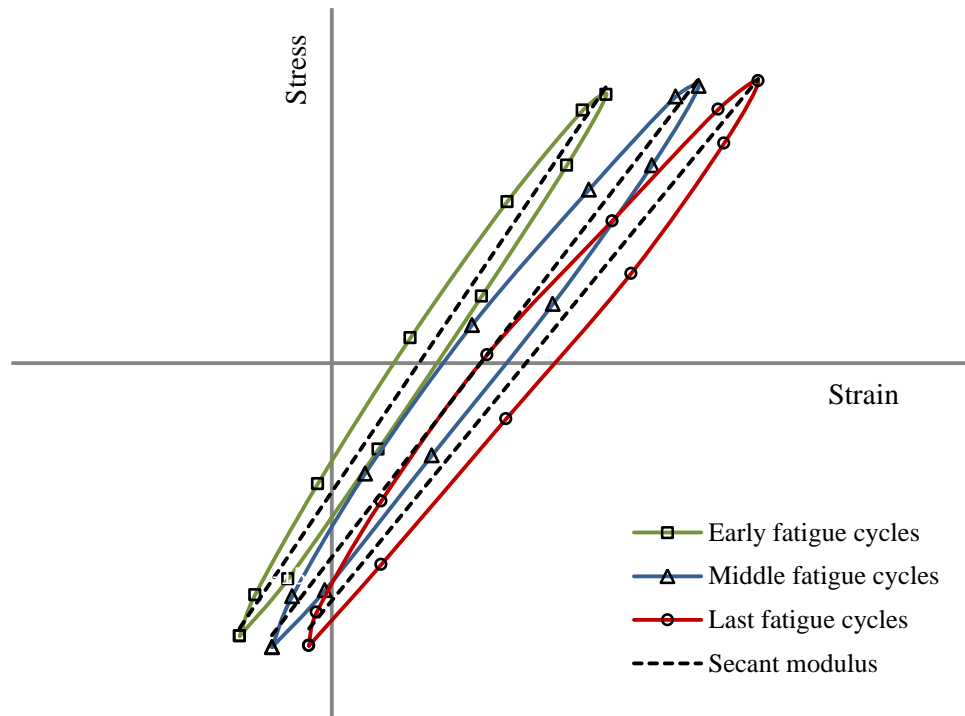


Figure 3.11 *Illustration of changes in absorbed energy (increase in loop area), secant modulus reduction (decrease in secant slope) and creep (point where secant line crosses the horizontal axis) as the cyclic fatigue progresses*

3.3.3.3 Consideration of a strain correction factor

Prior to establishing the S-N hysteresis loops, a correction factor was applied into the strain results, where two values of this factor were determined depending on the specimen shape. This is due to the reality that the two specimen transition sections (shoulders) between the grips and the gauge section are included in testing and the effect of these sections on the results must be excluded. These factors were determined using integral calculations (Appendix 1) and found to be 0.667 and 0.412 for the rectangular and circular specimens, respectively. Multiplying the initial strain results by these factors will provide the approximate strain occurred in the gauge sections and exclude the strain in the transition sections.

3.3.3.4 Fatigue cycles versus absorbed energy and modulus

In order to obtain plots of cycles to failure against either absorbed energy or secant modulus per loading cycle, the calculations of the energy and modulus were performed

starting from the 10th fatigue loading cycle followed by all the other examined cycles over the testing period and ending with the 1000th, 100th and 5th cycles before failure. Findings of the change in absorbed energy per loading cycle along with the reduction in secant modulus were compared diagrammatically, as appropriate, according to the variation in specimen shape and production method of each cement composition. This process included comparing the energy and modulus behaviour when various stress levels were used.

To obtain diagrams that show the behaviour of the absorbed energy per loading cycle as the cycles to failure progress, considering the logarithmically selected cycles only, each absorbed energy value (that was initially obtained in MPa and converted into kJ/m³) was plotted against the relevant cycle number on a log scale. The aim of this step was to observe any significant change in the amount of absorbed energy over the fatigue testing period to reflect the crack growth behaviour. Similarly, the relation between the change in modulus and fatigue life was represented on separate diagrams. The slope of the secant for each of the selected loops was plotted against the relevant cycle number on the log scale to assess the expected reduction in modulus over the fatigue life. This process was performed for the median specimen of each specimen type group at each stress level and the findings were compared for the two cements.

3.3.4 Fatigue crack growth in CT specimens

The fatigue crack length was measured at different points at each breakage of a gauge strand. As the breakage of each strand shows a step increase in voltage, the instantaneous crack length was identified using Equation 3.7.

$$a = a_0 + n(\Delta a) \quad (3.7)$$

where, n is the number of gauge strands broken at a certain stage and Δa is the crack growth increment that represents increase in crack length after the fracture of each strand ($\Delta a = 0.25$ mm).

Once the crack length was obtained at each stage, the crack growth per loading cycle was determined using Equation 3.8. Also, the stress intensity factor range ΔK was determined at each crack increment point according to Equation 3.9 (ASTM, 2013).

$$\left(\frac{da}{dN}\right)_i = \frac{a_i - a_{i-1}}{N_i - N_{i-1}} \quad (3.8)$$

where, $\frac{da}{dN}$ is the crack growth rate and i is the strand number ($i = 1, 2, 3, \dots, 20$).

$$\Delta K = \frac{\Delta P}{B\sqrt{W}} \frac{(2 + \frac{a}{W})}{(1 - \frac{a}{W})^{3/2}} \left[0.886 + 4.64\left(\frac{a}{W}\right) - 13.32\left(\frac{a}{W}\right)^2 + 14.72\left(\frac{a}{W}\right)^3 - 5.6\left(\frac{a}{W}\right)^4 \right] \quad (3.9)$$

where, ΔP is the difference between the maximum and minimum fatigue forces, W is the specimen width, B is the specimen thickness.

From the results of each testing specimen, two graphs could be generated depending on the validity of the obtained results. One graph was produced by plotting the measured crack lengths, at the time of strand breakage, against the associated number of cycles to failure, describing the relation between the crack growth and fatigue cycles. The other graph, which has been widely related to the use of compact tension specimens, describes the crack propagation rate as a function of the stress intensity factor. It has been reported that, when load amplitude is constant, the stress intensity factor increases with crack propagation for most specimen geometries (Bucci, 1981). It was considered therefore, the values of the stress intensity range should show an increase as the crack propagates. Paris' power law (Equation 2.17) was subsequently used to compare the findings for the tested CT specimens. To generate a power law fit, the data was presented on a log-log plot of da/dN versus ΔK . This was done in two ways: one was to generate a trend line fit for the data of each specimen individually and the other was to generate one fit for the data of all the identical specimens (i.e. the same material specimens).

3.4 POST-FATIGUE FAILURE INVESTIGATIONS

As fatigue failure mechanisms of a component or specimen can be largely described by the characteristics of the fracture surfaces at the point where the failure occurred, the fracture surfaces of specimens were examined further after being initially investigated for macroporosity, as discussed above. Many specimens of the testing groups were examined using an optical microscope, with particular focus on the median specimens. The aim was to investigate the existence and distribution of porosity and its role in developing fatigue cracks in addition to the effect of the opacifier fillers and the other additives. Due to having limited access to a scanning electron microscope, the examination of fracture surfaces using this device was performed only on the median specimens of those testing groups that were tested in fully reversed cyclic loading at $\pm 20\text{MPa}$ (total of 8 specimens). Differential Scanning Calorimetry (DSC) analysis was similarly conducted on the same specimens to consider the effect of each specimen shape and production method for the two cements on the degree of polymerisation.

3.4.1 Microscopic investigations of fracture surfaces

The SEM involved examining the eight median specimens of the testing groups fractured at the $\pm 20\text{MPa}$ stress type. The investigation of the fracture surfaces was performed using a scanning electron microscope (Hitachi, S4700 FE-SEM) from a lower magnification level (1mm scale bar on the micrograph), to allow the observation of a whole fracture surface, to higher magnification levels (down to $5\mu\text{m}$ scale bar) to provide a detailed description of the material's structure, distribution of the additives, the degree of cohesion between the cement matrix and the added elements and any resultant micro defects.

An optical microscope (Olympus, SZH-ILLD) was used to perform more frequent microscopic investigations for all testing groups, mainly to have general comparisons between the fracture surfaces in an attempt to see the effect of stress regime, along with the existence of stress concentrations, on controlling the initiation and propagation of fatigue cracks. A digital camera was used to obtain graphs of the fracture surfaces for the different specimen and stress types. Also, side views of the fractured gauge sections of particular specimens (mainly the medians) were photographed (approximately within

1mm from the fracture surface) to, first, have closer view to the moulded or machined surfaces for both specimen shapes and, second, to compare the “disconnection topography” of various specimens for all testing regimes and bone cement types.

3.4.2 Differential Scanning Calorimetry (DSC)

The amount of residual monomer has been reported to potentially affect the fatigue life of bone cement specimens (Lewis and Janna, 2003). Any variations in the degree of polymerisation (residual monomer) might influence the fatigue life of specimens depending on their chemical composition and their type. The aim of involving the DSC analysis was therefore to, first, estimate the degree of polymerisation for every specimen type of each cement and, second, find the significance of variations in the degree of polymerisation among all specimen types.

The specimens with the median fatigue life of those that were tested in fully reversed tension-compression of ± 20 MPa were involved in the analysis, thus representing the specimen types for all stress regimes. After fatigue failure, each of these median specimens was grinded using a clean and rough hand file at a fracture surface side to obtain a sufficient amount of “grated cement”. For each specimen type, a sample of approximately 5mg in weight was used for the DSC experiments. The sample was put in an aluminium pan in the DSC chamber (DSA-Q100, TA Instruments) with the use of another empty aluminium pan as a reference.

The analysis involved three successive thermal processes: (1) heating the sample from 25°C to 180°C, (2) cooling it to the initial start temperature of 25°C and (3) heating it for a second time to the 180°C temperature. The heat flow of the three processes (all at a rate of 10 °C/min) was plotted against the temperature to obtain three comparable heat flow behaviours for each bone cement composition and specimen type. The two heating processes (1 and 3) were compared together and the difference in heat flow between the two processes was considered as the difference in degree of polymerisation, as the exotherm that can be produced during the first heating process different from the second heating process is due to the non-reacted MMA monomer. The results for all specimen types were compared and the significance of variations in polymerisation degrees was statistically measured, using Student’s *t*-test.

CHAPTER 4. TOTAL FATIGUE LIFE

4.1 INTRODUCTION

This chapter examines and compares the fatigue life (number of cycles to failure) for all the specimen types and cyclic loading types and levels considered in the current study. The aim is thus to compare the fatigue performance when various stress regimes are used discussing the effect of these variations on controlling the fatigue longevity, apart from the fatigue crack propagation behaviour which is considered in the next chapter. Many of the reported studies that have examined fatigue of bone cement considered the total fatigue life only and analysed the results according to these findings, which is usually followed by observations of the fracture surfaces. When the effects of particular variables on the fatigue properties of the material were investigated, the fatigue life results were compared using various data analysis approaches. Among these, and apparently the most applicable approaches, are Weibull analysis (that includes determining the probability of fracture) and Wöhler analysis (that can be used to predict failure at unexamined stress levels). Accordingly, for the purpose of the current study, the fatigue results of all testing groups were compared using these two approaches, including both the two- and three-parameter Weibull distributions. The aims, therefore, are to (1) provide comparisons between the fatigue longevity of the various stress regimes, (2) predict the fatigue life at lower stress amplitudes and (3) examine the effect of the selected analysis approach, if any, on describing fatigue results.

4.2 METHODS

The test specimens were prepared, assessed and classified as described in Section 3.2.1. In order to perform the fatigue test and obtain fatigue life (number of cycles to failure), the specimens were fatigued to fracture in the manner detailed in Section 3.2.2. Once the sufficient number of specimens required for each testing group was tested, the fatigue data was analysed as described in Section 3.3.1 for Weibull analysis and as described in 3.3.2 for the S-N curve (Wöhler) analysis. Weibull distributions were examined using both the two- and three-parameter approaches to compare the fatigue results of the fully reversed tension-compression and the tension-tension stress regimes.

S-N analysis was performed for the fully reversed stresses only. In addition, after fatigue failure, the fracture surfaces of particular specimens (such as the median specimens or those with the longest and the shortest fatigue lives) were microscopically observed as described in Section 3.4.1. The DSC analysis was conducted as summarised in Section 3.4.2 to investigate the variations in the residual monomer and the effect of this factor on the final fatigue results.

4.3 RESULTS - WEIBULL ANALYSIS OF FULLY REVERSED TENSION-COMPRESSION FATIGUE TESTS

4.3.1 Fatigue results

Table 4.1 shows the number of cycles to failure for all specimens that were fatigue tested in fully reversed tension-compression conditions at ± 20 MPa. The cycles to failure results are classified according to specimen type (shape and production method) and listed in ascending order, excluding the specimens that were rejected according to the “1 mm pore” rejection criterion. Figure 4.1 illustrates the assessment of specimens according to this criterion as discussed in Section 3.2.2.5. The specimen shown in Figure 3.1a is an example of the specimens that had no obvious pores whereas that in Figure 3.1b represents the specimens that had one or more micropores (< 1 mm) in the fracture surface, where the specimens in both cases were accepted. The specimen in Figure 3.1c is an example of those that were rejected.

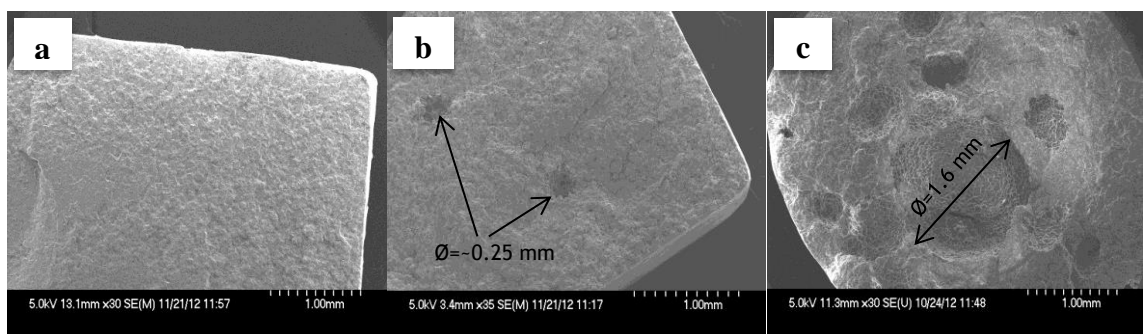


Figure 4.1 Illustration of porosity assessment of fracture surfaces after fatigue failure: (a & b) accepted specimens with no pores or pores diameter of ≤ 1 mm and (c) a rejected specimen with a pore diameter of > 1 mm

Table 4.1 Ranked fatigue results (cycles to failure) of all groups tested in fully reversed tension-compression of $\pm 20\text{MPa}$, classified according to specimen type and cement composition

Specimen	SmartSet GHV				CMW1			
	RDM	RMM	CDM	CMM	RDM	RMM	CDM	CMM
1	5,845	1,616	14,614	1,233	11,618	4,468	8,500	4,300
2	6,577	3,086	16,346	1,826	12,292	5,779	33,884	5,425
3	7,679	4,185	26,720	2,188	12,929	7,435	39,849	17,442
4	13,742	6,279	34,753	2,525	19,165	8,476	44,784	19,597
5	25,640	14,376	42,406	2,618	20,088	9,753	68,226	25,264
6	26,086	15,589	53,265	4,030	22,686	10,470	72,443	26,136
7	27,775	18,267	70,787	5,303	31,937	14,207	86,923	27,900
8	31,269	23,310	71,939	7,008	34,969	15,054	138,372	29,021
9	32,778	31,809	115,804	14,789	53,600	19,755	167,384	31,197
10	49,288	47,993	178,800	19,188	103,492	27,165	282,046	31,455
11	113,192			22,000				
12				59,256				
Mean	30,897	16,651	62,543	11,830	32,278	12,256	94,241	21,774
Median	26,086	15,589	53,265	5,303	22,686	10,470	72,443	26,136

4.3.2 Significance of variations in fatigue results: preliminary comparisons

The significance of variations between various sets of fatigue results are compared in Table 4.2. The use of ANOVA to assess the variations indicated significant differences between fatigue results when the four specimen types of each cement were compared against each other, giving p -values (the significance of variation at a 5% confidence level) of 0.003 and 0.001 for SmartSet GHV and CMW1, respectively. Comparison of the same specimen type of one cement against its counterpart in the other cement provided, in general, no significant differences apart from providing a p -value of 0.05 between the circular machined specimens of the two cements.

Within the same bone cement composition, comparison between various stress regimes showed variations in fatigue results, depending mainly on the specimen shape and production method which can be affected by the type of bone cement used. For SmartSet GHV, the most significant difference was found between the CDM and CMM

sets (p -value = 0.002), comparing the effect of production method on the fatigue life of circular specimens of this cement. A critically significant difference (p -value = 0.049) was seen between the RDM and CDM, providing an indicator of the effect of the difference in specimen shape when moulding was used. No significant differences were found between the rectangular specimens when either of the two production methods were used (p -value = 0.097) or between the machined specimens of both shapes (p -value = 0.240). For the CMW1 cement, however, comparisons between all the stress regimes revealed significant differences in fatigue lives, showing the more obvious influence of specimen shape and preparation technique on the fatigue life and behaviour.

Table 4.2 Significance of variations in results among various specimen types and cement compositions for the tension-compression stresses at $\pm 20\text{MPa}$

Comparison status	Statistical hypothesis test	p -value	Significance of variations
SmartSet GHV (RDM vs RMM vs CDM vs CMM)	ANOVA	0.003	significant
CMW1 (RDM vs RMM vs CDM vs CMM)	ANOVA	0.001	significant
RDM (SmartSet GHV vs CMW1)	Student's t -test	0.460	non significant
RMM (SmartSet GHV vs CMW1)	Student's t -test	0.200	non significant
CDM (SmartSet GHV vs CMW1)	Student's t -test	0.156	non significant
CMM (SmartSet GHV vs CMW1)	Student's t -test	0.050	critical
SmartSet GHV (RDM vs RMM)	Student's t -test	0.097	non significant
SmartSet GHV (CDM vs CMM)	Student's t -test	0.002	significant
SmartSet GHV (RDM vs CDM)	Student's t -test	0.049	significant
SmartSet GHV (RMM vs CMM)	Student's t -test	0.241	non significant
CMW1 (RDM vs RMM)	Student's t -test	0.021	significant
CMW1 (CDM vs CMM)	Student's t -test	0.006	significant
CMW1 (RDM vs CDM)	Student's t -test	0.018	significant
CMW1 (RMM vs CMM)	Student's t -test	0.012	significant

4.3.3 Weibull functions: two-parameter analysis

The graphical representation of the two-parameter Weibull functions, according to Equation 2.25, is shown in Figure 4.2. The relevant Weibull parameters (b & N_a) and the resultant fatigue performance index (I) for all functions are compared in Table 4.3. Clear differences can be seen between the fatigue longevity for the four specimen types. For both cement compositions, in general, greater fatigue performances were obtained when moulded specimens, particularly the circular cross-sections, were used. Machined

specimens of both shapes, in addition to providing the lowest performance, behaved in a reverse manner when comparing the two cement compositions with the greatest fatigue lives associated with the circular CMW1 specimens.

4.3.3.1 Comparison of fatigue performance indices

Considering the results in greater detail, significant variations were found between fatigue performances of specimen types, which can vary depending on the chemical composition. Considering the effect of production method on fatigue lives of the same shape specimens, rectangular moulded specimens of the same cement showed well above double the fatigue lives compared to the rectangular machined. These variations increased remarkably when comparing the effect of surface preparation method on the performance of the circular shape, which in turn varied depending on the bone cement composition. The results revealed more than 5.5 times greater fatigue performance for the circular moulded specimens made from the SmartSet GHV cement compared to the circular machined specimens of the same material. For a similar comparison of the CMW1 specimen, this factor of difference was found to be nearly 3.5.

Within the same production method and considering the effect of specimen shape only, 2 and 2.7 times greater fatigue performance indices were found when comparing the circular moulded specimens to the rectangular moulded ones for SmartSet GHV and CMW1, respectively. This difference, however, was not as great when comparing the fatigue performance indices that resulted from testing the circular machined specimens against the rectangular machined for both cements, with the largest difference between those when CMW1 was used (fatigue index ratio was only 1.5).

Considering the effect of cement composition solely, minimal advantage was obtained for the rectangular shape (either moulded or machined) of the CMW1 specimens compared to the SmartSet GHV counterparts. This trend of difference in the performance of both cements, however, increased noticeably when comparing the CDM sets providing a factor of 1.5 and, more significantly, when comparing the CMM sets with a factor of almost 2.5.

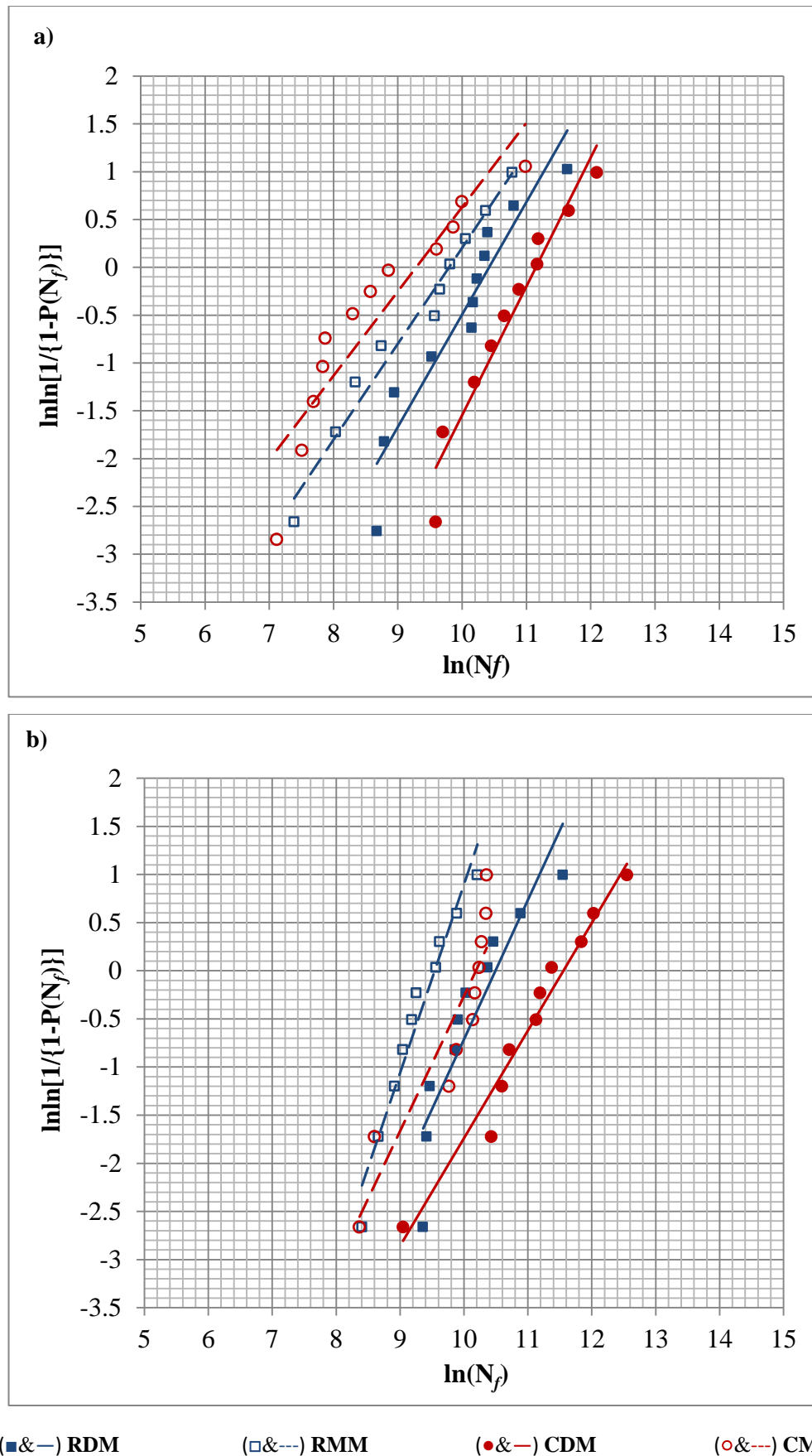


Figure 4.2 Plots of the two-parameter Weibull relationships showing the variations in fatigue behaviour of four different specimen types tested in fully reversed tension-compression (± 20 MPa) for (a) SmartSet GHV and (b) CMWI

Table 4.3 Summary of the determined values of the shape and scale parameters (two-parameter Weibull for the tension-compression stresses) and the resultant fatigue performance indices – based on the relevant functions in Figure 4.2

Specimen type	SmartSet GHV			CMW1		
	b	N_a /cycles	I /cycles	b	N_a /cycles	I /cycles
RDM	1.176	34,200	37,088	1.447	35,242	42,393
RMM	1.004	15,678	15,709	1.963	14,045	19,678
CDM	1.316	66,171	75,909	1.116	106,938	112,970
CMM	0.882	14,765	13,346	1.403	26,370	31,235

4.3.3.2 Probability density functions of Weibull distributions

All Weibull moduli (shape parameters) obtained from using the two-parameter Weibull analysis were low and below the expected symmetry range, indicating a high degree of variability, with the largest Weibull modulus being 1.963. The Weibull distributions skewed to the right for 6 of the 8 testing sets with ($1 < b < 2$). One set (RMM SmartSet GHV) provided exponential distribution ($b=1$) and another testing set (CMM SmartSet GHV) provided increasing failure probability ($b < 1$).

Apart from the overall skewness to the right, the shape of the probability density function among all specimen types differed (Figure A2.1 in Appendix 2). Therefore, the probability of failure between any two cycles to failure data points, which is represented by the area under the curve along the fatigue life between these two data points, appeared to differ depending on the shape of the density function curve which ends to the right at the highest cycles to failure number in a testing group identifying the point at (and after which) the probability of failure is 100%. Meanwhile, the spread of the distribution along the fatigue life variable, which was mainly controlled by the scale parameters, seemed to be dissimilar among the different groups.

It was observed, however, the shapes of the probability density functions of the same specimen type of the two test cements were closer for the moulded sets (either rectangular or circular) with the difference being mainly controlled by the scale parameter rather than the shape parameter, which was assessed by the distribution curve of one group extending in a narrower or wider fatigue life range (and higher or lower

curve peak) compared to the equivalent group in the other cement. Exceptionally, however, the shape of the CMM specimen type in both cements was found to be totally dissimilar. This was, of course, due to the larger difference between both the shape and scale parameters in one group compared to their corresponding values in the other group.

4.3.4 Weibull functions: three-parameter analysis

The graphical representation of the three-parameter Weibull functions is shown in Figure 4.3. The Weibull parameters (b , N_a & N_0) and the resultant fatigue performance index (I) for all functions are compared in Table 4.4. The trend of Weibull functions appeared to be similar to those obtained from the two-parameter analysis, with slight differences in fatigue behaviour for certain specimen types. The most obvious of these differences was the reverse behaviour in fatigue results of the RDM and the CMM of CMW1 specimens compared to each other, for the two- and three-parameter functions. Deviating from the two-parameter Weibull also, the graphical comparison of the three-parameter Weibull functions of the four testing specimen types for one cement against the equivalent methods in the other showed even clearer dissimilar behaviour, particularly among the RDM, RMM and CMM sets.

4.3.4.1 Comparison of fatigue performance indices

Variations in fatigue performance between the testing sets remained obvious, but not exactly the same to those reported within the two-parameter Weibull analysis. Considering the effect of production method on fatigue life, all the findings reported above for the two-parameter Weibull remained similar except for obtaining about 8.5 times greater fatigue performance between the circular moulded specimens made from the SmartSet GHV cement compared to the equivalent circular machined set (the factor of difference was 5.5 with the two-parameter analysis).

Considering the effect of specimen shape only, apparent differences were found that were less than those when the two-parameter Weibull analysis was used. Factors of 2.2 and 3.2 times greater fatigue performance were obtained when comparing the circular moulded specimen to the rectangular moulded for SmartSet GHV and CMW1, respectively. Also, the differences in fatigue performance approximately doubled when

using the three-parameter approach to compare the fatigue results of the circular machined specimen against the rectangular machined for both cements.

As for the effect of cement composition, the minimal fatigue performance advantage to the rectangular shape for both production methods, that was shown by the two-parameter Weibull to be in favour of the CMW1 specimens, appeared in favour of SmartSet GHV with the three-parameter approach. Greater fatigue lives by almost 1.5 times were found from comparing the CDM set of CMW1 against its SmartSet GHV equivalent (the same as in the two-parameter approach). Approximately 3.5 times superior fatigue performance index was obtained between the CMM specimens of CMW1 against its comparable SmartSet GHV set (this factor was only 2.5 with the two-parameter approach).

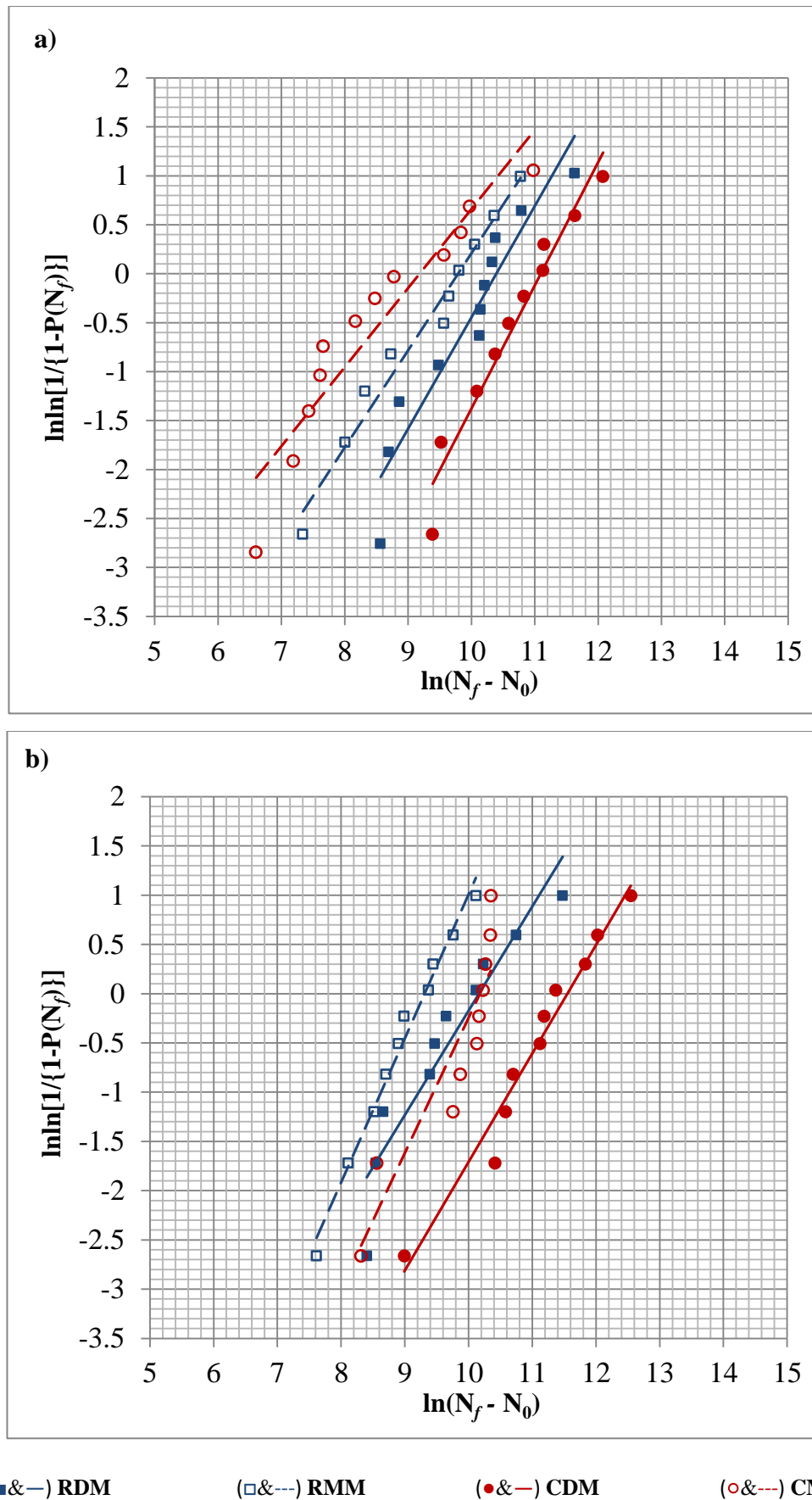


Figure 4.3 Plots of the three-parameter Weibull relationships showing the variations in fatigue behaviour of four different specimen types tested in fully reversed tension-compression (± 20 MPa) for (a) SmartSet GHV and (b) CMW1

Table 4.4 Summary of the determined values of the shape, minimum fatigue life and scale parameters (three-parameter Weibull at tension-compression) and the resultant fatigue performance indices – based on the relevant functions in Figure 4.3

Specimen type	SmartSet GHV				CMW1			
	b	N_0 /cycles	N_a /cycles	I /cycles	b	N_0 /cycles	N_a /cycles	I /cycles
RDM	1.137	590	33,282	35,489	1.059	7,150	33,233	34,199
RMM	0.992	75	17,869	17,797	1.461	2,440	13,481	16,295
CDM	1.257	2,664	68,588	76,898	1.101	469	104,666	109,825
CMM	0.808	498	10,142	9,117	1.372	221	26,477	31,013

4.3.4.2 Probability density functions of Weibull distributions

In general, all the obtained shape parameters were well below the expected symmetry range ($3 < b < 4$). Five out of the eight testing sets provided right skewness of the Weibull distributions ($1 < b < 1.5$). Two testing sets showed exponential distributions with $b \approx 1$ (RMM SmartSet GHV and RDM CMW1). One testing set (CMM SmartSet GHV) provided slightly greater failure probability at lower number of cycles ($b < 1$). Comparison of the three-parameter density functions of the moulded sets (Figure A2.1 in Appendix 2) showed similarity in terms of the shape parameter and varied slightly with regard to the fatigue life characteristic. When comparing the three-parameter distribution for each moulded specimen type to the equivalent two-parameter distribution, the results showed closer (or identical) fatigue life density distributions for the specimens that provided longer fatigue lives and less similarity at the shorter fatigue lives. The variations among the three-parameter density functions for the machined sets were slightly different and larger. The comparison of the rectangular machined sets for both cements (RMM), showed the greatest difference between the two- and three-parameter distributions. Smaller differences were seen between the two- and three parameter density functions for the CMM set of the SmartSet GHV cement, but with obviously different shape and characteristic parameters when comparing this specimen type set for the two cements, irrespective of the analysis approach being two- or three-parameter distribution.

4.4 RESULTS - WEIBULL ANALYSIS OF TENSION-TENSION FATIGUE TESTS

4.4.1 Fatigue Results

Table 4.5 compares the fatigue lives of all specimens that were tested in tension-tension stress between 2 and 20 MPa ($R = 0.1$). The fatigue results are arranged in ascending order and classified according to the specimen type (shape and production method) and comparing this for the two test cements.

Table 4.5 *Fatigue results (cycles to failure) for tension-tension (2-20 MPa), classified according to specimen type and cement composition*

Specimen	SmartSet GHV				CMW1			
	RDM	RMM	CDM	CMM	RDM	RMM	CDM	CMM
1	35,133	3,092	28,867	3,665	6,053	10,929	7,295	7,594
2	39,151	5,225	88,356	3,783	13,650	22,281	22,355	19,942
3	41,590	10,721	150,508	7,318	20,812	96,263	57,551	26,339
4	53,042	182,053	176,475	22,045	26,594	101,239	66,070	94,442
5	90,674	368,371	242,819	31,579	42,456	123,138	77,495	102,999
6	132,754	480,545	348,523	55,740	68,025	127,146	93,219	113,872
7	248,978	487,456	387,423	75,843	83,323	127,868	131,880	200,434
8	413,482	517,978	398,740	121,250	86,833	155,045	141,256	235,786
9	585,588	883,840	533,447	232,749	122,875	200,701	225,439	435,576
10	1,196,665	1,131,150	957,624	244,709	155,297	310,635	251,068	520,177
11	1,322,375		1,463,387				258,577	
Mean	378,130	407,043	434,197	79,868	62,592	127,525	121,110	175,716
Median	132,754	480,545	348,523	55,740	68,025	127,147	93,219	113,872

4.4.2 Significance of variations in fatigue results: preliminary comparisons

The initial comparisons to measure the significance of variations, among various groups tested in the tension-tension manner, using either Student's t -test or Analysis of Variance (ANOVA) are provided in Table 4.6. Contradictory to the findings of the tension-compression regimes, when comparing fatigue results of the four specimen types in each cement, no significant variations were found for either cement with p -

values of 0.139 and 0.169 for SmartSet GHV and CMW1, respectively. Also, differing from the fully reversed stress regimes, the comparison of the variations in fatigue results of the same specimen type from one cement with their equivalent from the other cement showed significant variations for three specimen types (RDM, RMM, and CDM with p -values of 0.024, 0.018 and 0.014, respectively). Non significant variations were found between the circular machined specimens (CMM) of both cements (p -value = 0.073).

Table 4.6 Significance of variations in results among various specimen types and cement compositions for the tension-tension stress regimes

Comparison status	statistical hypothesis test	p -value	Significance of variations
SmartSet GHV (RDM vs RMM vs CDM vs CMM)	ANOVA	0.139	non significant
CMW1 (RDM vs RMM vs CDM vs CMM)	ANOVA	0.169	non significant
RDM (SmartSet GHV vs CMW1)	Student's t -test	0.024	significant
RMM (SmartSet GHV vs CMW1)	Student's t -test	0.018	significant
CDM (SmartSet GHV vs CMW1)	Student's t -test	0.014	significant
CMM (SmartSet GHV vs CMW1)	Student's t -test	0.073	non significant

4.4.3 Weibull functions: two-parameter analysis

The two-parameter Weibull relationships for the fatigue results of the tension-tension stress regimes are compared in Figure 4.4. The values of the Weibull parameters of these functions and the calculated fatigue indices are provided in Table 4.7. For the SmartSet GHV testing sets, obvious variations appeared between the four specimen types in terms of fatigue lives and data scatter, where the clearest differences in behaviour were associated with the rectangular moulded specimens. For the CMW1, noticeably less variation in results was obtained. Exceptionally, the machined specimens of this cement showed closer or even greater trends of fatigue performance compared to the equivalent moulded specimens, different from that obtained from the machined specimens of the other cement and also from all the tension-compression regimes where the machined specimens showed clearer decreases in fatigue lives.

4.4.3.1 Comparison of fatigue performance indices

Considering the effect of surface production method only, two differences that appear to be worth mentioning between the fatigue performance indices of the same specimen

shape and material were found. One was between the RMM and RDM specimens made from CMW1 where the former production method provided a factor of 2.2 greater fatigue performance compared to the latter. Interestingly, this behaviour is totally opposite to that reported earlier for the equivalent tension-compression regime. With a larger difference gap, the CDM specimens made from SmartSet GHV provided 7.5 times greater fatigue performance compared to the same composition CMM specimens, providing a similar trend to the equivalent finding for the tension-compression regime (that showed a factor of 5.5).

For the same production method and focusing on the influence of specimen cross sectional shape for each cement, the circular moulded specimens provided 1.5 and 1.7 greater fatigue indices compared to the rectangular moulded for the SmartSet GHV and CMW1 specimens respectively, which are less than those obtained from the same comparisons of the tension-compression regimes. Dissimilarly, the circular machined specimens, compared to the rectangular machined ones, provided similar fatigue indices for one cement (a factor of difference of only 1.02 with a slight advantage to the rectangular machined specimens) and remarkably different fatigue indices for the other cement (a factor of 4.75 in favour of the rectangular machined specimens). Again, these findings differ noticeably from those obtained when the fully reversed tension-compression regimes were used.

In general, and considering the effect of bone cement type, the fatigue performance of SmartSet GHV testing groups provided significantly longer fatigue lives compared to the CMW1 specimens, with the exception of the CMM group of the SmartSet GHV cement which provided the lowest fatigue performance at all. The moulded specimens of the SmartSet GHV cement, compared to their CMW1 counterparts, provided 3.5 times greater fatigue performance when the circular shape was used and 4 times greater performance when the rectangular sections were tested. When considering the same comparison for the machined specimens, the rectangular shape of SmartSet GHV cement provided only 1.7 times greater fatigue lives compared to the equivalent CMW1 specimens. Providing a totally different tendency, however, the circular machined specimens of the former cement provided only one third of the fatigue performance obtained from the circular machined specimens of the latter cement.

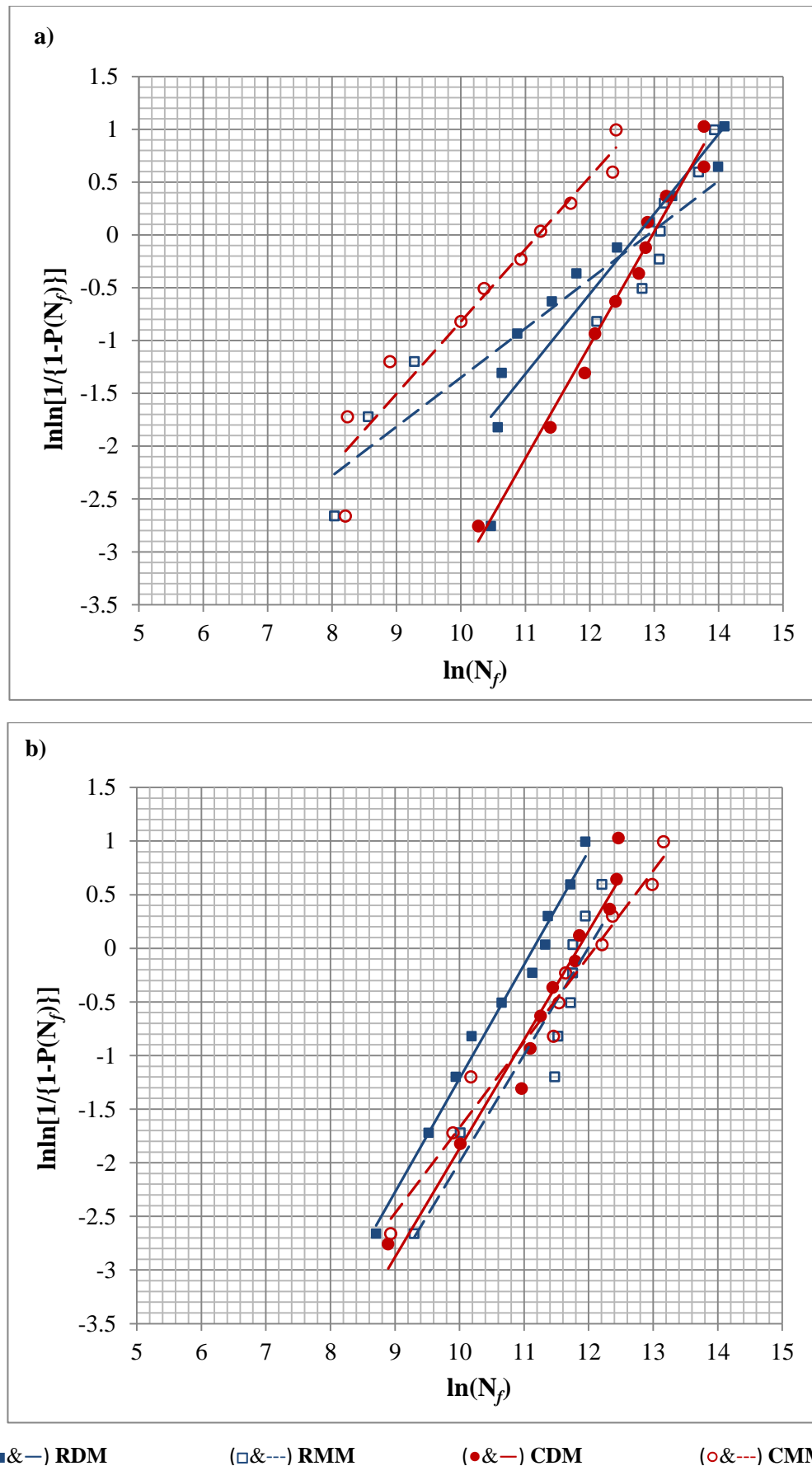


Figure 4.4 Plots of the two-parameter Weibull relationships showing the variations in fatigue behaviour of four different specimen types tested in tension-tension cyclic loading between 2 and 20 MPa for (a) SmartSet GHV and (b) CMW1

Table 4.7 Summary of the determined values of the shape and scale parameters (two-parameter Weibull at tension-tension) and the resultant fatigue performance indices – based on the relevant functions in Figure 4.4

Specimen type	SmartSet GHV			CMW1		
	b	N_a /cycles	I /cycles	b	N_a /cycles	I /cycles
RDM	0.757	344,552	299,780	1.061	73,130	75,327
RMM	0.465	420,837	286,972	1.000	162,755	162,327
CDM	1.073	442,413	458,296	1.014	133,252	134,182
CMM	0.684	73,130	60,482	0.797	178,872	159,688

4.4.3.2 Probability density functions of Weibull distributions

Generally, the Weibull shape parameters were not only below the symmetry range but also in a lower range between approximately $b \approx 0.4$ and $b \approx 1$. The shape of the probability distribution function was exponential for one specimen type (RMM of CMW1) and approximately exponential for three specimen types (CDM of SmartSet GHV and RDM and CDM of CMW1). All the remaining specimen types showed more increasing failure probability ($b < 1$), particularly for the rectangular machined specimens made from SmartSet GHV ($b = 0.465$).

The probability of failure can be much greater during the early and middle life cycles compared to the last life cycles, which can be estimated by the area under the curve of the probability function (Figure A2.2 in Appendix 2). Analysing the findings of the RDM specimens made from CMW1, for instance, the probability of reaching failure between 10,000 and 75,000 fatigue cycles is significantly greater than that can be obtained over the cycles between 75,000 and 150,000. In the cases where the b value was less than 1, the chance of recording earlier failure is greater. Apart from the obvious difference in the longest fatigue life that each specimen type provided, more similarity between the shapes of the distributions appeared among the different specimen types, particularly within the same cement, compared to that reported earlier for the tension-compression regimes.

4.4.4 Weibull functions: three-parameter analysis

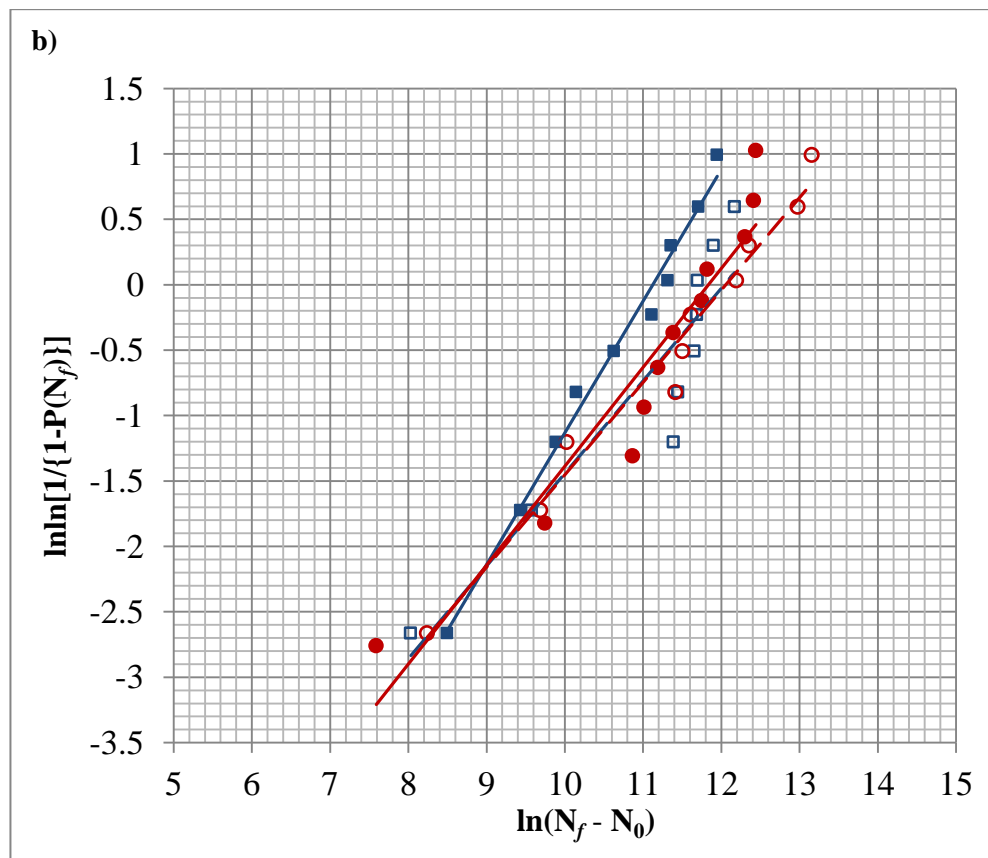
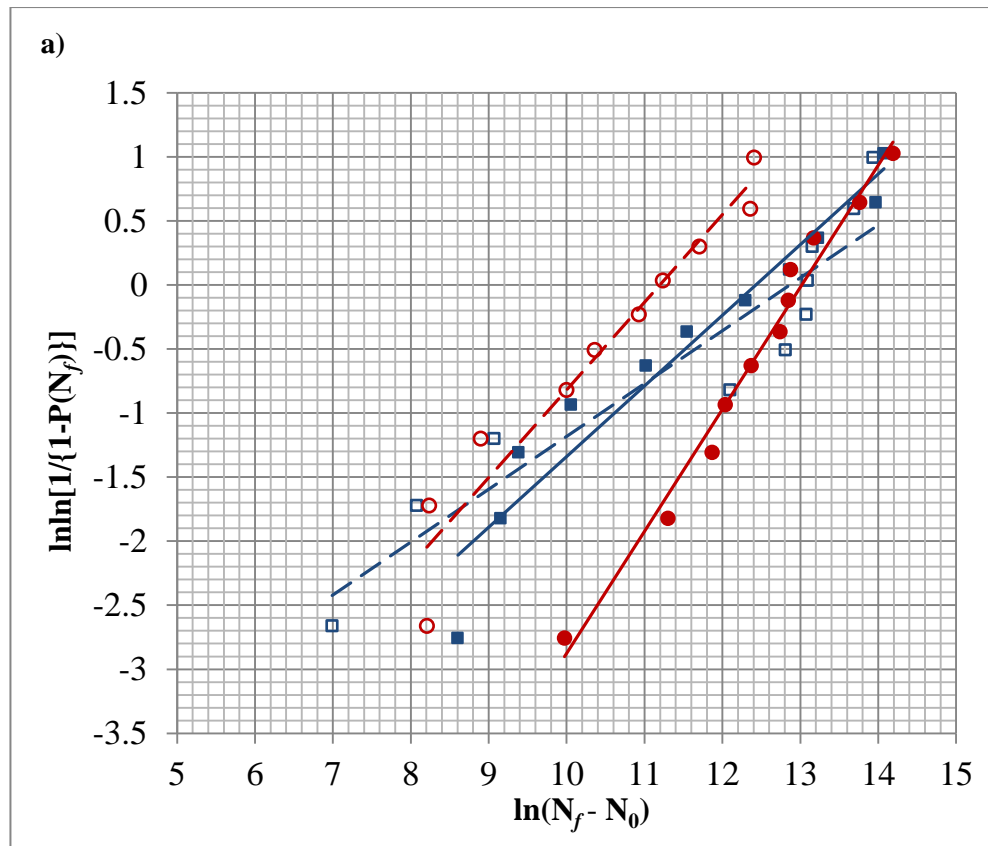
The graphical comparisons of the three-parameter Weibull relationships of the different specimen types tested in tension-tension are presented in Figure 4.5. The associated Weibull parameters and calculated fatigue indices are summarised in Table 4.8. In general, the order of the trends of fatigue behaviour for the different specimen types is similar to that obtained from the two-parameter Weibull. It should be noted, however, the shape and characteristic parameters were marginally different from those obtained for the two-parameter analysis, showing slight decrease for most of the groups.

4.4.4.1 Comparison of fatigue performance indices

The trend of differences between the fatigue performance indices is generally similar to that obtained from the two-parameter Weibull distributions. For most of the specimen groups, however, the fatigue index declined slightly in different ratios among the different groups, due to considering the third Weibull parameter (N_0) that lowered the Weibull moduli. Comparing the results of the two- and three-parameter approaches, the fatigue index of the RDM specimens made from SmartSet GHV showed the largest decrease ($\Delta I = 31\%$), leading this specimen type to indicate providing lower performance compared to its RMM equivalent. The other comparisons were not largely different from those reported for the two-parameter analysis, keeping the same substantial differences between the CDM and CMM of SmartSet GHV (a factor of 7.5) and between the RMM and RDM of CMW1 (a factor of 2.2).

4.4.4.2 Probability density functions of Weibull distributions

Due to having lower values of Weibull moduli with the three-parameter analysis compared to the two-parameter for many specimen types, the shape of the probability density functions of the specimen types were noticeably different when comparing those for the two approaches (Figure A2.2 in Appendix 2). Three specimen types, that were reported as exponential for the two-parameter approach (namely; RMM and CDM of CMW1 and CDM of SmartSet GHV), provided “less than exponential” curve shape. The shape of the other five specimen types were similar to their two-parameter counterparts, with the CMM specimen type of SmartSet GHV provided identical shape, of course, due to the third Weibull parameter being equal to zero for this case.



(■&—) RDM

(□&---) RMM

(●&—) CDM

(○&---) CMM

Figure 4.5 Plots of the three-parameter Weibull relationships showing the variations in fatigue behaviour of four different specimen types tested in tension-tension cyclic loading between 2 and 20 MPa for (a) SmartSet GHV and (b) CMWI

Table 4.8 Summary of the determined values of the shape, minimum fatigue life and scale parameters (three-parameter Weibull at tension-tension) and the resultant fatigue performance indices – based on the relevant functions in Figure 4.3

Specimen type	SmartSet GHV				CMW1			
	b	N_0 /cycles	N_a /cycles	I /cycles	b	N_0 /cycles	N_a /cycles	I /cycles
RDM	0.552	29,685	279,117	207,375	1.008	1,146	68,805	69,080
RMM	0.413	2,005	389,851	250,538	0.707	7,853	177,089	148,902
CDM	0.953	7,400	459,438	448,511	0.756	5,318	143,184	124,496
CMM	0.684	0	73,051	60,416	0.706	3,809	175,881	147,782

Except for having one specimen type to provide an exponential failure distribution (that is the RDM type of CMW1), the three-parameter analysis revealed all the other specimen types to provide increased (than exponential) failure probability. This probability, however, differed among specimen types depending on the Weibull modulus value. The highest Weibull modulus among these groups was slightly below 1 (CDM of SmartSet GHV) making the density function closer to being exponential. The lowest Weibull parameter associated with the RMM specimen type of SmartSet GHV ($b=0.413$), increasing the chance of reaching earlier failure compared to all the other specimen types.

4.5 RESULTS - WÖHLER (S-N) CURVES

4.5.1 General comparison of S-N curves of various specimen types

As can be seen from the S-N curves in Figure 4.6, obvious differences between fatigue lives were found when a range of stress regimes were used. For each bone cement structure, the effect of specimen shape in conjunction with surface preparation method is clearly evident. The longest fatigue life was constantly associated with the circular moulded specimens at all stress levels. Excluding this specimen type, the results appeared to be more dependent on the change in chemical composition where divergence in the trends of S-N curves was seen among the two cements. While the circular machined specimens for SmartSet GHV, for example, provided the shortest fatigue lives, this was not the case for CMW1 cement where the rectangular machined specimen type was the weakest in terms of resisting fatigue failure.

Apart from the outcome that fatigue results were largely controlled by the specimen shape and surface finish, it can also be deduced that, within the same cement composition, the trends of S-N curves can differ because of the data scatter. These trends can, in the first instance, be assessed visually and then numerically by the comparison of the slopes (regression coefficients) of the curves. For SmartSet GHV specimens, for instance, the S-N curve of the rectangular machined specimens (slope of -2.21) provided the most different trend compared to the other curves which showed less difference in changing the fatigue behaviour at different stress amplitudes. Likewise, for the CMW1, inequality was found between the slopes of the four curves with the lowest slope (-2.65) associated to the rectangular moulded specimen type. As testing was performed at higher stress levels than those encountered *in vivo* (as discussed in section 3.3.1), the decrease in the slope of an S-N curve may be used to indicate which specimen type might provide the lowest fatigue results at the *in vivo* stress levels, of course, compared to the other specimen types.

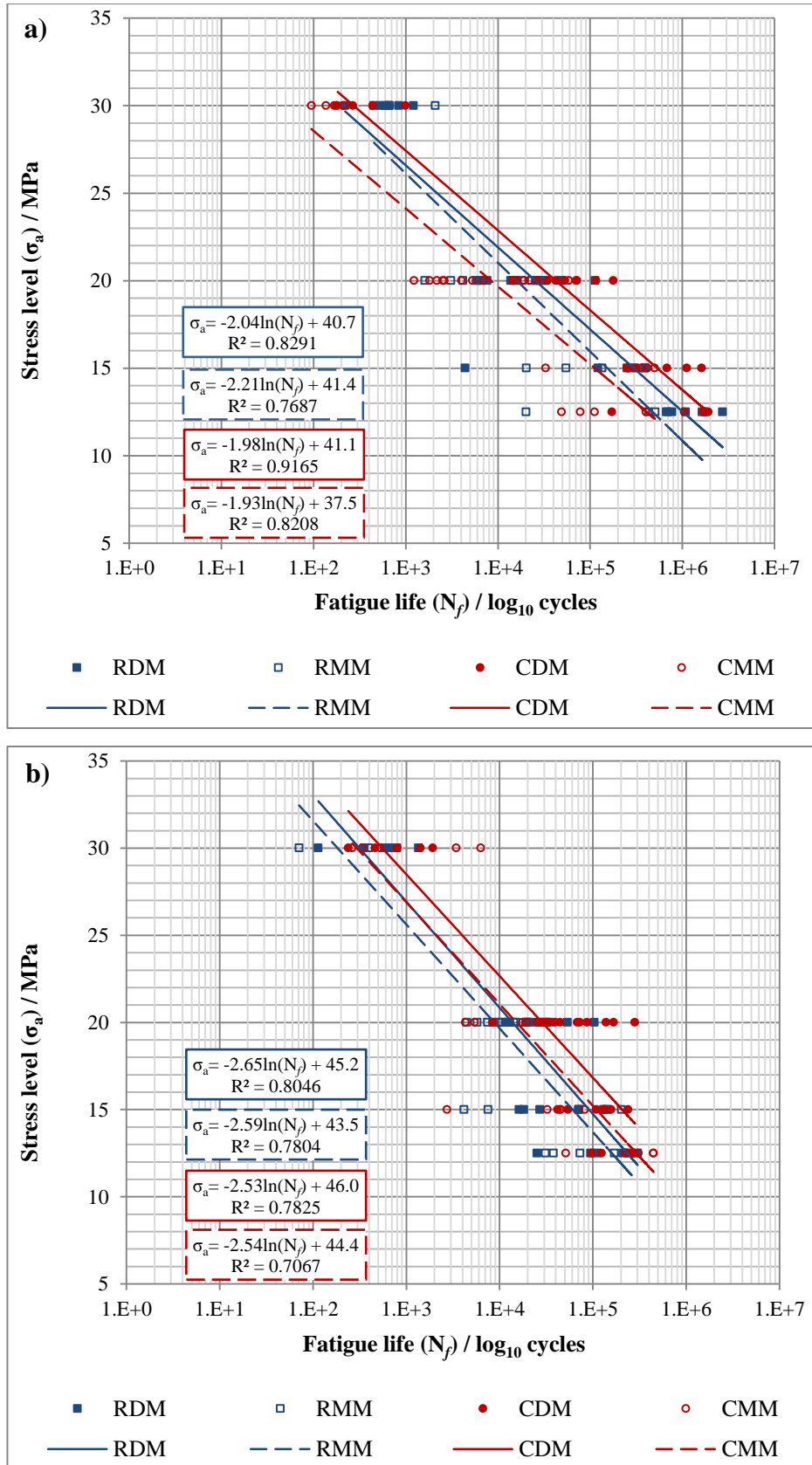


Figure 4.6 General comparison of *S-N* curves generated from testing at four fully reversed tension-compression stress levels, comparing fatigue behaviour of four specimen types for (a) SmartSet GHV and (b) CMW1 bone cements

4.5.2 Comparison of S-N curves of the same specimen type of different cements

This analysis considers the relation between two S-N curves generated from testing the two bone cements at the same conditions including specimen type and stress levels. As can be seen from Figure 4.7, the change in stress amplitude had different effects on the behaviour of S-N curves for the same specimen type of the two cements. For all specimen types, in general, a trend of providing greater fatigue lives was found at the higher stress levels (± 30 & ± 20 MPa), particularly for the circular shape, for the CMW1 specimens compared to the SmartSet GHV ones. However, at the lower levels (± 15 & ± 12.5 MPa), nearer the physiological stress, the fatigue trends were reversed, with SmartSet GHV showing the longer lives.

Figure 4.7a compares the fatigue behaviour of the two cements when the rectangular moulded specimens were used. Although the difference between the median specimens of the cements was less obvious at the higher stresses, the advantage for the SmartSet GHV to provide greater fatigue lives was more significant as the stress amplitude decreased to 15 MPa and the gap became even wider at the lowest stress of 12.5 MPa. This specimen type showed the largest difference between the gradients of the S-N curves of both cements (26%).

Similarly, Figure 4.7b shows a comparison between the S-N curves of the rectangular machined specimens of both cements. Once again, the difference between the fatigue lives, with greater performance to the SmartSet GHV, increased noticeably as the stress level declined towards the *in vivo* levels. This indication, which is reflected by the clear difference between the two curves gradients (22%), can also be assessed through the inconsistent change in the gap between the medians as the stress decreased.

The S-N curve diagram shown in Figure 4.7c includes comparing the trends of fatigue behaviour of the circular moulded specimens of both cements. This comparison confirms the indication that SmartSet GHV provides greater fatigue performance at the lower stresses. The difference between the gradients of the relevant S-N curves was again substantial (22%).

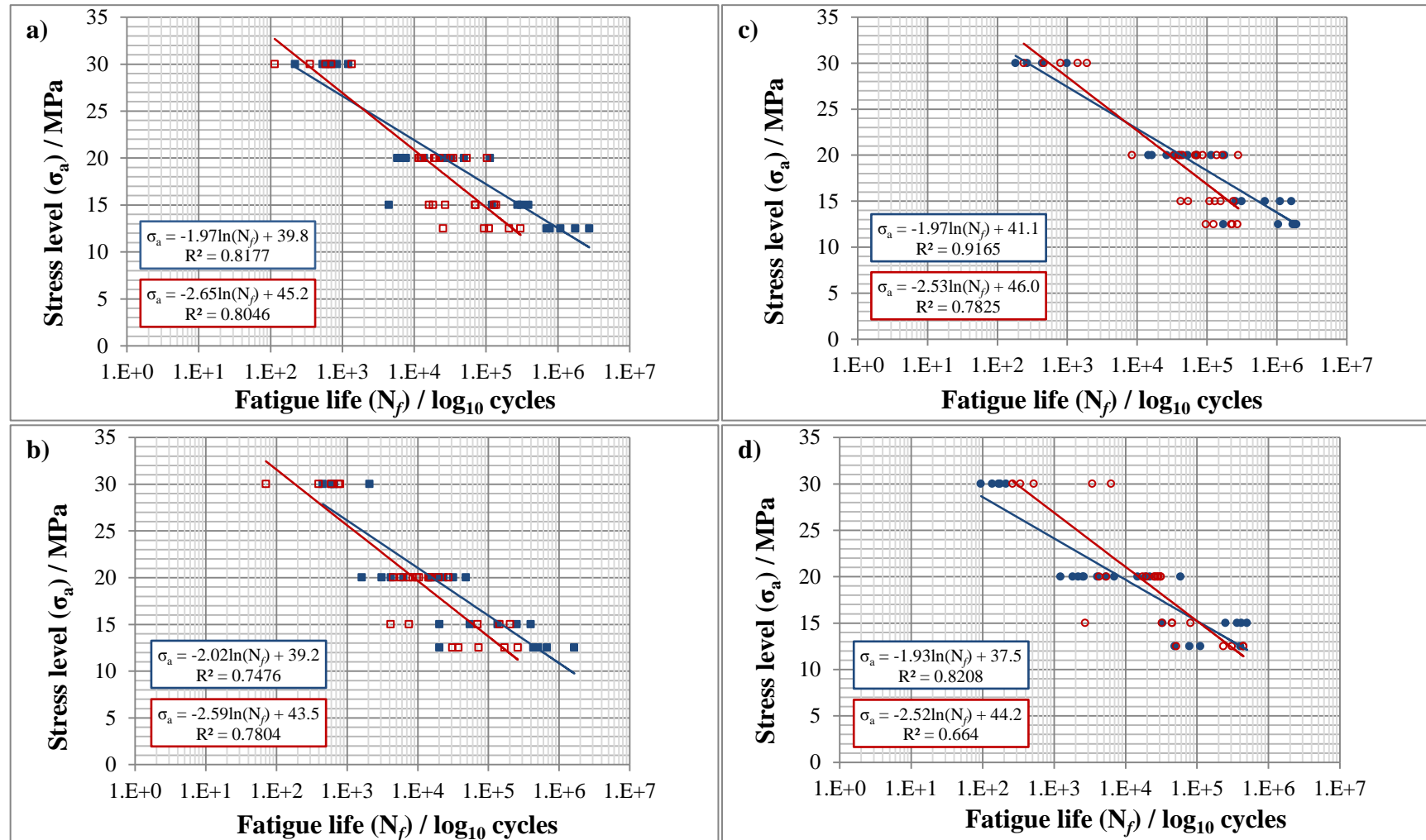


Figure 4.7 Comparison of S-N curves of SmartSet GHV cement (blue) and CMW1 cement (red) using specimen types of a) RDM, b) RMM, c) CDM and d) CMM.

For the circular machined specimens (Figure 4.7d), the longer fatigue life advantage in favour of CMW1 at the higher stress amplitudes was seen again. The trend of proving the opposite performance for the two cements at the lower stress levels was again apparent. Almost the same difference between the regression coefficients of the two S-N curves was determined (23%) showing, once again, dissimilarity in the increase of fatigue lives among the two cements comparing to each other as the stress level was decreased.

Thus, for all the specimen shapes, the differences in the gradients of the stress-life relationship ranged between 1.93 and 2.02 for SmartSet GHV, with intercepts between 37.5 and 41.1, whereas these differences in the gradients ranged from 2.52 to 2.65 for CMW1, with intercepts between 43.5 and 46.0. If all the results of the same cement are combined, regardless of specimen type, the stress-life relationship is given in Equations 4.1 and 4.2, for SmartSet GHV and CWM1 respectively. Although, for each cement, there are differences produced by the specimen shape and production method, the trend in the results is unaffected by the specimen specification.

$$\sigma_a = -1.91 \ln(N_f) + 38.87 \quad (4.1)$$

$$\sigma_a = -2.47 \ln(N_f) + 43.70 \quad (4.2)$$

4.5.3 The effect of individual stress levels

As clarified in the previous section, the fatigue results were found to be variously affected by the change in the maximum stress. Although the variations in fatigue lives were found mainly to be affected by the specimen type, the effect of the stress level appeared to have dissimilar effects on the cement compositions at the different stress levels. The fatigue results of the median specimens for all testing groups at each stress level are compared graphically in Figure 4.8, providing an indication of the variations in fatigue lives at different stress amplitudes. As reported below, and unless exceptionally highlighted, at all stress levels and for both specimen shapes, the moulded specimens provided the greatest fatigue performance compared to the machined types, however, with dissimilar degrees of variations at the different stress levels. Similarly, most of the stress regimes showed, in general, longer fatigue lives for the circular shape compared to the rectangular excluding the SmartSet GHV specimens that were tested at ± 30 MPa and only the circular machined tested at ± 20 MPa, where the fatigue lives were considerably shorter. Comparing the

fatigue behaviour of all specimen types at the examined stress amplitudes, more inconsistent findings were also seen.

At the highest stress amplitude (± 30 MPa) and within the same cement, variations in fatigue lives appeared between the circular moulded and circular machined with a 2.4 factor of difference for SmartSet GHV and 1.5 for CMW1, always with the moulded specimens demonstrating longer fatigue life. Comparing this for the rectangular shape, substantially less variation between the fatigue lives of both cements was determined with a maximum factor of difference of 1.2. Overall, slightly greater fatigue lives were obtained for the CMW1 specimens at this level in comparison to the SmartSet GHV counterparts.

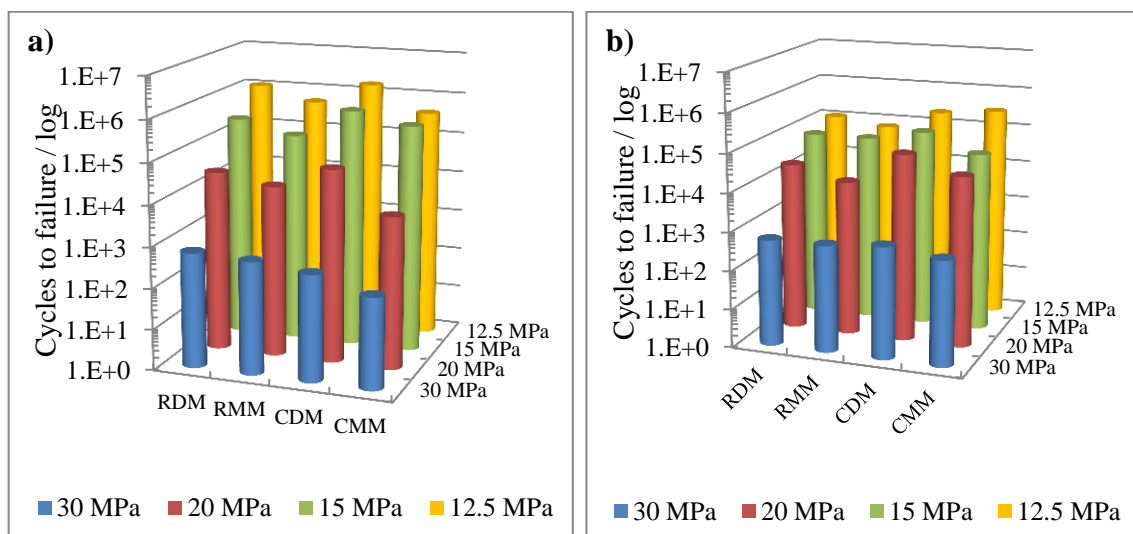


Figure 4.8 Comparisons of the median fatigue lives of different specimen types at different stress levels for (a) SmartSet GHV and (b) CMW1

At the next stress level (± 20 MPa), the variations between fatigue lives for different specimen types became more obvious. For SmartSet GHV, a factor of difference of 10 was found between the circular moulded and the circular machined specimens, which was only 1.7 when the rectangular specimens were compared. For CMW1, the comparable factors were 2.8 and 2.2, respectively. When comparing the same specimen type between the two cements, the factors of difference varied. This factor was 5 between the circular machined specimens and 1.4 between the circular moulded specimens showing, for both cases, greater fatigue performance associated with the CMW1 specimens. Considering the median results also, however, the rectangular specimens of SmartSet GHV showed somewhat higher fatigue lives compared to the corresponding CMW1 types, providing factors of 1.2 between the moulded and 1.5 between the machined.

At ± 15 MPa, as one would typically expect, longer fatigue lives, than those obtained from the higher stress levels, were recorded. It is worth mentioning though the degree of increase in fatigue lives among the different stress regimes was interestingly different. Moreover, these changes were obviously dissimilar for the two cements. For the SmartSet GHV specimens, a factor of difference of only 2 was found between the circular specimens (that was 10 in the higher stress regime) and a factor of 2 also appeared between the rectangular types (almost similar to that in the higher level). For CMW1, the factor of difference between the circular moulded and machined decreased from 5 in the previous stress level to 3 with this level. There was no difference between the median fatigue lives for the rectangular specimen types. Comparing the equivalent stress regimes for the two cements, and contrasting the results in the lower tested stress level, significantly longer fatigue lives were associated with the SmartSet GHV specimens, particularly when comparing the circular specimens. Factors of difference of approximately 4, 2, 5 and 8 were found between the RDM, RMM, CDM and CMM stress regimes, respectively.

At the lowest stress (± 12.5 MPa), within the same cement, the factors of difference between the rectangular moulded and rectangular machined specimens in both cements were similar to those obtained for the 15 MPa stress level. Considering the circular shape, however, a greater factor of difference was found between the moulded and machined specimens of the SmartSet GHV specimens; and the most exceptional finding was obtaining somewhat greater fatigue lives for the machined compared to the moulded specimens of the CMW1 (factor difference of 1.4). Also, as the S-N curves showed, even greater factors of difference were between the fatigue lives of a particular specimen type of SmartSet GHV cement compared to its counterpart in the CMW1 for three types. These factors were 10, 7 and 7.5 for the RDM, RMM and CDM stress regimes, respectively. Surprisingly, the CMM regime did not show such a difference.

As an overall description of the findings of the S-N analyses, the degree of variations between the S-N curves of different testing sets depended on the variable being considered in the comparison (specimen shape, production method, stress level or cement type). Greater fatigue performance was seen for the moulded specimen compared to the machined, particularly for SmartSet GHV, with the longest fatigue lives associated with the circular shape. The change in stress amplitude led to different alterations in fatigue lives when comparing a specimen set of one cement with their equivalents in the other, providing an initial indicator of how cement composition can influence the fatigue lives of various bone cement specimens that, in turn, can vary depending on the stress level.

4.6 RESULTS - POST-FATIGUE EXAMINATIONS

4.6.1 Microscopic observations of specimens' fracture and circumferential surfaces

Excluding the discarded specimens that had macropores in their gauge and shoulder sections with a total rejection rate of approximately 20%, the topography of the fracture surfaces of all specimens varied, depending essentially on the bone cement composition and inclusions that, in turn, seemed to be affected by the existence of other stress concentration raisers (manufacturing and microporosity defects). The stress level and type appeared to play a role in controlling the fatigue fracture mechanisms. At high stresses, particularly ± 30 MPa, smoother topography was observed on the majority of the fracture surfaces. In general, it can be said that fatigue fracture depended on the chemical composition, microporosity distribution, cement opacifier filler and the stress type and level applied. Rougher topography fracture surfaces were always associated with the SmartSet GHV specimens compared to the CMW1. Specimen shape and production method also influenced the severity of porosity and the other stress concentration raisers, thus affecting the fatigue fracture development.

Scanning electron micrographs (SEM) of the fracture surfaces of the eight median specimens tested in fully reversed tension-compression at ± 20 MPa are compared in Figure 4.9. Generally, the SmartSet GHV surfaces were rougher than the CMW1 surfaces. The micrographs indicate that, for CMW1 specimens, particularly the circular, the cracks started from many points on the circumference of the rectangular or circular fracture surfaces, growing towards the centre where the fracture growth rate is affected by the specimen type and cement composition. For the SmartSet GHV specimens, the crack routes are not as obvious showing more complicated disconnection topography that, at higher SEM magnifications, seemed to be largely controlled by the separation between the cement matrix and the accumulations of inclusions at many origins. The side view of the fracture surfaces of randomly selected specimens led to the conclusion that the "disconnection topography" between the upper and lower fracture surfaces of a specimen is affected by both sample type and cement composition.

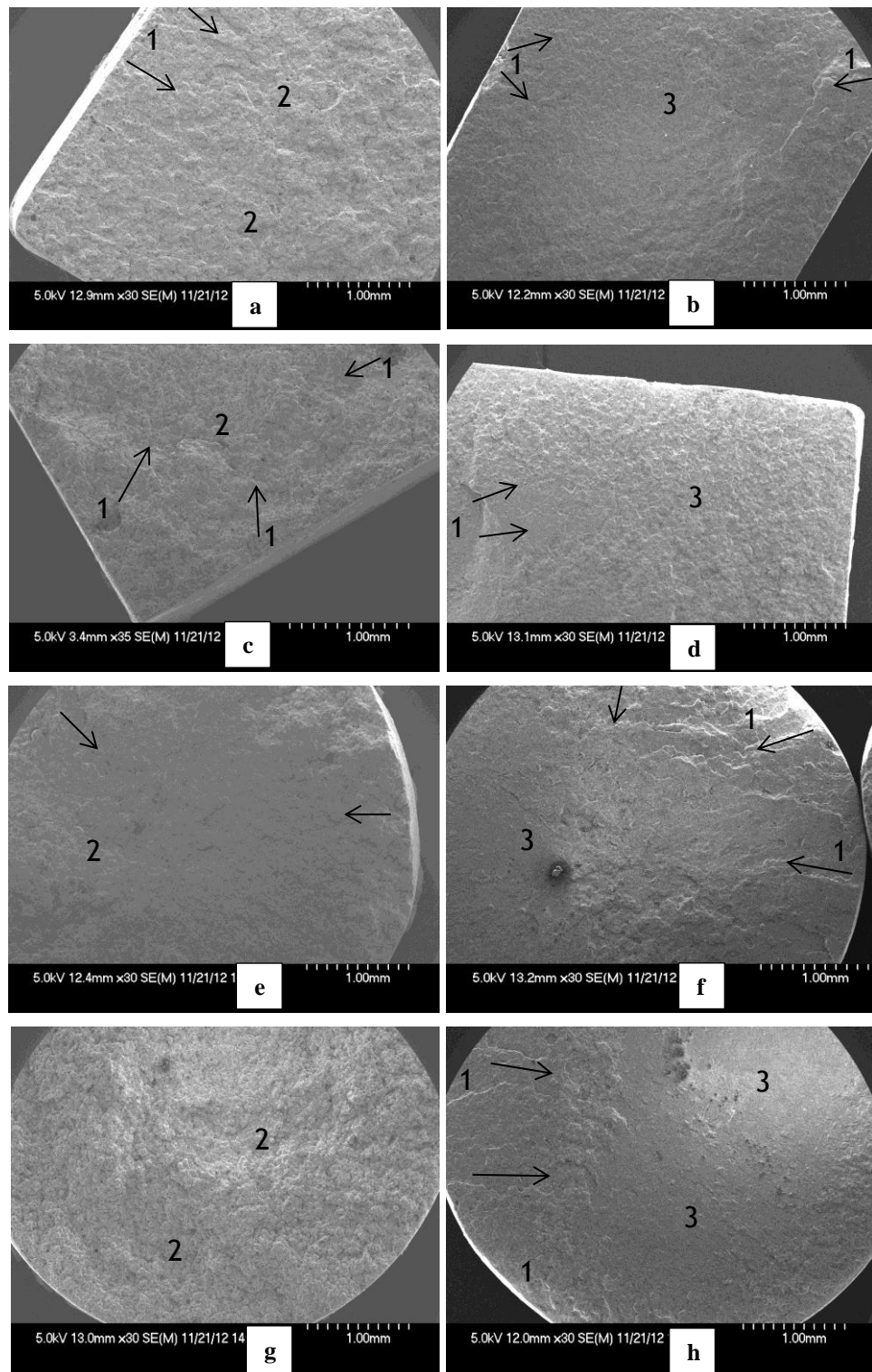


Figure 4.9 SEM of fracture surfaces of the median specimens of different specimen types of (a, c, e & g) SmartSet GHV and (b, d, f & h) CMW1, showing (a & b) RDM specimens, (c & d) RMM specimens, (e & f) CDM specimens and (g & h) CMM specimens. Possible crack origins indicated by number 1 where the arrows show the crack progress directions. Rougher (slower) crack growth areas for SmartSet GHV indicated by number 2 and smoother (faster) crack growth areas for CMW1 indicated by number 3. (All marker bars = 1mm)

In parallel with the SEM, the optical microscopic observations of wider range of specimens, but for all stress levels specimens, indicated that various reasons can control the fatigue life of specimens. The presence and distribution of porosity or inclusions led to recording shorter fatigue lives. These defects trigger fatigue fracture for particular specimen types in shorter time than others, depending meanwhile on the cement composition. It was also possible to have closer surface observations of the gauge sections where the effect of production method on both specimen shapes could be relatively assessed.

In terms of fracture surface investigations, the specimens that lie in the median and the long fatigue life range showed, in general, features similar to those compared in Figure 4.9 using the SEM system. For those specimens that provided short fatigue lives, the optical microscopic observations showed more obvious effect of the presence of pores and/or accumulation of inclusions within the fracture surface or, more severely, on both the circular or rectangular circumferences of specimens, with the latter being more influential.

4.6.2 Degree of polymerisation (DSC analysis)

The analysis of the DSC results indicated no significant differences between all specimen types. As can be generally deduced from the obtained graphs (Figure A3.1 in Appendix 3), for all specimens, initial heating of a small sample size (~ 5 mg) taken from the fractured bone cement specimens to 180°C, cooling it to room temperature and repeating the first heating process again provided no remarkable difference between the two heating processes. Although this indicated that the majority of the powder and the liquid reacted together after the mixing process and the end of the polymerisation process, further calculations considering the difference between the equivalent numerical results (data points) of the two heating processes showed that the degree of polymerisation was not total, reflecting the existence of small amounts of residual monomer. Table 4.9 compares the estimated degree of polymerisation for all specimen types.

Table 4.9 Comparison of the estimations of the degree of polymerisation for all specimen types

Specimen type	Degree of polymerisation %	
	SmartSet GHV	CMW1
RDM	90.0	86.0
RMM	92.5	93.0
CDM	82.0	91.0
CMM	84.5	92.0

4.7 DISCUSSION

4.7.1 Effects of specimen type

The results have shown that specimen shape and surface production method (specimen type) can significantly alter fatigue life of bone cement. Although the use of different analysis approaches has revealed some noticeable variations when comparing the fatigue results of different specimen types, this did not seem to change the overall trend of the fatigue behaviour, except when the stress regime parameters were different. It has been demonstrated that, in general, and when testing using the fully reversed stress mode in particular, testing of circular cross sectional specimens produced by moulding leads to recording substantially longer fatigue lives, compared to all other specimen types. These other types have also shown variations in fatigue lives amongst each other, with the more common trend being for the rectangular moulded specimens to provide greater fatigue performance. While the machined specimens have revealed greater probability of failure in shorter fatigue periods, it is not certain which shape of the machined specimens would provide longer fatigue lives, which seemed to be largely controlled by the differences in chemical composition.

4.7.1.1 Specimen cross-sectional area and size

The fatigue results of many materials can be variously affected by the specimen shape and size. Van Paepegen (2011), for instance, pointed out that, for fatigue testing of composites, the selection of an appropriate specimen shape is controlled by the nature of the composite being tested. He referred to the existence of some issues where a number of early attempts to use particular specimen profiles similar to those applied in testing of metals led to “unrepresentative modes of failure”. These concerns about the specimen shape has also been reported for fatigue testing of bone cement as to which specimen shape (rectangular or circular cross sectioned) is more appropriate and representative to the *in vivo* conditions. On the one hand, researchers such as Krause et al. (1988) and Cristofolini et al. (2000) believed the thickness of the rectangular specimens can provide closer simulation to the *in vivo* cement mantle. Other researchers, on the other hand, either preferred testing the circular shape or argued that testing either shape should be acceptable as reported by Lewis and Janna (2003) that “the controversy over test specimen shape is misplaced because *in vitro* fatigue tests are performed in order to characterise the bone cement material, rather

than the cement mantle". In an attempt to simulate the shape and stress conditions of the *in vivo* bone cement mantle more closely, Murphy and Prendergast (2003) subjected tubular specimens (thickness of 3mm) to multi-axial fatigue loading (axial stress through the taper grips and internal pressure to create both hoop and radial stresses). They concluded, according to their testing setups and findings, that the presence of multi-axial stresses can largely influence the variations in fatigue strength of bone cement.

Lewis and Janna (2003), when they examined the effect of specimen cross sectional shape, found that circular specimens provide greater fatigue lives compared to the rectangular. One limitation of their study is comparing only the moulded specimens of both shapes. While this current study has validated these findings for the moulded specimens, it has also shown that the circular cross sectional specimens after machining do not necessarily provide longer fatigue lives as compared to the rectangular equivalents, indicating that the fatigue properties are controlled by the production method as well.

The propensity of the circular specimens to generally provide greater fatigue strength, particularly when moulded, as demonstrated in this research can be attributed to several reasons. The most obvious reason is that the rectangular specimen has almost three times larger gauge section surface area (450 mm^2) compared to the circular cross-sectional specimen (157 mm^2), leading to surface area to volume ratios of 0.9 and 0.8 respectively, but with gauge lengths of 25 mm and 10 mm respectively. This is important since it has been demonstrated practically that many polymers, similar to several materials, to show early fatigue failure due to the initiation of cracks on the outer surface (Sawyer et al., 2008). This phenomenon appeared to apply to bone cement specimens tested in the current study, but with the influence of this factor being controlled by specimen shape, production method and cement type. The concept of testing specimens with internal micro- rather than macro-level porosity has provided a greater chance for fatigue cracks to start from the outer surface, particularly after machining.

Another reason that has been observed to contribute to recording shorter fatigue lives with the rectangular shape is the corners along the section length of the test specimens. These corners (as also shown in Hoey and Taylor (2009a) for plain acrylic glass specimens, thus pre-polymerised PMMA) seemed to increase the stress concentration along the rectangular specimens, which became more effective if pores or defects existed nearby the corners, providing the most obvious fatigue crack origins as illustrated by the micrographs in Figure 4.12 as these specimens showed the shortest fatigue lives in their groups. The

existence of similar defects near the circular circumference of the other specimen shape was not observed to lead to such reductions in the fatigue lives. Evans (2006b), in support of this deduction, stated that “arguably the effect of porosity is therefore an artefact of the specimen design, rather than a change in the properties of the material”. One aspect that is related to specimen shape effect which might need to be referred to here is the difference between the transitional section geometries (shoulders) of both specimen shapes (Figure 3.1 and Figure A1.1 and A1.2 in Appendix1), which could have some effect on load transfer into the gauge section since the circular shoulder provides more uniform load transitional geometry. However, investigations on the effect of this factor might need to be conducted in further research.

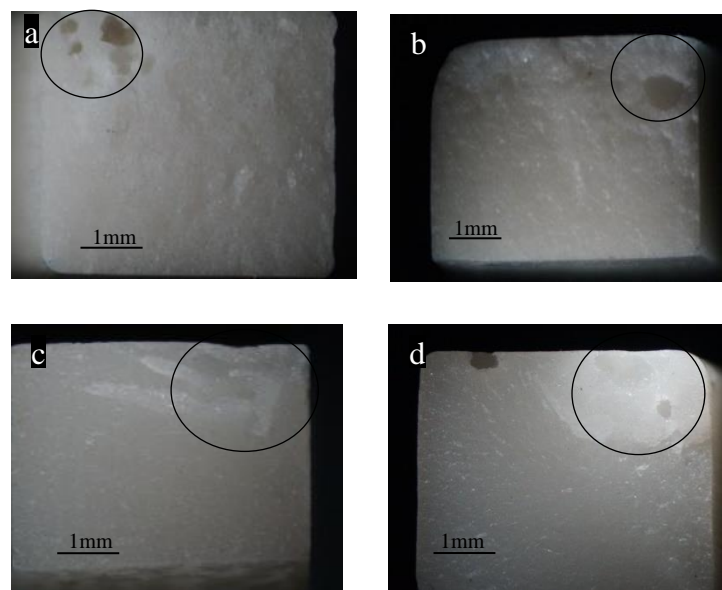


Figure 4.10 Examples of fracture surfaces that showed early failure of rectangular specimens due to localisation of pores or defects in the corners (circled) showing (a) for tension-tension and (b) for tension-compression of SmartSet GHV and (c) tension-tension and (d) tension-compression for CMW1. $R = 0.1$ and $R = -1$ respectively with a stress level of 20MPa (all marker bars = 1 mm).

The effect of specimen shape on controlling the degree of polymerisation has also been considered. Ram (1997) mentioned that the increased polymerisation enhances the tensile strength of polymers that is in principle comparable to the role of cross-linking in controlling the mechanical properties. For bone cement, Vallo et al. (1997) concluded that the residual monomer amount “acts as a plasticizer” that results in lower yield stress values, but more likely to improve the material’s toughness. Lewis and Janna (2003), for the cement specimens they tested, attributed the greater fatigue performance for the circular cross sectional specimens compared to the rectangular to the higher degree of

crystallinity for the former specimens. Although the findings of the current study have shown some difference in the degree of polymerisation when comparing the same specimen shapes of both cements (moulded and machined) against the other specimen shapes as provided in Table 4.9, it has been found that the variations in the degree of polymerisation due to the formation of specimens into two different shapes were statistically non significant (p -value of 0.17). This designates that, the effect of residual monomer on fatigue results, if any, would have occurred similarly in all specimen types making it of lower importance to consider the effect of this factor on the variations of fatigue results.

4.7.1.2 Surface preparation method (roughness)

Many studies have examined the effect of the procedures included in the moulding process, but not the moulding itself, on the final quality of produced specimens [e.g. Lewis (1999a), Graham et al. (2000), Dunne and Orr (2001) and Dunne et al. (2003)]. Considering the direct influence of changing the moulding protocol, Pennati et al. (2003) studied the effect of changing the moulding procedures, with no machining included, on fatigue properties of one bone cement (using rectangular specimens tested in zero-tension loading in air at room temperature) and concluded that fatigue strength results are greatly affected by specimen moulding technique with this factor being affected by the selected mixing and pressurisation processes. The study by Pennati et al. (2003) showed that adopting a “standard” moulding technique using a typical mould led to obtaining longer fatigue lives compared to other “new” moulding techniques they introduced and used for the aim of their study, where in all cases the specimens were made according to ISO 527-2 (i.e. rectangular cross sectioned).

This might be meaningful when it comes to reporting the potential reasons behind the enhancement of fatigue properties by moulding, particularly because of the moulding techniques involved in this current study. It has been clearly observed in this study that moulding is more likely to provide a thin well-coherent layer of the bone cement matrix that surrounds the whole structure of the specimen. Crawford et al. (1978) concluded that the presence of a “skin” layer on a moulded notch (rather than machined) of acetal copolymer specimens increases the fatigue properties by resisting fatigue crack initiation. In the current study, however, the formation of the outer protective layer has not always been well achieved, where, in some cases, the specimens were observed to have surface defects in the outer layer (Figure 4.11), leading to early fatigue failure of these specimens

which is likely to be one of the reasons to have wide variations between the high and low fatigue lives within the moulded specimens.

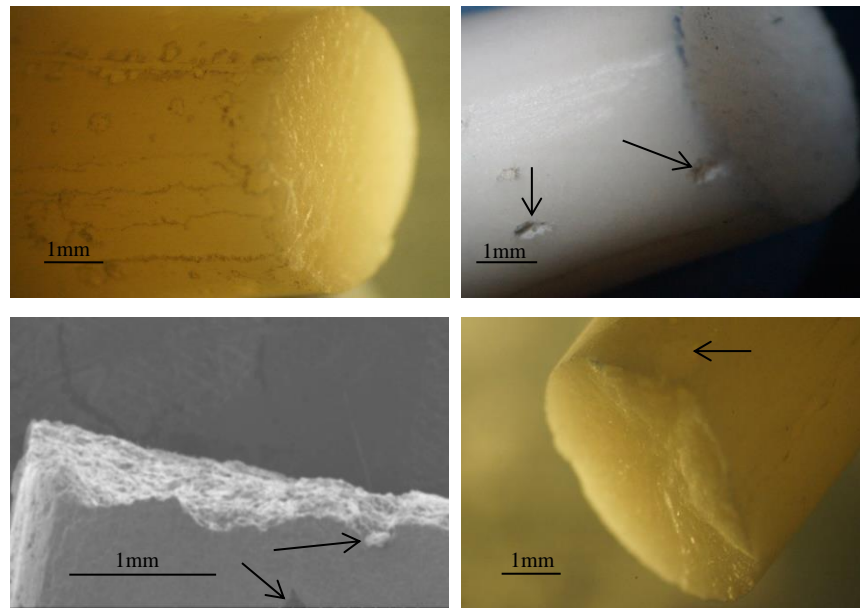


Figure 4.11 Examples of the defects observed on the outer surface of some moulded specimens (all marker bars = 1 mm)

In addition, it is well known that air bubbles form during the mixing and working of bone cement components, which are reduced by mixing vacuum systems, and moulding of the cement mixture causes the majority of these air defects to remain within the specimen. There is a great chance for the formation of some air bubbles due to the evaporation of the monomer during the early and hotter stages of the polymerisation process (Debrunner et al., 1976; Bishop et al., 1996) which can transfer towards the surface or stay within the specimens, providing both surface- and volume-distributed pores. In this regard, the notice reported in Bhambri and Gilbertson (1995) that “in some cases the crack initiated from internal defects in the presence of near-surface defects at the fracture plane” was also apparent in the current study. The fracture surfaces of many moulded specimens, however, have indicated that the severity of the pores formed within the specimen sections depends on the pore size and shape where the effect of these pores is, in turn, influenced by the position of the pores within the fracture surface such that, for both specimen shapes, the closer the pore to the outer surface the severer the effect. The influence of the stress type and magnitude on controlling the fatigue life seemed also to depend on the localisation of defects within the specimen.

In terms of the effect of machining on surface roughness and fatigue life, it has been observed that, in general, fatigue longevity declined significantly for the majority of the tested specimens (for both rectangular and circular cross sectioned) compared to the fatigue longevity achieved when the moulded specimens were used. This can be attributed to the interaction of several causes. Machining of the cast bone cement blanks leads to the removal of the outer “crack-resisting” layer provided by moulding; the observation that was also reported by Paravic et al. (1999). This change in the surface finish is more likely to contribute to recording shorter fatigue lives since, first, the internal pores and defects become emergent on the outer surface and, second, these pores and defects have severer crack initiation origins.

In addition to the decrease in surface quality due to machining, other reactions might exist leading to changes even in the properties of the material’s original structure. Being a polymer, polymethylmethacrylate bone cement has a relatively low modulus of elasticity [approximately 2.4 GPa (Webb and Spencer, 2007; Pelletier et al., 2010)]. Low moduli means that the polymer deflects elastically during the machining process which decreases its tolerability (Ashby, 1999). In addition, polymers in general have a chance to form free radicals during machining leading to the breakage of bonds at certain depths (Backman and Devries, 1969). It has also been reported the presence of shearing forces during fabrication processes can increase the chance of breaking the covalent bonds earlier (Hertzberg and Manson, 1980) where machining is likely to provide these conditions. Interpreting the results obtained in this study according to these concepts will certainly mean that the change in the surface properties due to machining of bone cement led to more potential crack initiation sites enhancing the occurrence of earlier fatigue failure.

The type and direction of machining also need to be considered, particularly when machining different specimen shapes. During machining of the rectangular specimens, the cutting tool moves longitudinally on the specimen surface machining the four specimen sides sequentially and removing the material in one direction, with the attention to provide as high surface quality as possible. When machining the circular cross sections, however, the specimen is maintained between two ends to allow the specimen to rotate using an adequate speed while the sharp cutting tool is fed to a certain depth of the specimen outer surface removing the material circularly in a longitudinal movement from one end to the other. After machining, the specimens will show fine machining lines (visible under the optical microscope) parallel to the load direction for the rectangular specimens and perpendicular to the load direction for the circular specimens. Nevertheless, the effect of

perpendicularity of the machining direction in relative to the testing axis for the circular specimens has been found to be influenced by the change in cement composition which can be more effective with the increase of accumulation of inclusions in the cement. The circular machined SmartSet GHV specimens have mostly provided shorter fatigue lives compared to the CMW1 counterparts, and vice versa for the rectangular.

4.7.2 Effects of cement powder inclusions

While the fatigue results have shown variations due to using different specimen types, the cement composition has meanwhile appeared to influence these variations. Although Weibull analysis has generally shown greater fatigue lives for the moulded specimens compared to the machined, the results have also revealed the degree of variations between fatigue lives of different specimen types can be controlled by the type of cement used. For example, the factor of difference between the fatigue performance indices (three-parameter Weibull of fully reversed tension-compression – Figure 4.3) was 8.5 between the circular moulded and circular machined specimens for SmartSet GHV which was only 3.5 for the CMW1 equivalent specimens. Also, within the same analysis, the rectangular machined specimens showed greater fatigue performance compared to the circular machined that was totally the opposite when the CMW1 was used. When testing at different stress levels, the S-N analysis (Figure 4.6) has provided wider comparison of the fatigue behaviour of different specimen types, showing the same general trend of the moulded specimen, particularly the circular, to provide longer fatigue lives. The degree of variations between different specimen types has also been shown to vary between the two cements. The analysis has again shown the reverse fatigue behaviour of both cements when using the two machined specimen types.

It has been shown in many studies, as introduced in Section 2.3.1.1, changes in chemical compositions or inclusions can variously alter fatigue properties. Davies et al. (1989), for instance, believed that chemical composition plays a role even greater than porosity stating that “the dominant determinant of the fatigue life of different commercially available bone cements is their basic composition not their porosity”. The findings of the current study have also demonstrated that variations in chemical inclusions can alter fatigue performance; however, these variations are altered by the selected package of stress regime (specimen specification and stress type and level). It is required, therefore, to suggest some possible reasons that contributed to controlling the fatigue longevity of the two cements examined in the current study leading them to reveal dissimilar or even opposite trends of

fatigue performance when using different specimen types. In other words, it is important to know how specimen shape and production method can variously describe the fatigue behaviour of different bone cements (as demonstrated by the analyses of the results) depending on the difference in additives. The SmartSet GHV specimens contain 9.76wt% zirconium dioxide and 2.87wt% gentamicin whereas CMW1 contains only 6.18wt% barium sulphate. This leads to estimated volume contents of 2.20 vol% zirconium dioxide and 1.70 vol% of barium sulphate in the specimens of SmartSet GHV and CMW1, respectively. This is important to highlight since it can be a vital factor in governing the fatigue life of bone cement, apparently depending on the surface production method. For materials in general, it has been reported that “the presence of inclusions by an order of magnitude larger than the machined surface roughness, generally overrides the effect of surface topography” (Novovic et al., 2004). The effect of the type and amount of additives on fatigue longevity of bone cement, however, seemed also to be influenced by the stress type and level (as discussed below).

To consider the effect of inclusions, it has been observed that, in general, SmartSet GHV fracture surfaces, in addition to including more additives, have indicated that the ZrO_2 opacifier particles have a greater tendency to agglomerate compared to the $BaSO_4$ particles within the CMW1. Figure 4.12 illustrates this observation comparing fracture surface of both cements at two magnification levels. This difference in opacifier content and distribution, along with the difference in the basic polymer structure of the cements, also provides a potential cause to have rougher fracture surfaces for SmartSet GHV compared to CMW1. One factor that might be worth considering when it comes to the random distribution of the opacifier particles, particularly for SmartSet GHV, is the effect of the mixing method used in this study. Whilst vacuum mixing is capable of reducing porosity to a large extent, it is not specifically aimed to provide even filler distributions with seemingly no mixing technique sufficient to solve this issue. While mixing by centrifugation, for instance, is conceptually thought to provide better fillers distribution and thus greater fatigue life, this is not always possible as can be deduced from several studies such as Rinnac et al. (1986), Davies et al. (1989) and Lewis et al. (1997).

In a similar way to the effect of porosity, when moulding, the inclusions seemed to provide less detrimental effect on fatigue life for both cements used in this study, with the difference among cements being largely affected by the stress level. Differently, machining the surface will lead to cutting through the accumulations of the opacifier inclusions near the surface producing, in some cases, severer crack initiation sites. The difference in

powder chemical composition has been shown in this study to lead to dissimilar fatigue longevity for both of the machined specimen shapes reflecting perhaps the difference between the filler response in both cements to the machining impact and direction since, for both Weibull and Wöhler analyses of the fully reversed fatigue loading, the rectangular machined specimens of SmartSet GHV provided longer fatigue lives compared to the CMW1 counterparts and vice versa for circular machined specimens.

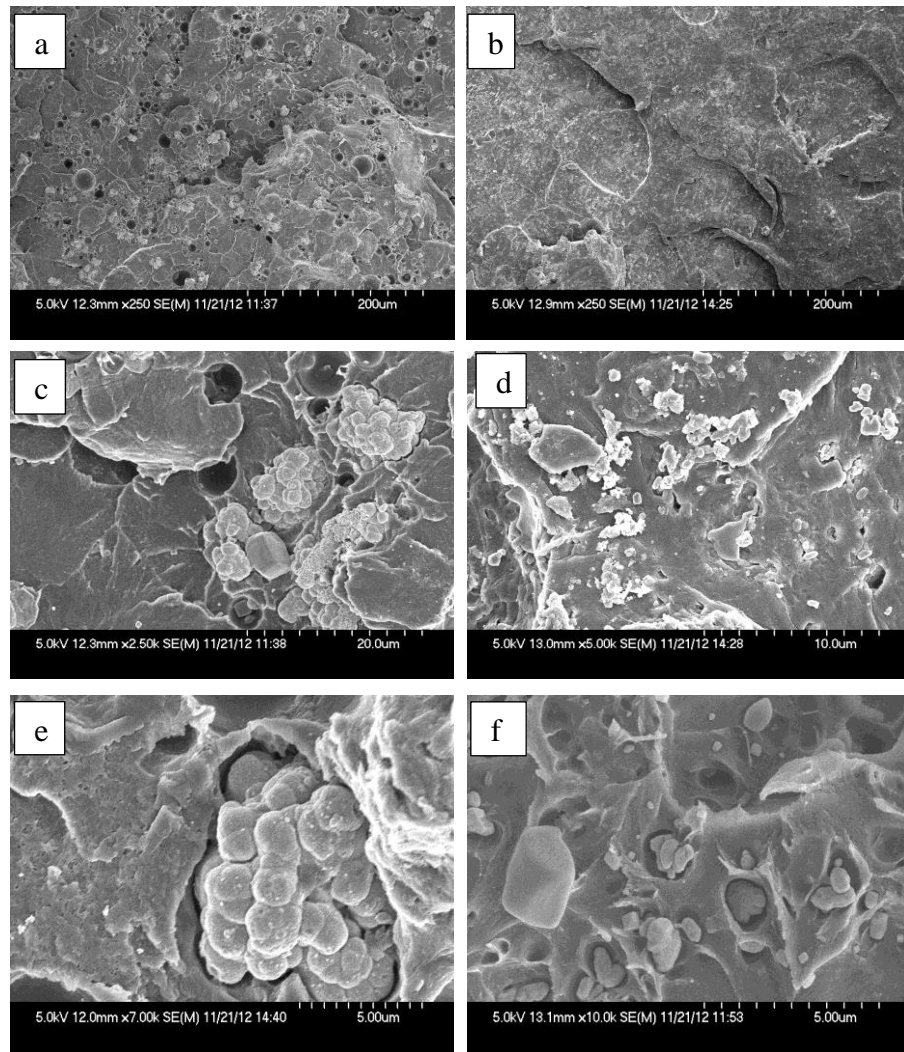


Figure 4.12 Micrographs of fracture surfaces compare the likely spread and accumulation of the two different opacifier particles in (a, c, e) SmartSet GHV and (b, d, f) CMW1, at three magnification levels (a & b marker bars =200µm, c & d marker bars =10µm and e & f marker bars =5µm).

4.7.3 Effects of stress type

Either fully reversed tension-compression stress (mean stress = 0) or tension only stress (mean stress > 0) has been particularly adopted in several *in vitro* studies, to better imitate

the *in vivo* fatigue conditions. However, the effect of tension and compression stresses in controlling the fatigue life of bone cement might be dissimilar under the *in vitro* and *in vivo* conditions. Gates et al. (1983) [also based on Carter et al. (1982)], stated that fatigue failure is primarily driven by the tensile segment during the fully reversed tension-compression with the effect of the compression segment being “small or negligible”. Dunne et al. (2014) pointed out that while *in vitro* tension can be a more important factor inducing cement failure than compression, tensile loading *in vivo* is not the only dominant mode, but rather complex combined stresses are more likely to occur. The tension-compression loading is, therefore, not only preferred in testing because this type of loading, as in Dowling (2007), provides a good indicator of fatigue performance of materials, but also more likely to exist *in vivo*.

For the findings of the current study, comparing the fatigue indices of the Weibull analyses (either two- or three-parameter) for the fully reversed tension-compression loading with that for the tension-tension loading (both stress types at a maximum stress of 20 MPa with $R = -1$ and $R = 0.1$, respectively) have indicated that stress type can be a key factor in governing fatigue life of bone cement specimens. Table 4.10 summarises the differences in fatigue performance when each of the stress loading types were applied on all specimen types.

Table 4.10 Comparison of the difference in fatigue performance index (I) for all specimen types at the fully reversed tension-compression (± 20 MPa) and tension-tension (2 to 20 MPa) stress conditions (based on the three-parameter Weibull analysis)

Specimen type	(SmartSet GHV)			I /cycles (CMW1)		
	I /cycles		Factor of difference in I	I /cycles		Factor of difference in I
	Tension-tension	Tension-compression		Tension-tension	Tension-compression	
RDM	207,375	35,489	6	69,080	34,199	2
RMM	250,538	17,797	14	148,902	16,295	9
CDM	448,511	76,898	6	124,496	109,825	1.1
CMM	60,416	9,117	6.5	147,782	31,013	5

It is fairly obvious, according to the results, that subjecting a specimen to tensile fatigue only would not be as detrimental as if the specimen was subjected to an alternating tension-compression loading, indicating that the compression cyclic segment accelerates the fatigue failure considerably. The fatigue results obtained from testing using the two

stress types have correspondingly been found to be affected by the specimen shape and production method. The effect of cement composition appeared also to be important when comparing the tension-tension stress regimes of one cement against those in the other cement. The combined effect of specimen shape, surface production method and cement composition appeared to be dissimilar among the two stress types, making the interpretation of fatigue results more complicated in terms of identifying the underlying factors that control the fatigue life of bone cements. There are several points, however, that should be highlighted in regard to these findings.

First, one mechanism that has usually been considered is the buckling of the rectangular specimens under the fully reversed tension-compression. While this is theoretically prospective, it seemed that buckling had not occurred during the fatigue testing of the rectangular specimens. This deduction has been provided after considering three indicators. Firstly, the Euler buckling load calculations (Appendix 4) showed that a compression stress levels of at least 31 and 35 MPa are required for the rectangular and circular specimens, respectively, to encounter buckling and these calculations assume that the entire distance between the grips is at the gauge length cross section so substantially underestimate the Euler buckling load. Secondly, the direct visual observations on a number of specimens during testing indicated no obvious buckling. Thirdly, the behaviour of the relevant stress-strain curves throughout testing provided stable behaviour similar to that for the circular specimens with no indication of any significant bending occurred on the specimens. Previously, Lewis and Janna (2003) compared fatiguing of the rectangular specimen shape to the circular shape, under fully reversed tension-compression of 15 MPa, and reported their results with no mention of examining the buckling phenomenon. The estimated buckling resistance in the current study can presumably be due to the reasonably small size of the rectangular specimens (half-sized ISO 527-2) with a sufficient cross sectional area of close thickness and width dimensions (nominally 4mm x 5mm). With thinner specimens, even of the same specimen length, the buckling phenomenon might have greater chance to occur.

Second, fatigue testing was performed at stress-controlled conditions which is different from Carter et al. (1982) and Gates et al. (1983) who adopted strain-controlled conditions. Obtaining incompatible results to that reported by those authors is accordingly possible since materials, as illustrated by Figure 2.2, can provide totally opposite (softening or hardening) deformation depending on the controlling parameter being stress or strain limit. Kindt-Larsen et al. (1995) found greater fatigue performance associated with Boneloc[®]

compared to Simplex P[®] under fully reversed strain conditions and vice versa under fully reversed stress conditions (Figure 2.7). They stipulated that the preference suggested by Carter et al. (1982) for using the strain-controlled conditions in fatigue testing of bone cement would only be correct if Boneloc[®] cement tended to provide greater fatigue performance *in vivo* compared to Simplex P[®] and other cements; the condition that has been oppositely approved according to many clinical reports such as Riegels-Nielsen et al. (1995), Nelsen and Wiig (1996) and Abdel-Kader et al. (2001). Testing under stress-controlled conditions therefore, as also demonstrated by Soltész (1994), is likely to provide more appropriate and reflective imitation to the loading of bone cement *in vivo* than the strain-controlled conditions.

Third, the maximum stress level adopted to compare the effect of stress type of 20 MPa seemed to be reasonably high for the fully reversed tension-compression regimes, leading the specimens, particularly the machined, to encounter earlier fatigue failure. The findings of the tension-tension tests did not reveal such short fatigue lives, indicating the essential role of the compression segment at this stress level in accelerating the failure of the specimens. At lower stress levels, however, the less influential effect of the compression phase in fatigue testing might exist since, as discussed in the next chapter, more slowly progressing growth in fatigue cracks are expected at these lower levels. However, further study including lower values of the maximum stress level for the tension-tension regimes (12.5 and 15 MPa to be compared to that for the fully reversed testing) is still needed to confirm or reject these suppositions.

4.7.4 Description of fatigue behaviour: effects of analysis approaches

For all analytical approaches used in this research, it has been clearly shown that fatigue results are dependent on the stress regime and cement composition used. The use of Student's *t*-test and ANOVA as parametric statistical comparison approaches as recommended in ASTM F2118, in addition to not providing a precise measurement of the degree of difference, may in particular cases be inappropriate as these approaches might decide a difference between two testing groups is non significant while the factor of difference is important. This matches the statement made by Lewis and Nyman (2000) regarding the inadequacy of using particular statistical analyses to conduct the pairwise comparisons for making accurate conclusions. Nevertheless, the use of these or similar statistical approaches would still be useful, but only in providing preliminary indicators for

fatigue life comparisons. The use of Weibull and Wöhler parameters and approaches, on the other hand, seemed to provide more precise comparisons of fatigue behaviours. Although the factors of difference between fatigue performance of various specimen types appeared to be affected by the adopted analysis approach (two-parameter Weibull, three-parameter-Weibull or S-N curve), this has not led to significant changes in the general trend of fatigue behaviour differences of all groups at any stress type and level. Yet, there are particular considerations that should be focused on regarding the use and findings of Weibull and Wöhler analyses.

For the Weibull analysis, the difference between the two- and three-parameter Weibull approaches in terms of describing fatigue life can be assessed from two perspectives. First, the use of both approaches (for both stress types at the examined stress level of 20 MPa) has not shown remarkable differences regarding the general trend of fatigue behaviour of all specimen types. There is no evidence, according to the findings of the current study, that switching between using either of these approaches is likely to provide major conflicts amongst results. Second, however, using one approach instead of the other can possibly lead to reporting different values of Weibull shape and fatigue characteristic parameters (and thus fatigue performance index), affecting the reported factors of difference. The decision as which approach is more applicable cannot be confidently made because, while the three-parameter distribution is thought to provide further flexibility (Evans et al., 2000) and improved estimates (Curtis and Juszczyk, 1998), this can be influenced by the judgment of the best locus of the French curve drawn to determine the third parameter (N_0) (Janna et al., 2005; Shigley and Mischke, 1989). Janna et al. (2005) suggested that the two-parameter or three-parameter Weibull functions is more appropriate fit when N_0 is less than or greater than zero, respectively. This appears to be an unclear deduction since N_0 (Weibull minimum fatigue life) cannot be less than zero, and assumed to be zero for the two-parameter Weibull. Lewis and Austin (1994) stated that the two-parameter Weibull analysis has been largely used while it is “inappropriate because its use implies that N_0 is zero”. In effect, the range within which lies the Weibull shape parameter (b), which is indeed affected by the minimum fatigue life parameter (N_0), can probably play the role in terms of providing distinguishably clear differences between the two- and three-parameter distributions. It has been pointed out that, at lower b values such that when $b = 1$, “the three-parameter Weibull reduces to that of the two-parameter exponential distribution” (Reliability Engineering Resources, 2002). For the exponential distribution ($b=1$), in particular, this is theoretically logical since the hazard functions (failure rate) for the two- and three-Weibull distributions are defined as Equations 4.3 and 4.4, respectively (Evans et

al., 2000). It is likely for fatigue of bone cement results to have right skewed Weibull distributions with high variability, but generally close to the exponential shape, as demonstrated in the current study, thus decreasing the significance of variations between the findings of the two Weibull approaches. Overall, however, it seems that careful use of the three-parameter Weibull distribution would lead to less biased conclusions.

$$\lambda = N_a N_f^{b-1} / N_a^b \quad (4.3)$$

$$\lambda = N_a (N_f - N_0)^{b-1} / N_a^b \quad (4.4)$$

The S-N curve analysis, in comparison, due to its specific excellence in comparing fatigue trends at different stress amplitudes, provided wider description of fatigue behaviour between all stress regimes (of the fully reversed tension-compression conditions). While it has, in general, indicated the same trends of fatigue performance provided by the Weibull analyses, it could interestingly show that fatigue lives of the same specimen type of two cements can provide dissimilar or opposite fatigue behaviour at different stress amplitudes. This finding provided by the S-N analysis would have been difficult to be noticed if the Weibull approaches were instead repeated for different stress levels. Also, the Weibull analysis requires at least double the number of specimens per testing group. If the linearity of the S-N curve, as assumed by Murphy and Prendergast (2000) who examined a range of stress levels between 13 and 25 MPa, can continue at lower levels than those examined in the current study (say down to 7 MPa that represents the average stress encountered *in vivo*), then the *in vitro* fatigue life can be estimated at these levels, which will be rather difficult to experimentally measure by direct testing due to being time consuming when using as low testing speed as 2 Hz; the frequency that is recommended by ASTM F2118 when the effect of test frequency on the particular cement in question is unknown. The endurance fatigue limit, however, needs to be identified for any examined cements, as the proposed linearity of the S-N curve can no longer be expected under this stress limit. The endurance limit has been reported as, for example, 3-4 MPa (run-out 1×10^7 cycles) when applying a 0.001 strain level on Simplex P[®] cement (Davies et al., 1987), 8.1 MPa (2×10^6 cycles) for fully reversed tension-compression fatigue test of CMWTM3 Cement (Lewis and Austin, 1994) and 9.2 MPa (1×10^7 cycles) for tension fatigue of Cemex[®] □RX cement (Bialoblocka-Juszczak et al., 2008).

4.8 CONCLUSIONS

- 1- Specimen type can variously affect the fatigue behaviour of bone cement. In general, moulded specimens, particularly with circular cross sections, tend to provide significantly greater fatigue lives. The behaviour is likely to be altered by the cement composition.
- 2- Moulding of specimens provides more crack resisting layers while machining can detrimentally affect their outer surfaces depending on the amount and type of particles included within the specimen, leading to the presence of these elements on the surface and thus creating more crack initiation sites.
- 3- There is no constant correlation between variability in fatigue behaviour and specimen type. One specimen type, compared to another, might show greater overall fatigue performance in conjunction with revealing greater variability.
- 4- Variability in fatigue results is governed by the presence of pores and defects within or on the surface of a specimen. This, however, seems to be differently influenced by specimen type and cement composition.
- 5- Tension-compression fatigue leads to significantly shorter fatigue life than tension only, indicating the role of the compression segment in accelerating fatigue failure which contradicts with older reports that compression has a minor effect. While the decrease in fatigue life due to the compression portion is apparent, it is differently influenced by specimen type and cement composition.
- 6- The selection of a particular stress level can be a key factor in describing fatigue behaviour of bone cements. Depending on the chemical composition, the fatigue behaviour of different specimens of bone cements can behave differently at high and low stress levels.
- 7- The overall trend of fatigue behaviour did not show any significant change when using two- and three-parameter Weibull nor when using the S-N analysis. The latter, however, can be more descriptive due to being specific when considering the effect of stress amplitude.

CHAPTER 5. BEHAVIOUR OF FATIGUE CRACK PROPAGATION

5.1 INTRODUCTION

The fatigue life of materials is controlled by two phases, crack initiation and crack propagation. For the *in vivo* fatigue of bone cement, crack growth has been reported to be the dominant failure mechanism (Topoleski et al., 1990). Further investigation of the factors that control fatigue crack development is important in describing the reasons behind fatigue failure. Since fatigue cracks initiate from pores or defects, particularly on the surface of specimens, it is vital to compare the behaviour of fatigue cracks for different specimen types. To consider the possible change in crack growth behaviour due to the change in chemical composition, comparing cements with different formulations is also relevant. These comparisons can be performed by examining the increase in absorbed energy per loading cycle during the fatigue testing period and, simultaneously, considering the reduction in secant modulus. Increasing absorbed energy indicates the generation of fatigue cracks and lower modulus also reflects the associated increase in accumulated fatigue damage. Further investigation of the cement composition effect on fatigue crack behaviour can be achieved by comparing the fatigue crack growth rate in pre-cracked specimens such as the compact tension (CT) specimens. In the current study, the concept of changes in absorbed energy and modulus was used as an indicator of the crack extension as the cyclic loading progresses, comparing this for the four specimen types of both cements. To validate the differences in fatigue crack behaviour obtained for the two cements, CT specimens (ASTM E647) were used to measure and compare the fatigue crack growth in these cements, as the CT specimens provide a great chance of monitoring the crack propagation in a controlled zone while meeting the constraints of linear elastic fracture mechanics (Vashishth et al., 1997).

5.2 METHODS

The developed MTS data logging procedure, in addition to measuring the total fatigue life of all specimens, was programmed to store the force-displacement data for each specimen throughout fatigue testing in the manner detailed in Section 3.2.2.3. After testing, for the median specimen of each stress regime, stress-strain curves were generated for selected

loading cycles and the instantaneous absorbed energy and secant modulus were both determined at each of these cycles as described in Section 3.3.3.2. The obtained absorbed energy and secant modulus values were plotted against the number of cycles to failure as explained in Section 3.3.3.4.

To measure the fatigue crack growth in the two cements, CT specimens were prepared as described in Section 3.2.3.1. As the ASTM E647 requires “a pre-crack that has been growing at or below the test load”, the crack measurement gauges were installed on the specimens as detailed in Section 3.2.3.2. A distance of 1mm was left between the “artificial”, that is machined, crack tip and the first strand of the crack propagation gauge to ensure that the start of gauge fracture occurred at more stable conditions of crack progress. The obtained data was analysed as described in Section 3.3.4.

5.3 ANALYSIS OF STRESS-STRAIN CURVES

The shapes of the stress-strain loops for the different stress regimes varied depending essentially on the cement composition, stress amplitude, and specimen type. For certain specimen types at certain stress levels, the effect of specimen shape and production method for a particular cement composition was more apparent. The analysis of these findings through the estimation of the change in the absorbed energy and reduction in modulus per load cycle has made the comparisons even more obvious. The change of the stress type (tension-compression or tension only) provided, as one would expect, different behaviour for the absorbed energy and modulus. However, the general trend of crack growth behaviour, represented by the change in energy and modulus, for the tension-tension stress type appeared similar to the findings at the lower stress levels used with the tension-compression testing, knowing that the amount of energy absorbed per cycle was approximately the half of that for the lowest tested, but not the equivalent, tension-compression level.

5.3.1 Stress-strain curves: fully reversed tension-compression fatigue

The shapes of the stress-strain curves varied depending on the bone cement composition. The effect of specimen type and more importantly the effect of production method were both apparent. Appendix 5 provides illustrations for the changes in the shape and size of

the stress-strain loops from the early fatigue cycles to the few final cycles before failure, comparing this for all specimen types of SmartSet GHV (Figure A5.1) and CMW1 (Figure A5.2). Considering both specimen type and cement composition, the stress-strain curves were similar at the low stress levels (± 12.5 and ± 15 MPa). This was not the case for the same comparison at the higher stress levels (± 20 and ± 30 MPa) where the shape and size of the hysteretic loops appeared to differ, showing clearer dependence on specimen type. The CMM specimens of SmartSet GHV, for instance, provided one of the largest changes in shape and size which became clearer during the final cycles before failure. The CMW1 counterparts provided less deformation and lower increases in loop size. The findings of these variations for all specimen types are discussed below on the basis of the expected changes in absorbed energy (increase in stress-strain loop area) and modulus (decrease in secant gradient of the loop).

5.3.1.1 Changes in absorbed energy

The amount of absorbed energy per loading cycle varied depending on the cement composition, specimen type and stress parameters (Figure 5.1). Apart from the fact that fatigue longevity was largely controlled by specimen type, the gradual increase in the absorbed energy was seen obviously clearer among the SmartSet GHV specimen types compared to the CMW1 specimens. The former cement specimen types showed variations in energy absorbed amongst each other that was not found for the latter cement specimens.

For SmartSet GHV (Figure 5.1a), the variations of the absorbed energy between the four specimen types were seen to be mainly affected by the stress level used. At the lower stresses of ± 12.5 and ± 15 MPa, the absorbed energy per loading cycle increased gradually and slowly throughout the testing period. At a higher stress of ± 20 MPa, the energy absorption progress in the moulded specimen was similar to that for the lower stress levels whereas in the machined specimens, particularly the circular, the absorbed energy amount started to increase rapidly well before reaching failure. At the highest stress of ± 30 MPa, the rapid increase started earlier for all specimen types, but the circular machined specimens provided remarkably higher increases in the energy absorption rate.

For CMW1 (Figure 5.1b), all specimen types showed similar behaviour, which was steady throughout the fatigue testing period, absorbing approximately the same amount of energy per loading cycle until only a few cycles before failure where the absorbed energy increased slightly. The absorbed energy per loading cycle at the highest stress level was, however, almost three times greater compared to the other stress levels.

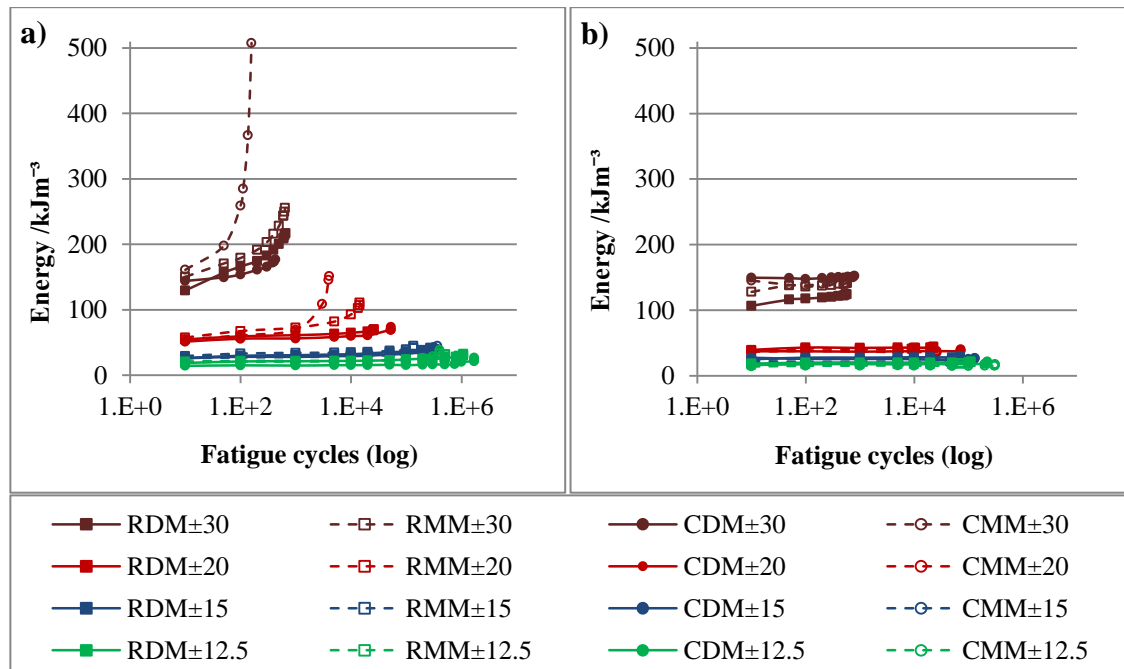


Figure 5.1 Variations in the increase in absorbed energy per fatigue cycle for the different specimen types tested in tension-compression, showing (a) SmartSet GHV and (b) CMW1 (note: RDM±30 refers to the RDM specimen type tested at stress levels of ±30 MPa etc.)

5.3.1.2 Changes in secant modulus

As can be seen from Figure 5.2a, the modulus appeared to decrease gradually for SmartSet GHV at the two lower stress levels until reaching a point well before failure where the modulus started to decrease more rapidly. At the two highest stress levels, the modulus started to decline rapidly from early fatigue cycles, particularly for all specimen types tested at ± 30 MPa and the machined specimens tested at ±20 MPa. At the 10th fatigue cycle, and considering all stress levels, the modulus started in a range between 2.1 and 2.8 GPa, giving an average of 2.45 GPa. At the 5th cycle before failure, this range declined to between 1.5 and 2.2 GPa with an average of 1.85 GPa (reduction in average of 25%).

For CMW1 (Figure 5.2b), a low reduction rate in modulus was seen during the testing period until reaching a point before failure where the modulus started to decline rapidly. At the 10th fatigue cycle of all specimens and stress levels, the modulus commenced with a range of between 2.2 and 3.1 GPa, providing an average of 2.65 GPa. At the 5th cycle before failure, this range became between 2.1 and 2.9 GPa to provide an average of 2.5 GPa (reduction in average of 6%). Table 5.1 compares the secant moduli for all specimen types of both cements at early fatigue life and few cycles before failure.

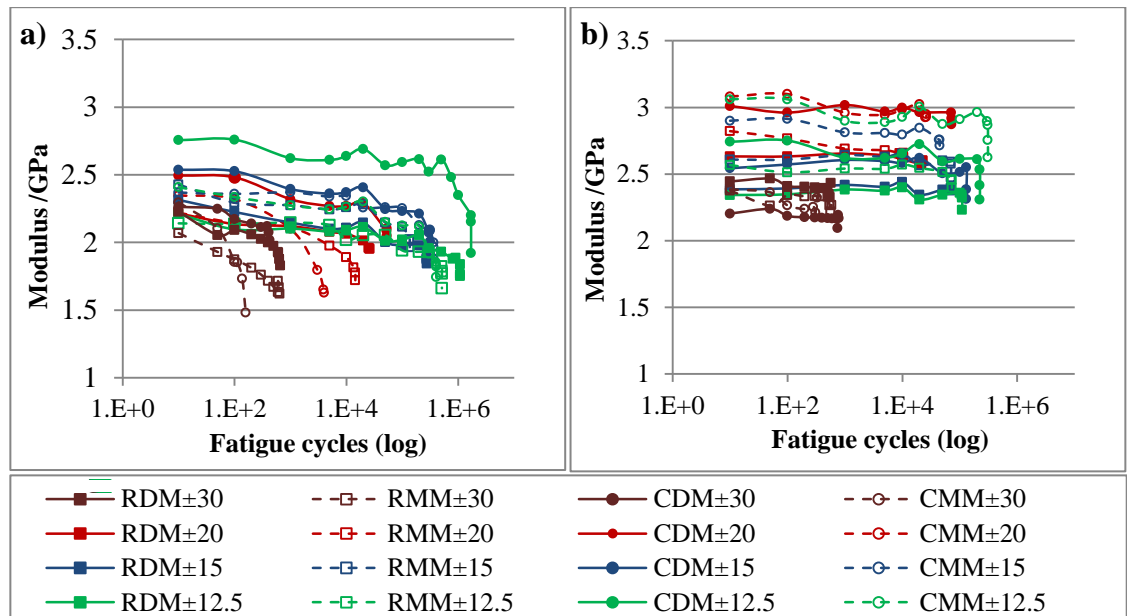


Figure 5.2 Variations in the reduction in modulus per fatigue cycle for the different specimen types tested in tension-compression, showing (a) SmartSet GHV and (b) CMW1 (note: RDM±30 refers to the RDM specimen type tested at stress levels of ±30 MPa etc.)

Table 5.1 Comparison of secant moduli of various specimen types tested in tension-compression measuring the modulus at an early fatigue cycle (the 10th cycle) and a late fatigue cycle (the 5th cycle before failure) with the total reduction in modulus in percentage between these two cycles

Stress levels	Specimen type	Modulus/ GPa (SmartSet GHV)			Modulus/ GPa (DePuy CMW1)		
		10 th Cycle	Last 5 th cycle before failure	Reduction average (%)	10 th Cycle	Last 5 th cycle before failure	Reduction average (%)
±12.5 MPa	RDM	2.21	1.75	21	2.34	2.23	5
	RMM	2.14	1.66	22	2.57	2.40	7
	CDM	2.76	1.92	30	2.74	2.31	16
	CMM	2.41	1.74	28	3.06	2.63	14
±15 MPa	RDM	2.31	1.84	20	2.39	2.38	0.5
	RMM	2.43	1.96	19	2.61	2.48	5
	CDM	2.53	2.01	21	2.54	2.31	9
	CMM	2.37	1.88	21	2.90	2.71	7
±20 MPa	RDM	2.21	1.95	12	2.63	2.60	1
	RMM	2.22	1.72	23	2.82	2.63	7
	CDM	2.49	2.05	18	3.01	2.87	5
	CMM	2.35	1.63	31	3.08	2.93	5
±30 MPa	RDM	2.23	1.83	18	2.44	2.43	0.5
	RMM	2.07	1.62	22	2.38	2.27	5
	CDM	2.26	2.02	11	2.20	2.17	1
	CMM	2.30	1.48	36	2.39	2.32	3

5.3.2 Stress-strain curves: tension-tension fatigue

For all testing specimen types, gradual increases in the area of the stress-strain loops were seen. Calculations, however, showed that the stress-strain loop area increased more quickly for the SmartSet GHV specimens compared to the CMW1 specimens. Figure A5.3 in Appendix 5 compares the stress-strain curves for all specimen types, considering the shape of the curves at early and late fatigue stages. The effect of specimen shape and production method was less obvious with tension-tension loading compared to the tension-compression test regimes. Three specimen types (RDM, RMM & CDM) of SmartSet GHV, however, showed about three times greater elongation when reaching the 5th cycle before failure, compared to the fourth specimen type (CMM) of the same cement and also compared to the all specimen types of CMW1 that showed similarity in elongation amongst each other. The findings also showed clearer reductions in modulus for the SmartSet GHV specimens. The changes in absorbed energy and modulus throughout testing were mainly controlled by the cement composition, with minimal effect of the specimen type which was seen to play a clearer role with the tension-compression regimes.

5.3.2.1 Changes in absorbed energy

For each cement individually, greater similarity was found between the different specimen types in terms of the absorbed energy behaviour. Specimen type controlled the fatigue longevity, but with no clear difference between the changes in absorbed energy among the same material specimens. During testing, the absorbed energy increased gradually for the SmartSet GHV specimen types till reaching a point well before failure where the amount of absorbed energy started to increase more rapidly (Figure 5.3a). For the CMW1 specimens, approximately the same amount of energy was absorbed per fatigue cycle throughout the testing period with no significant increases until close to the failure point where the energy absorbed increased slightly (Figure 5.3b).

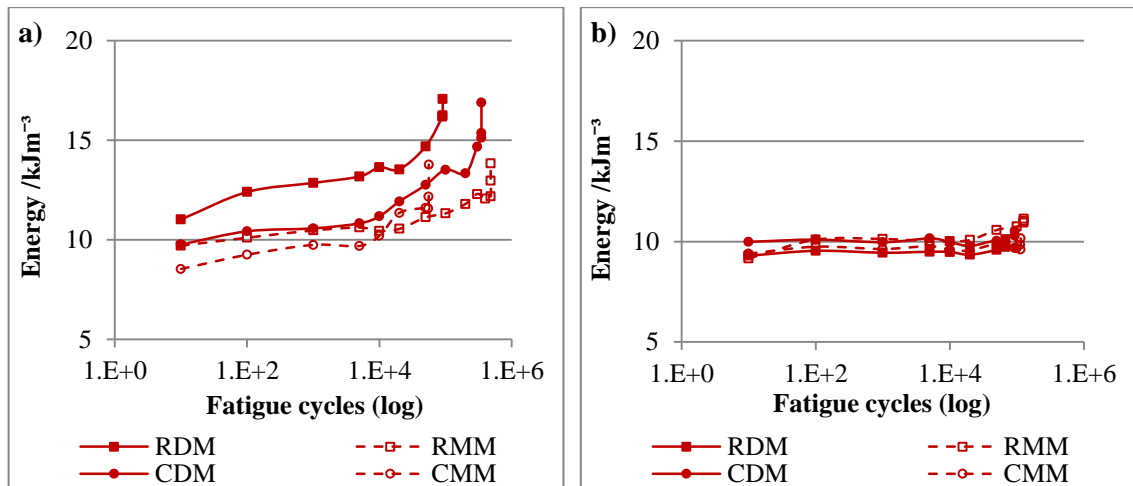


Figure 5.3 Variations in the increase in absorbed energy per fatigue cycle for the different specimen types tested in tension-tension, comparing (a) SmartSet GHV and (b) CMW1

5.3.2.2 Changes in secant modulus

Considering each cement composition individually, the trends of the reduction in secant modulus for the four specimen types were similar, particularly for the CMW1 specimen types. As can be seen from Figure 5.4 and Table 5.2, the decrease in modulus was more noticeable for the SmartSet GHV specimens showing total reductions of 17 to 24% between the 10th cycle and the 5th cycle before failure. This decline was only about 8% for the CMW1 specimens.

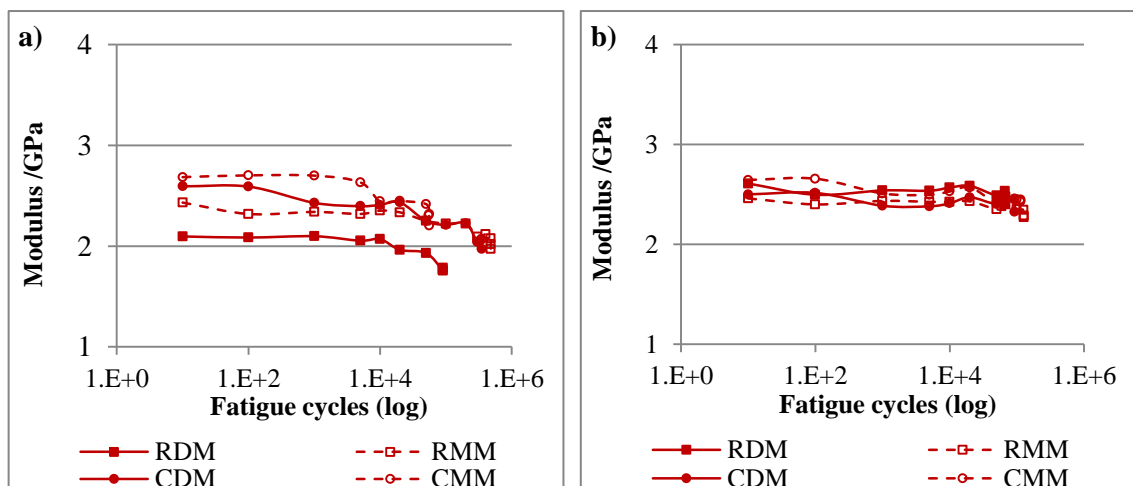


Figure 5.4 Variations in the reduction in modulus per fatigue cycle for the different specimen types tested in tension-tension, comparing (a) SmartSet GHV and (b) CMW1

Table 5.2 Comparison of secant moduli of various specimen types tested in tension-tension measuring the modulus at an early fatigue cycle (the 10th cycle) and a late fatigue cycle (the 5th cycle before failure) with the total reduction in modulus in percentage between these two cycles

Stress levels	Specimen type	Modulus / GPa (SmartSet GHV)			Modulus / GPa (CMW1)		
		10 th cycle	Last 5 th cycle before failure	Reduction average/ %	10 th cycle	Last 5 th cycle before failure	Reduction average/ %
Between 2 and 20 MPa	RDM	2.10	1.75	17	2.61	2.40	8
	RMM	2.43	1.97	19	2.46	2.27	8
	CDM	2.59	1.97	24	2.50	2.33	7
	CMM	2.68	2.20	18	2.64	2.43	8

5.4 FATIGUE CRACK GROWTH MEASUREMENT

5.4.1 Fatigue crack length vs. fatigue cycles

As indicated by the findings of the changes in absorbed energy and secant modulus, the same trend of difference in fatigue crack growth behaviour between the two tested cements was found when the CT specimens of both cements were subjected to fatigue loading. While the fatigue crack started to propagate increasingly in SmartSet GHV specimens from earlier loading cycles (or at least well before failure), showing progressively increased crack propagation as the fatigue cycles increase, the cracks seemed to not propagate or propagated at minimal rates for the CMW1 specimens till close to failure, after which the fatigue cracks propagated rapidly.

Over the investigated crack propagation length of 5mm (which is represented by the width of the crack gauge starting from 1mm after the CT pre-crack tip), all the SmartSet GHV specimens, as illustrated in Figure 5.5a, showed similar and constant increasing gradient in fracture growth rate over a length of approximately 3mm. The crack growth speed increased more rapidly over the remaining 2mm, accelerating the final failure. CMW1 specimens (Figure 5.5b), in comparison, showed no obvious increase in the crack length indicating significantly greater resistance to the crack development. Once the crack has started to grow, however, the specimens of this cement showed exceedingly rapid crack propagation leading to prompt failure. Table 5.3 shows the crack lengths at which failure occurred for the CT test specimens, comparing this for both test cements. Clearly, SmartSet GHV allowed the progress of longer fatigue cracks before reaching the failure

point compared to CMW1 that, in addition to showing fast crack growth, encountered failure at shorter crack length.

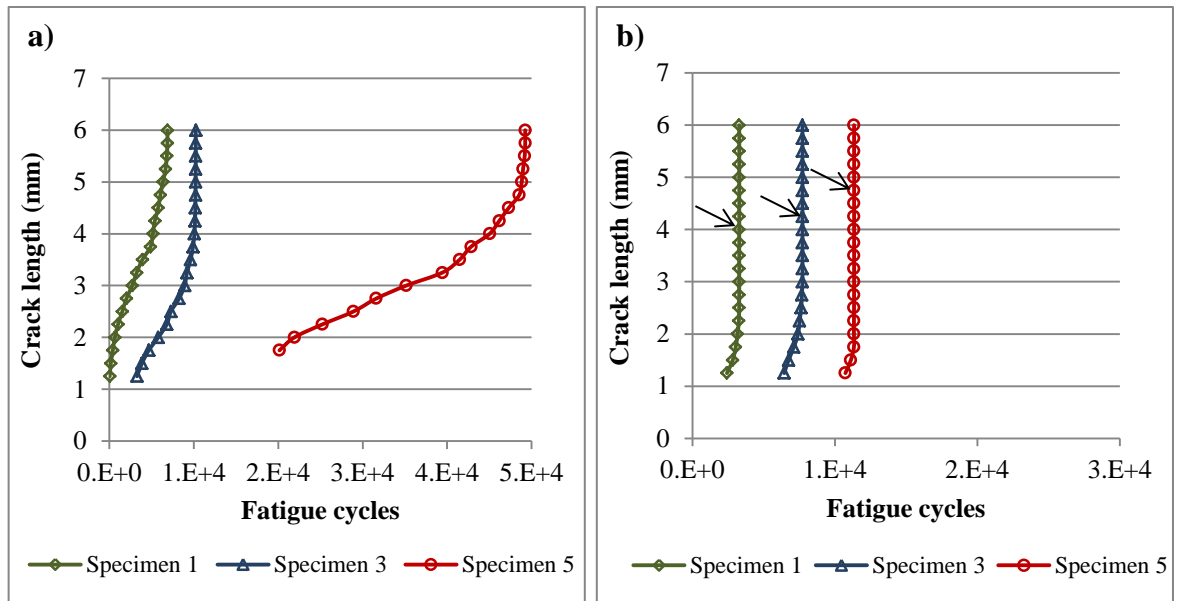


Figure 5.5 Comparison between the fatigue crack propagation in (a) SmartSet GHV and (b) CMW1 [low (Specimen 1), median (Specimen 3) and high (Specimen 5) performance specimens were used for each cement – the arrows show early failure points in CMW1]

Table 5.3 Comparison of fatigue crack lengths at the failure point for the two cements

Specimen No.	SmartSet GHV			CMW1		
	Total cycles to failure	No. of gauge strands broken at failure	Crack length at failure	Total cycles to failure	No. of gauge strands broken at failure	Crack length at failure
1	7,072	Strand No. 20 broke at 6,870 cycles	~ 6.00 mm	3,286	12	4.00 mm
2	9,085	Strand No. 20 broke at 9,091 cycles	~ 6.00 mm	3,628	18	5.50 mm
3	10,225	20	6.00 mm	7,724	13	4.25 mm
4	35,585	20	6.00 mm	10,613	17	5.25 mm
5	49,393	Strand No. 20 broke at 49,253 cycles	~ 6.00 mm	11,348	15	4.75 mm

5.4.2 Crack growth rate vs. stress intensity range

Most of the calculated fatigue crack growth rates were within the required range provided by ASTM E647 which recommends the use of the method described in this standard for $da/dN > 1.0 \times 10^{-8}$ mm/cycle at constant load amplitude. While the lowest crack growth rates were slightly greater than this limit for SmartSet GHV specimens (between 2.2×10^{-8} and 2.2×10^{-7} mm/cycle), they were well above this limit for CMW1 specimens (between 1.0×10^{-7} and 1.9×10^{-5} mm/cycle). Crack propagation rates below this limit are 'near-threshold' that correspond to early stages of crack propagation where the threshold stress intensity factor range (ΔK_{TH}) is representative of the value below which the crack will not propagate (Bucci, 1981). It should be noted, however, the lowest crack growth rates were higher for CMW1, compared to SmartSet GHV, because they largely describe the crack growth in CMW1 specimens over the last few fatigue cycling periods before failure. Otherwise, it is expected, according to the results, to have lower crack growth rates for this cement at early loading stages which might have existed before the breaking of the first strand of the crack measurement gauge.

Figure 5.6 shows a general description of the relationship between the crack growth rate and the stress intensity range comparing the trend for the two cements. The data obtained for the 5 data sets of each cement are plotted together with the regression line for each cement. The Paris' law representative equations for the combined sets are provided within the diagram showing the values of the C and n constants. It is to be noted that the lower number of data points for CMW1 reflects the effect of the fast crack growth on reducing the number of data points for this cement due to the breakage of more than one gauge strand over a single fatigue cycle period, particularly at later stages of cyclic loading. The data plots for the individual specimens (i.e. crack growth versus intensity range for each single specimen) are provided in Appendix 6.

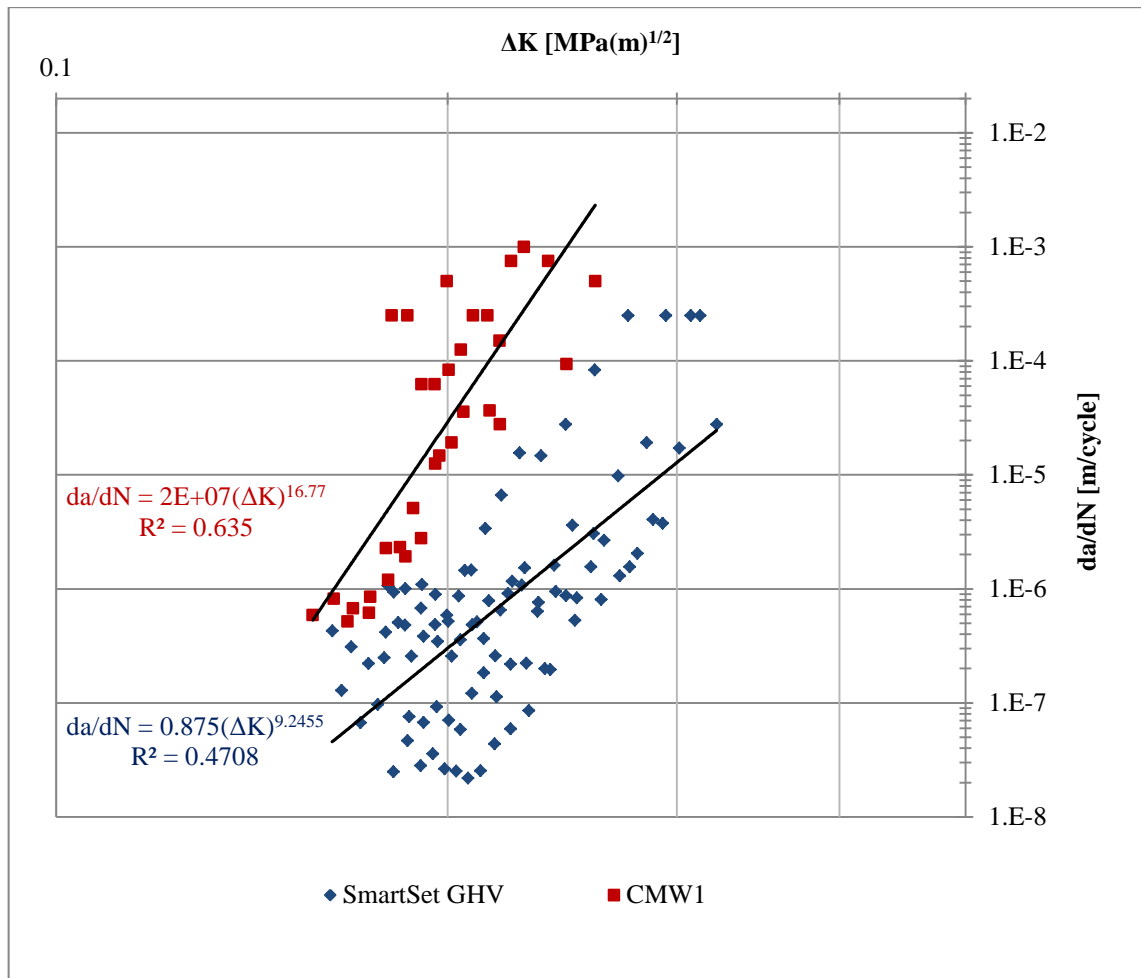


Figure 5.6 Comparison of the regression lines fitting the fatigue crack growth rate (da/dN) against the stress intensity range (ΔK) for SmartSet GHV and CMW1

5.5 DISCUSSION

5.5.1 Stress-strain cyclic curves as fatigue damage indicators

The investigation of the stress-strain curves (hysteresis loops) to indicate the progress of fatigue crack damage in the tested specimen types of the two bone cements has shown remarkable differences. The progressive changes in the absorbed energy and modulus shown as changes in the stress-strain loop area and the secant gradient respectively have indicated that fatigue crack behaviour can be variously affected by specimen shape and production method, however, the effect is largely controlled by bone cement composition. The selection of particular stress type and amplitude has also seemed to play a key role in controlling the behaviour of the changes in energy absorption and secant modulus, indicating the nature of fatigue crack behaviour in each specimen and cement.

5.5.1.1 Specimen type and composition

Recalling the discussion in chapter 4 (Section 4.7) regarding the effect of specimen specification and cement inclusions, the cyclic stress-strain relationships have provided detailed comparable indications for the crack progress behaviour in all specimen types. In chapter 4, the differences in fatigue lives were attributed to the variations in specimen specification and resultant porosity as stress concentration factors considering the role of cement composition without discussing the crack propagation mechanisms. In this chapter, the changes in absorbed energy and secant modulus per loading cycle are compared for different specimen types. The results have shown remarkable findings regarding the effect of specimen type which has been seen to be directed by the cement composition.

The results, according to the absorbed energy and secant modulus changes, have obviously indicated that SmartSet GHV specimens are less resistant to the fatigue damage. At high stress levels in particular, the machined specimens of this cement, especially the circular, have been found to absorb more energy and reduce the apparent modulus from earlier fatigue stages compared to the moulded specimens; the trend that have seen to become more obvious as the fatigue cycles progress, which demonstrates that machined specimen have low fatigue crack resistance properties. On the contrary, all the CMW1 cement specimen types did not seem to change the absorbed energy or modulus, and accordingly the crack propagation mechanisms, throughout the cyclic loading periods. However, once the crack has initiated in a specimen, which also occurs earlier in the machined specimens, the specimen shows failure immediately with no obvious crack resistance period. This reflects the importance of cement composition and inclusions as being a leading factor to control the effect of specimen type on describing fatigue crack behaviour, but the similarity in crack growth trends, as that found for the CMW1 specimens, does not necessarily mean fatigue lives are close. The effect of machining to enhance the fatigue crack propagation in SmartSet GHV can be due to the specific molecular weight and PMMA beads characteristics of this cement. Due to having different molecular weight and different PMMA particle size, the speed of crack propagation in the two cements would differ, regardless of specimen type. More discussion of the effect of the molecular and particle characteristics is provided in Section 5.5.2.3 below.

5.5.1.2 Stress type and amplitude effect

For the fully reversed tension-compression stress regimes, testing at a range of stress levels has shown significant variations in terms of the increase in absorbed energy and decrease

in modulus rates. All CMW1 specimen types, at all stress levels, have revealed stable progress for the increase in absorbed energy and the decrease in secant modulus at minimal rates. The results have also shown the change in stress amplitude within the examined range leads to similar behaviour in terms of energy absorption and stiffness reduction for all specimen types, apart from the variations in the absorbed energy amounts and modulus reduction rates per fatigue cycle at different stress levels that certainly led to differences in total fatigue life.

Dissimilarly, SmartSet GHV results have clearly shown that, on the one hand, there is a critical stress level that at or below which all specimen types can provide more stable and similar absorbed energy behaviour, at low absorption rates. On the other hand, exceeding this particular stress level can lead to clearer variations in terms of the increase in the absorbed energy amounts as the cyclic fatigue progresses. The reduction in modulus has tended to provide the same dissimilar behaviour below and above this stress level. While this stress level has been shown to exist at somewhat lower levels for the machined specimens (apparently between ± 15 and ± 20 MPa), it appeared to be higher for the moulded specimens (between ± 20 and ± 30 MPa).

For the tension-tension stress regimes, while examining the stress level of 20 MPa has revealed a similar trend of difference in energy and modulus changes when comparing the two cements, it has also shown close behaviour of these changes among all specimen types of the same cement. This might reflect the role that can stress type play in describing crack mechanisms. This is based on the findings that the application of tension-compression rather than tension-tension fatigue leads the specimen to successively absorb much more energy under the former loading compared to the latter. This leads to the consideration of other possible factors that can exist when fatiguing specimens, such as thermal stability and creep, considering the role of stress parameters in revealing these phenomena and how they both can possibly affect crack growth behaviour, as discussed below in Sections 5.5.1.3 and 5.5.1.4 respectively.

In general, a possible reason that might be involved in providing the dissimilarity in stress-strain behaviour between the two cement compositions at different stress types and amplitudes is the different impact that each stress can have on the craze zones and their expected growth prior to crack propagation. It has been stated for polymers that “the craze crack growth increases with stress” (Volynskii and Bakeev, 1995). This, however, does not necessarily mean a subsequent gradual crack growth since, as it has been demonstrated by Kambour (1968) for the stress-strain behaviour of the craze in glassy polymers, the craze

can be “much softer than the parent polymer, but capable of sustaining larger stresses and strains up to the point of failure” whereas, in this case, “craze failure is much more dependent on polymer molecular weight than craze formation”. These suppositions seem to apply to the stress-strain behaviour findings in the current study, for both stress types tested and more apparently at high stress levels, such that the crazes in CMW1 sustain stresses without leading to gradual crack growth whereas, in contrast, these crazes in SmartSet GHV can progress steadily, but well before failure leading to subsequent crack progresses. The role that the differences in molecular weight between the two cements can play in controlling crack growth mechanisms is discussed more fully in Section 5.5.2.3 below.

5.5.1.3 Thermal stability of test specimens

The general concept is that higher fatigue stress levels, as stated in Liu (2005) for polymers, leads to an increase in the hysteresis generated heat, where the extent of thermal heating is contributed to by the size of the stressed component and the heat loss from the surface area of the specimen and the flow rate of the fluid, such that the smaller the outer surface to volume ratio the greater the accumulated heating. Also, for bone cement in particular, it has been found that thermal stability can differ among cements because of the difference in opacifier type (Lewis et al., 2005b; Kjellson et al., 2007). For specimens used in the current study, the surface to volume ratios are 0.8 and 0.9 for the circular and the rectangular specimen shapes respectively, thus are reasonably close. Considering the cement composition, the difference in opacifier filler is less likely to show dissimilar thermal stability since both fillers (ZrO_2 and $BaSO_4$) are considered as ceramics and should have similar thermal properties. As for the effect of the antibiotic additives, while it has been reported in Webb and Spencer (2007) that a number of antibiotics such as flucloxacillin, penicillins, chloramphenicol and tetracycline are heat labile, it has also been reported that one of the basic considerations for bone cement antibiotics, in general, is to be heat stable (Gogia et al., 2009). Gentamicin sulphate, in particular, is thought to have “good thermostability” (Klemm, 2001), thus less likely to influence thermal stability of Smart Set GHV either during the polymerisation process or fatigue cyclic loading.

The difference in thermal stability, if any existed, would therefore be attributed to other variables including mainly the difference between the basic polymer structures of both cements. This, as can be seen from Table 3.1, might be due to the difference that CMW1 is based on polymethyl methacrylate (polymer) and SmartSet GHV is based on polymethyl methacrylate with methyl acrylate (copolymer). According to the data reported in Gaur et al. (1982), the glass transition temperatures for poly(methyl methacrylate) (PMMA) and

poly(methyl acrylate) (PMA) are 105 °C and 6 °C, respectively. Change in the specific heat capacity at these temperatures were reported, in the same study, as 33.5 and 42.3 J mol⁻¹ K⁻¹, respectively. According to the stress-strain behaviours of both cements, the consideration of variations in thermodynamic properties would be stress amplitude dependant, and would be more obvious in SmartSet GHV specimens. Herman et al. (1990) studied the fatigue failure mechanisms in engineering plastics, comparing acetal homopolymer (Delrin) and PMMA under bending stress conditions. They concluded that “the exact failure mechanism depends on the applied bending stress, with the higher stresses favouring thermal failure”. They reported the “changeover” stress between thermal and mechanical failure as 27 MPa for PMMA and 54 MPa for Delrin. For the findings of the current study, while the “changeover” stress levels, at which the absorbed energy behaviour changes remarkably, are apparent for the SmartSet GHV specimens, particularly the machined, as discussed above, it is still not evident that thermal instability is a major factor and further research might be needed to examine this phenomenon.

5.5.1.4 Consideration of creep contribution

Examining the tensile fatigue damage in the cement-bone interface, Kim et al. (2004) reported that the creep occurred due to fatigue dominates stiffness damage. In the current study, the stress-strain responses for all specimen types tested in tension-tension (maximum stress 20 MPa, R = 0.1) have indicated that, the creep properties generally seem to be governed by cement composition. The comparison of the hysteresis loop transition on the strain axis of the stress-strain plots, for all specimen types of both cements (Figure A5.3 in Appendix 5), has shown that, when close to failure, the SmartSet GHV specimens, except of the circular machined, tend to undergo approximately 3 times more creep compared to CMW1 specimens. Figure 5.7 illustrates this finding, comparing the median specimens for all groups. The tendency of the SmartSet GHV to provide greater ductility, shown by the gradual development of the fatigue damage, is related to the property of this cement to undergo creep. The circular machined specimens of this cement, due to encountering earlier fatigue failure, did not have adequate time to allow the creep to progress, but the creep trend was similar to that for the early stages of the other specimen types. Considering the test environment, Liu et al. (2005) found that SmartSet GHV reveals much more creep at body temperature than room temperature. For CMW1 specimens, it is quite obvious that the creep behaviour is similar among all specimens, with lower increase in creep rates compared to SmartSet GHV. While creep amounts appeared to be larger in one cement compared to the other, this indicates that creep might have

contributed into enhancing fatigue life for SmartSet GHV, but not necessarily the dominant factor.

In addition, the possibility of creep affecting fatigue longevity cannot be relied on for making final conclusions since results were compared only at one tension-tension stress level. It has been reported in different studies that the correlation between fatigue life and creep of bone cement is stress level dependent. Verdonschot and Huiskes (1995), for instance, concluded that higher stress levels leads to higher creep rates in bone cement. While Waanders et al. (2010a) suggested that, for the cement-bone interface damage mechanics, “at higher external stresses, creep is not capable of relieving peak cement stresses to such an extent that fatigue crack formation is attenuated”, they referred to the relatively increased contribution of creep into fatigue crack formation at lower stress levels. If this was the case, the more stable crack propagation found for the lower stress levels of the tension-compression regimes (mainly for SmartSet GHV) would be attributed, at least in part, to creep. Overall, however, while the effect of creep on fatigue crack propagation cannot be totally neglected, particularly when comparing the two cements, further investigations are still required to compare the effect of higher and lower tension-tension stress levels.

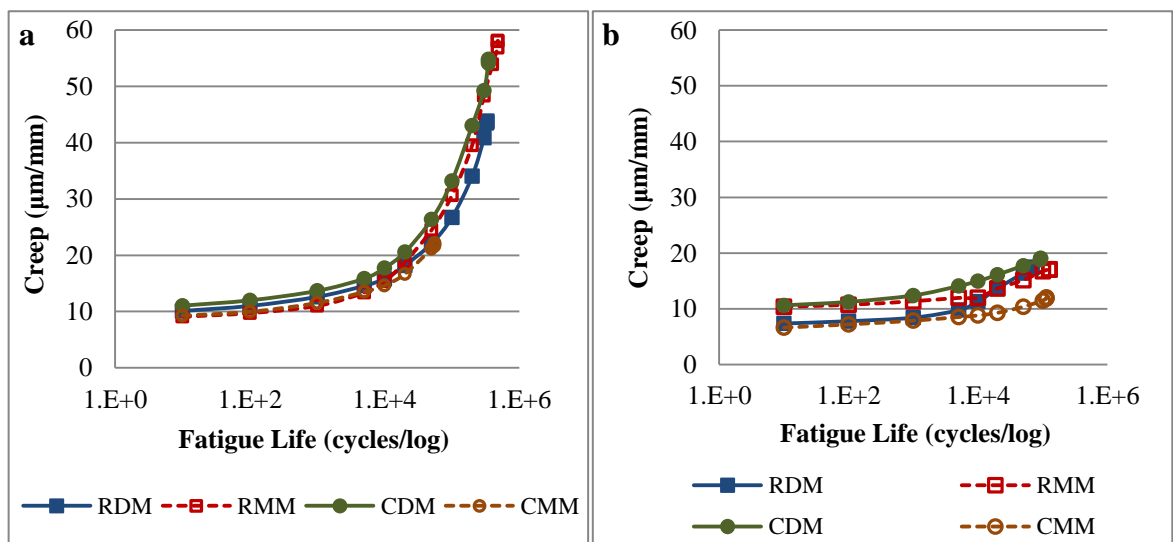


Figure 5.7 Comparable illustration of the strain creep behaviour for different specimen types of (a) SmartSet GHV and (b) CMW1 at 20 MPa tension-tension stress level ($R=0.1$).

5.5.2 Crack growth in CT specimens

5.5.2.1 Compliance to Paris' power law

Race and Mann (2008) proposed that two-power law fits are required to represent fatigue crack propagation rates in PMMA bone cement. Examining their findings along with those in Molino and Topoleski (1996) and Nguyen et al. (1997), they believed that the existence of “discontinuities in the log-log plot of da/dN versus ΔK ” is unavoidable and the data cannot be reduced to a single power law. It should be noted though, of these three studies, only Molino and Topoleski (1996) examined Simplex P along with the radiolucent Simplex and Plexiglas[®] while the other two studies examined the crack growth in Simplex P only, knowing that testing specimen and procedures were not identical. This is important to consider since, as mentioned in Bialoblocka-Juszczak et al. (2008) according to older studies, fracture properties of bone cement can be influenced by its chemical composition and testing procedures. Bialoblocka-Juszczak et al. (2008) tested the fatigue crack propagation in Cemex[®] RX considering this cement as “representative of a standard PMMA based bone cement”. They represented the combined data of five specimens to generate a single regression line described by Paris' law, obtaining a general coefficient of determination of 0.96.

One consideration of the current study was that a precise and correct identification of the “area of interest” during which the crack propagation would be driven by the stress intensity factor (macrocrack growth) and neglecting the irrelevant data points close to the crack tip of the CT specimen can perhaps lead to, first, reporting more representative results and, second, a greater chance to obtain a single fit of data points. The da/dN versus ΔK plots (Appendix 6) have shown variations in the coefficient of determination (R^2), where for the data sets of many specimens high coefficients (up to 0.98) were obtained and for few sets low coefficients (down to 0.35) were found. The individual plots of the high coefficients of determination might indicate that the Paris' law is followed over the examined area. The combination of the same cement data sets to have one representative trend line (Bucci, 1981; Ginebra et al., 2002; Bialoblocka-Juszczak et al., 2008), as can be seen from figure 5.6, has indicated that the two cements have distinct fracture properties. The combined data of CMW1 sets has also indicated that the change in stress intensity range occurs at higher increase in crack length compared to SmartSet GHV, with a greater m value for CMW1 (i.e. lower crack growth resistance). This dissimilarity in behaviour was perhaps because, as discussed above, CMW1 can have greater ability to resist crack growth and fracture at earlier fatigue stages, indicating delayed threshold stress

intensity factor range (ΔK_{TH}), followed by sudden and rapid crack propagation. Overall, the use of Paris' power law to examine fatigue crack growth in bone cement depends on the cement composition such that it can be more adequate and applicable for particular cements than others, providing that the testing protocol is appropriate.

5.5.2.2 Effects of molecular and particle characteristics

The molecular characteristics, including molecular weight and molecular weight distribution, are important in influencing the advancement of fatigue crack through the craze zone where higher molecular weight leads to increased craze strength (Pruitt, 2003). For bone cement, the formation of the craze zones is influenced by the molecular weight such that the higher the molecular weight the greater the fracture resistance (Ries et al., 2006). It has been reported by Liu et al. (2003) that both SmartSet GHV and CMW1 have similar narrow particle distributions, but, while SmartSet GHV powder has substantially greater molecular weight compared to CMW1 powder ($\sim 1 \times 10^6$ and 2×10^5 g/mol, respectively), the opposite is true for the molecular weights of the cements matrices. Liu et al. (2003) included that SmartSet GHV matrix has noticeably lower molecular weight than the CMW1 matrix ($\sim 5.5 \times 10^5$ and 9×10^5 g/mol, respectively). The variations in molecular weights of the two cements for both the matrices and the powder can have an important effect on the fatigue crack growth.

It was observed by Kim et al. (1977), for polymethylmethacrylate in particular, increasing the molecular weight from 1×10^5 to 4.8×10^6 g/mol led to a decrease in fatigue fracture growth rates by two orders of magnitude. It has been reported, however, while the reduction in molecular weight lowers fracture toughness, this does not necessarily lead to shorter fatigue life, but the decline in fatigue lives may occur if the molecular weight was greatly reduced (Graham et al., 2000). Therefore, on the one hand, the higher molecular weight for CMW1 matrix (approximately 1.6 times greater than SmartSet GHV) can be considered a possible reason for these variations in the fatigue crack growth behaviour between the two cements, particularly in terms of controlling the time to start propagation, while, on the other hand, the fatigue life behaviour reported in chapter 4 does not reflect this clear difference in crack propagation behaviour between the two cements where, for certain stress regimes, the fatigue lives were not significantly different when comparing the two cements.

In terms of the difference in the powder molecular weight between the two cements, this factor can also have an influence. Compared to CMW1, SmartSet GHV has higher powder

molecular weight associated with larger PMMA particle size. The mean diameter of the particles were reported in Liu et al. (2003) as 69 ± 2.1 and 44 ± 1.9 μm for SmartSet GHV and CMW1, respectively. Liu et al. (2005), in their study considering the mechanical characteristics of SmartSet GHV, stated “it is evident that most of the micro-cracks propagate around large PMMA beads, indicating a weak bonding between the large beads and the matrix”. This seems to be sensible since it matches the comparable observations of the fracture surfaces of both cements in the current study. Disconnection of the PMMA beads from the matrix in the SmartSet GHV fracture surfaces was much more obvious (Figure 5.8a) which can be more influential if the opacifier particles accumulate closer to the larger beads (Figure 5.8b). This can also be considered as one of the possible reasons to have rougher fracture surfaces for the SmartSet GHV (including all testing regimes for the rectangular and circular specimens used to test the fatigue life). Theoretically, this is possible since the lower fraction and the smaller size of CMW1 PMMA beads would be expected to exhibit greater matrix-bead bonding, resulting in superior resistance to crack growth.

When considering the difference that one cement (SmartSet GHV) includes antibiotic and the other cement (CMW1) is antibiotic free, the possible effect of molecular weight on fatigue properties would still exist. Rimnac et al. (1986) compared the fracture properties of different commercial bone cements (each with and without antibiotic) and attributed the variations in fracture toughness and fatigue crack propagation to the difference in molecular weights with no significant effect from the presence of antibiotics.

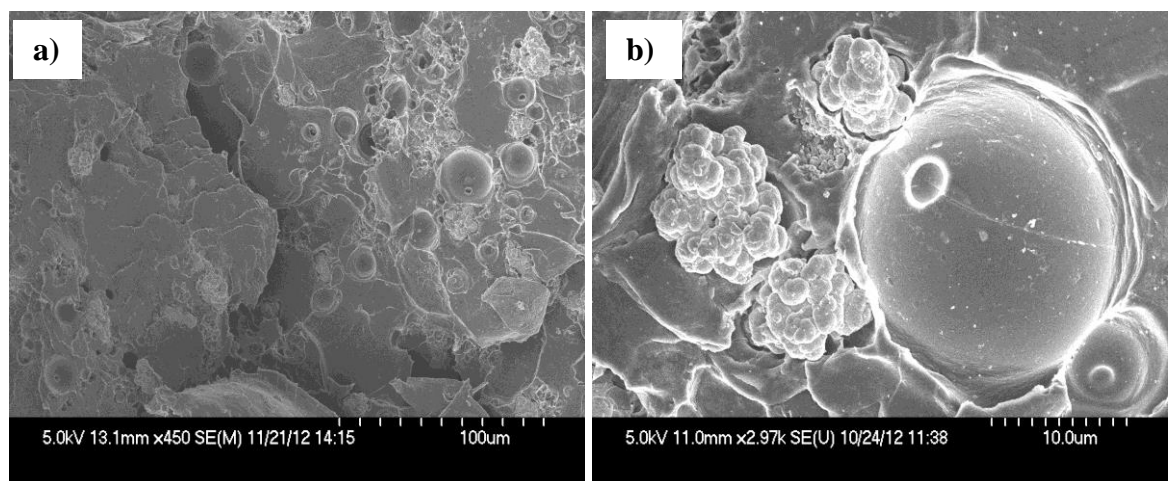


Figure 5.8 Micrographs of a SmartSet GHV fracture surface illustrating (a) the disconnection of the PMMA beads without being fractured (marker bar = $100\mu\text{m}$) and (b) interaction between a PMMA bead and accumulated ZrO_2 particles (marker bar = $10\mu\text{m}$).

In brief, the differences in both molecular weight and PMMA beads characteristics can apparently be considered among the main factors that can govern the fatigue fracture properties. Compared to CMW1, the lower molecular weight of SmartSet GHV matrix and the greater size of the PMMA beads within its structure seem to play a key role in providing slow fatigue crack propagation from earlier fatigue loading cycles. This means the crack would preferably grow within the weaker matrix extending through the bead-matrix interface as being the second weakest route. The occasional presence of accumulated opacifier, particularly adjacent to the beads, may have a contributing effect on crack behaviour. Reverse to SmartSet GHV, the higher matrix molecular weight and greater bonding between the PMMA beads and matrix in CMW1 can delay the crack progress within the bulk structure. Once the crack has started to progress in this cement, however, the bonding will no longer resist the crack propagation where a rapid increase in crack growth rate occurs over few cycles, leading to fast failure.

5.6 CONCLUSIONS

- 1- The progressive changes in stress-strain hysteretic behaviour during fatigue testing, by means of estimating the instantaneous absorbed energy and secant modulus for representative loading cycles, can be a valuable analysis and comparison criterion for, as a minimum, identifying the trend of fatigue crack propagation for different specimen and cement types.
- 2- In general, for all stress regimes used in this study, the absorbed energy increase and secant modulus reduction per loading cycle is much greater in SmartSet GHV than in CMW1, thus reflecting the sooner initiated and more gradual progressing cracks in the former cement leading to slow failure; the case that is reflected by the latter cement where rapid propagation of cracks occurs shortly prior to failure.
- 3- For the examined fully reversed tension-compression stress regimes, the increase in stress level upon SmartSet GHV specimens above certain level can lead to extremely rapid increase in the absorbed energy (i.e. more immediate fatigue damage). This changeover stress level, however, can be comparatively influenced by specimen specifications with the machined specimens being the most likely to reflect this aspect. In contrast, all CMW1 specimens tend to absorb a similar amount of energy throughout the fatigue loading period until close to failure.
- 4- The direct measurements of the crack growth rates in SmartSet GHV and CMW1, using the ASTM E647 standard technique, have validated the equivalent stress-

strain findings in terms of the difference in crack propagation behaviour of both cements. Again, the cracks tend to progress gradually in SmartSet GHV from well before failure while showing no clear propagation in CMW1 until close to failure.

- 5- Different cements can show different compliance to Paris' power law. The application can be much more suitable for particular cements (such as SmartSet GHV) than others (as CMW1). Whether or not the cement was following Paris' law, the application would still be of help in, at least, identifying if the crack propagation would at some stage be in agreement with this law.
- 6- While cement composition is essential in identifying the fatigue crack propagation behaviour, there is still some uncertainty about what underlying factors are dominant in governing the propagation process. It is suggested, however, the differences in molecular weight of the matrix and PMMA particle characteristics of the cements are more likely to have key roles in controlling crack behaviour.

CHAPTER 6. GENERAL DISCUSSION

The fatigue results and data analysis have clearly shown that the adoption of a particular fatigue testing stress regime is substantial in describing fatigue behaviour of bone cements. Each testing variable of the selected stress regime (i.e. specimen shape, specimen production method and stress type and amplitude) has been shown to be of particular importance. Stress regime influence, however, has been more evidently found to be cement composition dependent. Weibull analysis, either two- or three-parameter, of fatigue life results at a maximum stress level of 20 MPa (in fully reversed tension-compression or in tension-tension) have made it obvious that both specimen type and cement composition are important in terms of influencing fatigue life. The analysis has also shown that the type of fatigue loading, tension-compression or tension only, has a major effect on fatigue life. Using the S-N analysis to compare fatigue lives at a range of stress levels in fully reversed tension-compression has, first, emphasised the Weibull findings that moulded specimens, particularly the circular, tend to provide significantly longer fatigue lives compared to the machined and, second, revealed that testing at different stress levels can lead to dissimilar fatigue life behaviour for various cements such that a high stress level can be more damaging to one particular cement than another and vice versa. The investigation of the cyclic stress-strain curves (hysteresis loops) has provided further fatigue damage analysis indicating and comparing the damage development in all specimen types at the examined stress levels. Considering the variations in fatigue damage indicated by this analysis among the two test cements, the findings seemed largely to correlate to those obtained when CT specimens were used to measure fatigue crack propagation.

These findings have generally provided the indication that while the crack growth period, controlled by the stress intensity factor, can last longer for SmartSet GHV than CMW1 showing variations in crack growth resistance, it seems that fatigue life of bone cements, particularly at lower stress levels, is mainly identified by the crack initiation period (stress concentration factor) which can be governed by the specimen type. Specimen type is important since it can substantially alter the stress concentration raisers within or on the surface of the specimen; the variable that is in turn influence by cement type and stress parameters. At high stress levels, particularly in fully reversed tension-compression conditions, fatigue cracks initiate much earlier, particularly for machined specimens, shortening the crack resistance period.

The importance of specimen type in controlling the stress concentration factor, particularly when machined, can be related to the variations in the distribution and severity of the underlying stress concentration raisers such as porosity and cement inclusions. Regardless of the rejection of the specimens with macroporosity ($>1\text{mm}$), the presence of microporosity ($\leq 1\text{mm}$) in many specimens has been seen as a major factor in controlling fatigue life, which is also considered as one of the reasons to control the variability in fatigue results within the same testing group. Machining of test specimens, in addition to the possible damage of the original structure, produces severer micropores on the surface as also reported by Paravic et al. (1999). The direction of machining, which is controlled by the specimen shape, can also be important. While machined specimens of both specimen shapes tend to provide shorter fatigue lives, the cement chemical composition might also contribute in increasing or decreasing the fatigue life gap between the two specimens. For moulded specimens, the severity of surface micropores would be alleviated by the outer moulded layer. Similarly, the presence of cement additives such as the radiopaque opacifiers on a specimen surface that has been machined provides potential stress concentration origins, which can interact with the adjacent pores resulting in yet severer crack initiation sites. The cement composition and the included opacifier type can differently alter these stress concentration factors.

It is emphasised that machined specimens not only provide less relevant fatigue lives, particularly under tension-compression, but also, and more importantly, are less likely to represent the cement mantle *in vivo* due to the possible damage of the polymeric structure at the outer surface when machining and thus changing the material's original properties. This is important to report since as it is clear from the literature, and as it is also apparent in the review study by Lewis (2003a), many studies have used machined specimens, mostly with circular cross sectional shape, in fatigue testing of bone cement with no or insufficient consideration of the effect of this specimen production method. This has been irrespective of some reported suggestions that producing test specimens by machining can result in negative impact on their surfaces by introducing manufacturing cracks (Parchinski, 1977 in Krause et al., 1988) and causing interior pores to become surface pores (Paravic et al., 1999).

In general, moulded specimens can be much more reliable than machined specimens not only because they encounter importantly less manufacturing stresses and defects, but also because the bone cement is injected *in vivo* similar to the moulding process. It is to be considered though whilst moulding can be a better representative of the *in vivo* cement,

this is only to some extent and does not perfectly reflect the exact situation for various reasons. *In vivo*, the cement mantle in a joint replacement such as a total hip replacement has moulded surfaces, but not as smooth and uniform as test specimens, due the presence of two different types of *in vivo* interdigitations: cement-prosthesis and cement-bone interfaces. Femoral stems usually have roughed (grit blasted) or polished surfaces, which identifies the interface characteristics between the prosthesis and the cement in a cemented joint replacement. For cemented stems, while the polished stems are usually designed with a taper-slip to provide implant stability and long-term success (Shah and Porter, 2005), the stems roughened surfaces are used to assure greater cement-stem bonding (Berry, 2004). This can be important in identifying the cement-prosthesis interface characteristics which can be largely responsible for controlling the cement mantle failure.

Also, after preparing the internal surface of the bone by a rasping process, the interdigitation levels between the injected cement and the rasped bone can be different. Waanders et al. (2010b) concluded that cement-bone interface properties can be influenced by the degree of interdigitation depending on the bone structure:

“There are very strong positive relationships between the average interdigitation depth of the cement-bone interface and the strength and the stiffness as well as the contact area and strength and stiffness. It is likely that this relationship depends on the morphology of the bone.”

Whilst using the moulded specimens can be a more valuable option than machined, testing specimens with circular or rectangular cross sectional shapes cannot be easily decided. Considering the controversial reported in the literature as which specimen shape is more optimal to use in fatigue testing of bone cement, as discussed in Section 2.3.2.1, some points might be worth discussing and clarifying based also on the findings of the current study. The findings have validated the older outcome by Lewis and Janna (2003) that circular specimens afford greater fatigue performance than the rectangular ones; however, in terms of the reasons that can affect fatigue life of both specimen shapes, different reasons were given priority than those provided in Lewis and Janna (2003) as discussed in Section 4.7.1.1. Nevertheless, if the advantage of the circular moulded specimens being to provide longer fatigue lives was considered, the debate about which specimen shape to use would be of lower importance. When testing specimens for fatigue, the adopted stress type and level can be more important than the specimen shape of moulded specimens, considering the “misleading” fatigue results that can be obtained from machined specimens of both shapes.

It has been shown in this study, particularly for SmartSet GHV, that fully reversed tension-compression at higher stress levels than approximately 15 MPa for machined specimens and 20 MPa for moulded specimens can lead to greater acceleration in fatigue crack initiation and growth and thus shortening fatigue life substantially, resulting in unreliable findings when considering the *in vivo* stress conditions. Referring to the need of future work to validate their supposition, Lewis and Janna (2003) applied a stress level of 15 MPa under the fully reversed tension-compression conditions, on rectangular and circular moulded specimens, and suggested that fatigue tests would less likely provide a different trend than they obtained if testing was performed at lower stress levels than the 15 MPa level. Similarly, Lewis et al. (2003) applied the same stress level of 15 MPa under the same conditions on circular moulded specimens and gave the same suggestion, adding that while the stress level used is a major study limitation when considering *in vivo* conditions, it is still adequate to be used for the *in vitro* testing since they expected thermal softening to occur at higher stress levels and with increased frequency. They also referred to the need of future work to corroborate their suggestions “over a wide range of test stress levels”; the work that has been largely covered in the current research, considering different specimen shapes and production methods.

In contrast to the findings of the fully reversed fatigue conditions, when testing in tension-tension at a stress level of 20 MPa, the stress-strain behaviour and the relevant fatigue damage parameters have indicated that fatigue damage progress is much more similar for all specimen types of the same cement and apparently different when comparing the two tested cements. The absorbed energy amount per loading cycle was low compared to the equivalent maximum stress level for the tension-compression loading. Approximately a third lower absorbed energy has been found with this tension-tension stress level compared to the lowest examined fully reversed tension-compression stress level of 12.5 and 15 MPa. The amount of absorbed energy per loading cycle have been seen to increase remarkably above these stress levels enhancing the fatigue damage and thus shortening the fatigue life. It seems that, for the tension-tension stress type, even noticeably higher stress levels than 20 MPa would not provide significant changes in the absorbed energy and thus similarity in crack growth behaviour among specimens; this supposition still needs further research to be confirmed. At the same maximum stress level, the trend of bone cement specimens to withstand tension-tension much greater than tension-compression is attributed to the extra work per loading cycle that is applied on the specimens during the compression segment, leading them to absorb more energy and thus produce more fatigue damage per cycle. Overall, to be as close as possible to the *in vivo* conditions and to avoid

any unrelated testing drawbacks to exist during testing, such as thermal failure, it is suggested that, depending on the stress type used, adequate maximum stress levels should be adopted in fatigue testing. In all cases, particularly for the tension-compression testing, an appropriate specimen type should be used.

Having considered the importance of stress regime on describing the fatigue behaviour of bone cement, it is emphasised that this variation in fatigue behaviour is also governed by the chemical composition of test cements. The findings have made it quite clear that using different cements can lead to different fatigue behaviours that in turn depend on specimen type and stress parameters used. While, depending on the stress type and level, specimen shape and surface specification can be vitally important in identifying the severity of the stress concentration raisers including the added particles and porosity, fatigue crack propagation in bone cements seems to be largely influenced by the molecular weight of the cement matrix and PMMA beads characterisations. Depending on specimen shape and surface production method, stress raisers such as micropores on the surface of a specimen can largely control fatigue life of bone cement by facilitating the initiation of a fatigue crack at this defect followed by the formation of a craze zone that is also affected by the cement's molecular weight and PMMA particle size considering the possibility of the presence of different types of opacifier fillers and resultant porosity to contribute into enhancing crack growth. Accordingly, this can be provided as a possible reason for the variations in fatigue crack propagation behaviour of both test cements included in the current study.

CHAPTER 7. CONCLUSIONS AND FUTURE WORK

7.1 CONCLUSIONS

- 1- In general, fatigue behaviour of bone cement can be substantially influenced by the testing regime variables. Specimen shape, surface production method and stress parameters are all of importance. Each variable, particularly the last two, can play a major role in crack initiation, thus shortening the fatigue life. The stress parameters (type and level) can be vitally important also when it comes to the fatigue crack growth rate.
- 2- Irrespective of the data analysis approach used, moulded specimens, particularly the circular, show substantially longer fatigue lives than the machined specimens. This result is apparently because the moulded specimens have greater ability to resist the initiation of fatigue cracks from the micropores and any other defects on the outer surface. In all cases, the variability in fatigue results, which can be greater within the moulded specimen sets, is mostly governed by the variability in both the internal and the surface microporosity.
- 3- At the same maximum stress level, fully reversed tension-compression fatigue loading leads to substantially shorter fatigue lives compared to tension-tension loading. While this can be attributed to the additional mechanical work applied to the specimen during the compression segment of this type of cyclic loading, this reflects the important effect of the presence of the compression portion in conjunction with an equivalent tension portion, but does not necessarily mean that compression is more damaging than tension, particularly because bone cement is known to have greater compressive than tensile strength.
- 4- Bone cement, due to being a viscoelastic material, is generally expected to be sensitive to the stress amplitude applied. At or above a certain stress level, a bone cement material can be driven into the “low cycle” fatigue more quickly potentially due to the failure being contributed to by thermal effects. This “critical” stress level, however, depending on the chemical composition of the cement in question, can also be influenced by the type of specimen used particularly when comparing moulded and machined specimens.

- 5- The effects of the series of testing variables can be reflected by the stress-strain responses through the assessment of the changes in both the energy absorbed and secant modulus per loading cycle. For a particular cement composition (SmartSet GHV), certain specimen types at high stress levels, particularly the machined, can show rapid increases in the absorbed energy associated with noticeable reductions in secant modulus, from well before failure, indicating a similar trend of fatigue damage. In contrast, CMW1 tends to maintain approximately the same amount of absorbed energy per loading cycle with limited reductions in modulus, indicating that the crack propagates suddenly few cycles before failure.
- 6- In relation to, and validating the estimations of, the fatigue damage progress as seen by the stress-strain behaviours, when using pre-cracked specimens to measure the fatigue crack growth rate in both cement, similar trends of crack behaviour to those can be indicated by the changes in the hysteresis loop response were observed.
- 7- At the same stress conditions, while the specimen type can be the most important variable to control fatigue crack initiation depending also on the cement chemical composition, the crack propagation stage is more likely to be governed by the cement composition. The difference in molecular weight and PMMA particle characterisations are the most obvious factors to influence the fatigue crack growth.
- 8- Considering the *in vivo* stress conditions of bone cement, it is quite clear that certain *in vitro* testing regimes may be irrelevant. Machining of specimens and/or applying high stresses can lead to “undesirable” effects and, therefore, provide irrelevant fatigue life results.
- 9- Overall, it is suggested that applying fully reversed tension-compression loading on circular moulded specimens can be preferred for fatigue testing of bone cement because the tension and compression segments of this loading type, in addition to not resulting in “over-estimated” fatigue results, are present *in vivo* and the shape of this specimen type is both more adequate to this loading type and its moulding production method can be representative to the *in vivo* conditions. The *in vitro* loading levels should be maintained within a range of 12 to 20 MPa. The maximum stress of this range is suggested to provide greater chance for the fatigue failure to occur due to mechanical rather than thermal effects and the minimum stress level is suggested to minimize testing time and avoid obtaining run-out results that would be insignificant when it comes to the fatigue data analysis using either Weibull or S-N analyses, considering to test as closer as possible to the *in vivo* stress levels.

7.2 FUTURE WORK

- 1- The final conclusions in the current thesis have been made according to the fatigue results from testing in fully reversed tension compression conditions at a range of stress levels while the tension-tension regimes were limited to a single stress level. Although this has provided an indicator that stress type is important, performing further tension-only testing at all the other stress levels involved in the fully reversed loading would provide further details about the effects of stress level.
- 2- The results reported in this thesis have indicated that the compression portion of the fully reversed loading cycles can increase the fatigue damage rate substantially. This existed when both the tension and compression segments were alternately applied. It might be of significance therefore to conduct further testing to examine the effect of compression only (i.e. during compression-compression loading), again at a range of *in vitro* stress levels.
- 3- For each stress type and cement, further investigation of the critical stress levels at which thermal effects might occur can provide more comparable findings for the effects of using various testing regimes.
- 4- Since bone cement *in vivo* is expected to be subjected to more than one stress mode at a time, performing biaxial testing, under the same conditions and data analysis techniques used in the current work, can provide more useful results.
- 5- The S-N curves reported within the current thesis were generated as regression lines as performed in some previous studies. Other studies have generated the S-N curve as a line that crosses the data points of cycles to failure of each stress level at the 'mean'. It might be of significance to examine if there is any effect due to this difference in the S-N curve determination method.
- 6- In this thesis, strain occurred in the gauge of a specimen was estimated based on engineering calculations. Direct measurements of the gauge strain for a number of specimens using strain gauges or DIC (digital image correlation) system would help validate the 'engineering' based findings.

LIST OF REFERENCES

- Abdel-Kader, K. F. M., Allcock, S., Walker, D. I. & Chaudhry, S. B. 2001. Boneloc bone-cement: experience in hip arthroplasty during a 3-year period. *Journal of Arthroplasty*, 16, 811-819.
- Anderson, T. L. 2005. *Fracture mechanics: Fundamentals and Applications*, Boca Raton, USA, Taylor & Francis Group, LLC
- Ashby, M. F. 1999. *Materials Selection in Mechanical Design*, Oxford, UK, Butterworth-Heinemann.
- Askeland, D. R., Fulay, P. P. & Wright, W. J. 2011. *The Science and Engineering of Materials*, Stamford, USA, Cengage Learning.
- ASTM E647-13 2013 Standard Test Method for Measurement of Fatigue Crack Growth Rates. ASTM International, West Conshohocken, US
- ASTM F2118-03 2003 Standard Test Method for Constant Amplitude of Force Controlled Fatigue Testing of Acrylic Bone Cement Materials. ASTM International, West Conshohocken, US
- ASTM E739-91 2004 Standard Practice for Statistical Analysis of Linear or Linearized Stress-Life (S-N) and Strain-Life (ϵ -N) Fatigue Data. ASTM International, West Conshohocken, US
- ASTM C1239-07 2007 Standard Practice for Reporting Uniaxial Strength Data and Estimating Weibull Distribution Parameters for Advanced Ceramics. ASTM International, West Conshohocken, US
- Backman, D. K. & Devries, K. L. 1969. Formation of free radicals during machining and fracture of polymers. *Journal of Polymer Science: Part A-1*, 7, 2125-2134.
- Bargar, W. L., Brown, S. A., Paul, H. A., Voegli, T., Hseih, Y. & Sharkey, N. 1986. In vivo versus in vitro polymerisation of acrylic bone cement: effects on material properties *Orthopaedic Research Society*, 4, 86-89.
- Bauer, T. W. & Schils, J. 1999. The pathology of total joint arthroplasty.II. Mechanisms of implant failure. *Skeletal Radiology* 28, 483-497.
- Bauman, J. T. 2008. *Fatigue, Stress and Strain of Rubber Components*, Munich, Carl Hanser Verlag.
- Bergmann, G., Deuretzbacher, G., Heller, M., Graichen, F., Rohlmann, A., Strauss, J. & Duda, G. N. 2001. Hip contact forces and gait patterns from routine activities. *Journal of Biomechanics*, 34, 859-871.
- Berry, D. J. 2004. Cemented femoral stems: what matters most. *Journal of Arthroplasty*, 19 (Suppl.), 83-84.
- Bhambri, S. K. & Gilbertson, L. N. 1995. Micromechanisms of fatigue crack initiation and propagation in bone cements. *Journal of Biomedical Materials Research* 29, 233-237.

- Bhandari, V. B. 2010. *Design of Machine Elements*, New Delhi, Tata McGraw-Hill
- Bialoblocka-Juszczak, E., Baleani, M., Cristofolini, L. & Viceconti, M. 2008. Fracture properties of an acrylic bone cement. *Acta of Bioengineering and Biomechanics*, 10, 21-26.
- Bishop, N. E., Ferguson, S. & Tepic, S. 1996. Porosity reduction in bone cement at the cement-stem interface. *Journal of Bone & Joint Surgery (Br)*, 78-B, 349-356.
- Britton, J. C., McInnes, P., Weinberg, R., Ledoux, W. R. & Retief, D. H. 1990. Shear bond strength of ceramic orthodontic brackets to enamel. *American Journal of Orthodontics and Dentofacial Orthopedics*, 98, 348-353.
- Britton, J. R., Walsh, L. A. & Prendergast, P. J. 2003. Mechanical simulation of muscle loading on the proximal femur: analysis of cemented femoral components migration with and without muscle loading. *Clinical Biomechanics (Bristol; Avon)*, 18, 637-646.
- BSI 2012a *ISO 527-1: Plastics - Determination of tensile properties. Part 1: General principles*. The British Standards Institution, London, UK.
- BSI 2012b. *ISO 527-2: Plastics - Determinations of tensile properties. Part 2: Test conditions for moulding and extrusion plastics*. The British Standards Institution, London, UK.
- Bucci, R. J. 1981. Development of a Proposed ASTM Standard Test Methods for Near-Threshold Fatigue Crack Growth Rate Measurement *In: Hudak, S. J. & Bucci, R. J. (eds.) Fatigue Crack Growth Measurement and Data Analysis*. Philadelphia, US: American Society for Testing and Materials
- Carter, D. R., Gates, E. I. & Harris, W. H. 1982. Strain-controlled fatigue of acrylic bone cement. *Journal of Biomedical Materials Research: Part A*, 16, 647-657.
- Collins, J. A. 1993. *Failures of Materials in Mechanical Design: Analysis, Prediction, Prevention*, USA, John Wiley & Sons, Inc.
- Cotterell, B. 2010. *Fracture and Life*, London, Imperial College Press.
- Crawford, R. J., Klewpatinond, V. & Benham, P. P. 1978. Effects of moulded and machined notches upon the fatigue strength of an acetal copolymer. *Polymer* 20, 649-652.
- Cristofolini, L., Minari, C. & Viceconti, M. 2000. A methodology and criterion for acrylic bone cement fatigue tests. *Fatigue & Fracture of Engineering Materials & Structures*, 23, 953-957.
- Culleton, P., Prendergast, P. J. & Taylor, D. 1993. Fatigue failure in the cement mantle of an artificial hip joint. *Clinical Materials*, 12, 95-102.
- Cunnane, C. 1978. Unbiased plotting positions - a review. *Journal of Hydrology*, 37, 205-222.
- Curtis, R. V. & Juszczak, A. S. 1998. Analysis of strength data using two- and three-parameter Weibull models. *Journal of Materials Science*, 33, 1151-1157.
- Danzer, R., Supancic, P., Pascual, J. & Lube, T. 2007. Fracture statistics of ceramics - Weibull statistics and deviations from Weibull statistics. *Engineering Fracture Mechanics*, 74, 2919-2932.

- Davies, J. P., Burke, D. W., O'Connor, D. O. & Harris, W. H. 1987. Comparison of the fatigue characteristics of centrifuged and uncentrifuged Simplex P bone cement. *Journal of Orthopaedic Research*, 5, 366-371.
- Davies, J. P., Jasty, M., O'Connor, D. O., Burke, D. W., Harrigan, T. P. & Harris, W. H. 1989. The effect of centrifuging bone cement. *Journal of Bone and Joint Surgery (Br)*, 71-B, 39-42.
- Deb, S. & Koller, G. 2008. Acrylic Bone Cement: Genesis and Evolution. In: Deb, S. (ed.) *Orthopaedic Bone Cement*, Cambridge, England: Woodhead Publishing.
- Deb, S., Lewis, G., Janna, S. W., Vazquez, B. & San Roman, J. 2003. Fatigue and fracture toughness of acrylic bone cements modified with long-chain amine activators. *Journal of Biomedical Materials Research Part A*, 67, 571-577.
- Debrunner, H. U., Wettstein, A. & Hofer, P. 1976. The Polymerization of Self-Curing Acrylic Cements and Problems due to The Cement Anchorage of Joint Prosthesis In: Schaldach, M. & Hohmann, D. (eds.) *Advances in Artificial Hip and Knee Joint Technology*. Berlin: Springer Verlag.
- Dowling, N. E. 2007. *Mechanical Behaviour of Materials: Engineering Methods for Deformation, Fracture, and Fatigue*, New Jersey, Pearson Prentice Hall.
- Dunne, N., Clements, J. & Wang, J. S. 2014. Acrylic Cements for Bone Fixations in Joint Replacements. In: Revell, P. A. (ed.) *Joint Replacement Technology*. UK: Woodhead Publishing.
- Dunne, N. J. & Orr, J. F. 2001. Influence of mixing techniques on the physical properties of acrylic bone cement. *Biomaterials*, 22, 1819-1826.
- Dunne, N. J., Orr, J. F., Mushipe, M. T. & Eveleigh, R. J. 2003. The relationship between porosity and fatigue characteristics of bone cements. *Biomaterials*, 24, 239-245.
- Ehrenstein, G. W. 2001. *Polymeric Materials: Structure - Properties - Applications*, Munich, Germany, Carl Hanser Verlag.
- Ellyin, F. 1997. *Fatigue Damage, Crack Growth and Life Prediction*, London, Chapman & Hall.
- Evans, M., Hastings, N. & Peacock, B. 2000. *Statistical Distributions*, Canada, John Wiley & Sons.
- Evans, S. L. 2006a. Effects of porosity on the fatigue performance of polymethyl methacrylate bone cement: an analytical investigation. *Proceedings of the Institution of Mechanical Engineers, Part H: Journal of Engineering in Medicine*, 220, 1-10.
- Evans, S. L. 2006b. Fatigue of PMMA Bone Cement. In: Gdoutos, E. E. (ed.) *Fracture of Nano and Engineering Materials and Structures: Proceedings of the 16th European Conference of Fracture, Alexandroupolis, Greece, July 3-7, 2006*. The Netherlands: Springer.
- Faucher, B. & Tyson, W. R. 1988. On the determination of Weibull parameters. *Journal of Materials Science Letters*, 7, 1199-1203.

- Freitag, T. A. & Cannon, S. L. 1977. Fracture characteristics of acrylic bone cements. II. Fatigue. *Journal of Biomedical Materials Research Part A*, 11, 609-624.
- Fritsch, E., Rupp, S. & Kaltenkirchen, N. 1996. Does vacuum-mixing improve the fatigue properties of high-viscosity poly(methyl-methacrylate) (PMMA) bone cement? Comparison between two different evacuation methods. *Archives of Orthopaedic Trauma Surgery*, 115, 131-135.
- Gates, E. I., Carter, D. R. & Harris, W. H. 1983. Tensile fatigue failure of acrylic bone cement. *Journal of Biomechanical Engineering*, 105, 393-397.
- Garellick, G., Rogmark, C., Kärrholm, J. & Rolfson, O. 2012. *Swedish Hip Arthroplasty Register: Annual Report 2012*. Available: http://www.shpr.se/Libraries/Documents/AnnualReport_2012_Eng_WEB.sflb.ashx [Accessed 23/03/2015]
- Garellick, G., Kärrholm, J., Lindahl, H., Malchau, H., Rogmark, C. & Rolfson, O. 2013. *Swedish Hip Arthroplasty Register: Annual Report 2013*. Available: http://www.shpr.se/Libraries/Documents/AnnualReport_2013Eng.sflb.ashx [Accessed 23/03/2015]
- Gaur, U., Lau, S., Wunderlich, B. B. & Wunderlich, B. 1982. Heat capacity and other thermodynamic properties of linear macromolecules: VI. Acrylic polymers. *Journal of Physical and Chemical Reference Data* 11, 1065-1089.
- Gelb, H., Schumacher, H. R., Cuckler, J., Ducheyne, P. & Baker, D. G. 1994. In vivo inflammatory response to polymethylmethacrylate particulate debris: effect of size, morphology and surface area. *Journal of Orthopaedic Research*, 12, 83-92.
- Ginebra, M. P., Albuixech, L., Fernandez-Barragan, E., Aparicio, C., Gil, F. J., San Roman, J., Vazquez, B. & Planell, J. A. 2002. Mechanical performance of acrylic bone cements containing different radiopacifying agents. *Biomaterials*, 23, 1873-1882.
- Gogia, J. S., Meehan, J. P., Di Cesare, P. E. & Jamali, A. A. 2009. Local antibiotic therapy in osteomyelitis. *Seminars in Plastic Surgery*, 23, 100-107.
- Gough, H. J. & Pollard, H. V. 1935. The Strength of Metals under Combined Alternating Stresses. *Proceedings of the Institution of Mechanical Engineers* [Online], 131. Available: <http://pme.sagepub.com/content/131/1/3.citation> [Accessed 10/06/2013].
- Graham, J., Pruitt, L., Ries, M. & Gundiah, N. 2000. Fracture and fatigue properties of acrylic bone cement: the effects of mixing method, sterilization treatment, and molecular weight. *Journal of Arthroplasty*, 15, 1028-1035.
- Halim, T., Burgett, M., Donaldson, T. K., Savisaar, C., Bowsher, J. & Clarke, I. C. 2014. Profiling the third-body wear damage produced in CoCr surfaces by bone cement, CoCr, and Ti6Al4V debris: A 10-cycle metal-on-metal simulator test. *Proceedings of the Institution of Mechanical Engineers, Part H: Journal of Engineering in Medicine*, 228, 703-713.
- Hansen, D. & Jensen, J. S. 1990. Prechilling and vacuum mixing not suitable for all bone cements: Handling characteristics and exotherms of bone cements. *Journal of Arthroplasty*, 5, 287-290.

- Hardinge, K. 1983. *Hip Replacement: The Facts - With Chapters on Other Joint Replacements*, Oxford, UK, Oxford University Press.
- Harper, E. J. 1998. Bioactive bone cements. *Proceedings of the Institution of Mechanical Engineers, Part H: Journal of Engineering in Medicine*, 212, 113-20.
- Harper, E. J. & Bonfield, W. 2000. Tensile characteristics of ten commercial acrylic bone cements. *Journal of Biomedical Materials Research (Applied Biomaterials)*, 53, 605-16.
- Harrigan, T. P., Kareh, J. A., O'Connor, D. O., Burke, D. W. & Harris, W. H. 1992. A finite element study of the initiation of failure of fixation in cemented femoral total hip components. *Journal of Orthopaedic Research*, 10, 134-144.
- Harris, J. 2006. *Fuzzy Logic Applications in Engineering Science*, Dordrecht, The Netherlands, Springer.
- Hasenwinkel, J. M., Lautenschlager, E. P., Wixson, R. L. & Gilbert, J. L. 2002. Effect of initiation chemistry on the fracture toughness, fatigue strength, and residual monomer content of a novel high-viscosity, two-solution acrylic bone cement. *Journal of Biomedical Materials Research* 59, 411-421.
- Havelin, L. I., Engesaeter, L. B., Espehaug, B., Furnes, O., Lie, S. A. & Vollset, S. E. 2000. The Norwegian Arthroplasty Register: 11 years and 73,000 arthroplasties. *Acta Orthopaedica Scandinavica*, 71, 337-353.
- Herman, W. A., Hertzberg, R. W. & Manson, J. A. 1990. The influence of loading history on fatigue in engineering plastics. *Journal of Materials Science*, 25, 434-440.
- Hertzberg, R. W. 1996. *Deformation and Fracture Mechanics of Engineering Materials*, John Wiley & Sons, Inc.
- Hertzberg, R. W. & Manson, J. A. 1980. *Fatigue of Engineering Plastics*, New York, USA, Academic Press.
- Hoey, D. & Taylor, D. 2009a. Comparison of the fatigue behaviour of two different forms of PMMA. *Fatigue & Fracture of Engineering Materials & Structures*, 32, 261-269.
- Hoey, D. & Taylor, D. 2009b. Quantitative analysis of the effect of porosity on the fatigue strength of bone cement. *Acta Biomaterialia*, 5, 719-726.
- Hoppel, C. P. R. & Pangborn, R. N. 1994. The evaluation of fatigue damage in short fiber-reinforced styrene-maleic anhydride. In: Mitchell, M. R. & Buck, O. (eds.) *Cyclic Deformation, Fracture, and Non-Destructive Evaluation of Advanced Materials*. Philadelphia, PA: American Society for Testing and Materials.
- James, S. P., Jasty, M., Davies, J., Piehler, H. & Harris, W. H. 1992. A fractographic investigation of PMMA bone cement focusing on the relationship between porosity reduction and increased fatigue life. *Journal of Biomedical Materials Research* 26, 651-662.
- Janna, S., Dwiggins, D. P. & Lewis, G. 2005. A new, reliable, and simple-to-use method for the analysis of a population of values of a random variable using the Weibull probability distribution: application to acrylic bone cement fatigue results. *Bio-Medical Materials and Engineering*, 15, 349-355.

- Janssen, D., Aquarius, R., Stolk, J. & Verdonshot, N. 2005a. The contradictory effects of pores on fatigue cracking of bone cement. *Journal of Biomedical Materials Research Part B: Applied Biomaterials*, 74, 747-753.
- Janssen, D., Stolk, J. & Verdonshot, N. 2005b. Why would cement porosity reduction be clinically irrelevant, while experimental data show the contrary. *Journal of Orthopaedic Research*, 23, 691-697.
- Jasty, M., Davies, J. P., O'Connor, D. O., Burke, D. W., Harrigan, T. P. & Harris, W. H. 1990. Porosity of various preparations of acrylic bone cements. *Clinical Orthopaedics and Related Research*, 259, 122-129.
- Jasty, M., Maloney, W. J., Bragdon, C. R., O'Connor, D. O., Haire, T. & Harris, W. H. 1991. The initiation of failure in cemented femoral components of hip arthroplasties. *Journal of Bone and Joint Surgery (Br)* 73, 551-558.
- Jeffers, J. R., Browne, M. & Taylor, M. 2005. Damage accumulation, fatigue and creep behaviour of vacuum mixed bone cement. *Biomaterials*, 26, 5532-5541.
- Johnson, J. A., Provan, J. W., Krygier, J. J., Chan, K. H. & Miller, J. 1989. Fatigue of acrylic bone cement - effect of frequency and environment. *Journal of Biomedical Materials Research*, 23, 819-831.
- Kambour, R. P. 1968. Stress-strain behaviour of the craze. *Polymer Engineering and Science*, 8, 281-289.
- Kane, R. J., Yue, W., Mason, J. J. & Roeder, R. K. 2010. Improved fatigue life of acrylic bone cements reinforced with zirconia fibers. *Journal of the Mechanical Behavior of Biomedical Materials*, 3, 504-511.
- Kim, D. G., Miller, M. A. & Mann, K. A. 2004. Creep dominates tensile fatigue damage of the cement-bone interface. *Journal of Orthopaedic Research*, 22, 633-640.
- Kim, S. 2008. Changes in surgical loads and economic burden of hip and knee replacements in the US: 1997–2004. *Arthritis & Rheumatism (Arthritis Care & Research)*, 59, 481-488.
- Kim, S. L., Skibo, M., Manson, J. A. & Hertzberg, R. W. 1977. Fatigue crack propagation in poly(methyl methacrylate): Effects of molecular weight and internal plasticization. *Polymer Engineering & Science*, 17, 194-203.
- Kindt-Larsen, T., Smith, D. B. & Jensen, J. S. 1995. Innovations in acrylic bone cement and application equipment. *Journal of Applied Biomaterials* 6, 75-83.
- Kjellson, F., Abdulghani, S., Tanner, K. E., McCarthy, I. D. & Lidgren, L. 2007. Effect of iodixanol particle size on the mechanical properties of a PMMA based bone cement. *Journal of Materials Science: Materials in Medicine*, 18, 1043-1051.
- Klemm, K. 2001. The use of antibiotic-containing bead chains in the treatment of chronic bone infections. *Clinical Microbiology and Infection*, 7, 28-31.
- Krause, W. & Mathis, R. S. 1988. Fatigue properties of acrylic bone cement: review of the literature. *Journal of Biomedical Materials Research*, 22 (A1 Suppl.), 27-53.

- Krause, W. R., Grimes, L. W. & Mathis, R. S. 1988. Fatigue testing of acrylic bone cements: statistical concepts and proposed test methodology. *Journal of Biomedical Materials Research*, 22, 179-190.
- Kühn, K. 2000. *Bone Cement: Up-to-Date Comparison of Physical and Chemical Properties of Commercial Materials*, Berlin, Springer-Verlag.
- Kühn, K. 2005. Properties of bone cement: what is bone cement? In: Breusch, S. & Malchau, H. (eds.) *The Well-Cemented Total Hip Arthroplasty*, Heidelberg: Springer Medizin Verlag.
- Kühn, K., Ege, W. & Gopp, U. 2005. Acrylic bone cements: composition and properties. *Orthopedic Clinics of North America*, 36, 17-28.
- Kurtz, S. M., Villarraga, M. L., Zhao, K. & Edidin, A. A. 2005. Static and fatigue mechanical behavior of bone cement with elevated barium sulfate content for treatment of vertebral compression fractures. *Biomaterials*, 26, 3699-3712.
- Lee, Y., Pan, J., Hathaway, R. & Barkey, M. 2005. *Fatigue Testing and Analysis: Theory and Practice*, USA, Elsevier Inc.
- Lennon, A. B. & Prendergast, P. J. 2005. Evaluation of cement stresses in finite element analysis of cemented orthopaedic implants. *Journal of Biomedical Engineering*, 123, 623-628.
- Lewis, G. 1999a. Effect of mixing method and storage temperature of cement constituents on the fatigue and porosity of acrylic bone cement. *Journal of Biomedical Materials Research Part B: Applied Biomaterials*, 48, 143-149.
- Lewis, G. 1999b. Effect of two variables on the fatigue performance of acrylic bone cement: mixing method and viscosity. *Bio-Medical Materials and Engineering*, 9, 197-207.
- Lewis, G. 2000. Relative roles of cement molecular weight and mixing method on the fatigue performance of acrylic bone cement: Simplex P versus Osteopal. *Journal of Biomedical Materials Research Part B: Applied Biomaterials*, 53, 119-130.
- Lewis, G. 2003a. Fatigue testing and performance of acrylic bone-cement materials: state-of-the-art review. *Journal of Biomedical Materials Research Part B: Applied Biomaterials* 66B, 457-486.
- Lewis, G. 2009. Properties of antibiotic-loaded acrylic bone cement for use in cemented arthroplasties: a state-of-the-art review. *Journal of Biomedical Materials Research Part B: Applied Biomaterials*, 89, 558-574.
- Lewis, G. & Austin, G. E. 1994. Mechanical properties of vacuum-mixed acrylic bone cement. *Journal of Applied Biomaterials*, 5, 307-314.
- Lewis, G. & Janna, S. 2003. Effect of test specimen cross-sectional shape on the in vitro fatigue life of acrylic bone cement. *Biomaterials*, 24, 4315-4321.
- Lewis, G., Janna, S. & Bhattaram, A. 2005a. Influence of the method of blending an antibiotic powder with an acrylic bone cement powder on physical, mechanical, and thermal properties of the cured cement. *Biomaterials*, 26, 4317-4325.

- Lewis, G., Janna, S. & Carroll, M. 2003. Effect of test frequency on the in vitro fatigue life of acrylic bone cement. *Biomaterials*, 24, 1111-1117.
- Lewis, G. & Li, Y. 2010. Dependence of in vitro fatigue properties of PMMA bone cement on the polydispersity index of its powder. *Journal of the Mechanical Behaviour of Biomedical Materials*, 3, 94-101.
- Lewis, G. & Nyman, J. S. 2000. Toward standardization of methods of determination of fracture properties of acrylic bone cement and statistical analysis of test results. *Journal of Biomedical Materials Research Part B: Applied Biomaterials*, 53, 748-768.
- Lewis, G., Nyman, J. S. & Trieu, H. H. 1997. Effects of mixing method on selected properties of acrylic bone cement. *Journal of Biomedical Materials Research Part B: Applied Biomaterials*, 38, 221-228.
- Lewis, G. & Sadhasivini, A. 2004. Estimation of the minimum number of test specimens for fatigue testing of acrylic bone cement. *Biomaterials*, 25, 4425-4432.
- Lewis, G., Van Hooy-Corstjens, C. S., Bhattaram, A. & Koole, L. H. 2005b. Influence of the radiopacifier in an acrylic bone cement on its mechanical, thermal, and physical properties: barium sulfate-containing cement versus iodine-containing cement. *Journal of Biomedical Materials Research Part B: Applied Biomaterials*, 73, 77-87.
- Lezarus, M. D., Cuckler, J. M., Schumacher, H. R., Ducheyne, P. & Baker, D. G. 1994. Comparison of the inflammatory response to particulate polymethylmethacrylate debris with and without barium sulphate. *Journal of Orthopaedic Research*, 12, 532-541.
- Liptáková, T., Lelovics, H. & Nečas, L. 2009. Variations of temperature of acrylic bone cements prepared by hand and vacuum mixing during their polymerization. *Acta Bioengineering and Biomechanics*, 11, 47-51.
- Liu, A. F. 2005. *Mechanics and Mechanisms of Fracture: An Introduction*, USA, ASM International
- Liu, C. Z., Green, S. M., Watkins, N. D., Baker, D. & McCaskie, A. W. 2005. Dynamic creep and mechanical characteristics of SmartSet GHV bone cement. *Journal of Materials Science: Materials in Medicine*, 16, 153-160.
- Liu, C. Z., Green, S. M., Watkins, N. D. & McCaskie, A. W. 2003. On the particle size and molecular weight distributions of clinical bone cements. *Journal of Materials Science Letters*, 22, 1147-1150.
- Madigan, S., Towler, M. R. & Lewis, G. 2006. Optimisation of the composition of an acrylic bone cement: application to relative amounts of the initiator and the activator/co-initiator in Surgical Simplex® P. *Journal of Materials Science: Materials in Medicine*, 17, 307-311.
- Malchau, H., Herberts, P., Garellick, G., Söderman, P. & Eisler, T. 2002. Prognosis of total hip replacement: Update of Results and Risk-Ratio Analysis for Revision and Re-revision from the Swedish National Hip Arthroplasty Register 1979-2000. *The Swedish Hip Arthroplasty Register* [Online]. Available: <http://www.shpr.se/Libraries/Documents/AAOS2002.sflb.ashx> [Accessed 30/04/2014].
- Mann, K., Miller, M. A., Race, A. & Verdonschot, N. 2009. Shear fatigue micromechanics of the cement-bone interface: An in vitro study using digital image correlation techniques.

Journal of Arthopaedic Research, 27, 340-346 Manson, S. S. (ed.) 1971. *Metal Fatigue Damage: Mechanism, Detection, Avoidance and Repair*, Baltimore, USA: American Society for Testing and Materials.

McCartney, L. N. 1996. Stress transfer mechanics: Methods that should be the basic of life prediction methodology. In: Johnson, W. S., Larsen, J. M. & Cox, B. N. (eds.) *Life Prediction Methodology for Titanium Matrix Composite*, West Conshohocken, US: American Society for Testing and Materials.

McClintock, F. A. & Argon, A. S. (eds.) 1966. *Mechanical behaviour of materials*, Massachusetts, USA: Addison-Wesley.

Mehlhoff, M. A. & Sledge, C. B. 1990. Comparison of cemented and cementless hip and knee replacements. *Arthritis and Rheumatism*, 33, 293-297.

Milella, P. P. 1999. A fatigue crack growth theory based on energy considerations: Further developments on small crack behaviour and R ratio. In: Panontin, T. L. & Sheppard, S. D. (eds.) *Fatigue and Fracture Mechanics*, West Conshohocken, PA American Society for Testing and Materials.

Milella, P. P. 2013. *Fatigue and Corrosion in Metals*, Italy, Springer.

Minari, C., Baleani, M., Cristofolini, L. & Baruffaldi, F. 2001. The effect on the fatigue strength of bone cement of adding sodium fluoride. *Proceedings of the Institution of Mechanical Engineers, Part H: Journal of Engineering in Medicine*, 215, 251-253.

Mitchell, M. R. 1996. Fundamentals of Modern Fatigue Analysis for Design *ASM Handbook, Vol 19, Fatigue and Fracture*, USA: ASM International.

Mitchell, W., Matthews, J. B., Stone, M. H., Fisher, J. & Ingham, E. 2003. Comparison of the response of human peripheral blood mononuclear cells to challenge with particles of three bone cements in vitro. *Biomaterials*, 24, 737-748.

Mittemeijer, E. J. 2010. *Fundamentals of Materials Science: The Microstructure-Property Relationship Using Metals as Model Systems*, Berlin Springer-Verlag.

Moet, A. & Aglan, H. 2003. Fatigue failure mechanisms. In: Lampman, S. (ed.) *Characterization and Failure Analysis of Plastics*. USA: ASM International.

Molino, L. N. & Topoleski, L. D. 1996. Effect of BaSO₄ on the fatigue crack propagation rate of PMMA bone cement. *Journal of Biomedical Materials Research*, 31, 131-137.

Monge Jodra, V., Sainz De Los Terreros Soler, L., Diaz-Agero Perez, C., San Requejo, C. M. & Plana Farras, N. 2006. Excess length of stay attributable to surgical site infection following hip replacement: a nested case-control study. *Infection Control and Hospital Epidemiology*, 27, 1299-1303.

Moran, C. G. & Horton, T. C. 2000. Total knee replacement: the joint of the decade: A successful operation, for which there's a large unmet need. *British Medical Journal*, 320, 820.

Murphy, B. P. 2001. *Aspects of the fatigue behaviour of acrylic bone cement*. Doctor of Philosophy Thesis, University of Dublin.

- Murphy, B. P. & Prendergast, P. J. 1999. Measurement of non-linear microcrack accumulation rates in polymethylmethacrylate bone cement under cyclic loading. *Journal of Materials Science: Materials in Medicine*, 10, 779-781.
- Murphy, B. P. & Prendergast, P. J. 2000. On the magnitude and variability of the fatigue strength of acrylic bone cement. *International Journal of Fatigue*, 22, 855-864.
- Murphy, B. P. & Prendergast, P. J. 2003. Multi-axial fatigue failure of orthopedic bone cement - experiments with tubular specimens. *Journal of Materials Science: Materials in Medicine*, 14, 857-61.
- Nelsen, A. R. & Wiig, M. 1996. Total hip arthroplasty with Boneloc: loosening in 102/157 cases after 0.5-3 years. *Acta Orthopaedica Scandinavica*, 67, 57-59.
- Nguyen, N. C., Maloney, W. J. & Dauskardt, R. H. 1997. Reliability of PMMA bone cement fixation: fracture and fatigue crack-growth behaviour. *Journal of Materials Science: Materials in Medicine*, 8, 473-483.
- NJR 2013. *National Joint Registry for England, Wales and Northern Ireland: 10th Annual Report 2013*. Available: http://www.njrcentre.org.uk/njrcentre/Portals/0/Documents/England/Reports/10th_annual_report/NJR%2010th%20Annual%20Report%202013%20B.pdf [Accessed 23/03/2015].
- Novovic, D., Dewes, R. C., Aspinwall, D. K., Voice, W. & Bowen, P. 2004. The effect of machined topography and integrity on fatigue life. *International Journal of Machine Tools & Manufacture*, 44, 125-134.
- Paravic, V., Nobel, P. C., Alexander, J. W., Leibs, T. R. & Elliot, A. 1999. Effect of specimen preparation on porosity and fatigue life: a study of centrifuged and handmixed cement. *45th Annual Meeting, Orthopaedic Research Society* Anaheim, California.
- Pelletier, M. H., Lau, A. C. B., Smitham, P. J., Nielsen, G. & Walsh, W. R. 2010. Pore distribution and material properties of bone cement cured at different temperatures. *Acta Biomaterialia*, 6, 886-891.
- Pennati, G., Villa, T. & Dubini, G. 2003. Influence of specimen molding technique on fatigue properties of a bone cement. *Journal of Applied Biomaterials and Biomechanics*, 1, 148-153.
- Pilliar, R. M., Blackwell, R., Macnab, I. & Cameron, H. U. 1976. Carbon fiber-reinforced bone cement in orthopedic surgery. *Journal of Biomedical Materials Research*, 10, 893-906.
- Pokluda, J., Sandera, P. & Hornikova, J. 2005. *Analysis of Roughness-Induced Crack-tip Shielding in Terms of Size Ratio Effect*, Lancaster, PA, ASTM International.
- Polák, J. 2003. Cyclic deformation, crack initiation, and low-cycle fatigue. In: Milne, I., Ritchie, R. O. & Karihaloo, B. (eds.) *Comprehensive Structural Integrity: Fracture of Materials from Nano to Macro (Vol. 4)*. Amsterdam: Elsevier Pergamon.
- Pruitt, L. A. 2003. Fatigue testing and behaviour. In: Lampman, S. (ed.) *Characterization and Failure Analysis of plastics*. USA: ASM International.

- Quinn, J., Joyner, C., Triffit, J. T. & Athanasou, N. A. 1992. Polymethylmethacrylate-induced inflammatory macrophages resorb bone. *Journal of Bone and Joint Surgery (Br)*, 74-B, 652-658.
- Race, A. & Mann, K. A. 2008. Fatigue crack propagation rates in PMMA bone cement cannot be reduced to a single power law. *Journal of Biomedical Materials Research Part B: Applied Biomaterials*, 86, 278-282.
- Ram, A. 1997. *Fundamentals of Polymer Engineering*, New York, Plenum Press.
- Ramaniraka, N. 2002. Thermal bone necrosis at the bone-cement interface after cemented total hip arthroplasty: a finite element analysis *In: Leyvraz, P. F., Pioletti, D., Quinn, T. & Zysset, P. (eds.) European Orthopaedic Research Society*, Lausanne, Switzerland: EPFL Press.
- Ramulu, M. 1999. Characterization of Surface Quality in Machining of Composites. *In: Jahanmir, S., Ramulu, M. & Koshy, P. (eds.) Machining of Ceramics and Composites*.
- Reliability Engineering Resources. 2002. *Characteristics of the Weibull Distribution* [Online]. Available: <http://www.weibull.com/hotwire/issue14/relbasics14.htm> [Accessed 14/10/2014].
- Riegels-Nielsen, P., Sørensen, L., Andersen, H. M. & Lindequist, S. 1995. Boneloc cemented total hip prostheses. Loosening in 28/43 cases after 3-38 months. *Acta Orthopaedica Scandinavica*, 66, 215-217.
- Ries, M. D., Young, E., Al-Marashi, L., Goldstein, P., Hetherington, A., Petrie, T. & Pruitt, L. 2006. In vivo behaviour of acrylic bone cement in total hip arthroplasty. *Biomaterials*, 27, 256-261.
- Rinnac, C. M., Wright, T. M. & McGill, D. L. 1986. The effect of centrifugation on the fracture properties of acrylic bone cements. *Journal of Bone and Joint Surgery (Am)*, 68-, 281-287.
- Roques, A., Browne, M., Thompson, J., Rowland, C. & Taylor, A. 2004. Investigation of fatigue crack growth in acrylic bone cement using the acoustic emission technique. *Biomaterials*, 25, 769-778.
- Rosato, D. V., Schott, N. R., Rosato, D. V. & Rosato, M. G. (eds.) 2001. *Plastics Engineering Manufacturing and Data Handbook*, USA: Kluwer Academic Publishers.
- Sabokbar, A., Fujikawa, Y., Brett, J., Murray, D. W. & Athanasou, N. A. 1996. Increased osteoclastic differentiation by PMMA particle-associated macrophages. *Acta Orthopaedica Scandinavica*, 67, 593-598.
- Sauer, J. A. & Richardson, G. C. 1980. Fatigue of polymers. *International Journal of Fracture*, 16, 499-532.
- Sawyer, L. C., Grubb, D. T. & Meyers, G. F. 2008. *Polymer Microscopy*, New York, USA, Springer.
- Schierholz, J. M. & Beuth, J. 2001. Implant infections: a haven for opportunistic bacteria. *Journal of Hospital Infection*, 49, 87-93.

- Schijve, J. 2009. *Fatigue of Structures and Materials*, USA, Springer Science+Business Media, B.V.
- Schoellner, C., Fuerderer, S., Rompe, J. D. & Eckardt, A. 2003. Individual bone cement spacers (IBCS) for septic hip revision - preliminary report. *Archives of Orthopaedic and Trauma Surgery*, 123, 254-259.
- Shah, N. & Porter, M. 2005. Evaluation of cemented stems. *Orthopedics*, 28 (Supplements), S819-S825.
- Shigley, J. E. & Mischke, C. R. 1989. *Mechanical Engineering Design*, New York, USA, McGraw-Hill.
- Slane, J., Vivanco, J., Meyer, J., Ploeg, H. L. & Squire, M. 2014. Modification of acrylic bone cement with mesoporous silica nanoparticles: effects on mechanical, fatigue and absorption properties. *Journal of the Mechanical Behavior of Biomedical Materials*, 29, 451-461.
- Soh Fotsing, B. D., Ango, G. F. & Fogue, M. 2010. Statistical techniques of sample size estimating in fatigue tests. *International Journal of Engineering and Technology*, 2, 477-481.
- Soltész, U. 1994. The influence of loading conditions on the life-times in fatigue testing of bone cements. *Journal of Materials Science: Materials in Medicine*, 5, 654-656.
- Spurgeon, C. H. 2009. Energy Release Rate. In: Kumar, P. (ed.) *Elements of Fracture Mechanics*, New Delhi: TaTa McGraw-Hill.
- Starke, G. R., Birnie, C. & van den Blink, P. A. 1998. Numerical modelling of cement polymerisation and thermal bone necrosis. In: Middleton, J., Jones, M. L. & Pande, G. N. (eds.) *Computer Methods in Biomechanics & Biomedical Engineering - 2*, Amsterdam, the Netherlands: Gordon and Breach Science
- Stillwell, W. T. 1987. *The Art of Total Hip Arthroplasty*, London, Grune & Stratton.
- Stryker. 2006. Simplex P Bone Cement Products. Available: http://www.endoroot.com/modules/newbb/dl_attachment.php?attachid=1275321230&post_id=29506. [Accessed 09/05/2014].
- Suresh, S. 1998. *Fatigue of Materials*, New York, USA, Cambridge University Press.
- Swanson, S. R. (ed.) 1974. *Handbook of Fatigue Testing*, Philadelphia: ASTM.
- Tanner, K. E., Wang, J., Kjellson, F. & Lidgren, L. 2010. Comparison of two methods of fatigue testing bone cement. *Acta Biomaterialia*, 6, 943-952.
- Teoh, S. H. 2000. Fatigue of biomaterials: a review. *International Journal of Fatigue*, 22, 825-837.
- Theodoroua, D. J., Theodoroua, S. J., Duncana, T. D., Garfinb, S. R. & Wonga, W. H. 2002. Percutaneous balloon kyphoplasty for the correction of spinal deformity in painful vertebral body compression fractures. *Journal of Clinical Imaging*, 26, 1-5.
- Toksvig-Larsen, S., Franzen, H. & Ryd, L. 1991. Cement interface temperature in hip arthroplasty. *Acta Orthopaedica Scandinavica*, 62, 102-105.

- Tong, J., Zant, N. P. & Heaton-Adegbile, P. 2006. Fatigue Failure in reconstructed Acetabula - A Hip Simulator Study. In: Gdouts, E. E. (ed.) *Fracture of Nano and Engineering Materials and Structures - Proceedings of the 16th European Conference of Fracture*, Alexandroupolis, Greece, July 3-7, 2006.
- Topoleski, L. D., Ducheyne, P. & Cuckler, J. M. 1990. A fractographic analysis of in vivo poly(methyl methacrylate) bone cement failure mechanisms. *Journal of Biomedical Materials Research*, 24, 135-154.
- Topoleski, L. D., Ducheyne, P. & Cuckler, J. M. 1993. Microstructural pathway of fracture in poly(methyl methacrylate) bone cement. *Biomaterials*, 14, 1165-1172.
- Topoleski, L. D., Ducheyne, P. & Cuckler, J. M. 1995. The effects of centrifugation and titanium fiber reinforcement on fatigue failure mechanisms in poly(methyl methacrylate) bone cement. *Journal of Biomedical Materials Research: Part A*, 29, 299-307.
- Vallo, C. I., Cuadrado, T. R. & Frontini, P. M. 1997. Mechanical and fracture behaviour evaluation of commercial acrylic bone cements. *Polymer International*, 43, 260-268.
- Van De Belt, H., Neut, D., Uges, D. R., Schenk, W., R., V. H. J., Van Der Mei, H. C. & Busscher, H. J. 2000. Surface roughness, porosity and wettability of gentamicin-loaded bone cements and their antibiotic release. *Biomaterials*, 21, 1981-1987.
- Van Paepegen, W. 2011. Fatigue testing methods for polymer matrix composites In: Guedes, R. M. (ed.) *Creep and Fatigue in Polymer Matrix Composites*. Cambridge, UK Woodhead Publishing.
- Vashishth, D., Behiri, J. C. & Bonfield, W. 1997. Crack growth resistance in cortical bone: concept of microcrack toughening. *Journal of Biomechanics*, 30, 763-769.
- Verdonschot, N. & Huiskes, R. 1995. Dynamic creep behaviour of acrylic bone cement. *Journal of Biomedical Materials Research*, 29, 575-581.
- Vishay. 2014. *Special Use Sensors - Crack Propagation Sensors* [Online]. Vishay Precision Group. Available: <http://www.vishaypg.com/docs/11521/crackpro.pdf> [Accessed 18/07/2014].
- Volynskii, A. L. & Bakeev, N. F. 1995. *Solvent Cracking of Polymers*, Amsterdam, The Netherlands, Elsevier science B. V.
- Waanders, D., Janssen, D., Mann, K. A. & Verdonschot, N. 2010a. The effect of cement creep and cement fatigue damage on the micromechanics of the cement-bone interface. *Journal of Biomechanics*, 43, 3028-3034.
- Waanders, D., Janssen, D., Mann, K. A. & Verdonschot, N. 2010b. The mechanical effects of different levels of cement penetration at the cement-bone interface. *Journal of Biomechanics*, 43, 1167-1175.
- Wallbridge, N. & Dowson, D. 1982. The walking activity of patients with artificial hip joints. *Engineering in Medicine* 11, 95-96.
- Wang, J. S., Diaz, J., Sabokbar, A., Athanasou, N., Kjellson, F., Tanner, K. E., McCarthy, I. D. & Lidgren, L. 2005. In vitro and in vivo biological responses to a novel radiopacifying agent for bone cement. *Journal of the Royal Society Interface*, 2, 71-78.

-
- Webb, J. C. J. & Spencer, R. F. 2007. The role of polymethylmethacrylate bone cement in modern orthopaedic surgery. *The Journal of Bone and Joint Surgery [Br]*, 89-B, 851-857.
- Weibull, W. 1951. A statistical distribution function of wide applicability. *Journal of Applied Mechanics*, 18, 293-297.
- Weibull, W. 1961. *Fatigue Testing and Analysis of Results*, Oxford, London, New York and Paris, Pergamon Press.
- Wykman, A. G. & Sanderjöö, G. A. 1995. Low polymerization temperature with Boneloc®: in vivo measurements in 11 hip replacements. *Acta Orthopaedica Scandinavica*, 66, 218-219.
- Yang, D. T., Zhang, D. & Arola, D. 2010. Fatigue of the bone/cement interface and loosening of total joint replacements. *International Journal of Fatigue*, 32, 1639-1649.

APPENDICES

Appendix. 1 Calculations of strain correction factors for testing specimens

The axial displacement of a test specimen occurs along the gauge section and the two transitional sections (shoulders) between the gauge and the grips over the total length as shown in Figure A1.1a and Figure A1.2 for circular and rectangular cross sectional specimens, respectively. Equation A1.1 shows the relation between the total displacement and strain over all the sections included in testing which is constantly controlled by Equation A1.2. To determine the percentage of displacement and accordingly the strain in the gauge section only, Equations from A1.2 to A1.5 were used to rewrite Equation A1.1 to provide Equations A1.6 and A1.7.

$$\delta_t = \int_0^{\ell_t} \varepsilon d\ell \quad \text{A1.1}$$

$$\delta_t = \delta_g + 2\delta_s \quad \text{A1.2}$$

where, δ_t = total displacement, ε = strain, ℓ_t = sum of the gauge and two shoulders lengths, δ_g = gauge displacement and δ_s = shoulder displacement

$$\varepsilon = \frac{F}{E} \times \frac{1}{A_i} \quad \text{A1.3}$$

where, A_i = instantaneous area, F = applied force and E = Young's modulus

$$\delta_g = \frac{F}{E} \times \frac{\ell_g}{A_g} \quad \text{A1.4}$$

where, δ_g = gauge displacement, ℓ_g = gauge length and A_g = gauge section area.

$$\delta_t = \frac{F}{E} \int_0^{\ell_t} \frac{1}{A_i} d\ell \quad \text{A1.5}$$

$$\frac{\delta_g}{\delta_t} = \frac{\frac{\ell_g}{A_g}}{\int_0^{\ell_t} \frac{1}{A_i} d\ell} \quad \text{A1.6}$$

$$\frac{\delta_g}{\delta_t} = \frac{\frac{\ell_g}{A_g}}{2 \int_0^{\ell_s} \frac{1}{A_s} d\ell_s + \frac{\ell_g}{A_g}} \quad \text{A1.7}$$

where, ℓ_s = shoulder length, A_s = instantaneous shoulder cross sectional area.

A1.1 Correction factor for the rectangular cross sections

When considering the rectangular shape, the calculations of the cross sectional areas for the gauge (constant) and the shoulders (instantaneous) were obtained using Equations A1.8 and A1.9, respectively. As illustrated by Figure A1.1b, a slide with area of A_s was integrally used to estimate the strain over the shoulders, where the instantaneous shoulder width (slide length) was calculated using Equation A1.10.

$$A_g = t \times w_g \quad \text{A1.8}$$

$$A_s = t \times w_s \quad \text{A1.9}$$

$$w_s = 2w_v + w_g \quad \text{A1.10}$$

where w_s = instantaneous shoulder width, w_g = gauge width, t = Specimen thickness and w_v = the increase in shoulder width throughout the shoulder length starting from gauge width.

Therefore, Equation A1.7 can be rewritten as in Equation A1.11 and A1.12.

$$\frac{\delta_g}{\delta_t} = \frac{\frac{\ell_g}{t \times w_g}}{2 \int_0^{\ell_s} \frac{1}{t \times w_s} d\ell_s + \frac{\ell_g}{t \times w_g}} \quad \text{A1.11}$$

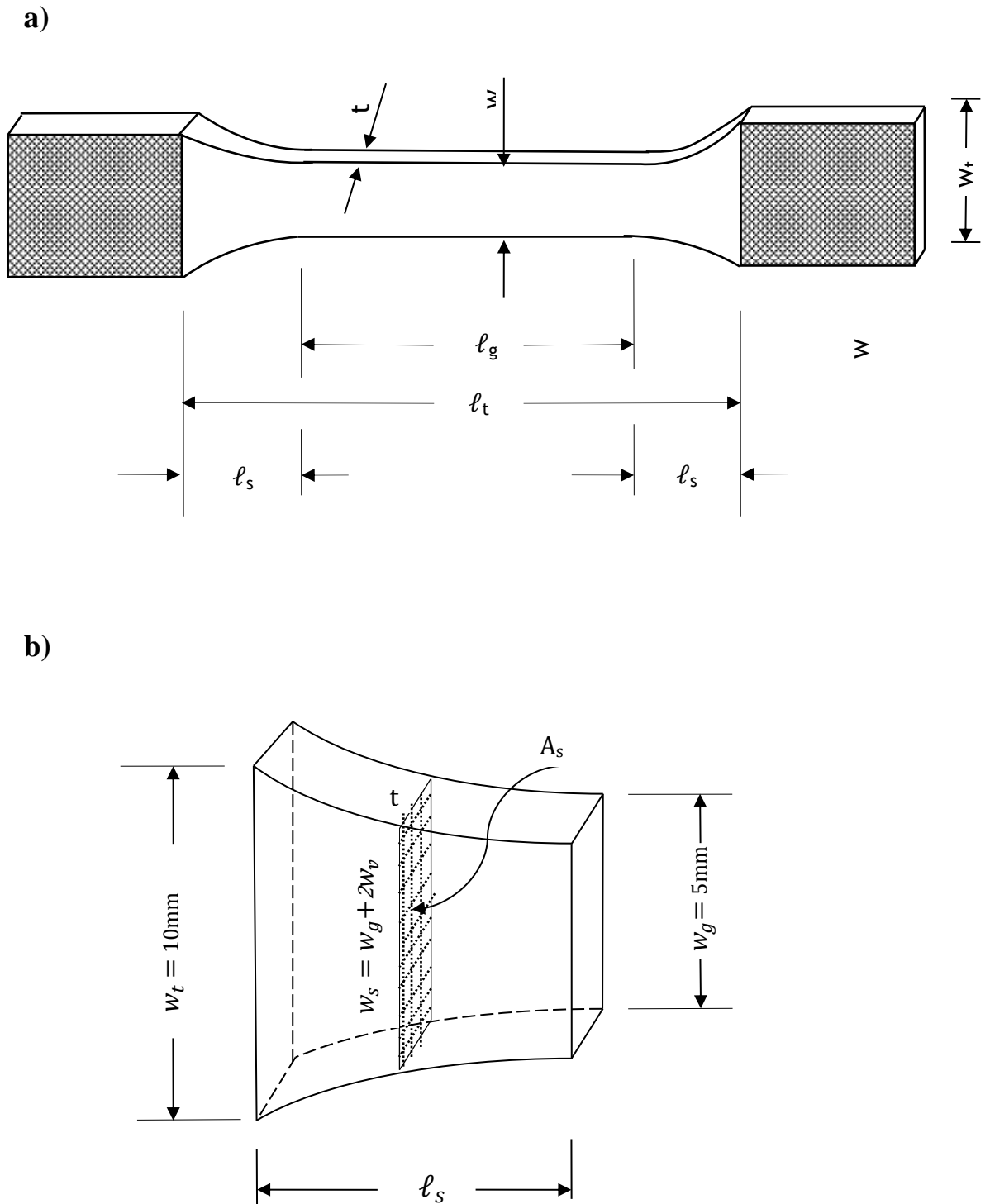
$$\frac{\delta_g}{\delta_t} = \frac{\frac{\ell_g}{t \times w_g}}{2 \int_0^{\ell_s} \frac{1}{\frac{w_t - w_g}{t (2 \int_0^2 dw_v + w_g)}} d\ell_s + \frac{\ell_g}{t \times w_g}} \quad \text{A1.12}$$

Substituting the values of ℓ_g (25 mm), w_g (5 mm), ℓ_s (10 mm), t (4 mm), w_t (10 mm) and w_g (5 mm) in Equation A1.12 provides the following:

$$\frac{\delta_g}{\delta_t} = 0.67 \quad \text{A1.13}$$

Therefore, the strain in the gauge length ε_g can independently be calculated where,

$$\varepsilon_g = 0.67 \frac{\delta_t}{l_g} \quad \text{A1.14}$$



l_g = gauge length = 25 mm, l_s = shoulder length = 10mm, l_t = total length included in testing = $l_g + 2l_s$, w_t = grip width = 10mm, w_g = gauge section width = 5 mm, A_s = shoulder instantaneous area & w_s = shoulder instantaneous width

Figure A1.1 a) Rectangular specimen parameters and b) a specimen shoulder showing the slide used for calculating the instantaneous area by integration

A1.2 Correction factor for the circular cross sections

The instantaneous cross sectional area of each shoulder of the circular specimens can be represented as a circle of radius r . If $(0, r)$ is a point on the curvature of a circular cross sectional profile (curve radius R), the formula for the circle of this curve is given in Equation A1.13, where b is the smallest radius of the curvature profile and l is the longitudinal length of the profile. Therefore, calculation of the cross sectional area of the profile at the point $(0, r)$, which is the area of the circle of the radius r , can be calculated using equation A1.14 [the plus-minus (\pm) sign was replaced by the minus ($-$) sign only due to being relevant to the considered geometry].

$$r = (b + R) \pm \sqrt{(R^2 - l^2)} \quad \text{A1.13}$$

$$A = \pi r^2 = \pi [(b + R) - \sqrt{(R^2 - l^2)}]^2 \quad \text{A1.14}$$

The instantaneous area for the shoulder cross section was accordingly determined according to Equation A1.15, where r_g is the radius of the gauge section. Applying this into Equation A1.7 will lead it to be rewritten as in Equation A1.16.

$$A_s = \pi \left[(r_g + R) - \sqrt{(R^2 - \ell_s^2)} \right]^2 \quad \text{A1.15}$$

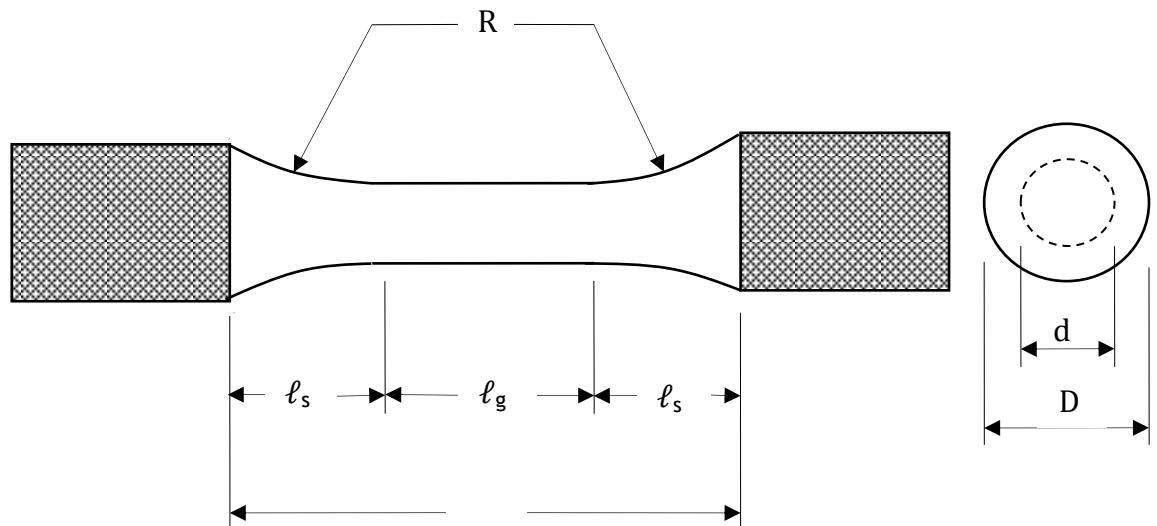
$$\frac{\delta_g}{\delta_t} = \frac{\frac{\ell_g}{A_g}}{\frac{2}{\pi} \int_0^{\ell_s} \frac{1}{\left[(r_g + R) - \sqrt{(R^2 - \ell_s^2)} \right]^2} d\ell_s + \frac{\ell_g}{A_g}} \quad \text{A1.16}$$

Solving the integration part of Equation A.16 using Simpson's rule and substituting the values of ℓ_g (10 mm), r_g (2.5 mm), ℓ_s (8 mm) and R (10 mm) provides:

$$\frac{\delta_g}{\delta_t} = 0.41 \quad \text{A1.16}$$

Thus, the strain in the gauge section ε_g can be determined where,

$$\varepsilon_g = 0.41 \frac{\delta_t}{\ell_g} \quad \text{A1.16}$$



l_g = Gauge length = 10 mm, l_s = Shoulder length = 8mm, l_t = Total length included in testing = $l_g + 2l_s$, $d=2r_0$ = Gauge diameter = 5mm & D = Grip diameter = 8.5 mm

Figure A1.2 *Circular specimen parameters*

Appendix. 2 Probability density functions

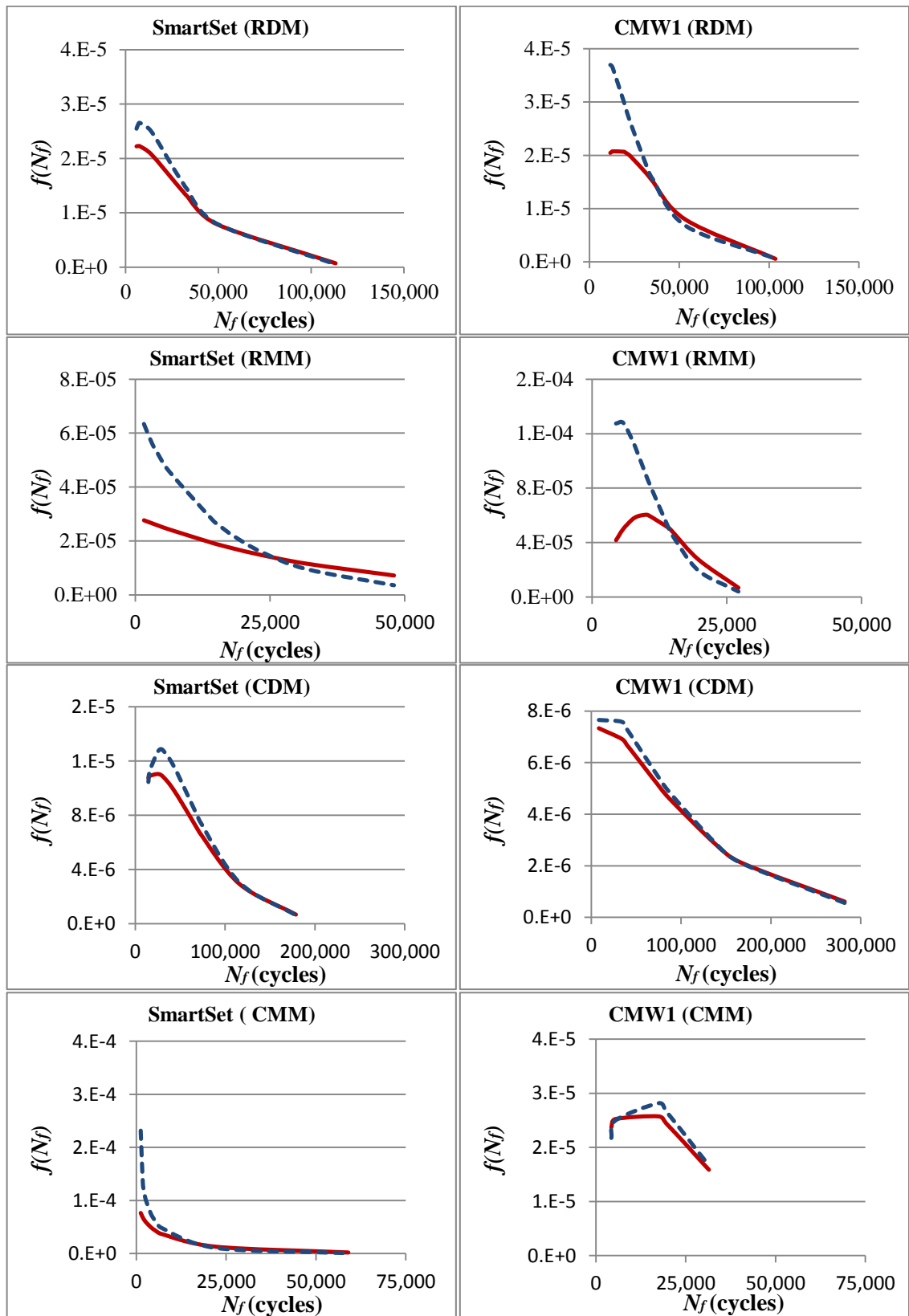


Figure A2.1 The probability density functions of the two-parameter (solid curves) and three-parameter (dotted curves) Weibull distributions for all specimen types tested in fully reversed tension-compression loading ($\pm 20\text{MPa}$)

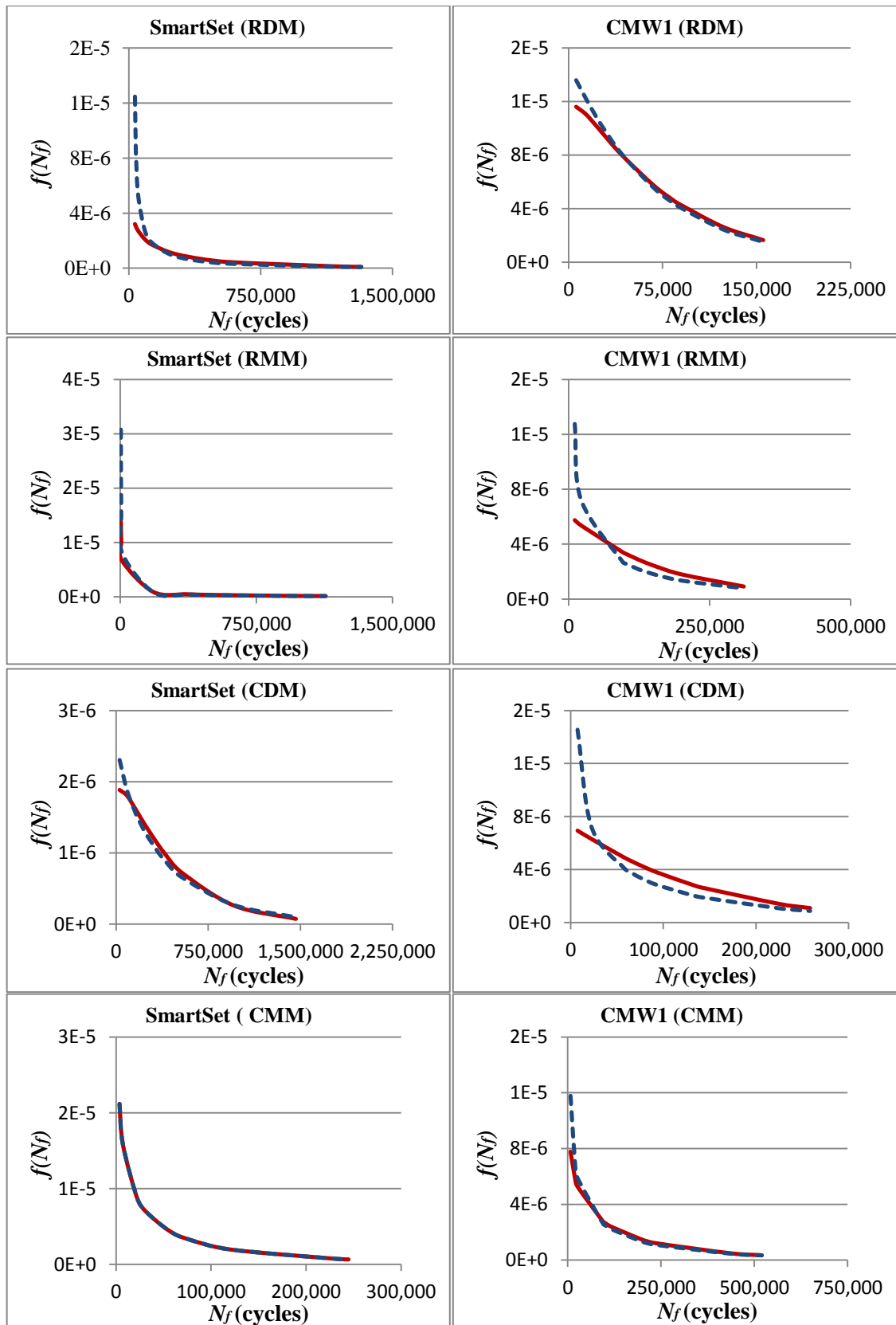
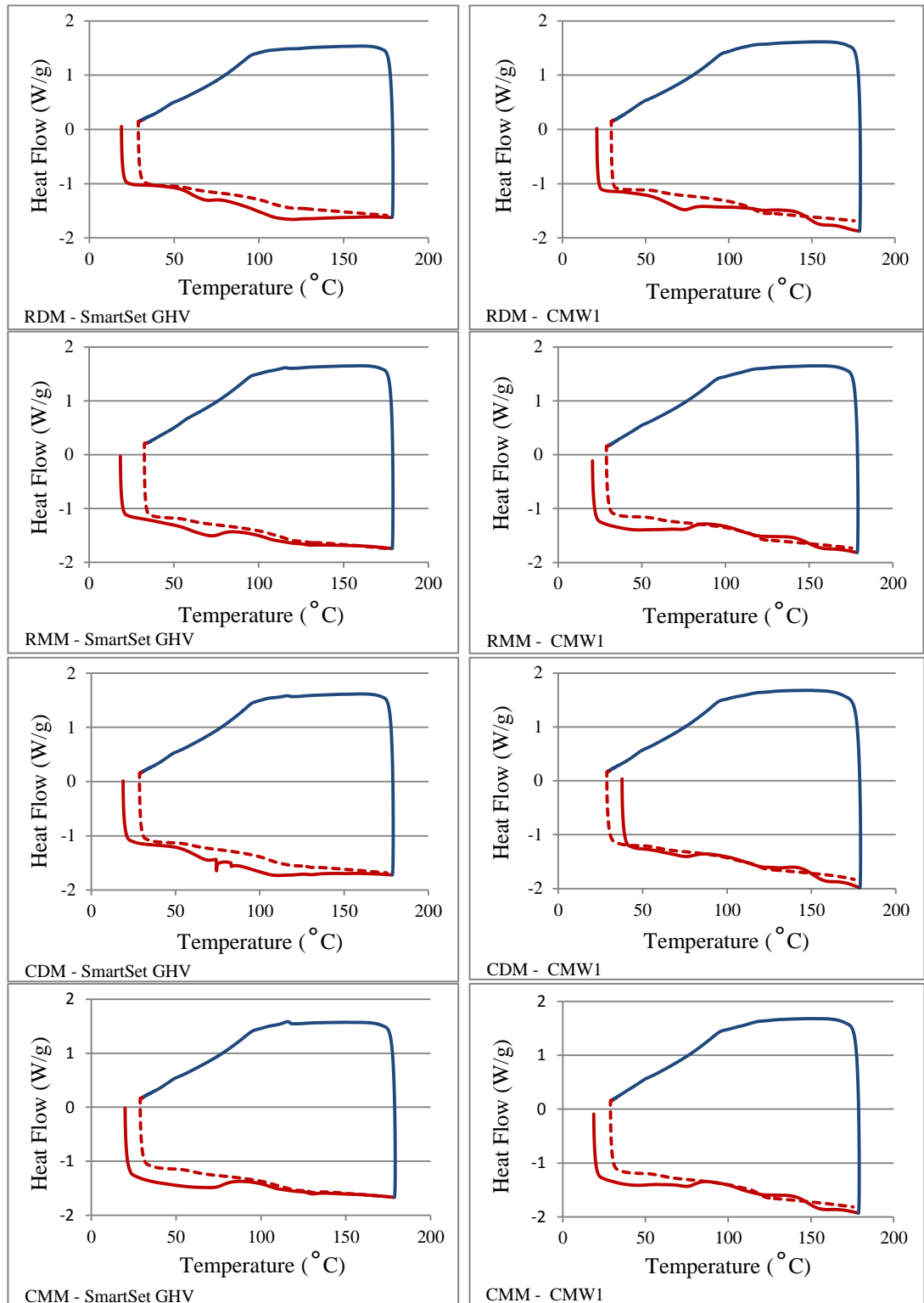


Figure A2.2 The probability density functions of the two-parameter (solid curves) and three-parameter (dotted curves) Weibull distributions for all specimen types tested in tension-tension cyclic loading

Appendix. 3 DSC analysis



— Process 1 (heating to 180°C) — Process 2 (cooling to ~25°C) - - - Process 3 (second heating to 180°C)

Figure A3.1 Comparison of the DSC results for specimen types of SmartSet GHV and CMW1

Appendix. 4 Euler buckling load calculations

The critical load at and above which the buckling would occur is:

$$P_{critical} = \pi^2 \frac{EI}{l^2} \quad (A4.1)$$

where E is Young's modulus, l is the effective length and I is the polar moment of inertia.

For the rectangular cross sections:

$$I = \frac{1}{3} bh^3 \quad (A4.2)$$

And for the circular cross sections:

$$I = \frac{\pi r^4}{2} \quad (A4.3)$$

where b and h are the thickness and width of the rectangular sections and r is the radius of the circular sections.

Considering that testing on a specimen included the gauge section and the shoulders, the effective length l was substituted for in Equation A4.1 by the total length of the gauge section and the two shoulders. Young's modulus was assumed to be 2400 MPa. Therefore, the critical loads for nominal specimens were estimated as:

$P_{critical} = 621$ N for the rectangular specimens corresponding to a stress of 31 MPa

$P_{critical} = 685$ N for the circular specimens corresponding to a stress of 35 MPa

Appendix. 5 Stress-strain behaviour

A5.1 Stress-strain behaviour of the median specimens of the fully reversed tension-compression fatigue (SmartSet GHV)

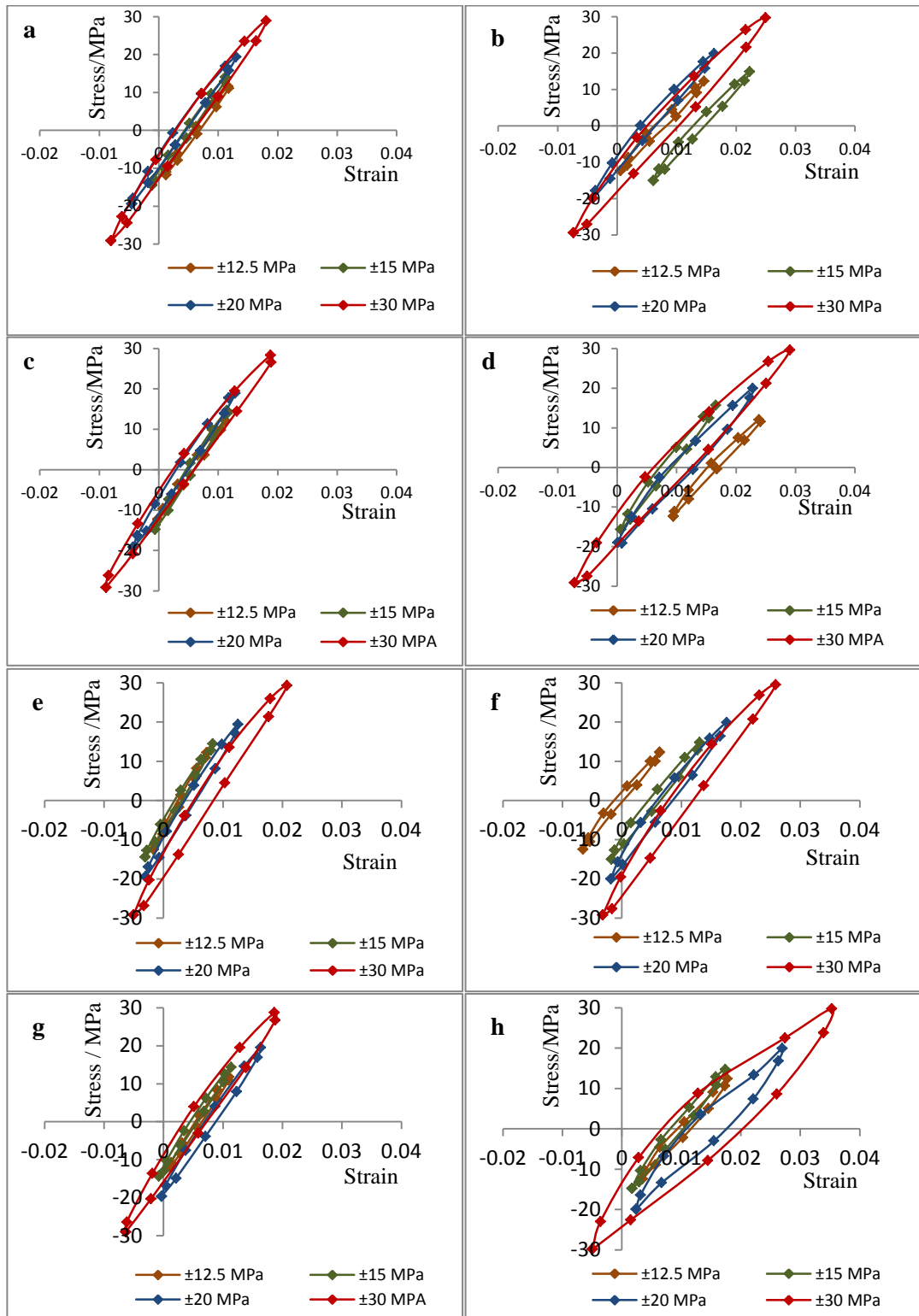


Figure A5.1 Comparison of stress-strain curves at early and late fatigue cycles in SmartSet GHV for different specimen types: RDM (a and b), RMM (c and d), CDM (e and f) and CMM (g and h) where a, c, e and g show the loops at the 10th cycle and b, d, f and h show them at the 5th cycle before failure.

A5.2 Stress- strain behaviour of the median specimens of the fully reversed tension-compression fatigue (CMW1)

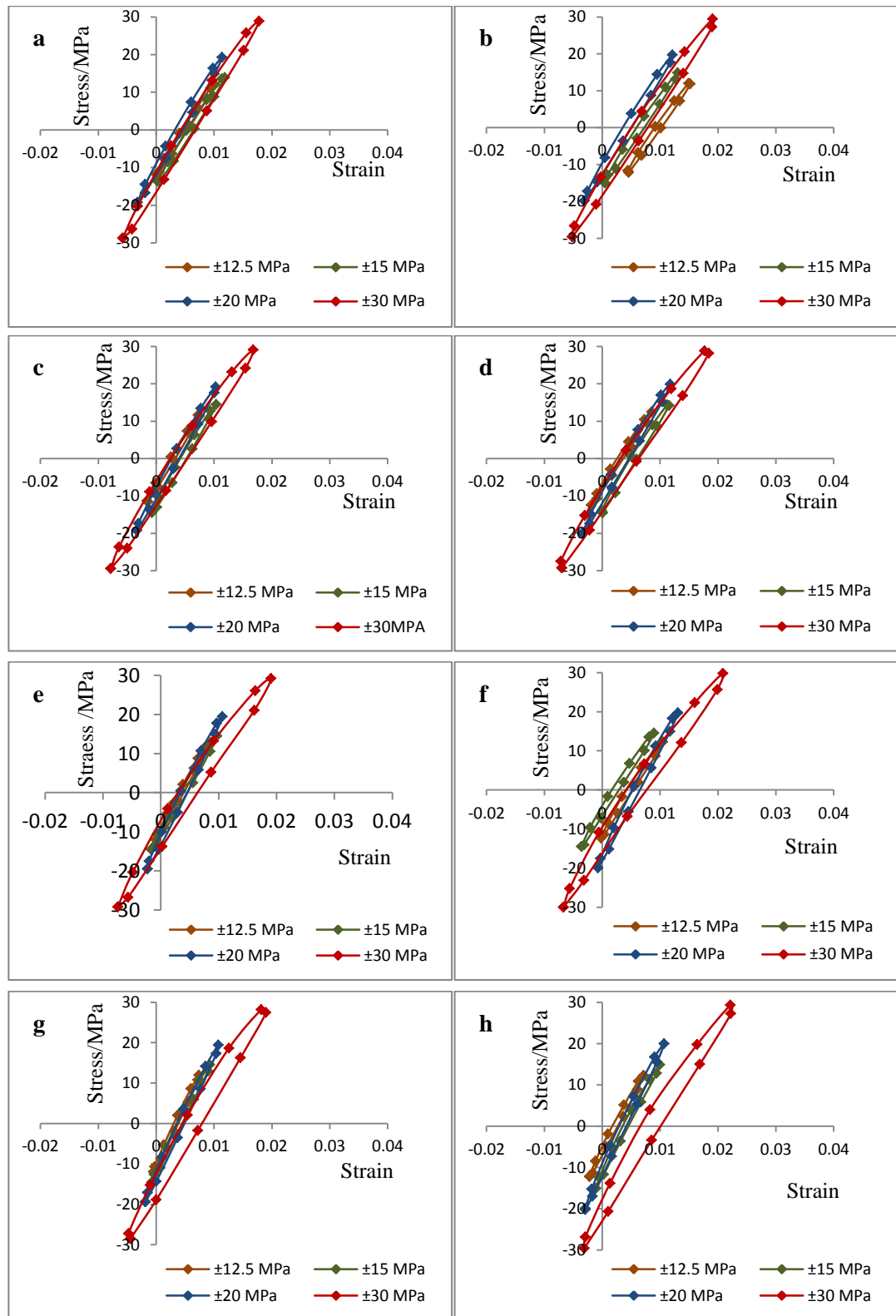


Figure A4.2 Comparison of stress-strain curves at early and late fatigue cycles in CMW1 for different specimen types: RDM (a and b), RMM (c and d), CDM (e and f) and CMM (g and h) where a, c, e and g show the loops at the 10th cycle and b, d, f and h show them at the 5th cycle before failure

A5.3 Stress-strain behaviour of the median specimens of the tension-tension fatigue (SmartSet GHV vs. CMW1)

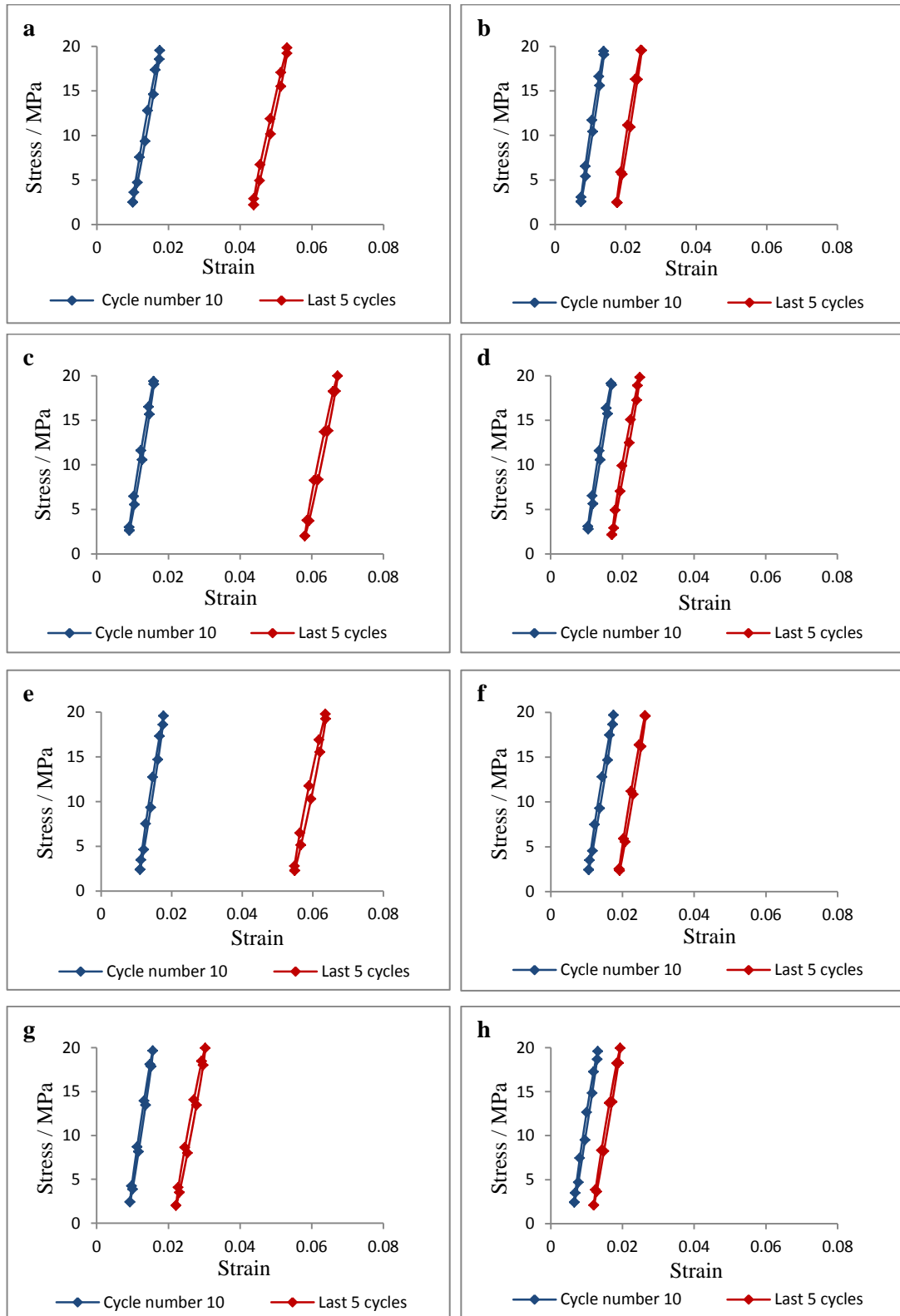


Figure A.3 Comparison of stress-strain curves at early (10^{th}) and late (5^{th} before failure) fatigue cycles for different specimen types: RDM (a and b), RMM (c and d), CDM (e and f) and CMM (g and h) where a, c, e and g are for SmartSet GHV and b, d, f and h for CMW1.

Appendix. 6 da/dN versus ΔK plots for individual specimens

A5. 1 SmartSet GHV

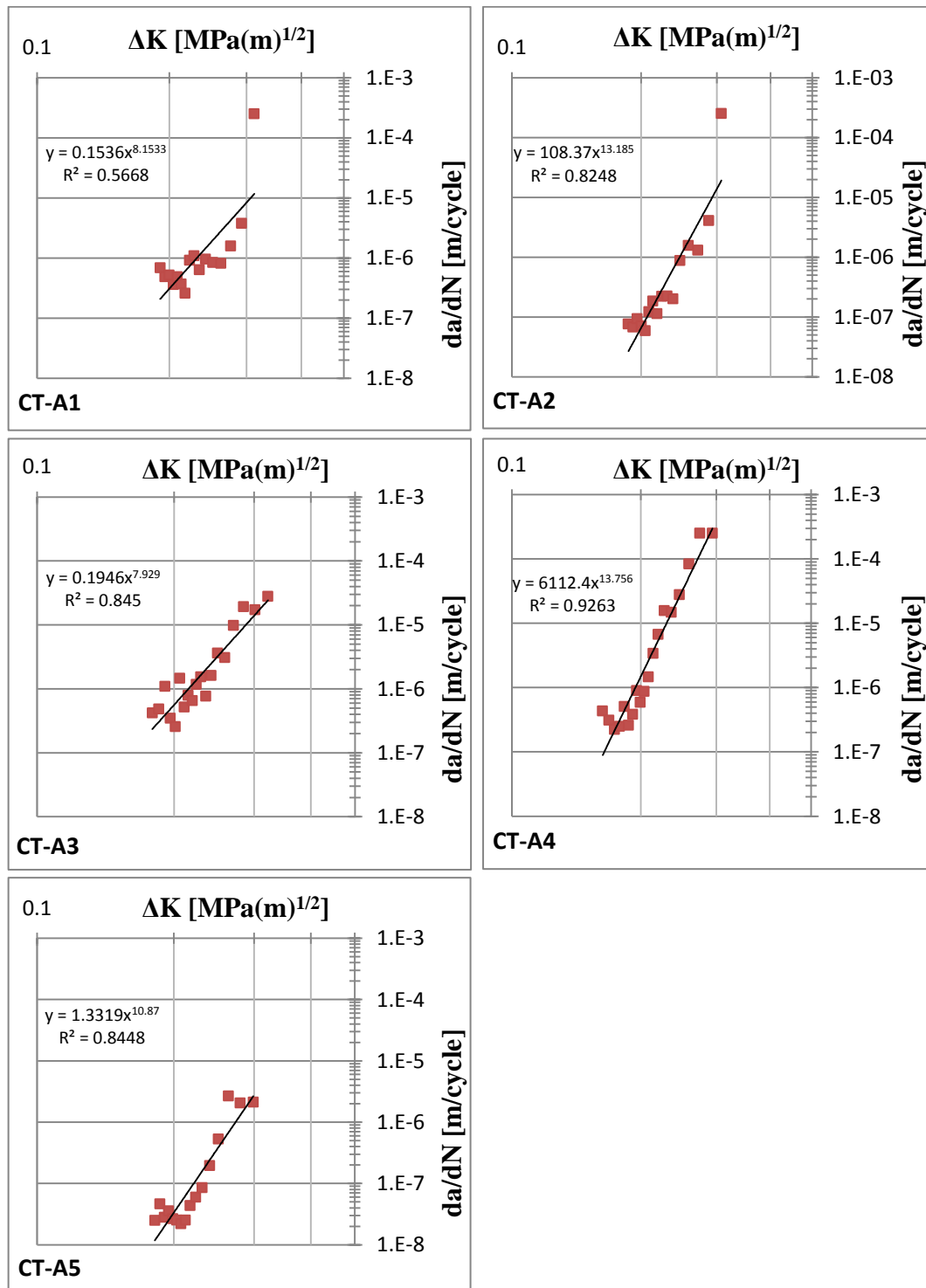


Figure A5.1 The individual regression fittings of the fatigue crack growth rate (da/dN) against the stress intensity range (ΔK) for SmartSet GHV specimens

A5.2 CMW1

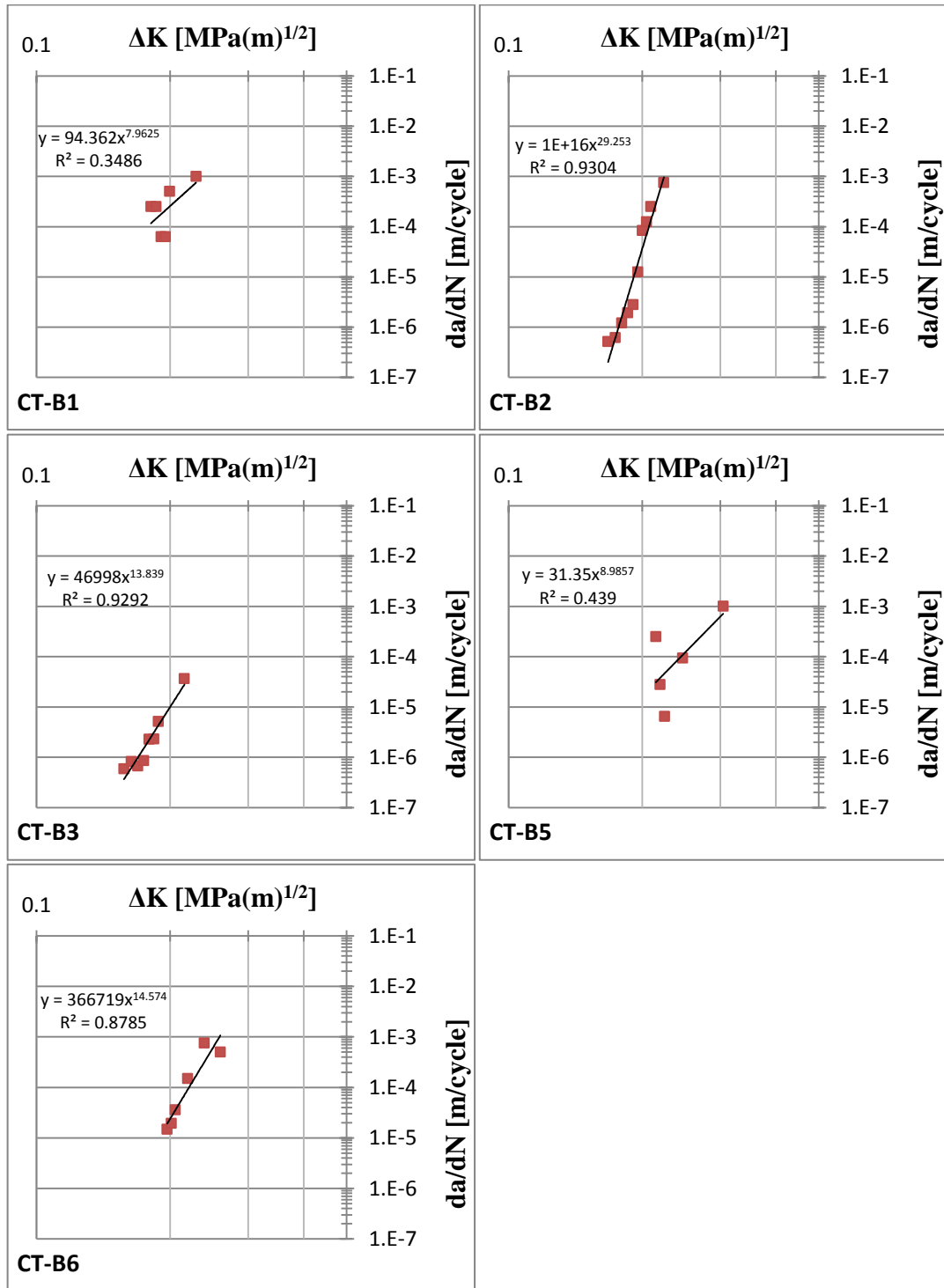


Figure A5.1 The individual regression fittings of the fatigue crack growth rate (da/dN) against the stress intensity range (ΔK) for CMW1 specimens

PUBLICATIONS

P.1 CONFERENCE ABSTRACTS

Effects of Specimen Configuration and Cross Sectional Area on the Fatigue Characteristics of Bone Cement

Emadeddin Sheafi, K. Elizabeth Tanner

UK Society for Biomaterials, Nottingham, UK, June 2012

Comparison of Fatigue Crack Growth in Two Bone Cements under Various Stress Regimes

Emadeddin Sheafi, K. Elizabeth Tanner

25th European Conference on Biomaterials, Madrid, Spain, September 2013

Fatigue Characterization of Two Bone Cements Tested Using Various Methods over a Range of *In Vitro* Stress Amplitudes

Emadeddin Sheafi, K. Elizabeth Tanner

26th European Conference on Biomaterials, Liverpool, UK, August-September 2014

P.2 JOURNAL PAPER

Effects of test sample shape and surface production method on the fatigue behaviour of bone cement

E.M. Sheafi, K.E Tanner

Journal of the Mechanical Behavior of Biomedical Materials, Volume 29, January 2014, Pages 91–102

Effects of Specimen Configuration and Cross Sectional Area on the Fatigue Characteristics of Bone Cement

Emadeddin Sheafi, K. Elizabeth Tanner

School of Engineering, University of Glasgow, Glasgow, G12 8QQ e.sheafi.1@research.gla.ac.uk

INTRODUCTION

A range of test methods have been used to measure the fatigue behaviour of bone cements. The tests have used machined or moulded surfaces and rectangular e.g. [1] or circular cross-sections e.g. [2] and tension only e.g. [1] or fully reversed tension-compression e.g. [2]. The results have been presented as S-N (or Wöhler) curves or after Weibull analysis.

However, only two previous studies have compared the same cements with different test regimes [3, 4]. They found variations in fatigue behaviour when testing four different cements using two different methods: tension only on ISO 527 directly moulded samples and tension-compression on ASTM F218 machined samples. The fatigue life showed a factor of 2 difference between the two most extreme cements using tension-compression on ASTM F218 machined samples while the difference in the fatigue lives was a factor of 15 for tension only on ISO 527 directly moulded samples. The current study investigates systematically the effect of specimen shape and preparation method on the *in vitro* fatigue life.

EXPERIMENTAL METHODS

Test specimens were prepared either directly cast or machined down from oversized cast samples. Sample shapes were either rectangular dumbbell samples according to ISO 527 standard or cylindrical dumbbell samples according to ASTM F2118. Both these samples have a nominal cross-sectional area of 20mm², however there are differences in the surface area of the gauge section. Samples were fatigue loaded to failure in fully reversed tension-compression stress level at ±20 MPa, at 37 °C in continuously flowing saline.

Data analysis used Weibull analysis, plotting Weibull numbers against the natural logarithm of cycles to failure. The Weibull (*W*) number was calculated using Eqn 1

$$W = \ln \ln \left[\frac{1}{1 - P(N_f)} \right] \quad (3.1)$$

where P_f is the probability of failure.

Furthermore energy absorbed per load cycle and the secant modulus were calculated at different stages of the loading time to track the initiation and progress of failure in the four types of samples.

RESULTS AND DISCUSSION

Weibull analysis (Figure 1) showed some differences in the cement behaviour, depending on the sample shape and

production method. The analysis also showed variations in absorbed energy (figure 2) and secant modulus (stiffness) as the samples progressed to failure.

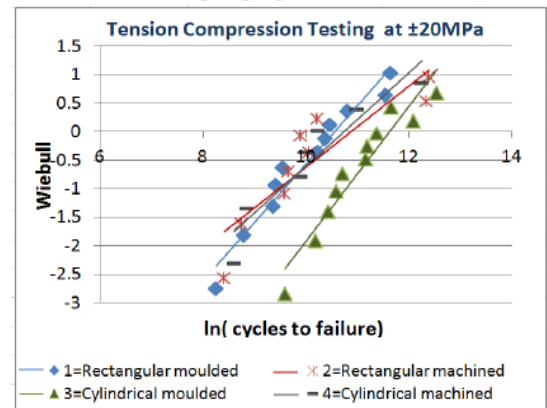


Figure 1 Weibull number versus ln(cycles to failure)

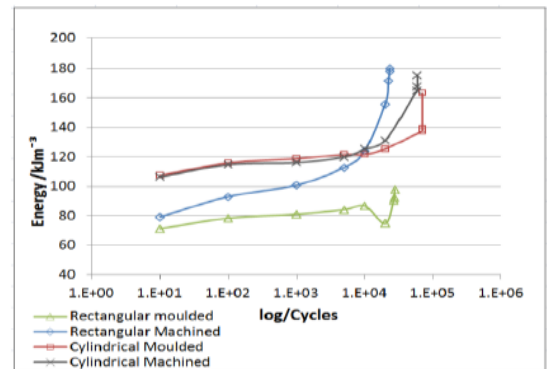


Figure 2 Variations in energy absorbed with load cycles

CONCLUSIONS

Sample shape and production method altered the measured fatigue life of the cements. Crack initiation and propagation were seen as increases in the energy absorbed and reduction in the secant modulus

REFERENCES

1. E.J. Harper & W. Bonfield, J Biomed Mater Res 53-A, 605-616, 2000.
2. G. Lewis *et al.*, J Biomed Mats Res, 73-B, 77-87, 2005.
3. G. Lewis & S. Janna, Biomaterials 24, 4315-4321, 2003.
4. K.E. Tanner *et al.*, Acta Biomaterialia, 6, 943-952, 2010.

ACKNOWLEDGMENTS

ES is supported by a Libyan Government scholarship. CWM is thanked for the supply of bone cement and mixing systems.

Comparison of Fatigue Crack Growth in Two Bone Cements under Various Stress Regimes

Emadeddin Sheafi, K. Elizabeth Tanner
School of Engineering, University of Glasgow, UK,
e.sheafi.1@research.gla.ac.uk

INTRODUCTION

Numerous testing methods have been applied to measure the fatigue life of bone cement leading to inconsistent reported results. Test specimens have been produced by moulding or machining to obtain rectangular (e.g. Harper & Bonfield¹) or circular (e.g. Lewis *et al.*²) cross sectional samples. Testing has been performed in tension-compression or tension-tension. Under the same other conditions, the effects of these variations in stress regimes on fatigue crack growth have not been compared. Previous studies have examined fatigue of bone cement comparing moulded against machined circular samples for one cement in tension-tension³, rectangular against circular moulded for three cements at one level of tension-compression⁴, or tension-tension of rectangular moulded versus tension-compression of circular machined of four cements⁵. The current study compares the growth of fatigue cracks in different sample types of two cements under two tension-compression stress levels.

EXPERIMENTAL METHODS

Two different bone cement compositions were used: SmartSet GHV Gentamicin and DePuy CMW1. Test specimens were manufactured with rectangular (ISO 527) or circular (ASTM F2118) cross sections. This was achieved after direct moulding of the dough or machining of oversized cast rods. Four sample types were obtained: rectangular moulded (RDM), rectangular machined (RMM), circular moulded (CDM) and circular machined (CMM). At least 5 samples from each category were tested to failure in fully reversed tension-compression at ± 15 or ± 20 MPa at 3Hz in saline at 37°C. As fracture growth can be tracked via the increase in energy absorption per load cycle, the energy absorbed of the median samples was calculated at different stages during testing to compare the failure progress in these samples.

RESULTS AND DISCUSSION

Fatigue crack growth can be affected by the stress regime depending on cement composition (Fig. 1). At the higher stress, rapid increases in energy were seen in SmartSet GHV particularly with machined samples. At the lower stress, this rise was substantially slower and less diverse. With CMW1, similar energy behaviour was observed for all sample shapes with a large range in the cycles to failure.

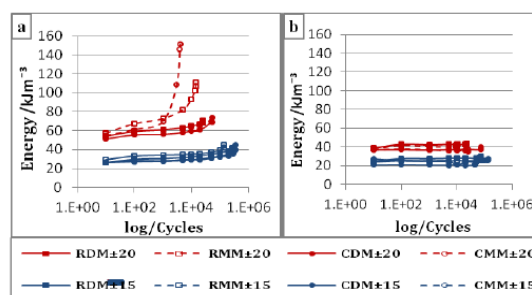


Figure 1 Variations in energy absorption over fatigue cycling at ± 15 & ± 20 MPa of (a) SmartSet and (b) CMW1

CONCLUSIONS

Depending on the energy absorption concept, crack growth can be clearly tracked for particular stress regimes and compositions. Testing methods are therefore important and identifying 'optimal' ones is essential.

REFERENCES

1. Harper EJ and Bonfield W, JBMR (2000),53-A:605-616.
2. Lewis G *et al.*, JBMR, 73-B, 77-87, 2005.
3. Paravic V *et al.*, ORS, 45th Mtg (1999),184.
4. Lewis G and Janna S, Biomaterials (2003),24:4315-4321
5. Tanner KE *et al.*, Acta Biomater (2010),6:943-952

ACKNOWLEDGMENTS

ES is supported by a Libyan Government scholarship. The authors thank DePuy CMW for the supply of bone cement and mixing systems.

Fatigue Characterization of Two Bone Cements Tested Using Various Methods over a Range of *In Vitro* Stress Amplitudes

E.M. Sheafi and K.E. Tanner

School of Engineering, University of Glasgow, Glasgow, UK, e.sheafi.1@research.gla.ac.uk

INTRODUCTION

Inconsistency in results of *in vitro* fatigue testing of bone cements has been reported. One possible reason for this variation is the use of a wide range of testing regimes, with limited consideration to the possible effects of the testing method and stress amplitude on the measured fatigue behaviour of various bone cement compositions. The effect of testing method (moulded or machined surfaces of rectangular or circular specimen shapes), but at only one stress level (± 20 MPa), has previously been examined¹ using two cements and significant variations in fatigue lives were found. An earlier study² considered only the effect of specimen cross sectional shape (produced by moulding), again at one stress level (± 15 MPa), showing longer fatigue lives for the circular specimens of the three cements tested. In terms of considering the effect of stress level, one study³ compared the fatigue behaviour of four bone cements. Fully reversed loading at five stress levels of circular machined specimens was compared to one level stress of tension-tension of rectangular moulded specimens. Significantly less range of differences was reported between the fatigue lives of the cements when the former method was used.

In the current study, the fatigue behaviour of two bone cements was compared over a range of *in vitro* fully reversed tension-compression stress levels. The process was comparably performed for different specimen types, followed by S-N analysis.

EXPERIMENTAL METHODS

Two different bone cement compositions were used: SmartSet GHV Gentamicin (including 2.9wt% ZrO₂ opacifier) and unmedicated DePuy CMW1 (including 6.2wt% BaSO₄ opacifier). Test specimens were manufactured by both direct moulding and machining as rectangular (ISO 527) or circular (ASTM F2118) cross sectional shapes. Four specimen types were produced: rectangular moulded (RDM), rectangular machined (RMM), circular moulded (CDM) and circular machined (CMM), providing four test specimen types. After a minimum of a week soaking in 37°C saline, at least 5 specimens from each category of both cements were tested to failure at each of four fully reversed tension-compression stress amplitudes: ± 12.5 , ± 15 , ± 20 and ± 30 MPa. Cycles to failure for each specimen was recorded and an S-N curve for each specimen testing method was established by plotting the maximum stress levels against the log of cycles to failure. S-N diagrams were produced which compare fatigue behaviour of the two cements in a specific specimen production and shape method.

RESULTS AND DISCUSSION

The S-N diagrams are shown in Figure 1. Each diagram compares the fatigue behaviour of the two cement

compositions for one type of specimen shape and surface finish. Generally, over the tested *in vitro* stress range, the results showed reverse fatigue performance of the two compositions such that SmartSet GHV, in comparison to DePuy CMW1, provided shorter fatigue lives at the highest stress levels and obviously longer lives as the stress amplitude decreased towards the *in vivo* levels. The results, meanwhile, showed differences in fatigue lives among the testing methods which also varied within the individual stress level.

This implies that the fatigue fracture of different cements can perhaps be dissimilarly and even contradictorily controlled by the adopted stress regime starting with the type of specimen used and ending with the stress amplitude allocated.

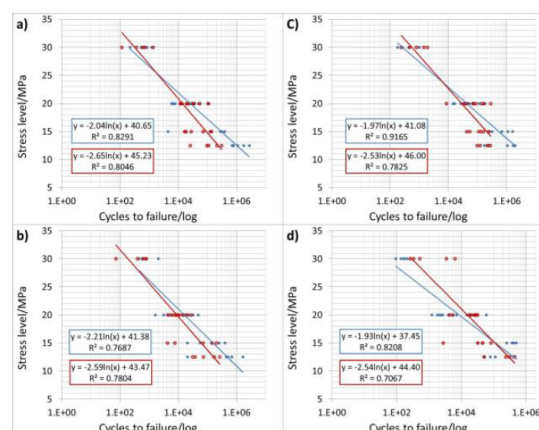


Figure 1 Comparison of S-N curves of SmartSet cement (blue) and DePuy CMW1 cement (red) using testing methods of a) RDM, b) RMM, c) CDM & d) CMM

CONCLUSIONS

Description of fatigue behaviour of bone cements can largely be driven by the selection of the specimen type along with the stress parameters. Thus, when measuring the fatigue life of bone cement, the effect of the stress regime is to be considered, unless an optimal criterion is agreed upon.

REFERENCES

1. E.M. Sheafi & K.E. Tanner, J Mech Behav Biomedical Materials, 29, 91-102, 2014.
2. G. Lewis & S. Janna, Biomaterials 24, 4315-4321, 2003.
3. K.E. Tanner *et al.*, Acta Biomaterialia, 6, 943-952, 2010.

ACKNOWLEDGMENTS

The authors thank DePuy CMW for the supply of the bone cements and mixing devices. The Libyan Government is thanked for providing ES with a scholarship.



Available online at www.sciencedirect.com

ScienceDirect

www.elsevier.com/locate/jmbbm

Research Paper

Effects of test sample shape and surface production method on the fatigue behaviour of PMMA bone cement



E.M. Sheafi*, K.E. Tanner

School of Engineering, James Watt South Building, University of Glasgow, Glasgow G12 8QQ, United Kingdom

ARTICLE INFO

Article history:

Received 29 April 2013

Received in revised form

14 August 2013

Accepted 19 August 2013

Available online 2 September 2013

Keywords:

Polymethylmethacrylate

Bone cement

Fatigue

Sample shape

Sample surface preparation method

Weibull analysis

Absorbed energy

ABSTRACT

There is no consensus over the optimal criterion to define the fatigue life of bone cement *in vitro*. Fatigue testing samples have been made into various shapes using different surface preparation techniques with little attention being paid to the importance of these variations on the fatigue results. The present study focuses on the effect of test sample shape and surface production method on the fatigue results. The samples were manufactured with two cross sectional shapes: rectangular according to ISO 527 and circular according to ASTM F2118. Each shape was produced using two methods: direct moulding of the cement dough and machining from oversized rods. Testing was performed using two different bone cements: SmartSet GHV and DePuy CMW1. At least 10 samples of each category were tested, under fully reversed tension-compression fatigue stress at ± 20 MPa, to allow for Weibull analysis to compare results. The growth of fatigue cracks was observed by means of the changes in the absorbed energy and apparent modulus. It was found that fatigue crack growth can be altered by the sample shape and production method; however it is also dependent on the chemical composition of the cement. The results revealed that moulded samples, particularly those based on the ASTM F2118 standard, can lead to up to 5.5 times greater fatigue lives compared to the machined samples of the same cement. It is thus essential, when comparing the fatigue results of bone cement, to consider the effect of production method along with the shape of the test sample.

© 2013 Elsevier Ltd. All rights reserved.

1. Introduction

Polymethylmethacrylate (PMMA) based bone cement has been used in cemented joint arthroplasty since the 1960s. The role of this polymeric substance is to fill the gap between the bone and the implant connecting them together and working as a grout transferring the loads generated from gravity and muscle actions. Fatigue failure of the cement

mantle has been considered a major issue that leads to many undesirable consequences. Fundamentally, the key mechanical functions of bone cement reduce after cement failure. Biologically, the fracture of the mantle leads to the detrimental production and spread of PMMA and opacifier particles. The presence of these cement particles increases bone resorption (Quinn *et al.*, 1992; Sabokbar *et al.*, 1996) and leads to various biological responses depending on particle shape

*Corresponding author. Tel.: +44 141 330 2416; fax: +44 141 330 4343.

E-mail address: e.sheafi.1@research.gla.ac.uk (E.M. Sheafi).

and size (Gelb et al., 1994; Mitchell et al., 2003) as well as the type of opacifying agent included (Mitchell et al., 2003; Lezarus et al., 1994; Wang et al., 2005). More importantly, concerns have been raised regarding the likely contribution of this failure in accelerating aseptic loosening, the cause of approximately 75% of all revisions of both cemented and uncemented total hip replacements (Malchau et al., 2000).

These facts have made it vitally important to investigate variables that control the fatigue behaviour of bone cement. *In vitro*, much research has been performed on this aspect using various testing methods. The factors such as chemical formulation, storage temperature, viscosity, mixing method and resultant porosity have been examined extensively with variations in results. The inconsistency in the reported results has generated the question as what controls these variations in fatigue behaviour. Lewis and Nyman (2000) examined the literature pointing out that 'a plethora of test conditions have been used' adding that 'many literature parametric studies employed inappropriate statistical methods' and 'these studies have not addressed the issue of possible interactions between the parameters being investigated'.

It is widely reported that fatigue life of elements can variously be affected by many design variables including, but not limited to, manufacturing method, cross section and geometry and cyclic deformation mode. Fatigue testing specimens are usually designed and tested in such a way that 'the required test conditions are simulated as closely as possible' (Swanson, 1974). The manufacturing methods can be classified, as in Bhandari (2007), into three categories: casting processes (e.g. mould casting), deformation processes (e.g. extrusion) and material removal or machining processes (e.g. milling). Although casting can be 'one of the easiest methods to convert the raw material into finished component' (Bhandari, 2007), the most common method in preparing fatigue specimens is to machine them from non-waisted oversized rods, presuming that the specimen is not overheated or excessively stressed by the machining process (Swanson, 1974). The material removing approach is particularly applicable for specimens with circular sections that are cyclically loaded under various deformation modes including rotating bending (Suresh, 1998). One main aspect that has been reported to relate to the significance of the selection of a particular manufacturing process is the resultant surface roughness and integrity. The greater the deviation from a polished surface the lesser the material strength since the rougher surfaces provide more local stress concentration sites that enhance the initiation of microcracks which propagate leading to fatigue failures (Mott, 2004). Various standards have been published to help in providing guidelines for preparing specimens and testing the properties of materials such as those published in the ISO and ASTM standards. The ISO standards, for example, include specific standards that describe the procedures to be followed when preparing testing specimens by injection and moulding (e.g. ISO 293) or machining from compression- or injection-moulded rods (e.g. ISO 2818). Despite the consideration that fatigue failures depend essentially on surface conditions where a high fraction of fatigue cracks progress from the surface, it seems there is no specific manufacturing process to provide the 'best' surface quality of a component or specimen for all

materials as this can largely be controlled by the properties of the shaped material as well as the manufacturing conditions.

In terms of sample profile, fatigue specimens can be either unnotched (smooth) or notched to produce a stress concentration site in the failure section where the latter is characterised by the elastic stress concentration factor (Dowling, 2007). Specimens are designed with a particular shape of the gauge section providing circular or rectangular cross sectional areas. Review of the literature shows that a typical fatigue life testing specimen generally is divided into three to five regions: the gauge section in the centre of the specimen that has a significantly reduced cross sectional area compared to the other parts of the specimen, two grip ends to be used for fixing the specimen in the testing machine, and two transitional sections between the gauge and the grips through which the cross area is gradually reduced from the grips to the gauge section. The specimens, particularly the circular, can be either solid or hollow as appropriate to represent the real-life conditions. Although the cross sectional shapes are mainly limited to rectangular or circular, the geometries of the gauge and non-gauge sections vary largely depending upon the properties of the material being tested. Generally, two main criteria should be considered when designing fatigue specimens: (1) ensuring the occurrence of the failure in the gauge section and (2) avoiding the presence of stress raisers unless deliberately required (Swanson, 1974). The stress concentrations mentioned in the latter criterion such as notches are included in specimens for special testing requirements as the Compact Tension specimens used in measuring the fatigue crack growth rate within a material.

In addition to specimen production method and profile, the effect of cyclic deformation mode and type should also be considered. A component or specimen might encounter a single direction stress (uniaxial) or interference of two (biaxial) or more (multiaxial) stresses. Fatigue stresses are classified depending upon the position and direction of the applied cyclic load. To assess the fatigue properties of a material, fatigue samples are cyclically loaded by applying axial tension and/or compression, bending or torsion loads as required. Combinations of different stresses such as axial tension and torsion can exist simultaneously. These combined stresses lead to more complex situations as the stresses might differ in phase or frequency or both depending on the sources of cyclic loading (Dowling, 2007). An early study by Gough and Pollard (1935), for instance, proposed an elliptical quadrant criterion to consider the combined effect of, and the relation between, the bending stress and the torsion stress in metals considering their fatigue limits in single load cases. With either mode, one of the following stress types is usually performed in fatigue testing: fully reversed tension-compression, zero-tension or tension-tension stress. The selection of the appropriate stress type is made depending on the conditions that a material would encounter in 'real life'.

Considering the application of the previous procedures for bone cement, it is significant to identify which sample preparation techniques and stress regimes have specifically been used and reported. A review by Lewis (2003) states that 'two categories of specimen fabrication methods have been used, these being moulding into a rod or plate and then machining to final

dimensions and direct moulding, in a polymeric or metallic mould, without or with external pressurisation, into final dimensions'. Although specimen cross sections are generally made to provide rectangular or circular shapes, the geometry of test specimens has varied (Lewis and Nyman, 2000). More concern and debate, however, has been reported regarding the effect of the cross sectional shape rather than the geometry of a specimen. Cristofolini et al. (2002), for instance, used a 4 mm thickness flat dumbbell shape according to ISO 527 'in order to approximate the *in vivo* cement mantle thickness closely'. Similarly, a different geometry of a 5 mm thickness flat shaped specimen was earlier suggested by Krause et al. (1988) to represent the cement mantle *in vivo*, but to be used in testing with 'an appropriate testing protocol' they introduced. In contrast, many studies have preferred testing a circular shape according to specific standards such as ASTM F2118. Lewis and Janna (2003), nonetheless, argue that using either shape should be acceptable as the aim is to characterise the material *in vitro*. Limited discussion, however, has considered the influence of surface preparation on fatigue behaviour of bone cement specimens. Although it has been suggested that mouldable samples would be preferable to machined (Krause et al., 1988; Paravic et al., 1999; Lewis and Nyman, 2000), both sample production methods are being used.

As for the effect of deformation mode on fatigue behaviour of bone cement, there are no particular studies to specifically investigate this factor. Most studies, however, applied only one mode preferring to use uniaxial tension or compression cyclic deformation modes. Tension-tension or tension-compression stress types, in particular, have been reported in the cement mantle *in vivo* (Lewis and Nyman, 2000). Tension-compression loading above all can be particularly preferred because this loading, according to Dowling (2007), provides a good indicator of fatigue performance of materials. Due to these considerations, only very few studies have applied other stress deformation modes such as bending rotating or three point bending of bone cement specimens.

As yet, there is no comprehensive study to compare the effect of variations in both shape and surface finish in the presence of any deformation mode and type. Three previous studies have variously compared different cements under the same conditions involving no more than two testing regimes. Paravic et al. (1999) compared the fatigue behaviour of moulded versus machined circular cross sectional samples that were made from a single cement and were subjected to various tension only peak stress levels. They found apparent longer fatigue lives when the samples were moulded. Another study by Lewis and Janna (2003) compared the fatigue behaviour of rectangular and circular cross sectional shapes using only the moulded sample production method for three bone cements. A factor of difference between 2 and 36 times was found from this work. A more recent study by Tanner et al. (2010) tested four bone cements comparing two methods of fatigue testing where the first method tested rectangular moulded samples under single stress level tension only, followed by Weibull analysis, and the second method performed Wöhler analysis of circular machined samples of the same cements under various stress levels. They found that the difference in fatigue lives between the cements was up to a factor of 15 when the moulded

rectangular with Weibull analysis was used and only a factor of 2 when the machined circular and Wöhler analysis method was used.

The aim of the current study is to test and compare fatigue behaviour of two different bone cements using two dumbbell sample shapes: half sized rectangular cross sectional according to ISO 527 (hereinafter called rectangular) or circular cross sectional according to ASTM F2118 (hereinafter called circular). Each of these shapes was produced by either direct moulding or machining from oversized cast bars. Single stress level fully reversed tension-compression was used and fatigue results of various sample types were compared by means of Weibull statistical analysis. In addition, initiation and propagation of cracks were investigated through comparing the absorbed energy per loading cycle for each sample type by means of hysteresis loops.

2. Materials and methods

2.1. Materials

Two different high viscosity bone cements were used. Smart-Set GHV (containing gentamicin) and DePuy CMW1 (no gentamicin) were produced and supplied by DePuy CMW as powder (40 g) and liquid (18.88 g) portions. Each cement has a different opacifying filler in its powder to make the cement visible on X-rays. The GHV powder contains 14.37 wt% zirconium dioxide as an opacifier (9.76 wt% in the mixture) whereas the CMW powder contains 9.1 wt% barium sulphate instead (6.18 wt% in the mixture). Table 1 compares the chemical compositions of the two bone cements (DePuy (2012)).

2.2. Samples preparation

The powder and liquid components were vacuum-mixed at room temperature using the CEMVAC mixing system (DePuy CMW, Blackpool, UK) following the manufacturer's instructions focusing in particular on mixing time, waiting time and working time for each cement. Four PTFE moulds were used to produce four types of samples as follows:

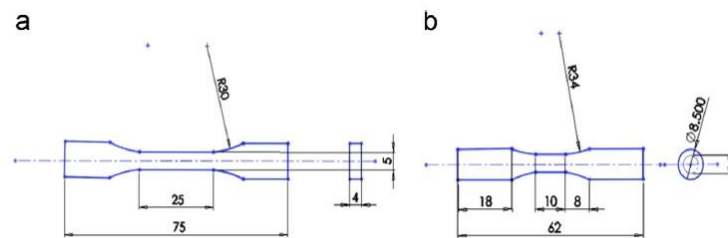
1. Rectangular directly moulded dumbbell samples (RDM)
2. Rectangular moulded and then machined dumbbell samples (RMM)
3. Circular directly moulded dumbbell samples (CDM)
4. Circular moulded and then machined dumbbell samples (CMM)

The moulded and machined rectangular samples were made according to ISO 527 - type 1BA (BSI Standards, 2012) as shown in Fig. 1a whereas the moulded and machined circular samples were made according to ASTM F2118 (ASTM Standards, 2003) as shown in Fig. 1b. Both sample shapes have a nominal gauge cross sectional area of approximately 20 mm². The difference in the two sample shapes is important because of the resultant differences in gauge surface areas, gauge volumes and surface area to volume ratios (Table 2).

Table 1 – The powder and liquid chemical contents of SmartSet GHV and DePuy CMW1 (from J&J website)*

Composition of bone cement powder:	SmartSet GHV		DePuy CMW1	
	%w/w	g	%w/w	g
Polymethylmethacrylate	0	0	88.85	35.54
Methylmethacrylate/methacrylate copolymer	80.45	32.18	0	0
Benzoyl peroxide	0.96	0.384	2.05	0.82
Gentamicin sulfate	4.22	1.688	0	0
Barium sulphate	0	0	9.1	3.64
Zirconium dioxide	14.37	5.748	0	0
Composition of bone cement liquid:				
Methylmethacrylate	97.5	18.408	98.5	18.5968
N,N-Dimethyl-p-toluidine	≤ 2.5	≤ 0.47	≤ 1.5	≤ 0.282
Hydroquinone	75 ppm	75 ppm	75 ppm	76 ppm

* The contents represent a 40 g unit (40 g powder and 18.88 g liquid).

**Fig. 1 – Test specimen shapes (a) rectangular according to ISO 527 and (b) circular according to ASTM F2118 (units in mm).****Table 2 – Sample shapes and variations in cross and surface areas and surface area to volume ratios.**

	Gauge cross sectional area (mm ²)	Surface area of gauge section (mm ²)	Volume of gauge section (mm ³)	Surface area to volume ratio
Rectangular	20	450	500	0.9
Circular	19.64	157.14	196.43	0.8

To produce these samples, the doughy cement mixture was injected during the working time into a mould which was immediately, before reaching the hardening time, pressurised to 50 bar for 20–30 min. This was to ensure the formation of the required sample shapes with limited porosity and to eject the excess cement. The samples were then removed from the mould and incubated at 37 °C for 24 h to guarantee initial completion of the polymerisation process. The oversized rectangular and circular samples were machined to the final shape and, along with the moulded samples, were initially assessed visually under strong light for porosity. Specimens that had pores greater than 1 mm in diameter were defined as ‘macro-pores’ and less than 1 mm as ‘micro-pores’ (Cristofolini et al., 2002; Bialoblocka-Juszczak et al., 2008). Accordingly, samples with large pores (>1 mm) were rejected. This assessment hypothesis has been criticised because it ‘will result in comparisons of limited clinical relevance’ (Prendergast et al., 2002). However, it is argued that the cross sectional areas of the samples are too small and directly exposed to the experimental fatigue stress; whereas *in vivo* the stress is distributed over the larger area of the

cement mantle. The basic aim is to fatigue test the cement material not the specimens themselves since the large voids will occupy significant ratios of the gauge volumes, resulting in earlier failure in a test sample compared to the *in vivo* mantle. As for the opinion that this porosity rejection consideration is not relevant to the real applications *in vivo*, the effect of porosity on fatigue strength has already been reported to not match when it comes to comparing the *in vivo* and *in vitro* findings (Janssen et al., 2005; Ling and Lee, 1998). After porosity assessment, all samples were soaked in 0.01 M phosphate buffered saline (PBS) at 37 °C for a period of 1–6 weeks prior to testing. It is recommended that specimens should continually be maintained in the PBS solution between 7 and 60 days (ASTM F 2118-03, 2003).

2.3. Mechanical testing

The samples were subjected to fully reversed tension-compression fatigue testing at a stress of ±20 MPa at 3 Hz. An MTS – 858 Mini Bionix[®]II was used to perform testing and record all the required data according to a specified procedure. During testing,



Fig. 2 – Close up of a specimen fully covered by sprayed saline during testing.

the samples were covered by continuously flowing PBS solution at 37 °C (Fig. 2). The testing data was recorded logarithmically throughout the testing period by the MTS program, that is the first 10 cycles from each hundred until 1000 cycles were recorded, followed by the first 10 cycles from each thousand until 10,000 cycles were recorded and so on. The collected data included recording 10 force and displacement data points for each tensile-compressive loading cycle. At least 10 samples were tested and accepted for each sample type of each cement to have sufficient samples to perform the two parameter Weibull analysis. Lewis and Sadhasivini (2004) estimated the minimum adequate number of bone cement samples in fatigue testing to be either 7 or 11 samples for the two and three parameter Weibull distributions respectively. Samples that were tested and subsequently found to have macro pores (>1 mm) in their fracture surfaces, which could not be detected in the initial porosity assessment before testing, were excluded from the analysis.

2.4. Weibull analysis

Fatigue testing data was investigated using Weibull analysis to compare the fatigue behavior of the four sample types. The number of cycles to failure of the samples in each set were ranked in ascending order to plot the logarithm of life data ($X = \ln N_f$) against Weibull reduced variate (Y) that is determined using Eq. (1) which requires calculating the cumulative probability of failure $P(N_f)$ using Bernard's approximation (Eq. (2)) where i is the sample rank in a particular population and n is the total number of samples in the population ($i=1, 2, 3, \dots, n$). Fatigue results for all sample types were subsequently presented according to their cement formulation on two comparable graphs to obtain four two-parameter Weibull

relationships (regression lines) for each cement.

$$Y = \ln \ln \left[\frac{1}{1-P(N_f)} \right] \quad (1)$$

where,

$$P(N_f) = \frac{i-0.3}{n+0.4} \quad (2)$$

The two-parameter Weibull distribution relationship is given in Eq. 3 (Hertzberg, 1996; Askeland et al., 2011). The exponential form of this function is given in Eq. 4 (Weibull, 1951, 1961; Shigley and Mischke, 1989; Danzer et al., 2007; ASTM C 1239-07, 2008; Soh Fotsing et al., 2010).

$$\ln \ln \left[\frac{1}{1-P(N_f)} \right] = b \ln(N_f) - b \ln(N_a) \quad (3)$$

$$P(N_f) = 1 - \exp \left[- \left(\frac{N_f}{N_a} \right)^b \right] \quad (4)$$

where, $P(N_f)$ is the probability of failure after N_f stress cycles, N_a is the characteristic fatigue life (also known as the scale parameter) and b is the Weibull modulus (also known as the shape parameter). The importance of Eq. (3) is that the left hand side of the equation represents the Weibull variate where the higher this number, the greater the fatigue performance. The right hand side of the equation is dependent on the variables b and N_a . The Weibull modulus is a measure of skewness of data away from a certain optimal range (normally $3 < b < 4$) during which "approximate symmetry is obtained along with a good approximation to the normal distribution" (Shigley and Mischke, 1989) and that "large b 's skew the distribution to the left and small b 's skew the distribution to the right" (Shigley and Mischke, 1989). If all b values are below this range, the dispersion of the N_f data is relatively measured so that the higher the b value the lesser the dispersion. The scale parameter N_a is obtained as the value below which 63.2% of the N_f results lie. Once b and N_a were obtained, the fatigue performance index I was calculated for each data set according to Eq. (5), introduced originally by Britton et al. (1990) when they investigated the shear bond strengths of dental ceramics. This approach has been reported to measure the fatigue performance of bone cement in several studies such as Dunne et al. (2003), Lewis (1999a, 1999b) and Janna et al. (2005). It is worth mentioning that the Weibull mean has similarly been used as an indicator, along with or, instead of I in other studies including Lewis and Janna (2003), Lewis (1999a) and Lewis et al. (2003). The results in this study were compared according to the I indicator and, meanwhile, to see if there is any significance of variations in the fatigue results, the cycles to failure data of relevant testing sets were compared using other statistical approaches, as appropriate, including Student's t-test and the analysis of variance (ANOVA).

$$I = N_a \sqrt{b} \quad (5)$$

2.5. Analysis of the hysteresis behaviour

To provide deeper analysis to the fatigue results, hysteresis loops were used to compare the absorbed energy and apparent modulus per loading cycle for all sample types. Weibull

analysis considers only the fatigue life (i.e. the last recorded load cycling data point before failure), but provides no clear indications of how cracks initiate and propagate. The idea of using the absorbed energy concept is built on what has widely been reported regarding the relation between the fatigue crack growth and the hysteresis energy. This energy based criterion is generally divided into two categories depending on which hypothesis is being considered: the amount of absorbed energy is constant and independent of the number of cycles to failure or the amount of absorbed energy changes as the cycles to failure progress (Ellyin, 1997). To simplify the process, it is supposed that 'a fatigue crack growth can be thought of as resulting from energy dissipation (or energy absorption) in the plastic zone' (McCartney, 1996). The change in energy absorption, however, is theoretically attributed to the creation of new free surfaces within the crack zone (Milella, 1999), reflecting the process of crack initiation and propagation. The general relation between the change in absorbed energy and apparent modulus is that the increase in energy follows the same trend as the decrease in moduli (Hoppel and Pangborn, 1994).

To compare the fatigue damage in samples according to these assumptions, the data of a 'typical sample' from each testing group, that is the one closest to the median cycles to failure, was selected to compare a total of 8 median samples. The force and displacement data of these samples was collected as explained above and was converted into stress-strain after selecting data points of certain loading cycles throughout testing so that the 10 data points of the 10th, 100th, 1000th, 5000th, 10000th, 20000th, 50,000th cycles were included in the analysis. To ensure observing the crack growth behaviour adequately before failure, cycles of the reversing counter positions 5, 100 and 1000 were also considered. Each point of the 10 data points of each of these cycles includes calculating the instantaneous stress and strain. It should be clarified that two different correction factors were applied into the strain results depending on the sample shape. This is due to the reality that the two sample

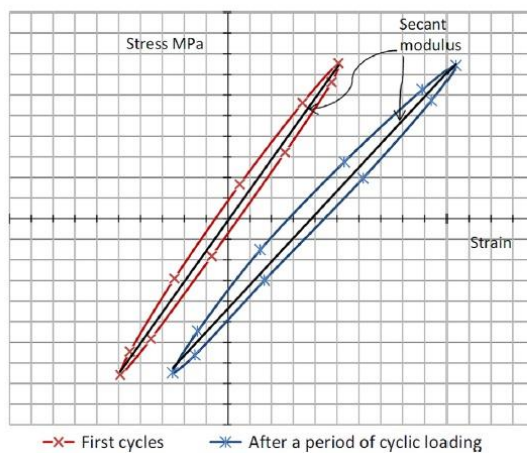


Fig. 3 – A schematic of the possible change in absorbed energy and modulus throughout testing (from actual test results).

shoulders between the grips and the gauge section are included in testing and the effect of these shoulders on the results must be excluded. These factors were determined using integral calculations and found to be 0.667 and 0.412 for the rectangular and circular samples respectively. Multiplying the initial strain results by these factors will provide the approximate strain occurred in the gauge sections. Once this correction has been considered, the absorbed energy during each of the selected cycles, represented by the area inside the hysteresis loops (Fig. 3), was estimated using the Trapezoidal Integration Rule by means of Microsoft Excel spreadsheets. Additionally, the secant modulus at the same cycle was calculated, which is equal to the slope of the straight line that connects the highest and lowest points in the loop. In order to obtain plots of cycles to failure against absorbed energy per loading cycle and secant moduli, the calculation of the energy and modulus were performed starting from the 10th fatigue loading cycle (loop 1 in Fig. 3) followed by all the other examined cycles and ending with the 5th cycle before failure (loop 2 in Fig. 3).

2.6. Comparison of fracture surfaces

Initial investigation of fracture surfaces were performed using an optical microscope. Scanning electron micrographs of the fracture surfaces of the eight median cycles to failure samples were also compared. The aim was to verify if there are any distinct features associated with particular sample types in terms of fatigue fracture behaviour.

3. Results

3.1. Weibull analysis

The fatigue testing results for different sample types comparing these for SmartSet GHV and DePuy CMW1 are presented in Fig. 4 plotting the natural logarithm of cycles to failure against Weibull number. The exclusion of invalid samples according to the macro porosity assessment led to an overall average of 23% of samples to be discarded, approximately two thirds of which occurred after testing. Table 3 summarises the calculated values of the two Weibull parameters; namely the shape parameter or Weibull modulus (b) and the characteristic fatigue life parameter (N_a). The table also shows the calculated values of the fatigue performance index (I) for each testing set which depends on the two parameters values. Due to the fact that this work considers the effect of three parameters simultaneously; namely, sample shape, surface roughness and cement composition, the results presented in Fig. 4 and Table 3 make it possible to assess the effect of a particular parameter and compare it to another, depending on the Weibull functions and the fatigue performance indices. For example, the effect of the shape parameter can be compared for samples that were made from SmartSet GHV for a specific surface production method. In this case, for the moulding conditions, the I index is double for the circular ($I=75,909$ cycles) compared to the rectangular ($I=37,088$ cycles). Considering the machining conditions only, however,

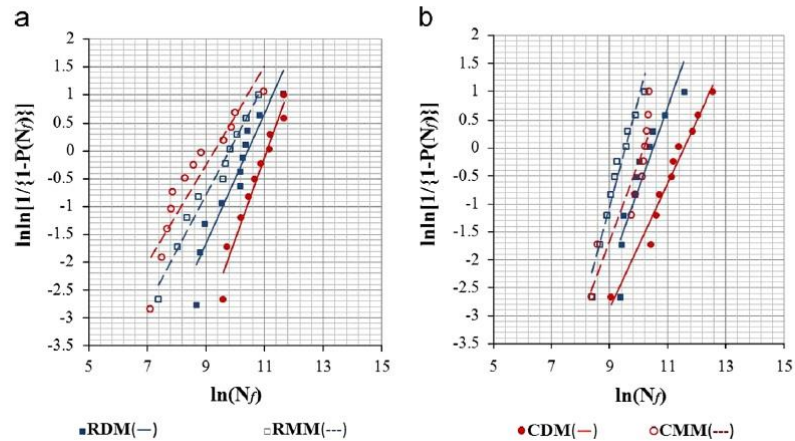


Fig. 4 – Plots of the two-parameter Weibull relationships showing variations in fatigue behaviour of four different sample types of (a) SmartSet GHV and (b) DePuy CMW1 bone cements.

Table 3 – Summary of the determined values of the shape and characteristics Weibull parameters and resultant fatigue performance index

Sample type	SmartSet GHV			DePuy CMW1		
	<i>b</i>	<i>N_a</i>	<i>I</i>	<i>b</i>	<i>N_a</i>	<i>I</i>
RDM	1.176	34,200	37,088	1.447	35,242	42,393
RMM	1.004	15,678	15,709	1.963	14,045	19,678
CDM	1.316	66,171	75,909	1.116	106,938	112,970
CMM	0.817	14,765	13,346	1.403	26,370	31,235

* *N_a* and *I* in cycles.

the fatigue indices are almost equal for the circular and rectangular shapes ($I=14,765$ and $15,678$ cycles respectively).

In general and regardless of bone cement type, moulded specimens showed significantly longer fatigue lives compared to the machined specimens ($p=0.00002$). The results showed 2.5–5.5 times greater fatigue performance indices for the moulded specimens ($I=37,088$, $42,393$, $75,909$ & $112,970$ cycles) compared to the machined specimens ($I=15,709$, $19,678$, $13,346$ & $31,235$ cycles). The greatest performance is associated, in particular, with the circular moulded specimens ($I=75,909$ & $112,970$ cycles). Compared to their rectangular counterparts ($I=37,088$ & $42,393$ cycles), these circular samples achieved 2–2.7 times longer fatigue lives.

Variations in the performance of various samples were also found to depend on the bone cement formation. On the one hand, for the rectangular shape, either moulded or machined, there were no significant differences between the fatigue lives of the SmartSet GHV and DePuy CMW1 samples ($I=42,393$ & $19,678$ cycles and $I=37,088$ & $15,709$ cycles respectively with p -value of 0.125). There was no evident effect of production method on the fatigue of this rectangular sample shape. On the other hand, however, significant differences in results were determined between the four sets of the circular shape ($p=0.001$). The circular moulded DePuy CMW1 samples showed 1.5 times greater fatigue index ($I=112,970$ cycles) and the circular machined 2.3 greater fatigue index ($I=31,235$ cycles)

compared to the comparable SmartSet GHV samples ($I=75,909$ & $13,346$ cycles respectively). These results also indicate that, contradictory to the rectangular samples, the effect of production method of circular samples on the fatigue can vary depending on formulation. From Fig. 4 and comparing the samples of both cements with regard to production method only, it can also be seen that samples that were produced by direct moulding showed similar fatigue behaviour trends; whereas the samples produced by machining showed the reverse trend where the rectangular machined samples performed better with the SmartSet GHV gentamicin and vice versa with the DePuy CMW1.

In terms of dispersion in fatigue results, all the Weibull moduli (b values) obtained in this work were clearly below the symmetry range. The Weibull distributions skewed to the right for 6 of the 8 testing sets with $b > 1$. One testing set (RMM SmartSet GHV) provided exponential distribution ($b=1$) and only one set (CMM SmartSet GHV) provided increasing failure probability ($b < 1$).

3.2. Hysteresis energy and stiffness

The calculated results from the stress-strain data are presented in Fig. 5. Generally, similar absorbed energy and stiffness behaviour were seen among the four sample types made from DePuy CMW1 (Fig. 5b and d) regardless of the

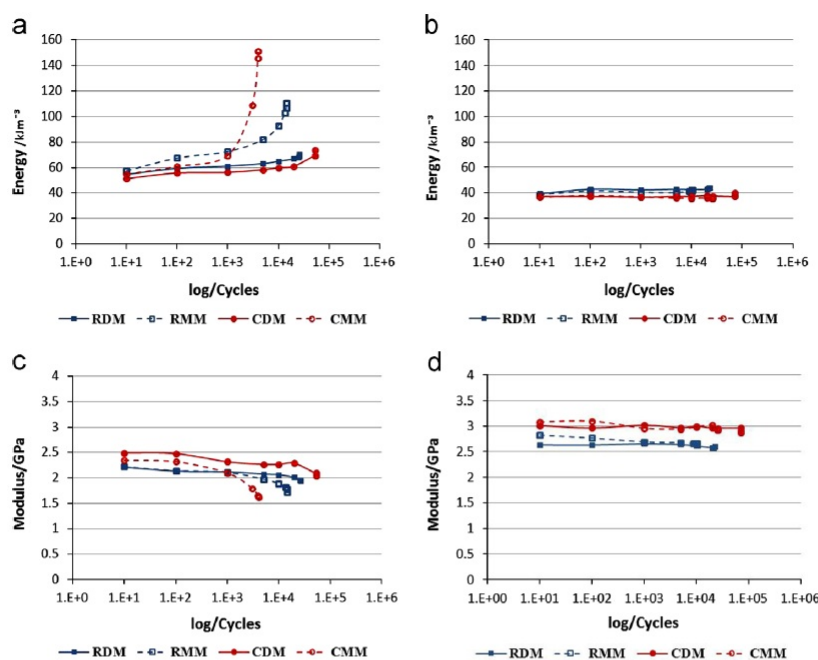


Fig. 5 – Comparison of (a and c) absorbed energy and (b and d) secant modulus variations throughout testing for (a and c) SmartSet GHV and (b and d) DePuy CMW1.

differences in fatigue lives. For the four sample types made of SmartSet GHV, obvious variations in the hysteresis energies and moduli can be seen (Fig. 5a and c), indicating variations in crack propagation among these samples with the highest crack growth speed associated with the machined samples and lower speed for the moulded samples. Comparing the two cements, the fatigue cracks initiate earlier and propagate faster in the SmartSet GHV samples.

3.3. Topography of fracture surfaces

The microscopic view of the fracture surfaces showed similarity between the samples within the same cement (Fig. 6). Generally, the SmartSet GHV surfaces were rougher compared to the DePuy CMW1 surfaces. It seems that the cracks start from many points on the circumference of the rectangular or circular fracture surfaces, growing towards the centre where the fracture growth rate is affected by the sample type and cement composition. The side view of the fracture surfaces of randomly selected samples (not shown) led to the conclusion that the ‘disconnection topography’ between the upper and lower fracture surfaces of a sample is affected by both sample type and cement composition.

4. Discussion

The results have shown significant variations in fatigue behaviour. Test materials have revealed up to 5.5 times greater fatigue performance when testing samples produced

by direct moulding rather than moulding and machining ($p=0.00002$). The longer lives of the moulded samples can be attributed to a few causes. One reason, which has also been reported by Paravic et al. (1999), is that machining of cast rods leads to removal of the outer layer of the material which exposes the internal pores, hence increasing the surface initiation of fractures. Similar to the effect of machined surface porosity, polymers in general have a chance to form free radicals during machining leading to the breaking of bonds at certain depths (Backman and Devries, 1969) which can alter the tensile and fatigue characteristics. Interpreting the results according to this concept will certainly mean that more potential crack initiation sites existed on the machined samples leading to earlier failure. When moulded, the effect of the degree of interaction between the mould and the bone cement material has been reported by Tanner et al. (2010), however, compared to the machining, it provides less severe surface fracture initiators.

Within the same production method, circular moulded samples provided greater fatigue performance, including the two cement materials, compared to the rectangular counterparts ($p=0.003$). Comparing the circular to the rectangular samples produced by machining, however, provided opposite behaviour in results as can be seen in Fig. 4. Statistically, however, there is no importance of these variations between the four testing sets within this production method ($p=0.27$). Overall, longer fatigue lives were more likely to be obtained when testing circular rather than rectangular samples. Similar findings, using different bone cements, have been published particularly when comparing circular moulded against

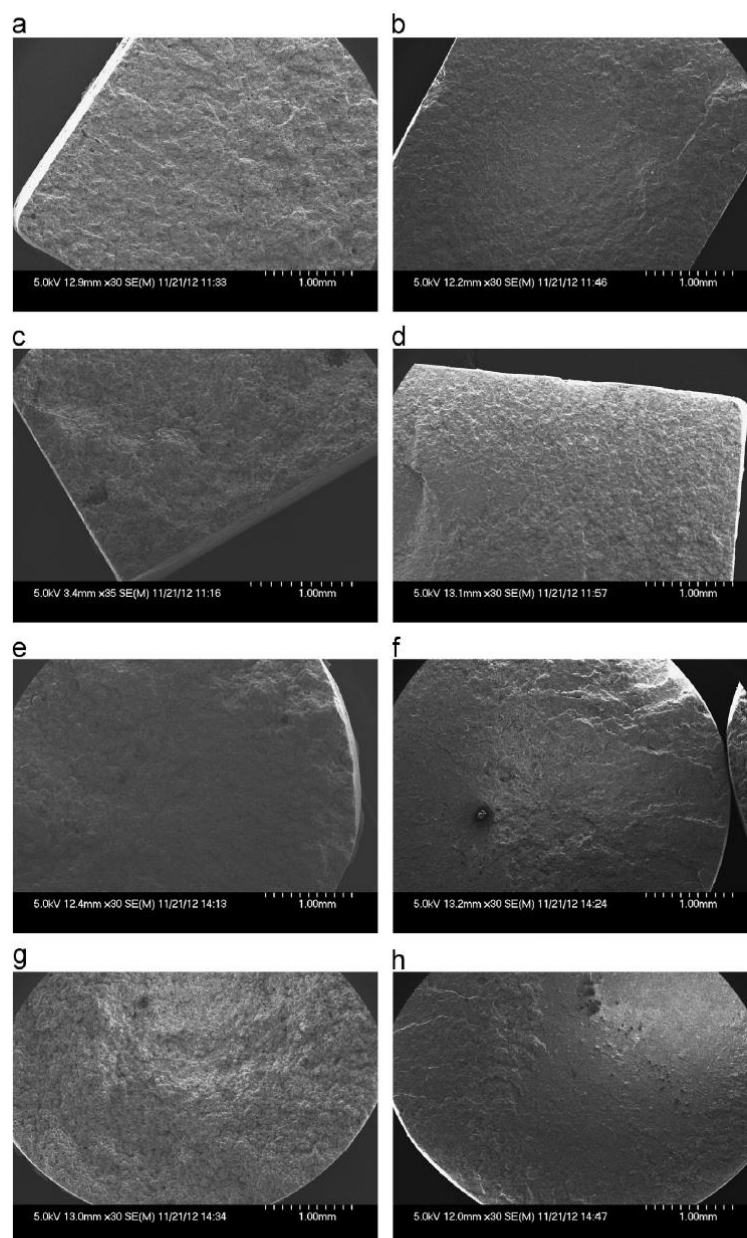


Fig. 6 – SEM of fracture surfaces of the median samples of different sample types of (a, c, e and g) SmartSet GHV and (b, d, f and h) DePuy CMW1 Showing (a and b) rectangular directly moulded, (c and d) rectangular machined, (e and f) circular directly moulded and (g and h) circular machined.

rectangular moulded (Lewis and Janna, 2003) and circular machined against rectangular moulded specimens, but at different fatigue stress types (Tanner et al., 2010). This trend in behaviour can be due to a combination of reasons. Rectangular samples have nearly three times larger nominal gauge surface area compared to the circular ones (450 mm² and 157 mm² respectively). This is important since the rectangular specimens have potentially more surface pores

increasing the number of crack initiation sites. It is necessary to consider also the effect of the difference between the two sample shapes in terms of surface area to volume ratios. The nominal ratios are 0.8 and 0.9 for the circular and rectangular samples respectively, providing a minimal advantage in crack resistance for the circular specimens. Another reason is that rectangular specimens have sharp corners forming stress concentration regions along the gauge length, whereas the

circular samples are free of corners. A few of the rectangular moulded samples, in particular, had accumulations of small pores at these edges, providing weaker regions enhancing the creation of fractures that lead to premature failures. These were less likely to be seen in the rectangular machined samples because they were largely removed during machining. Another cause that has been reported is the residual monomer in each sample shape and its possible variation due to the degree of polymerisation. Lewis and Janna (2003) found that the residual liquid monomer content for the circular specimens can be about 10% lower than that for the rectangular samples. The study concluded that the higher crystalline structure correlated to the circular shape led to the greater fatigue performance.

Among the two cement formations (Fig. 4), similarity in behaviour has emerged between each moulded shape in the two materials ($p=0.46$ and 0.16 for rectangular and circular respectively). Machined samples in the two materials behaved in a reverse way, yet no significant difference ($p=0.27$) of these variations was found when comparing the machined sets against each other. Nevertheless, a critical p -value ($p=0.05$) was determined when comparing the circular machined sets of the two cements. To investigate this indistinct correlation further, the two sets can be evaluated according to the fatigue performance index. The weakest sample type was the circular machined SmartSet GHV providing clearly lower fatigue index ($I=13,346$ cycles) compared to its DePuy CMW1 equivalent ($I=31,235$ cycles). As these two sample sets were produced, machined and tested in the same manner, the difference in results can only be due to the variations in chemical structure and additives. The former samples contain 9.76 wt% of zirconium dioxide and 2.87 wt% gentamicin whereas the latter set contains only 6.18 wt% of barium sulphate. When considering the densities of PMMA and the opacifiers, this leads to volume contents of 1.70 vol% for barium sulphate and 2.20 vol% for zirconium dioxide. After machining, therefore, the outer surface of the GHV samples had greater chance for the additives to arise that in some cases are surrounded by pores or voids increasing the crack initiations. This aspect might similarly be behind the trend between the fatigue lives of the rectangular machined samples of the SmartSet GHV and DePuy CMW1 though it is not statistically significant ($I=15,709$ and $19,678$ cycles respectively and $p=0.2$).

Having discussed some possible factors that can variously affect fatigue behaviour of bone cement depending on sample shape, production method and/or chemical structure, it is worth studying what factors have meanwhile controlled the variation in fatigue results within one testing group. The highest Weibull modulus value ($b=1.963$) associated with the DePuy CMW1 rectangular machined samples showing the lowest variation in results. This correlation, however, is reasonably at low performance of cycles to failure ($I=19,678$ cycles). That means, in this group, there is no specific factor seemed to have obviously affected one sample rather than the others. The greatest variation in results has been found with the GHV circular machined samples ($b=0.817$). This category has also shown the lowest fatigue index ($I=13,346$ cycles) as discussed above. Nine out of 13 samples failed particularly early, in the range between 1000 and 7000 cycles.

When investigating the fracture surfaces of these samples and comparing them to the equivalent GHV circularly moulded samples ($I=75,909$), similar amorphous structure of the fracture surfaces could be seen with the exception that the topography and circumference of the fracture surface for the machined samples seemed to be rougher than for the moulded ones. This result is presumably because machining process has led to the exposure of more crack initiators.

The investigation of crack behaviour through the hysteresis loops has largely clarified the process of crack initiation and propagation in all sample types. As can be seen in Fig. 5, the trends of the increase in absorbed energy and reduction in modulus (stiffness) are similar for DePuy CMW1 samples and varied for SmartSet GHV. Focusing on DePuy CMW1 results only, it can be understood that cracks remained steady with no obvious increase in growth until the last 1000 cycles (Fig. 5b and d). Differently, however, the absorbed energies and moduli for the SmartSet GHV samples showed substantial variations in results (Fig. 5a and c). In general, for this cement, the cracks initiate earlier and grow more rapidly than those in the DePuy CMW1 cement. This propagation of fatigue cracks is significantly faster with the SmartSet GHV machined samples compared to the moulded ones. Although this approach could substantially explain the variations in fatigue results among samples made of the SmartSet cement, the similarity and stability shown in crack behaviour amongst the DePuy CMW1 samples make it difficult to interpret the fatigue results of these samples in the light of the energy absorption concept. However, it does indicate that cracks in the DePuy CMW1 cement provide superior resistance to fracture growth within the fatigue testing period until a point close to the failure where the crack increases rapidly. This failure, however, as the fatigue life results showed, occurs earlier in the machined samples regardless of the apparent similarity in crack growth behaviour. That is to say, the higher increase in absorbed energy or reduction in modulus in one sample type compared to another does not constantly mean the former type provides shorter fatigue life. For example, the CDM samples made of SmartSet GHV showed clearer increases in energy and decreases in modulus compared to the RMM and CMM samples made of DePuy CMW1, while the fatigue life results of the former cement set were superior.

5. Conclusions

- This study has provided an emphasis that greater fatigue performance is achieved when moulded samples are used in testing. It has meanwhile validated the findings of Lewis and Janna (2003) that circular moulded samples, in particular, provide longer fatigue lives than rectangular moulded samples [I ratios (circular: rectangular)=2 for SmartSet GHV and 2.7 for DePuy CMW1, $p=0.003$].
- It has been shown that the effect of sample shape and production method themselves can be influenced by the type of bone cement used. Although no significant differences have been observed between the rectangular samples in both cements [I ratios (DePuy CMW1: SmartSet GHV)=1.13 for moulded and 1.27 for machined], clearer

variations in fatigue behaviour have been found between the circular samples of the two cements [I ratios (DePuy CMW1: SmartSet GHV)=1.5 for moulded and 2.4 for machined).

- Machining of samples can variously affect the outer surface of the sample depending on the amount and type of particles included in the cement matrix, leading to the presence of these elements on the surface creating more crack initiation sites.
- The investigation and analysis of the hysteresis loops, as increases in absorbed energy and reductions in secant modulus, have provided important indications of fatigue crack initiation and growth. Sample shape and production method have been found to significantly alter crack behaviour in the SmartSet GHV cement, whereas these variations were less conspicuous with the DePuy CMW1 cement.
- Overall, it is emphasised, when comparing fatigue results reported in the literature, variations in testing regimes must be considered.

Acknowledgements

The authors thank all those who have contributed to achieving this work. Appreciation is particularly to the Libyan Government for funding the research and DePuy CMW for providing the bone cement materials and mixing devices. Iskandar Vasiev is thanked for performing the electron microscopy.

REFERENCES

- Askeland, D.R., Fulay, P.P., Wright, W.J., 2011. *The Science and Engineering of Materials*, Sixth ed. Cengage Learning, Stamford.
- ASTM Standards, 2003. F2118-03, Standard Test Method for Constant Amplitude of Force Controlling Fatigue Testing of Acrylic Bone Cement Materials. American Society for the Testing and Materials, West Conshohocken, PA, US.
- ASTM Standards, 2008. C 1239-07, Standard Practice for Reporting Uniaxial Strength Data and Estimating Weibull Distribution Parameters for Advanced Ceramics. American Society for the Testing and Materials, West Conshohocken, PA, US.
- Backman, D.K., Devries, K.L., 1969. Formation of free radicals during machining and fracture of polymers. *Journal of Polymer Science Part A*, 2125–2134.
- Bhandari, V.B., 2007. *Design of Machine Elements*. Tata McGraw-Hill, New Delhi.
- Bialoblocka-Juszczak, E., Baleani, M., Cristofolini, L., Viceconti, M., 2008. Fracture properties of an acrylic bone cement. *Acta of Bioengineering and Biomechanics* 10, 21–26.
- Britton, J.C., McInnes, P., Ledoux, W.R., Retief, D.H., 1990. Shear bond strength of ceramic orthodontic brackets. *American Journal of Orthodontics and Dentofacial Orthopedics* 98, 348–353.
- BSI Standards, 2012. ISO 527-2, *Plastics – Determination of Tensile Properties; Part 2: Test Conditions for Moulding and Extrusion Plastics*. British Standards Institution, London, UK.
- Cristofolini, L., Minari, C., Viceconti, M., 2002. Methodology and criterion for acrylic bone cement fatigue tests. *Fatigue and Fracture of Engineering Materials and Structures* 23, 953–957.
- Danzer, R., Supancic, P., Pascual, J., Lube, T., 2007. Fracture statistics of ceramics – Weibull statistics and deviations from Weibull statistics. *Engineering Fracture Mechanics* 74, 2919–2932.
- DePuy, C.M.W., 2012. DePuy orthopaedic gentamicin bone cements. Available from: (https://www.jnjgatewayifu.com/eLabelingContent/Dpo/USENG/CMWeifu001_84324.pdf) (accessed 29.02.12).
- Dowling, N.E., 2007. *Mechanical behaviour of materials: Engineering methods for deformation, fracture, and fatigue*. Pearson. Prentice Hall, New Jersey.
- Dunne, N.J., Orr, J.F., Mushipe, M.T., Eveleigh, R.J., 2003. The relationship between porosity and fatigue characteristics of bone cements. *Biomaterials* 24, 239–245.
- Ellyin, F., 1997. *Fatigue damage, crack growth and life prediction*. Chapman & Hall, London.
- Gelb, H., Schumacher, H.R., Cuckler, J., Ducheyne, P., Baker, D.G., 1994. In vivo inflammatory response to polymethylmethacrylate particulate debris: effect of size, morphology and surface area. *Journal of Orthopaedic Research* 12, 83–92.
- Gough, H.J., Pollard, H.V., 1935. The strength of metals under combined alternating stresses. *Proceedings of the Institution of Mechanical Engineers*. Available from: (<http://pme.sagepub.com/content/131/1/3.citation>) (accessed 07.08.13).
- Hertzberg, R.W., 1996. *Deformation and Fracture Mechanics of Engineering Materials* fourth ed. John Wiley & Sons, Inc., Canada.
- Hoppel, C.P.R., Pangborn, R.N., 1994. The evaluation of fatigue damage in short fiber-reinforced styrene-maleic anhydride. In: Mitchell, M.R., Buck, O. (Eds.), *Cyclic Deformation, Fracture, and Non-Destructive Evaluation of Advanced Materials*. American Society for Testing and Materials, Philadelphia, PA.
- Janna, S., Dwiggin, D.P., Lewis, G., 2005. A new, reliable, and simple-to-use method for the analysis of a population of values of a random variable using the Weibull probability distribution: application to acrylic bone cement fatigue results. *Bio-Medical Materials and Engineering* 15, 349–355.
- Janssen, D., Stolk, J., Verdonschot, N., 2005. Why would cement porosity reduction be clinically irrelevant, while experimental data show the contrary. *Journal of Orthopaedic Research* 23, 691–697.
- Krause, W.R., Grimes, L.W., Mathis, R.S., 1988. Fatigue testing of acrylic bone cement: statistical concepts and proposed test methodology. *Journal of Biomedical Materials Research Part B Applied Biomaterials* 22, 179–190.
- Lewis, G., Janna, S., Carroll, M., 2003. Effect of test frequency on the in vitro fatigue life of acrylic bone cement. *Journal of Biomedical Materials Research Part B Applied Biomaterials* 48, 143–149.
- Lewis, G., Janna, S., 2003. Effect of test specimen cross-sectional shape on the in vitro fatigue life of acrylic bone cement. *Biomaterials* 24, 4315–4321.
- Lewis, G., Nyman, J.S., 2000. Toward standardization of methods of determination of fracture properties of acrylic bone cement and statistical analysis of test results. *Journal of Biomedical Materials Research Part B Applied Biomaterials* 53, 748–768.
- Lewis, G., Sadhasivini, A., 2004. Estimation of the minimum number of test specimens for fatigue testing of acrylic bone cement. *Biomaterials* 25, 4425–4432.
- Lewis, G., 1999a. Effect of mixing method and storage temperature of cement constituents on the fatigue and porosity of acrylic bone cement. *Journal of Biomedical Materials Research Part B Applied Biomaterials* 48, 143–149.
- Lewis, G., 1999b. Effect of two variables on the fatigue performance of acrylic bone cement: mixing method and viscosity. *Bio-Medical Materials and Engineering* 9, 197–207.
- Lewis, G., 2003. Fatigue testing and performance of acrylic bone-cement materials: state-of-the-art review. *Journal of*

- Biomedical Materials Research Part B Applied Biomaterials 66B, 457-486.
- Lezarus, M.D., Cuckler, J.M., Schumacher, H.R., Ducheyne, P., Baker, D.G., 1994. Comparison of the inflammatory response to particulate polymethylmethacrylate debris with and without barium sulphate. *Journal of Orthopaedic Research* 12, 532-541.
- Ling, R.S., Lee, A.J., 1998. Porosity reduction in acrylic cement is clinically irrelevant. *Clinical Orthopaedics and Related Research* 355, 249-253.
- Malchau, H., Herberts, P., Soderman, P., Oden, A., 2000. Prognosis of total hip replacement: update and validation of results from the Swedish National Hip Arthroplasty Register 1979-1998. 67th Annual meeting of the American Academy of Orthopedic Surgeons, Orlando; Available from: (<http://www.shpr.se/Libraries/Documents/AAOS2000NHR.sflb.ashx>) (accessed 02.04.13).
- McCartney, L.N., 1996. Stress transfer mechanics: methods that should be the basic of life prediction methodology. In: Johnson, W.S., Larsen, J.M., Cox, B.N. (Eds.), *Life Prediction Methodology for Titanium Matrix Composite*. American Society for Testing and Materials, West Conshohocken, US.
- Milella, P.P., 1999. A fatigue crack growth theory based on energy considerations: Further developments on small crack behaviour and R ratio. In: Panontin, T.L., Sheppard, S.D. (Eds.), *Fatigue and Fracture Mechanics*. American Society for Testing and Materials, West Conshohocken, PA.
- Mitchell, W., Matthews, J.B., Stone, M.H., Fisher, J., Ingham, E., 2003. Comparison of the response of human peripheral blood mononuclear cells to challenge with particles of three bone cements in vitro. *Biomaterials* 24, 737-748.
- Mott, R.L., 2004. *Machine Elements in Mechanical Design*. Pearson Education, New Jersey.
- Paravic, V., Nobel, P.C., Alexander, J.W., Leibs, T.R., Elliot, A., 1999. Effect of specimen preparation on porosity and fatigue life a study of centrifuged and hand mixed cements. In: *Proceedings of the 45th Annual Meeting, Orthopaedic Research Society*. Anaheim, California.
- Prendergast, P.J., Murphy, B.P., Taylor, D., 2002. Letter to editor. *Fatigue and Fracture of Engineering Materials and Structures* 25, 315-316.
- Quinn, J., Joyner, C., Triffitt, J.T., Athanasou, N.A., 1992. Polymethylmethacrylate-induced inflammatory macrophages resorb bone. *Journal of Bone and Joint Surgery* 74-B, 652-658.
- Sabokbar, A., Fujikawa, Y., Brett, J., Murray, D.W., Athanasou, N.A., 1996. Increased osteoclastic differentiation by PMMA particle-associated macrophages. *Acta Orthopaedica Scandinavica* 67, 593-598.
- Shigley, J.E., Mischke, C.R., 1989. In: *Mechanical Engineering Design*, fifth ed. McGraw-Hill, New York.
- Soh Fotsing, B.D., Ango, G.F., Fogue, M., 2010. Statistical techniques of sample size estimating in fatigue tests. *International Journal of Engineering and Technology* 2, 477-481.
- Suresh, S., 1998. *Fatigue of Materials*. Cambridge University Press, New York.
- Swanson, S.R. (Ed.), 1974. *Handbook of Fatigue Testing*. American Society for Testing and Materials, Philadelphia.
- Tanner, K.E., Wang, J.S., Kjellson, F., Lidgren, L., 2010. Comparison of two methods of fatigue testing bone cement. *Acta Biomaterialia* 6, 943-952.
- Wang, J.S., Diaz, J., Sabokbar, A., Athanasou, N., Kjellson, F., Tanner, K.E., McCarthy, I.D., Lidgren, L., 2005. In vitro and in vivo biological responses to a novel radiopacifying agent for bone cement. *Journal of the Royal Society Interface* 2, 71-78.
- Weibull, W., 1951. A statistical distribution function of wide applicability. *Journal of Applied Mechanics* 18, 293-297.
- Weibull, W., 1961. *Fatigue Testing and Analysis of Results*. Pergamon Press, London.